Studies of the meteorology and climatology of Ross Island and the Ross Ice Shelf, Antarctica

A thesis submitted in partial fulfilment of the requirements for the Degree of Doctor of Philosophy in Physics at the University of Canterbury by

Jack H. J. Coggins

University of Canterbury, 2013

This thesis documents a series of studies performed on the lower atmosphere over the region of the Ross Ice Shelf, Antarctica, and its surroundings. In particular, much of the thesis focuses on the area in the vicinity of Ross Island, a mountainous protrusion in the far north-west of the permanent floating ice shelf. Weather in both the smaller and larger regions is naturally complex and generated by a range of localised and larger scale interactions.

In order to better understand the meteorology of the Ross Ice Shelf, including Ross Island, we produce a synoptic climatology of the region based on surface wind output provided by the ERA Interim reanalysis. Output is taken from 1979 to 2011 and thus represents a much longer time scale than covered by previous studies of Ross Ice Shelf winds. The climatology is generated through a clustering routine based on the widely-used k-means technique. The results of the routine are discussed and we find that the reanalysis is capable of representing the previously reported features of the region. Cluster composites are also shown to be coherent between reanalysis output and data collected by *in situ* monitoring devices. We confirm that the Ross Ice Shelf Air Stream (RAS), a jet of fast-moving air that propagates from the Siple Coast across the ice shelf, is a robust feature of the climatology of the region and we find that it has a large impact on the surface temperature. The analysis is continued with reference to two widely studied modes of internal variability, the Southern Annular Mode (SAM) and El Niño-Southern Oscillation (ENSO), which are known to affect local conditions in the Ross Sea region via modulation of the Amundsen-Bellingshausen Sea low. Reanalysis output and results from the clustering routine allow us to examine the impacts of these modes upon the Ross Ice Shelf and Ross Sea in unprecedented detail. Further, we are able to tie changes in the mean pattern to variability within and between particular clusters, allowing us to ascertain the dominant synoptic patterns in forcing the mean variability. The impact on surface temperatures for both modes is found to be high and significant, which we explain with reference to changes in circulation patterns.

We further use the results of the clustering algorithm to explore the climatology of the region surrounding Ross Island. By producing composites of local *in situ* records based on the clustering technique described previously, we are able to generate a climatology of the region that is not hampered by gaps in the observational record. We find that the climate of Ross Island is sensitive to RAS events, due to the ability of strong flows to dramatically increase the temperature. At Scott Base, on the southern tip of the Hut Point Peninsula, the temperature is found to be particularly sensitive to these events. McMurdo Station, which is located less than 3 km away, is observed to be much less sensitive, due to the modulation of synoptic flows by localised topographic influences. Particularly salient is the difference in temperature trends between these two locations, which we show to be statistically significant in the annual and seasonal means from 1979 onwards. By applying a novel temperature reconstruction technique based on the output of the clustering routine, we are able to assess the contribution of changes in circulation to temperature trends at these two locations. We conclude that a large amount of the change in temperature at Scott Base can be explained through circulatory variability over the Ross Ice Shelf. However, the trend at McMurdo Station can not be explained using this technique and may be the result of extremely localised forcing.

Data availability in Antarctica is widely known to be low, due to the relative sparsity of observations and ongoing problems with data collection due to extremely inhospitable conditions and challenging logistical considerations. The lack of data at the mesoscale has hampered the understanding of localised processes in the Antarctic atmosphere that may be important for forecasting. Through the development

and deployment of a distributed system of atmospheric sensors called "SNOW-WEB", we have taken steps to address this issue in the vicinity of Ross Island. We report on the short-term deployment of the system in the summer of 2011/12 and on the data collected during that time. We perform a comparison with output from the Antarctic Mesoscale Prediction System (AMPS), a mesoscale forecast model employed in forecasting for the region, in order to highlight the utility of SNOW-WEB data collection and the accuracy of the model forecasts. Moreover, we perform experiments with the polar-modified Weather Research and Forecasting (WRF) model, in order to ascertain whether an improved topographic representation of the region surrounding Ross Island is capable of improving forecast accuracy. Topographic representation is considered particularly important in Antarctica, as the strong static stability of the lower atmosphere dictates that near-surface flows are highly sensitive to the underlying terrain. Accordingly, we find that the model representation of a strong wind event in the vicinity of Ross Island in December 2011 is much improved between a 1 km and 0.25 km grid. The high density of data collected by the SNOW-WEB network during this period was paramount in the validation of the high resolution model grids. The study also illustrates the importance of adequate representation of processes in the wider region, as Ross Island is observed to be sensitive to changes in conditions over the Ross Ice Shelf.

Deputy Vice-Chancellor's Office
Postgraduate Office

UNIVERSITY OF CANTERBURY
Te Whare Wānanga o Waitaha
CHRISTCHURCH NEW ZEALAND

Co-authorship Form

This form is to accompany the submission of any thesis that contains research reported in co-authored work that has been published, accepted for publication, or submitted for publication. A copy of this form should be included for each co-authored work that is included in the thesis. Completed forms should be included at the front (after the thesis abstract) of each copy of the thesis submitted for examination and library deposit.

Please indicate the chapter/section/pages of this thesis that are extracted from co-authored work and provide details of the publication or submission from which the extract comes:

Chapter 6, SNOW-WEB: A new technology for Antarctic meteorological monitoring, published in Antarctic Science, 2013 (Coggins et al., 2013).

Please detail the nature and extent (%) of contribution by the candidate:

Jack H. J. Coggins was the lead author of this article; contribution: 70%.

Certification by co-authors:

If there is more than one co-author then a single co-author can sign on behalf of all.

The undersigned certifies that:

- the above statement correctly reflects the nature and extent of the PhD candidate's contribution to this co-authored work;
- in cases where the candidate was the lead author of the co-authored work he or she wrote the text.

Name: Signature: Date:

Deputy Vice-Chancellor's Office
Postgraduate Office

UNIVERSITY OF CANTERBURY
Te Whare Wānanga o Waitaha
CHRISTCHURCH NEW ZEALAND

Co-authorship Form

This form is to accompany the submission of any thesis that contains research reported in co-authored work that has been published, accepted for publication, or submitted for publication. A copy of this form should be included for each co-authored work that is included in the thesis. Completed forms should be included at the front (after the thesis abstract) of each copy of the thesis submitted for examination and library deposit.

Please indicate the chapter/section/pages of this thesis that are extracted from co-authored work and provide details of the publication or submission from which the extract comes:

Parts of the Introduction chapter, and large sections of analysis carried out in chapter 3, accepted to the International Journal of Climatology (September, 2013).

Please detail the nature and extent (%) of contribution by the candidate:

Jack H. J. Coggins was the lead author of this article; contribution: 70%.

Certification by co-authors:

If there is more than one co-author then a single co-author can sign on behalf of all.

The undersigned certifies that:

- the above statement correctly reflects the nature and extent of the PhD candidate's contribution to this co-authored work;
- in cases where the candidate was the lead author of the co-authored work he or she wrote the text.

Name: Signature: Date:

Acknowledgements

I would like to thank my supervisor, Adrian McDonald, for taking me on as a PhD student and for support and encouragement throughout the course of the project. I would also like to thank my secondary supervisor, Wolfgang Rack, for enlightening discussions throughout the project. I also wish to thank Jack Baggaley for additional support.

I travelled to Antarctica several times over the course of the project and I wish to thank the staff of Scott Base for their hospitality, the science and field staff for support in SNOW-WEB deployment, and Antarctica New Zealand for logistical support. I would also like to thank the technical staff of the University of Canterbury Physics Department, especially Graeme Plank and Matt Pannell, for work on the development of the SNOW-WEB network of weather stations. Two anonymous reviewers commented on the SNOW-WEB chapter and I must thank them for the improvements that they suggested to the manuscript. Thanks also go to Iman Soltanzadeh and Peyman Zawar-Reza at Gateway Antarctica for providing the polar-WRF model output and for aid in interpreting its results, and for the information included in table 7.1. John and Liz Cassano visited the department during my time here and I wish to thank them for discussions regarding clustering techniques and the climate of the Ross Ice Shelf. I must also thank the students of the Atmospheric Physics research group, past and present, including: Ben Jolly, Simon Parsons, Simon Fullick, Nikolai Kruetzmann, Madeleine Smith, Fraser Dennison, Robert Ward and Rachel Soja; for interesting discussions on many subjects throughout my time here and for making the department a genuinely pleasant place to work. Ben Jolly, Simon Parsons, Robert Ward and Tim Delaney also aided in SNOW-WEB deployment and retrieval in Antarctica and for that I am grateful. Outside of the department, I would like to thank all of my friends in Christchurch and my flatmates. I owe a debt of gratitude to my good friend Holly Painter, who provided much support via the internet and who proof-read parts of the thesis. Laura Azzani deserves special mention for providing encouragement through the thesis writing stage.

Data used throughout the thesis came from a variety of sources. I wish to thank Kevin Manning for providing archived Antarctic Mesoscale Prediction System output for the summers of 2010/11 and 2011/12. Antarctic automatic weather station data were provided by the programmes of the University of Wisconsin, Madison, New Zealand's Nation Institute of Water and Atmospheric Research (NIWA), and the Nation Climatic Data Center (NCDC). Long-term monthly means for Antarctic manned stations were provided by the READER (REference Antarctic Data for Environmental Research) database, a project of the Scientific Committee on Antarctic Research (SCAR). We also employed data from the ERA Interim reanalysis, a project of the European Centre for Medium-Range Weather Forecasts (ECMWF), and the NCEP-DOE reanalysis, provided by the National Oceanic & Atmospheric Administration (NOAA). Satellite imagery was provided by the Landsat Image Mosaic Of Antarctica (LIMA) project, and topographical data by Radarsat Antarctic Mapping Project (RAMP) digital elevation model.

I wish to gratefully acknowledge the University of Canterbury for supporting my studies through the funding of a doctoral scholarship, and the New Zealand Ministry of Foreign Affairs and Trade for the funding of a Ross Sea Dependency Scholarship.

Finally, I would like to acknowledge the contributions of the examiners, Andrew Orr and James Renwick, towards the accuracy and readability of the manuscript.

Contents

List of Figures

List of Tables

Chapter 1

Introduction

This thesis is concerned with the meteorology and climate of the Ross Ice Shelf and surrounding regions of Antarctica. Special attention is given to the mountainous region of Ross Island in the far north-west of the shelf, due to the complex interplay observed there between local and synoptic influences, and the presence of two year-round manned bases on the island. In brief, the meteorology of both the smaller and wider regions are described through the production of a synoptic climatology based on ERA Interim output, an observational field campaign, and the development of a mesoscale model.

The Ross Ice Shelf (RIS) is located between the two major grounded Antarctic ice sheets and distributed almost symmetrically about the dateline. To its western and south-western flank is the high barrier of the Transantarctic Mountain range, and to the north, the Ross Sea. A topographic map of the region is displayed in figure 1.1. At the surface of the shelf, net northward atmospheric outflow has been shown to occur (Parish and Bromwich, 2007). The source of the outflow originates in down-slope flows which impinge on the ice shelf from both East Antarctica, through steep glaciers in the Transantarctic Mountains (Bromwich, 1989b; Breckenridge et al., 1993), and West Antarctica, via the gentler slopes of the Siple Coast ice floes (Bromwich et al., 1992; Bromwich and Liu, 1996). Confluence zones of the continental near-surface flow have been shown to occur in these locations by katabatic wind models (Ball, 1960; Parish and Bromwich, 1987) and output of the Antarctic Mesoscale Prediction System (AMPS) (Powers et al., 2003; Parish and Bromwich, 2007) (see section 2.2).

Drainage flows have been shown to be enhanced by cyclonic disturbances over the Ross Sea to the north of the permanent ice shelf (Bromwich et al., 1992, 1993). Notably, interaction of synoptic scale cyclones at the north-eastern margin of the ice shelf and drainage flows has been observed to induce an effect, coined the Ross Ice Shelf Air Stream (RAS) (Parish et al., 2006), in which flow from West Antarctica propagates across the shelf towards the north and north-west and is further fed by katabatic drainage along the Transantarctic Mountains (Bromwich et al., 1992; Seefeldt and Cassano, 2008, 2012). It appears that such flows are reinforced by a barrier wind regime (Schwerdtfeger, 1984) (see section 2.3) on the western margin of the shelf. Stably stratified air advected from the east is dammed against the Transantarctic Mountains, generating a pressure gradient perpendicular to the barrier which produces an enhanced low-level jet directed towards the north and north-west (O'Connor et al., 1994; Seefeldt et al., 2007; Steinhoff et al., 2009; Nigro et al., 2012b).

The seasonality of the RAS phenomenon was investigated by Parish et al. (2006) and Seefeldt and Cassano (2008, 2012), who reported that the effect is persistent and appears year-round, although RAS

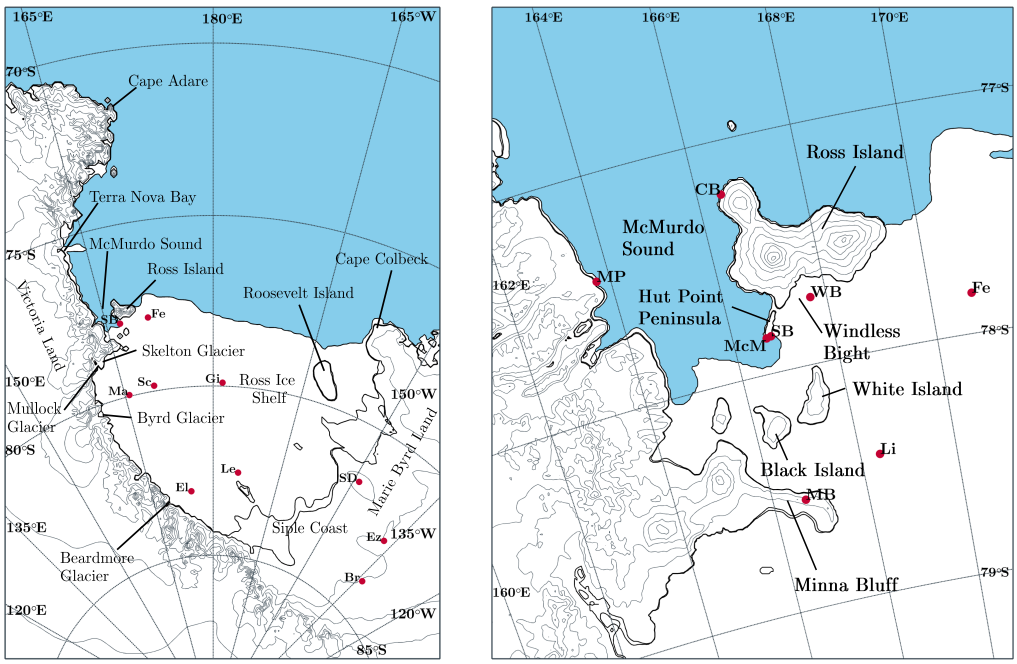

(a) Ross Ice Shelf map

(b) Ross Island map

Figure 1.1: Maps of greater Ross Ice Shelf and Ross Sea region (a), and Ross Island region (b). Sea is shown in blue and land and permanent ice in white. Ice cover around the sea margins is variable, such that depiction of the ice edge is approximate and for visual purposes only. Topographic contours shown are at 10 m, 80 m, 500 m and then every 500 m to 4000 m. Topographic data are sourced from the Radarsat Antarctic Mapping Project (RAMP) (Liu et al., 2001). Red dots show the location of AWS units used throughout the thesis.

seems to be most prevalent outside of summer months. During strong wind events in the RIS region, warming is observed at the surface of the ice shelf, which is visible as dark patches in satellite thermal infrared imagery (Bromwich et al., 1992; Carrasco and Bromwich, 1993a), although work by Steinhoff et al. (2009) suggests this pattern may also represent cloud formation. Warming signatures at the surface during strong wind events have also been confirmed by surface observations (Holmes et al., 2000). The warming effect is perhaps counter-intuitive, as air advected into the region has its origins on the cold, high-altitude ice sheets. The signature is explained by a combination of adiabatic warming, due to the movement of air towards sea-level, and subsequent turbulent vertical mixing, due to high wind speeds (Bromwich, 1989b). The strong temperature inversion over the ice shelf (Connolley, 1996) is then disrupted, and the surface warms.

The temperature reaction to strong winds on the ice shelf is remarkable and as such, the frequency of strong wind events over long time periods may have a profound impact on the surface climate. Large temperature gradients between East Antarctica, West Antarctica, and the ocean to the north (King and Turner, 1997) also dictate that the temperature of the ice shelf is likely to be highly dependent on the origin of the dominant flow. Given that circulation in the region is known to be influenced by several large-scale modes of variability, which are discussed later in this section, it seems likely that the surface temperature of the ice shelf may show some dependence on the wider region. Strong winds over the sea

to the north of the RIS also influence polynya formation (Bromwich et al., 1993) and consequently the production and advection of sea ice and highly saline Antarctic bottom water (Stammerjohn et al., 2008; Tamura et al., 2008; Comiso et al., 2011).

Ross Island, a mountainous protrusion from the permanent ice shelf, is located at the northern end of the RAS, and the area surrounding the island experiences a complicated surface flow regime, due to the transition of flow from the essentially flat ice shelf to the topographically complex region on the south side of the island. For reference, we show a map of Ross Island, with major features annotated in figure 1.1.

The primary Antarctic research facilities of both New Zealand and the United States are located on the tip of the Hut Point Peninsula, on the south side of Ross Island. The American station, McMurdo, was established in 1957 and has since recorded daily weather conditions with only minor interruptions. Scott Base was founded by New Zealand in the following year, and also has an almost complete climatic record. The distance between the two stations is ≈ 2.2 km. Data from both of the stations are available from SCAR's READER database (Turner et al., 2004) as highly quality controlled monthly averages. The two stations represent by far the longest instrumental records from this region of Antarctica.

The prevailing southerly flow on the ice shelf has been shown to produce a high pressure region in the wide bay to the south of Ross Island, known as Windless Bight (O'Connor and Bromwich, 1988; Seefeldt et al., 2003), as statically stable surface flow cannot overcome the high chain of mountains that lines Ross Island from west to east (see section 2.1). Further, the damming of flow along the Hut Point Peninsula, on the south-west of the island, generates a barrier wind regime that causes the wind at Scott Base, to be from the north-east (Sinclair, 1982). During times of strong winds from the south flow may be able to pass over the Hut Point Peninsula. Under these conditions, the wind at Scott Base tends to be strong and directed from the south or south-east. Similar conditions are also experienced to the south of the peninsula at Pegasus Runway (Holmes et al., 2000).

The occurrence of surface flow over the remainder of the island is unlikely due to the extreme altitude of the mountains there. Accordingly, during strong southerly wind events on the ice shelf, strong winds are observed either side of Ross Island in McMurdo Sound and the Ross Sea (Bromwich, 1988; Seefeldt et al., 2003; Monaghan et al., 2005), caused by the splitting of the southerly flow around the island.

Despite a growing body of knowledge on the dynamics of the RIS circulation, the climatic effects are not yet well understood, the investigation of which forms the bulk of the first half of this thesis. This lack of understanding is, at least in part, due to the nature of the Antarctic in situ climate record, which is short and thinly spread (Turner et al., 2004; Lazzara et al., 2012) compared to lower latitudes and the Northern Hemisphere. Consequently, and perhaps most importantly given current research priorities, climatic trends computed across the continent are not as well constrained as those in data-rich areas (Turner et al., 2005; Turner and Overland, 2009).

In order to investigate the climatology of the RIS and surrounding regions, with particular emphasis on the contribution of individual circulation patterns to the mean state, in chapter 3 we use a k-means clustering routine applied to surface wind conditions drawn from the ERA Interim reanalysis (Dee et al., 2011). The aim of such an analysis is to split high time-resolution data (6 hourly) over an extended period (1979-2011) into broad circulation patterns that can be readily interpreted, such that the climate can be assessed on synoptic time-scales.

Whilst a significant number of automatic weather station (AWS) records exist on the RIS (Lazzara et al., 2012), and have been used previously to investigate dynamical and climatic aspects of the region

(O'Connor et al., 1994; Slotten and Stearns, 1987; Reusch and Alley, 2004; Seefeldt et al., 2007), inconsistencies and gaps in the records mean that this data source is not optimal for long-term investigations of climatic variability. We use the ERA Interim reanalysis as it provides consistent records of multiple atmospheric variables at temporal and spatial resolutions that allow us to investigate the synoptic climatology of the region for an extended time period. Before employing the output of the clustering algorithm to study climatological changes however, we must first establish that it is able to adequately depict the known atmospheric features of the region, which is the primary focus of chapter 3 of this thesis.

The subsequent chapter then continues in this vein, and describes the application of the results of chapter 3 to the investigation of the variability of the climate of the region with two large-scale modes, which are described presently.

The Southern Annular Mode (SAM) is the leading mode of extra-tropical variability at monthly timescales in the Southern Hemisphere (Gong and Wang, 1999; Thompson and Wallace, 2000). The mode represents the predominantly zonally symmetric periodic strengthening and weakening of the dominant large-scale pressure and wind patterns around Antarctica. A thorough description of SAM if given in section 2.6.

In the positive (SAM+) phase, negative pressure and geopotential height anomalies are observed over Antarctica and the surrounding ocean. Positive anomalies occur in the mid-latitudes, the circumpolar trough shifts to the south, and circumpolar westerly winds are strengthened. The opposite conditions are observed during the negative SAM (SAM-) phase.

SAM phases are associated with variability in the wavenumber-3 structure around the Southern Ocean (Raphael, 2004; Kidston et al., 2009), which introduces some non-annular structure to the predominantly zonally symmetric pattern. An especially large degree of variability has been shown to occur in the Ross, Amundsen and Bellingshausen Seas (Bracegirdle, 2012; Fogt et al., 2012a; Turner et al., 2012), associated with SAM. In this region, a climatological low pressure zone exists, known as the Amundsen-Bellingshausen Sea (ABS) Low, which is generated by flow splitting around the Antarctic topography (Baines and Fraedrich, 1989; Lachlan-Cope et al., 2001; Fogt et al., 2012b) and thus pressure in the region is extremely variable on monthly time scales (Connolley, 1997). The literature surrounding SAM is reviewed in section 2.6.

The deepening of the ABS low under SAM+ conditions has been proposed as responsible for observed trends in sea ice in the Ross and Bellingshausen Seas (Stammerjohn et al., 2008; Turner et al., 2009b; Comiso et al., 2011) via wind-driven advection.

The El Niño-Southern Oscillation (ENSO) is a coupled ocean/atmosphere mode that is manifested in the tropical Pacific (Trenberth, 1997; Trenberth and Caron, 2000). Anomalous deep convection associated with ENSO has been shown to propagate variability to high latitudes via a Rossby wave train which crosses the South Pacific Ocean (Hoskins and Karoly, 1981; Mo and Paegle, 2001) and the modulation of Hadley and Ferrel cells and associated jets (Chen et al., 1996; Yuan, 2004). ENSO is discussed at length in section 2.7 and a review of the effects of ENSO on Antarctica and the Southern Ocean is given by Turner (2004).

As for SAM, a high degree of ENSO variability is observed in the ABS region (Turner et al., 2012). A weaker low and increased frequency of blocking is observed under El Niño (warm event) conditions (Renwick, 1998; Renwick and Revell, 1999), and some authors have observed that the low shifts eastward (Cullather et al., 1996; Bertler et al., 2004), although Turner et al. (2012) warned that this shift is not

statistically significant. The opposite conditions are observed in the La Niña phase.

Through the modulation of the ABS low, ENSO has been shown to increase precipitation in West Antarctica under La Niña conditions (Cullather et al., 1996; Bromwich et al., 2000; Genthon and Cosme, 2003). ENSO influences on the temperature of the Antarctic Peninsula (Marshall and King, 1998; Harangozo, 2000) and West Antarctic and surrounding oceans (Kwok and Comiso, 2002b,a; Schneider et al., 2012b) have also been demonstrated, which are characterised by increased warm (cold) advection to the east (west) of the ABS low during the La Niña phase. This circulation-driven mechanism has also been recognised as influencing the sea ice extent in the Ross, Amundsen and Bellingshausen Seas (Simmonds and Jacka, 1995; Liu et al., 2004; Yuan, 2004; Stammerjohn et al., 2008).

In the RIS region, which is located on the western flank of the ABS low, winds are directly affected by the strength and position of the pressure minimum (Fogt et al., 2012b; Turner et al., 2012). Accordingly, circulation in the region has been demonstrated to be dependent on the phase of both SAM (Fogt et al., 2012a; Cohen et al., 2013) and ENSO (Markle et al., 2012; Cohen et al., 2013). To the west of the ice shelf, in the McMurdo Dry Valleys, strong winds have also been shown to be more frequent under SAM+ and La Niña conditions (Bertler et al., 2006; Speirs et al., 2010, 2012).

The observed temperature at long-period weather stations in the north-west of the ice shelf shows covariability with both modes (Gillett et al., 2006; Marshall, 2007; Gillett et al., 2008; Fogt et al., 2012a; Schneider et al., 2012b; Yu et al., 2012), and both have been implicated in forcing trends in the region (Bertler et al., 2004; Marshall, 2007; Gillett et al., 2008; Schneider et al., 2012a). Temperature covariability has also been shown across the wider region (Kwok and Comiso, 2002a; van den Broeke and van Lipzig, 2004).

Although some of the temperature dependence of SAM has been explained via the isolating influence of circumpolar westerly winds (van den Broeke and van Lipzig, 2004; Marshall, 2007), a detailed regional study of the influence of these modes at the surface has yet to be performed. The results of the clustering analysis of chapter 3 are a powerful tool for investigating variability in the Ross Sea region, as the mean state of the atmosphere is an integrated measure of the occurrence of the clusters defined in chapter 3. Consequently, changes in the mean state can be better understood with reference to changes in the underlying meteorological conditions, as represented by the clusters. In chapter 4, we will further the results of the surface climate study of CMJ2013, via an application of the clustering results to variability in the region coinciding with the phases of SAM and ENSO.

Of further interest are historical temperature trends in the Ross Ice Shelf region, which are often difficult to characterise and interpret due to the historical lack of data from the continent. The READER database (Turner et al., 2004) does however catalogue climate data from a series of manned-stations across the continent, most available from the 1950s. Temperature trends at Scott Base have been shown to be variable between seasons and sensitive to start and end dates. Bertler et al. (2004) described a cooling at Scott Base in summer between 1986 and 2000, and suggested that the decreasing trends could be due to changes in circulation due to the increasing tendency towards La Niña conditions during the time period. Turner et al. (2005) reported cooling in the autumn and warming in the winter and spring from 1971 to 2000. However, they also showed warming in all seasons when the time period began in 1958. Similarly, Turner and Overland (2009) showed year-round warming at Scott Base and McMurdo Station from 1951 to 2006. Both Marshall (2007) and Gillett et al. (2008) showed that the increasingly positive tendency in the phase of SAM caused cooling in the region. This may explain the disparity in the later period, as SAM trends have been shown to be largest from the late 1970s onwards (Marshall, 2003) and are thought to occur due to ozone forced trends (Thompson and Solomon, 2002; Thompson et al., 2011).

Schneider et al. (2012a) reported year-round warming at Scott Base from 1958 to 2008, although only the spring value was statistically significant. In the period from 1979 to 2008, they found cooling in all seasons except spring.

Spring warming at Scott Base has been associated with equivalent changes in West Antarctica, an area where temperature trends are particularly contentious due to the extreme paucity of historical surface records (Schneider et al., 2012a). In this region, multiple reconstruction efforts have statistically inferred trends from available records using combinations of data sources (Monaghan et al., 2008; Steig et al., 2009; O'Donnell et al., 2011), but the size, extent, and timing of trends differs between reconstruction techniques.

Schneider et al. (2012a) reviewed several data sources and reconstructions for the springtime of 1979-2008. From their collation of results (in particular, their figure 3), it is clear that the sources agree on a net warming over the West Antarctic and Ross Ice Shelf, although the magnitude of the warming and its spatial pattern varies between sources. Recently, the study of Bromwich et al. (2012) has suggested that Byrd Station, on the West Antarctic plateau, is one of the most rapidly warming regions on the Earth's surface due to circulation changes associated with anomalous tropical convection (Ding et al., 2011; Schneider et al., 2012a) and the increasing tendency of in-phase SAM and ENSO events (Fogt et al., 2011).

The West Antarctic region is known to be sensitive to cyclonic activity (Nicolas and Bromwich, 2011a). The observed drainage of West Antarctic air onto the Ross Ice Shelf (Bromwich and Liu, 1996) and the sensitivity of both regions to variability of the low pressure centre in the Amundsen-Bellingshausen Seas (Fogt et al., 2012b; Turner et al., 2012) directly links the climate of the Ross Ice Shelf to that of the plateau, suggesting that the proposed mechanism for West Antarctic warming may also impact upon the Ross Ice Shelf region, although the signal may be complicated and weaker due to the distances involved and multiple influences on the ice shelf.

In section 2.8 we show examples of READER database trends (fig. 2.7), in which warming signatures of McMurdo Station are noticeably higher than those of Scott Base. The reason for this disparity is unknown. This is particularly important given the surroundings of the stations, as the historic lack of data in the region means that the stations represent the entirety of the *in situ* climate record in the region before the introduction of reliable AWS units in the mid-1980s (Lazzara et al., 2012). Scott Base records have been employed in the continental reconstructions of several studies (Monaghan et al., 2008; Steig et al., 2009; O'Donnell et al., 2011). As such, it is naturally important to fully understand the nature of the trends in the observational record and ascertain how well they might represent the wider area.

Due to the location of Ross Island at the tail end of the RAS, before being able to understand the temperature trends at these bases, it is first necessary to understand the impact of synoptic conditions upon the smaller region. While past studies of the climate, in particular the wind dynamics, of the Ross Island region have aided the understanding of the area, research has tended to focus on mean conditions over long periods (Sinclair, 1982, 1988), isolated case studies or short period model output (Bromwich, 1988; O'Connor and Bromwich, 1988; Seefeldt et al., 2003), or individual field seasons (Liu and Bromwich, 1993). A climatology of the region was performed by Monaghan et al. (2005) using one year of the finest grid resolution AMPS output (June 2002 to May 2003). The study focused on annual and seasonal mean depictions of the wind field, pressure, temperature and cloud fraction of the McMurdo Sound area, as described by AMPS. However, the time period of the study was rather short, and the onus on prevailing conditions.

The development of the clustering algorithm of chapter 3 affords us the opportunity to apply established results to the topographically detailed area of Ross Island. The ERA Interim reanalysis employed in chapter 3 is considered too coarse a resource to adequately depict the climate and wind flows of the area (see section 3.2). As such, we employ weather stations from a variety of Antarctic research programmes to represent cluster conditions around Ross Island. By necessity, this limits the time duration of the record compared to that of chapter 3, as reliable weather stations were only introduced into the region beginning in the mid-1980s. However, the cluster analysis and subsequent grouping of records based on the synoptic conditions allows us to study the effects of synoptic forcing upon the Ross Island region over a longer time period than has been attempted before. In this chapter, we then apply this knowledge further to better understand the observed trends at Scott Base and McMurdo Station and how they relate to changes in synoptic circulation in the wider region.

As mentioned previously, the AWS record available for Antarctica is not adequate to investigate long-term climatic variability, due to gaps and inconsistencies in data. Investigation of the mesoscale meteorology of the continent has also suffered, due to the large spatial gaps between AWS locations. This problem is rather apparent during investigations of the local climate of Ross Island detailed in chapter 3, where complex topography produces intricate surface flows which are not well-captured by reanalyses (see section 3.2.3) or pre-existing AWS units.

While improvements have been made in the AWS network distribution (Lazzara et al., 2012), Antarctic AWS are still relatively thinly spread, particularly in the continental interior. Furthermore, as a result of the extreme weather of the continent and the difficulties and cost in transport and logistics, it is inevitable that AWS systems occasionally fail, leading to gaps in an already sparse dataset. Quality control can become problematic with particularly remote stations, as there exist no reference data to compare suspect records. Research into localized effects has also suffered because of the sparse nature of AWS sites and coarseness of model grids, particularly in the complex coastal margins.

Thus, the problems with current AWS design and spread are twofold: firstly, there is a lack of redundancy within the AWS network, secondly, small-scale meteorological and climate effects are ill-understood, due to a paucity of data at kilometre scales.

Over the summer Antarctic field season of 2011/12, a team from the University of Canterbury carried out tests of a novel meteorological monitoring system called SNOW-WEB, which is reported on in chapter 6.

The SNOW-WEB system consists of a network of simple, cost-effective weather stations that can be deployed efficiently in snow- and ice-covered conditions. The system is equipped with GPS technology for accurate positioning and time-keeping, and the potential for measuring ice shelf movement. Individual stations carry onboard wireless transceivers, enabling them to transfer data in real time and be controlled remotely from manned bases in the region or via an internet interface. The system adds redundancy to data collection as a large number of stations can be deployed in a small area, ensuring data collection continues if one or more stations were to fail due to high wind events or other malfunctions. SNOW-WEB provides a large volume of spatially detailed data over the deployment area that would not be captured by a single AWS.

The distributed nature of the SNOW-WEB system can aid with the validation of gridded datasets, which is important in Antarctica due to the sparsity of *in situ* data meaning that model output is often difficult to verify. The lack of data is particularly acute above the surface, and results in meteorological studies tending to be heavily dependent on model output as a source of information on which to perform

analyses.

A particularly well-used source is output from the AMPS (Powers et al., 2003, 2012), which has been used extensively in the study of meteorology of the continent and is most often used in conjunction with observational records to lend credence to the model output. The original AMPS forecast model was based on the polar MM5 (fifth generation Pennsylvania State University - National Center for Atmospheric Research Mesoscale Model) (Bromwich et al., 2001; Cassano et al., 2001). Two particularly salient examples of its use in research are given by Monaghan et al. (2005) and Steinhoff et al. (2008), who used the highest resolution AMPS grid, which is centred on Ross Island, to produce a climatology of the area and investigate a single strong wind event, respectively.

The current generation of AMPS is based on the polar-modified Weather Research and Forecasting (polar-WRF) Model and has a high resolution grid (1.66 km) centred on Ross Island to aid in the numerical prediction of strong winds, specifically for aircraft logistical purposes.

Powers (2007) used AMPS output based on the polar-WRF to investigate a cyclonic disturbance on the ice shelf and to assess its representation in the model output, while Nigro et al. (2012b) used AMPS output to investigate knob-flows at the south of the Ross Ice Shelf. Other studies that have used syntheses of polar-WRF and AWS data sources include, Zawar-Reza et al. (2010), who studied surface flows on the Darwin-Hatherton Glacier, and Tastula and Vihma (2011), who performed validation experiments for the winter of 1998, with a comparison against the standard WRF model. An in-depth validation of the polar-WRF model via its use in AMPS was provided by (Nigro et al., 2011) using a self-organising mapping technique. Further, Bromwich et al. (2013) performed a continent-wide assessment of the model and highlighted the importance of boundary condition forcing. These reports, and the assessment of the polar-WRF by studies which have employed its output, have shown that in general the model is a reliable data source.

In the final section of chapter 6 we test output of the AMPS forecast model against the data collected during the SNOW-WEB deployment, in order to ascertain if the highest resolution AMPS grid adequately captures the local scale modulation of the synoptic scale forcing discussed in chapters 3 and 5.

In an analysis of the original generation of AMPS, Bromwich et al. (2005) reported that a large increase in the accuracy of model output in the Ross Island region was observed when the spacing of the nested grid covering the region was decreased from 10 km to 3.3 km. Further, in the assessment of the polar-WRF version of AMPS, Powers (2007) notes a similar increase in the accurate prediction of strong winds using a higher resolution grid. As described previously, flow direction in the area is dominated by local topography, and as such, improving the parametrisation of the landscape was seen to enhance the model description of the surface winds.

These results, and those from the final section of chapter 6 inform the final chapter of this thesis, in which we compare two runs of the polar-WRF model to Antarctic AWS and SNOW-WEB records, in order to ascertain if an increase in the resolution of the grid around Ross Island is able to improve the model representation of that region. We test two versions of the same model and vary only grid specification and time steps, over a 59 hour period beginning at 15:00 (UTC) 20 December 2011, and ending at 01:00 (UTC) 23 December 2011.

During this period the Ross Ice Shelf is subject to synoptic developments that impact heavily upon the conditions at Ross Island and cause a large amount of variability in a relatively short time frame. As such, the events studied capture a range of conditions at Ross Island, due to both synoptic and localised forcing, and hence highlight the importance of interplay between the two. It is during the time period

studied that the strongest winds of the summer of 2011/12 were recorded at the Scott Base AWS. To be able to accurately predict these conditions is especially important for summer logistics, when the frequency of air traffic to and from Ross Island is at its peak.

The first chapter of this thesis consists of a literature review, which details the state of knowledge of the Antarctic atmosphere. This chapter also serves to introduce concepts that will be drawn upon throughout the rest of the thesis. We discuss well-known meteorological features of the continent, with an emphasis on the region surrounding the Ross Ice Shelf, due to its salience to the remainder of the studies. We also discuss climatic influences on the continent such as the Southern Annular Mode and El Niño-Southern Oscillation, and we finish the chapter with a synopsis of continental surface temperature trends.

Chapter 2

The meteorology and climate of Antarctica and environs

The high latitude position of the Antarctic continent ensures that it is cold on a global scale. During winter the continent is subject to a complete lack of sunlight, while in the summer, weak insolation is strongly reflected by the high albedo ice surface (Grenfell et al., 1994; Wendler et al., 2004). The Antarctic ice mass resembles a high dome, centred slightly off the pole, and is almost zonally symmetric. As a consequence of the lack of high topography in the region surrounding the cold continent, a band of circumpolar westerly winds propagates unimpeded in an annulus around the Southern Ocean. This is in contrast to equivalent latitudes in the Northern Hemisphere. These winds are generated by the pressure gradient induced by the thermal contrast between polar and sub-tropical regions, and effectively isolate the surface of the continent from intrusions of warm air from lower latitudes. The steep slopes of the coastal margins of the continent further restrict the movement of warm air and moisture into the continental interior. The combination of these conditions ensure that Antarctica is the coldest continent on Earth. This chapter provides an overview of the meteorology and climate of the continent and a review of the atmospheric research that has been performed concerning the region.

Radiative heat loss at the surface of the Antarctic ice sheets often generates strong inversion conditions, in which the lower atmosphere warms with height (Phillpot and Zillman, 1970; Connolley, 1996). A host of dynamics, which are capable of generating intensely strong, and in some areas, persistent winds, are associated with these stably stratified conditions in the thin layer above the surface. Static stability conditions are discussed further in section 2.1. We discuss the surface wind field of the ice sheets and surrounding permanent ice shelves in some detail in sections 2.2 and 2.3, focusing in particular on areas and dynamics that are relevant for the remainder of the thesis.

The topography and surface wind field of the continent has further been shown to aid in the generation of the thermally direct meridional polar cell, which transports air north in the lower layers of the troposphere and south in the upper (James, 1989; Parish, 1992). The hemispheric impacts of the cell are known to be large, and the instability that the circulation produces in the circumpolar trough, a band of low pressure that circles Antarctica around the 60 °S parallel, is responsible for a highly cyclogenetic area that has a deep impact on the coastal margins of the continent. We discuss the large scale motion of the region and associated synoptic cyclone formation in section 2.4. A further result of this motion, and the phase difference in seasonal temperature changes between low and high latitudes, is the Semi-Annual

Figure 2.1: Map of Antarctica with major features and selected research stations labelled. Reproduced from Turner et al. (2004).

Oscillation, which we discuss in section 2.5.

The Antarctic atmosphere is subject to many oscillations on interannual and interdecadal time scales. For the purposes of this thesis, we will focus on describing two modes of internal variability, which have been shown to have large impacts on the surface climate of the continent, and have been implicated in the forcing of temperature trends in some areas. We will focus on the Southern Annular Mode (section 2.6); a see-saw of pressure anomalies between high and mid-latitudes; and the El Niño-Southern Oscillation (section 2.7); a tropically forced ocean/atmosphere coupled mode, that impinges on the Antarctic climate through an atmospheric teleconnection.

Finally, much emphasis has been placed on the characterization of Antarctic temperature trends in recent years. This has proved difficult on the continent due to a lack of historical observations. The details of patterns of changing temperature are only just emerging and portray a complex interplay between circulatory forcing mechanisms. Trends over the continent are covered in section 2.8.

For reference, a map of Antarctica with major regions indicated is shown in figure 2.1.

2.1 Static stability

The high degree of radiative heat loss at the surface layer of the Antarctic atmosphere causes the lower levels to often exist in inversion conditions: cold air at the surface of the ice sheets is denser and hence negatively buoyant relative to the air above it, which is warmer. The temperate inversion is often

described in terms of the gradient of potential temperature in the vertical coordinate, z. Potential temperature, $\theta = T(p_0/p)^\kappa$, describes the temperature of an air parcel at pressure p and temperature T, if that parcel was compressed or expanded adiabatically to a pressure of p_0, usually defined as 1000 hPa. κ is the ratio of the gas constant of dry air R_d to the specific heat at constant pressure c_p. The potential temperature is a useful quantity for examining atmospheric dynamics, firstly, as it is conserved in dry adiabatic processes, and secondly, because its vertical structure describes the static stability of the dry atmosphere. Following the description of Holton (1992), if the potential temperature is a function of height, then the atmospheric lapse rate ($\Gamma \equiv -\partial T/\partial z$) will differ from the dry adiabatic lapse (Γ_d) rate by:

$$\frac{T}{\theta}\frac{\partial \theta}{\partial z} = \Gamma_d - \Gamma \tag{2.1}$$

If $\Gamma < \Gamma_d$, such that the temperature decreases less quickly with height than the adiabatic lapse rate, then $\partial\theta/\partial z > 0$. Under these conditions, an air parcel displaced adiabatically upwards will undergo changes which mean it will be denser than the air around it and so falls back towards its equilibrium position. A parcel displaced adiabatically downwards is less dense than the air surrounding it and so rises. This situation is thus deemed to be statically stable. Conversely, if under $\partial\theta/\partial z < 0$ conditions a parcel of air is displaced upwards, it will be less dense than the air surrounding it, and therefore will continue to rise. Of course, this situation is unstable.

Under stable conditions, a displaced parcel of air is subject to a restoring force, and *buoyancy oscillations* can occur, which are described by the equation:

$$\frac{D}{Dt}\delta z = -N^2 \delta z \tag{2.2}$$

where D/Dt is the derivative with respect to time, following the motion of the parcel and δz is the vertical distance away from the equilibrium position. N is the Brunt-Väisälä frequency, where:

$$N^2 = g\frac{d\ln\theta}{dz} \tag{2.3}$$

The general solution to equation (2.2), is $\delta z = A\exp iNt$, where A is a constant. Thus, if $N^2 > 0$, oscillatory motion results. If $N^2 = 0$, then no restoring force exists, and oscillatory motion does not occur. If $N^2 < 0$, then the solution tends to increase exponentially, which reflects the instability described previously. The static stability conditions for dry air can then be summarised as:

$$\frac{\partial\theta}{\partial z} > 0 \qquad \text{statically stable} \tag{2.4}$$

$$\frac{\partial\theta}{\partial z} = 0 \qquad \text{statically neutral/adiabatic} \tag{2.5}$$

$$\frac{\partial\theta}{\partial z} < 0 \qquad \text{statically unstable} \tag{2.6}$$

In Antarctica, the surface air is often colder than the air above it. This results in exceptionally stable conditions in the surface layer, as $\partial\theta/\partial z$ is large, and thus a parcel displaced upwards will be negatively buoyant compared to the air around it. This stability has significant consequences for the surface meteorology of Antarctica for two reasons: firstly, the combination of the stable conditions and

sloping topography generates the large-scale katabatic winds that cover the surface of the continent, which are detailed in section 2.2. Secondly, the high static stability dictates that air often flows around rather than over topography, which constrains wind flows to topographic conditions and causes barrier flow effects, which are discussed in section 2.3, and fast-flowing convergence zones in the Antarctic hinterland. The degree of topographic constraint is described mathematically by the Froude number, a dimensionless measure that describes the ability of stratified air to flow over an object. The number is effectively a ratio of the kinetic energy of a parcel of air at the surface to the energy that the same parcel requires to overcome atmospheric stratification. Using the notation of Lynch and Cassano (2006), it is given by:

$$Fr = \frac{V}{\sqrt{gH\Delta\theta/\theta}} \quad , \tag{2.7}$$

where V is the component of the velocity that acts perpendicularly to the barrier of height H. $\Delta\theta$ is the potential temperature difference between the surface and the top of the barrier, and θ is the potential temperature of the parcel. In the case that Fr is greater than one the parcel is able to pass over the barrier, whereas if it is less than one the parcel is blocked. The latter condition is favoured if the air is statically stable, if the barrier is high, or if V is small, either due to a low wind speed or barrier-parallel flow. Above the surface, air will be blocked up to the critical dividing streamline height, and above this be able to pass over the barrier. A schematic representation of varying Froude numbers is provided by Stull (1988) (pg. 602). In Antarctica, despite strong wind speeds, the high stability of the cold surface air and the existence of high barriers dictate that Fr is rarely more than 1, which impacts heavily upon flows, especially in coastal zones.

2.2 Katabatic winds

Katabatic (from the Ancient Greek meaning *descending*) winds at the surface of the continent are gravity driven, down-slope flows that occur widely in Antarctica due to the negative buoyancy of the surface atmosphere. Winds of this type are almost ubiquitous over the ice slopes in the winter. In the summertime, weak insolation can warm the surface and hence weaken the inversion, resulting in positive lapse conditions (Phillpot and Zillman, 1970). The diurnal aspect of the heating also introduces a summertime diurnal cycle into the incidence and strength of katabatic winds (Zhou et al., 2009) that is absent in the winter.

Ball (1960) described a simple two-layer mathematical treatment of katabatic forcing. The lower layer is presumed to be colder than the upper, which represents a simplistic approximation to inversion conditions. The treatment is discussed at length by Lynch and Cassano (2006). We show their schematic of the simplified inversion layer structure in figure 2.2. Using their notation, and defining the x-axis to be along the slope and the y-axis to be across the slope, the dynamics are described by:

$$0 = -\frac{1}{\rho}\frac{\partial p}{\partial x}\bigg|_{top} - g\frac{\Delta\theta}{\bar{\theta}}\frac{\partial z}{\partial x} + fv - C_D V u, \tag{2.8}$$

$$0 = -\frac{1}{\rho}\frac{\partial p}{\partial y}\bigg|_{top} - fu - C_D V v. \tag{2.9}$$

Equation (2.8) represents the slope-parallel wind component. The first term on the right hand side

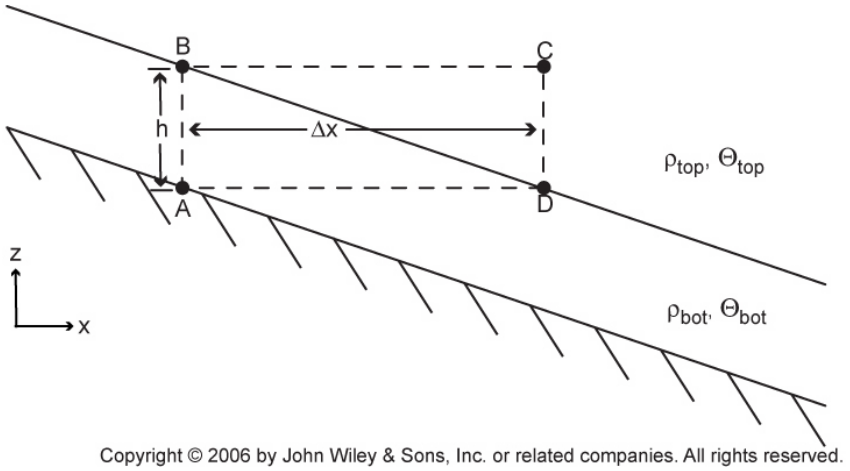

Figure 2.2: Vertical cross-section through the two-layer atmosphere used to represent katabatic winds. h is the depth of the inversion layer, $h/\Delta x$ is the slope of the ice sheet surface, ρ is the density, and Θ is the potential temperature. The subscripts *bot* and *top* refer to the bottom and top layers respectively. Figure and label reproduced from Lynch and Cassano (2006).

describes the force generated by the synoptic pressure (p) gradient, this is assumed to be confined to the layer above the inversion, hence *top*. ρ is the density of air. The second term on the right hand side describes the force due to the temperature inversion. g is the acceleration due to gravity, and z the height of the ice terrain. $\bar{\theta}$ is the mean potential temperature of the two layers. $\Delta\theta$ is the strength of the temperature inversion, and hence gives an indication of the static stability of the two-layer model. For a stably stratified atmosphere this term dictates a force directed down-slope. If there is no slope or no temperature inversion then the term goes to zero. The third term is the Coriolis force; $f = 2\Omega \sin\phi$ is the Coriolis parameter, where Ω is the angular frequency of the Earth's rotation and ϕ is the latitude. This term is thus negative in the Southern Hemisphere. v is the cross-slope wind speed. The final term is a quadratic representation of friction; C_D is a constant, V the scalar wind speed, u the down-slope wind component. Equation (2.9) has almost the same structure, except it lacks the second term of equation (2.8), as the y-axis is defined to be perpendicular to the terrain slope. Any change in the height of the inversion layer is assumed to be small relative to the horizontal distance scale. Thus, the katabatic force is dependent on the ratio of potential temperature difference between the two layers to the potential temperature of the lower layer, gravity, and the gradient of the slope. Other forces involved are the synoptic pressure gradient, which is assumed to be small compared to the katabatic force term, Coriolis, and friction. The katabatic force is directed along the fall-line, while the Coriolis force acts to turn flows to the left in the Southern Hemisphere. The resulting katabatic flows (in a steady-state scenario) are thus directed slightly to the left of the fall line, as an equilibrium between katabatic, Coriolis and frictional forcing. In reality, the strongest katabatic winds are observed tens of metres above the surface, due to the reduction in the frictional force with altitude (Seefeldt and Cassano, 2008).

The simple model of Ball (1960) was used by Parish (1982) and Parish and Bromwich (1987) to model the surface air-flow of East Antarctica and the continent as a whole, respectively. Further, and increasingly complicated, continental-scale modelling experiments were performed by Parish and Waight (1987), Parish and Bromwich (1991), Hines et al. (1995), van Lipzig et al. (2004) and Parish and Bromwich (2007). Results are generally similar and depict a continent-wide wind regime in which cold, negatively buoyant air from the plateau effectively 'falls' towards sea-level at an angle slightly to the

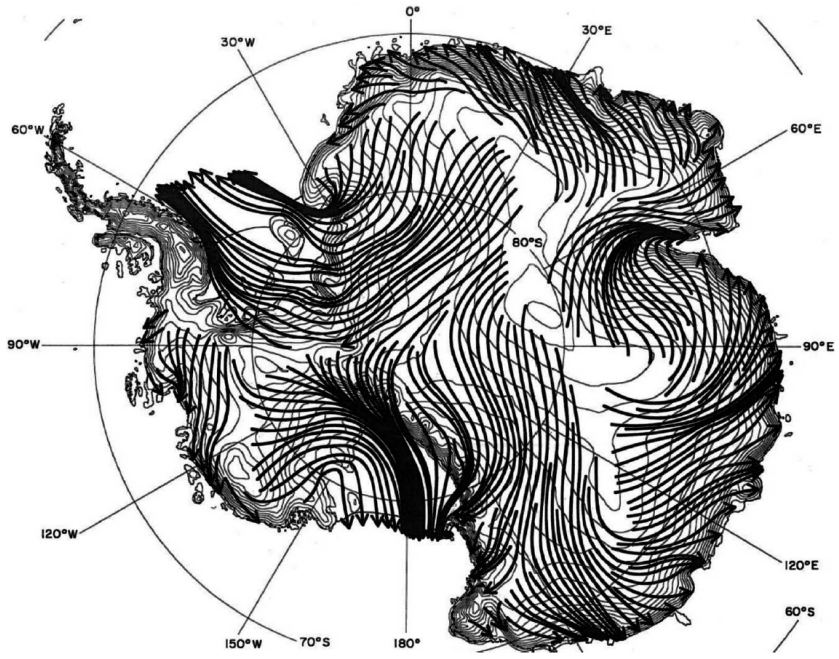

Figure 2.3: Mean streamlines at $\sigma = 0.9983$ over Antarctica from the June 2003 to May 2004 AMPS archive. Figure and label reproduced from Parish and Bromwich (2007).

left of the topographic fall line. To illustrate, we show the near-surface wind streamlines from AMPS archive, as reported by Parish and Bromwich (2007) in figure 2.3. The importance of the topography cannot be understated in the dynamics of the region. That the strength of the flow is dependent on the topographic gradient dictates that the wind speed over the highest parts of the Antarctic Plateau is weak and the direction variable, while towards the coast, as the gradient increases, the flow becomes much stronger and more unidirectional. The pattern has been confirmed by numerous observational and modelling studies (Wendler and Kodama, 1984; Renfrew, 2004; King et al., 2006; Zhou et al., 2009). Regions of confluence around the continent also serve to enhance the speed and determine the direction of the flow. The high static stability of near-surface air dictates that it flows around, rather than over, topographic barriers, as identified in section 2.1, and thus strong flows are observed in regions where the topography acts to channel air into narrow corridors. This is apparent in figure 2.3. These channels are more common around the edges of the continent where the topography is also generally the steepest. Confluence zones are a prominent feature of continental flow maps, and have been widely examined in observational studies over coastal regions of the continent, including glaciers in the Transantarctic Mountains at the western and southern margin of the Ross Ice Shelf (Bromwich, 1992; Bromwich et al., 1992; Breckenridge et al., 1993; Zawar-Reza et al., 2010), Terra Nova Bay (Bromwich, 1989a,b; Marshall and Turner, 1997; Cogliani et al., 1996; Knuth and Cassano, 2011), the Siple Coast (Bromwich and Liu, 1996; Liu and Bromwich, 1997), Adelie Land (Loewe, 1972; Parish et al., 1993; Pettre et al., 1993), Coats Land (Renfrew and Anderson, 2002; Renfrew, 2004; Renfrew and Anderson, 2006), Mawson (Dare and Budd, 2001), and East Antarctica (Allison et al., 1993; Zhou et al., 2009). A review of katabatic signatures for many research stations in East Antarctica was given by Mather and Miller (1966).

What are now known to be confluence zones, particularly those at Cape Denison and Port Martin in Adelie Land, posed a difficult problem for early meteorologists. In their vicinity, winds were recorded to be hurricane force for days on end (Loewe, 1972), which was not predicted by katabatic forcing, in which

wind speeds are only high whilst a pool of cold, negatively buoyant air exists upstream. It was only after adequate topographic mapping of the continent had been accomplished that it became understood that the channelling action of topography meant that these locations have an almost inexhaustible cold pool over the expanse of the plateau. The descending air is funnelled into a smaller cross-section at the coast and hence results in strong and persistent winds (Parish, 1982; Parish and Bromwich, 1987).

While katabatic flow is heavily influenced by the surface temperature field of the Antarctic ice sheets, one of the most important aspects of the flow is its ability to force changes in the temperature. Satellite-borne thermal infrared imagery shows dark signatures of air descending through glaciers in the Transantarctic Mountains (eg. Kurtz and Bromwich (1983); Bromwich (1989b); Breckenridge et al. (1993)). These signatures were interpreted as being due to a combination of blowing snow within the near-surface jet and the turbulent downward vertical advection of warmer air from above the surface inversion (Bromwich, 1989b). The warming mechanism proceeds as follows: air descending from the high plateau is adiabatically compressed as it falls towards sea-level and hence warms. The katabatic jet is fastest flowing just above the surface due to the reduced effects of friction away from the ice sheet, while air on the ice sheets is subject to a strong temperature inversion. The fast moving katabatic jet causes turbulence within the surface layer, and thus the warmer air aloft is transported to the surface, disrupting the inversion layer in the vicinity of the jet. Hence, katabatic flows appear to be warmer than the air around them. In fact, it is only surface air in the vicinity of the jet that is warmer than the surroundings; the average temperature in the jet column is still likely to be colder than the surroundings, due to its high-altitude and cold origins (Bromwich, 1989b). Other katabatic flows have been shown to cool their destinations due to the advection of cool air (van As and van Den Broeke, 2007). Vihma et al. (2011) investigated the thermal effects of katabatic winds using a two-dimensional numerical model under clear-sky, mid-winter conditions. They found that the thermal response of the atmosphere at the foot of the ice sheet to katabatic drainage was subject to variability depending on the height and gradient of the slope. Larger and steeper slopes result in increased surface warming as stronger winds are able to form, introducing more turbulence. Adiabatic warming is also greater when the flow has fallen through a larger distance. Results of Vihma et al. (2011) were supported by available observations. They further found that persistent drainage causes a cold pool of air to form over coastal sea ice, which subsequently generates a thermal wind in opposition to the katabatic flow if it is not removed under the influence of a synoptic pressure gradient. This pooling effect can cause a phenomenon known as a hydraulic jump (Lamb, 1952), in which a relatively fast mass of moving air meets a stationary or slow moving mass, and can cause anomalously calm conditions in coastal areas. Hydraulic (or katabatic) jumps have also been investigated by Pettre and Andre (1991) and Yu et al. (2005). A further relevant example is given by Steinhoff et al. (2008), in which a hydraulic jump is caused by a strong flow on the Ross Ice Shelf encountering a high-pressure stagnation zone in the vicinity of Ross Island.

The large amount of literature notwithstanding, there is still some ambiguity in the forcing mechanism that generates winds that are often described as katabatic. Many *katabatic* flows, especially around the coast, have been observed to be reinforced by synoptic conditions (eg. Marshall and Turner (1997); Turner et al. (2009a)), raising questions about their dominant forcing mechanism. Parish and Cassano (2001) and Parish and Cassano (2003b) noted that the directional constancy of winds over the Antarctic ice slopes shows little seasonal variation, and are often strong in summer despite there being a much reduced level of katabatic forcing at this time. Parish and Cassano (2003b) performed numerical simulations of the flow over the ice sheets, both with and without explicit long-wave radiation specification. The latter conditions were used as an example where katabatic forcing is unable to occur and hence the

wind is almost entirely dependent on the synoptic pressure gradient. Very similar surface wind fields were established under both conditions; synoptic pressure gradients were modified by the underlying terrain, and thus produced a wind-field that is similar to that of the katabatic example, highlighting the confining influence of the Antarctic topography on the surface wind field. The authors warn against describing a wind as katabatic simply due to its persistence, directional constancy, and the fact that it blows down-slope. In order to entirely understand the forcing nature of the wind, the separate terms of the dynamical equations must be examined to identify the relative magnitudes of forcing terms. This process requires upper level information on the boundary layer temperature inversion that is often not available. However, using numerical models, this type of analysis has been performed by Parish and Cassano (2003a) and van den Broeke and van Lipzig (2003) at a continental scale. The reports agreed that both types of forcing were important but disagreed about their relative influence in different regions. For instance, Parish and Cassano (2003a) conclude that synoptic forcing is most important over the steep coastal slopes, while katabatic forcing dominates in the interior. van den Broeke and van Lipzig (2003) state that synoptic control dominates in the interior due to the relatively gentle slopes. In the steep hinterland katabatic forcing appeared to be the dominant mechanism. Both studies focused on the mid-winter month of July, although the analysis of Parish and Cassano (2003a) was drawn only from one year, while that of van den Broeke and van Lipzig (2003) used a fourteen year model integration. Despite some disparity in results, the two reports both identify that labelling a wind *katabatic* simply because it flows downhill is likely to be inaccurate. Seefeldt and Cassano (2012) investigated wind conditions over the Ross Ice Shelf and environs. Their analysis of the vertical structure of the potential temperature and wind indicated that regions upwind of the Transantarctic Mountain glaciers showed large temperature inversions and were dominated by katabatic forcing. Conversely, in West Antarctica temperature inversions were less pronounced and the area was more prone to synoptic forcing. The distinction is made in part by the greater influence of maritime intrusions onto West Antarctica, due to its relatively low and gentle slope compared to East Antarctica, allowing synoptic cyclones in the Southern Ocean to penetrate farther south (Liu and Bromwich, 1997; Nicolas and Bromwich, 2011a). In the high-elevation areas of the East Antarctic plateau, katabatic forcing is the dominant mechanism, due to the inability of the synoptic influence to penetrate past the steep coastal margins. This results in the boundary layer of East Antarctica being colder and more stable, and thus more capable of katabatic forcing.

2.3 Barrier winds: the Ross Ice Shelf and Ross Island

A second wind dynamic that is prevalent in the coastal regions of Antarctica is that of the barrier wind (Schwerdtfeger, 1984). In areas in which strong lower-level flows encounter high topography it is unlikely that the air will have the energy to surpass the barrier, due to the highly stable nature of the Antarctic boundary layer, as discussed in section 2.1. If the flow towards the barrier is persistent, this can lead to the damming of cold air against the barrier, increasing the height of the inversion layer and producing a pressure gradient that is directed perpendicularly outwards from the barrier. Over time, the pressure gradient force forms an equilibrium with the Coriolis force, if at a large enough scale, resulting in a geostrophic wind flow parallel to the barrier.

In Antarctica, barrier flows have been observed in several regions (Schwerdtfeger, 1984), including the Antarctic Peninsula. The area that has appeared to attract the most attention, however is the Ross Ice Shelf, which is subject to a large and frequent example of the phenomenon. This is of primary

importance, as much of the work contained within this thesis is associated with this vicinity. The regime is produced by synoptic scale or mesoscale cyclonic forcing over the Ross Ice Shelf, when an easterly flow impinges on the high barrier of the Transantarctic Mountains at the western margin of the shelf. In this region the Transantarctic Mountains have an average altitude of approximately 2000 m, and rise steeply from the flat ice shelf to the east. Airflow from the east is dammed against the mountains, resulting in a strong southerly flow. Examples of the incidence of such conditions are given by O'Connor et al. (1994) for the impacts of both synoptic and mesoscale cyclones. Further observational studies (Stearns and Wendler, 1988; Seefeldt et al., 2007) have confirmed the existence of such flows using data from the American Antarctic Program's (USAP) automatic weather station (AWS) project (Lazzara et al., 2012). However, due to the lack of available high-resolution observations, particularly above the surface, in recent years researchers have turned to the operational forecasts of AMPS (Powers et al., 2003), which have been shown to be particularly reliable (Bromwich et al., 2003, 2005; Powers, 2007; Nigro et al., 2011, 2012a), to better resolve the dynamics of the situation. A particularly strong and destructive incident was described by Steinhoff et al. (2008), in which a combination of conditions produced wind speeds so high that the anemometer at McMurdo Station, Ross Island, was blown away. Nigro et al. (2012b) examined the dynamics of barrier winds and associated knob-jets on the extruding Prince Olav Mountains of the Dufek Coast at the south of the Ross Ice Shelf. Both of these studies highlight the fact that surface observations are not sufficient to fully analyse barrier regimes, as quite often the pressure gradient which generates such regimes is not manifest at the surface, but a few hundred metres above it.

The combination of cyclonic forcing of the barrier wind regime, and katabatic outflow from glaciers in the Transantarctic Mountains and the Siple Coast produces a wind regime over the ice shelf that has come to be known as the Ross Ice Shelf Air Stream (RAS) (Parish et al., 2006). RAS was first investigated with the use of satellite-borne thermal infrared cameras, as the stream displays the characteristic surface warming signature of strong Antarctic flows described previously (Bromwich et al., 1992, 1993; Carrasco and Bromwich, 1993b; Bromwich et al., 1994). A stream of warm, fast moving air was observed crossing the Ross Ice Shelf from the Siple Coast in the south-east, traversing parallel to the barrier of the Transantarctic Mountains, and turning to the north. Initially, these flows were called *katabatic*, despite the forcing clearly not being gravity driven (the Ross Ice Shelf is essentially flat). Surges were associated with synoptic scale cyclones located at the north-east margin of the shelf, over Marie Byrd Land. The RAS was investigated by Parish et al. (2006) using archived AMPS output of the one year period of November 2001 - October 2002. They found that a combination of synoptic, barrier, and katabatic dynamics forced the phenomenon and that there were three wind maxima in the area: in the vicinity of the Dufek coast, later studied by Nigro et al. (2012b); to the south of Cape Adare, also modelled by Buzzi et al. (1997); and at the tip of Minna Bluff. Peaks over the ice shelf were considered to be part of the RAS effect, but the definition of RAS dictates that an uninterrupted low-level jet must propagate from the Siple Coast along the Transantarctic Mountains for the phenomenon to be said to occur. They discussed the generation of the surface jet by a combination of katabatic and synoptic forcing, and a large barrier flow component. The air stream was further investigated by Seefeldt and Cassano (2008) using five years of AMPS output, the longest period then available of consistent grid-sizes. They performed a synoptic classification using a self-organising maps (SOM) technique applied to column-averaged wind speeds to capture the behaviour of low-level jets. They found that the most prominent jets were those from glaciers in the Transantarctic Mountains, that drain air from the East Antarctic Plateau. However, also present was the RAS, which they defined as the linking of several, sometimes separate, jets along the Transantarctic Mountains. Synoptic forcing was deemed to be necessary for the generation of the effect. Steinhoff et al. (2009) studied a single RAS event using AWS data, satellite imagery and AMPS output.

They focused on the moist processes involved, and reported that the RAS phenomenon was likely to cause cloud signatures over the ice shelf due to moisture advection from West Antarctica. They suggested that cloud signatures following the flow may have been mistaken for warm surface signatures in thermal infrared images in the past (c.f Bromwich et al. (1992),Carrasco and Bromwich (1993b)). Very recently, Seefeldt and Cassano (2012) studied the RAS with AMPS output and the SOM technique. They focused on winds at the 13 m and 150 m levels, and found that the effect was best represented at the higher level due to the reduction in frictional effects. They reported that, while the stream appears to be present throughout the year, is it most prevalent in the winter months. This is clearly to do with its dynamic origins. Firstly, RAS is associated with synoptic cyclone activity in Marie Byrd Land, which occurs most commonly outside of the summer. Secondly, the katabatic and barrier dynamics are dependent on the existence of stably stratified air and a temperature inversion over the ice shelf. These conditions are more often satisfied in the winter.

A notable second barrier wind regime occurs in the vicinity of Ross Island, which is a relatively small protrusion from the Ross Ice Shelf and situated at the north-west margin of the permanent ice. Ross Island may be a minor feature compared to the Antarctic ice sheets and Transantarctic Mountains, but its high and steep mountains, Erebus (3,794 m) and Terror (3,230 m), named for the exploration ships of James Clark Ross, rise dramatically from the ice shelf and constitute a considerable barrier. The Hut Point Peninsula, a low ($\sim 200\ m$) feature compared to Mounts Erebus and Terror, protrudes from the south-west side of the island. To the south are located White and Black Islands, and Minna Bluff, a high barrier which effectively shelters the region to the south of Ross Island from southerly winds (Holmes et al., 2000). The island is situated downstream of glaciers in the Transantarctic Mountains prone to katabatic drainage and the Ross Ice Shelf barrier flow and hence is often subject to strong and persistent winds from the south (Monaghan et al., 2005). Hence, a dynamically similar situation to that of the Transantarctic Mountains is observed. Early explorers noted wind directions taken from instruments and inferred from sastrugi, and correctly interpreted that the prevailing south wind was dammed by the island's topography (Simpson, 1919), producing an anomalously calm stagnation zone in the deep bay on the south side of the island known as Windless Bight. The pressure gradient force generated by the damming, directed outwards from the bight, causes the wind to split around the island, while the north-easterly prevailing wind at Scott Base, at the tip of the Hut Point Peninsula, similarly results from the turning of the wind by the barrier (Sinclair, 1988). The pressure distribution from automatic weather stations was interpolated by Slotten and Stearns (1987), who conjectured that a barrier regime existed in the area following the suggestion of Schwerdtfeger (1984). Bromwich (1988) described the phenomenon using satellite thermal infrared imagery and surface observations. O'Connor and Bromwich (1988) used weather station data, synoptic charts, and soundings from the McMurdo Station radiosonde to investigate the dynamics of the effect. Strong southerlies at Scott Base were observed only when synoptic cyclones in the Ross Sea advected warm, maritime air over the area. This air is less statically stable than that over the ice sheets, and thus it is able to surmount the Hut Point Peninsula, turning the prevailing north-easterly wind to the south. Liu and Bromwich (1993) observed the region using a SODAR (SOnic Detection And Ranging) device during the 1990/91 summer season and considered the source of the south wind encountering Ross Island. They found a distinct diurnal variation in the strength of the blocking, and associated it with diurnal variation in the katabatic source of air from glaciers to the south. Seefeldt et al. (2003) performed a numerical model study on the region and described the pressure and potential temperature fields in some detail for both high and low wind speeds. They found that in the event of a strong wind, the flow is able to pass over the topography to the south of Ross Island and the Hut Point Peninsula, even if it is stably stratified, which is consistent with Sinclair (1988)'s

observation that the strongest winds observed at Scott Base are from the south. However, the height of the mountains on Ross Island meant that surface flow is invariably not strong enough to pass over them, producing stagnation on the windward side (in Windless Bight) and in the lee of the island. The year-long study of Monaghan et al. (2005) using high-resolution AMPS output showed quasi-stationary vortices in the lee of the island that are shed via the von Kármán mechanism. Of further interest are the strong winds that form at the eastern and western boundaries of the island as flow converges at the pointed capes. These winds cause polynyas to form that can last for several days in the winter (Bromwich, 1988), and instigate the breakout of ice in the vicinity early in the melt season, making open water available relatively early in the spring. As such, some of the most southern penguin rookeries can be found in these locations (O'Connor and Bromwich, 1988). By examining empirical relationships between strong wind events at the Pegasus North weather station, to the south of the Hut Point Peninsula, Holmes et al. (2000) were able to place strong wind events in the region into a wider context. The authors reported that high winds at the runway often coincided with an east-west pressure gradient across the ice shelf, an increase in the temperature difference between Pegasus North and Minna Bluff, indicating the onset of unstable conditions, and temperature increases to the south of Ross Island, indicating the onset of strong winds there.

2.4 Large-scale circulation and synoptic activity

The high inner plateau of Antarctica acts as a cold pool up to the mid-troposphere and as such, dense, sinking air is found surrounding the pole. This produces a climatologically high pressure region over the internal ice sheets and anticyclonic geostrophic circulation around the ice cap (Parish and Cassano, 2003a; Parish and Bromwich, 2007), which is observed above the lower katabatic layer. Prolonged clear sky conditions allow more radiation from the surface to escape the lower atmosphere, and so the cooling is reinforced. This mechanism is also of great importance in the generation of katabatic flows via the generation of strong temperature inversions. The large-scale katabatic drainage over the Antarctic ice sheets has a large impact on the surface climate of the sheets and surrounding ocean. This drainage is also an integral part of the large-scale motion of the Southern Hemisphere. Parish and Bromwich (2007) interpreted drainage at the surface with respect to the mass balance of the Antarctic atmosphere, and concluded that katabatically and synoptically forced flows caused a net outflow from the surface of the continent, and thus forms one leg of the *polar cell*. A large temperature gradient over the Southern Ocean caused by the cold outflow meeting warmer air from the ocean-covered lower latitudes generates the semi-permanent polar front, an intensely baroclinic zone around the 60 °S parallel. The baroclinicity of the region, with emphasis on its topographic origins, was numerically modelled and investigated by Walsh et al. (2000). Rising air in the vicinity of 60 °S produces a region of low pressure, and thus the region is known as the Antarctic circumpolar trough (ACT). The combination of baroclinic and thermal instabilities ensure that this region experiences a large degree of synoptic cyclogenesis (Simmonds and Keay, 2000; Uotila et al., 2011). To the north of the ACT lies the region of the greatest north-south pressure gradient. In this zone, a band of westerlies propagates around the continent, uninhibited by topography except for the barrier of the Antarctic Peninsula. The final leg of the polar cell occurs in the mid- and upper-troposphere, where winds are generally directed towards the pole. At these altitudes, convergence causes cyclonic motion about the pole, known as the circumpolar vortex. The meridional circulation was numerically modelled by James (1989), Parish and Bromwich (1991) and Parish (1992). Parish et al. (1994) further experimented with a numerical model in reproducing the flow.

They performed experiments with and without the Antarctic topography present, in order to determine the modification of the meridional flow by topographically induced katabatic winds. They found that the position and intensity of the ACT was inherently linked to the Antarctic terrain, and that the Semi-Annual Oscillation (see section 2.5) was reproduced effectively only when the topography was present within the model. Parish and Bromwich (1998) reported a case study of the interaction of katabatic flows with a synoptic-scale cyclone during mid-winter 1988. They found that a disrupted branch of the polar cell in the mid- and upper-troposphere was responsible for a prominent pressure decrease over the ice sheets. A thorough treatment of the Antarctic mass balance is given by Parish and Bromwich (2007) using one year of output from AMPS.

A notable exception to the predominantly zonal structure of the ACT is the climatologically low pressure region observed in the vicinity of the Amundsen and Bellingshausen Seas (ABS). This area of low pressure has been referred to under several monikers, and even occurs in the Ross Sea in some seasons (Fogt et al., 2012b; Turner et al., 2012), but we will refer to it as the ABS low throughout this thesis. Other low pressure regions are apparent to the east of the Weddell Sea and to the immediate north of Prydz Bay, generating a zonal wavenumber 3 pattern around the coast of the continent (Raphael, 2004). These regions represent deep embayments into the south and thus have much lower topography than their surroundings. The rotational tank experiments of Baines and Fraedrich (1989), using realistic Antarctic topography, confirmed that the low pressure in these areas is fundamentally caused by the interaction of the topography with the mean westerly flow. They suggested that the low pressure areas and cyclonic motion were the result of flow splitting around the Antarctic topography coupled with the conservation of potential vorticity. The Antarctic atmosphere is strongly coupled in the vertical, and thus the depressions are observed throughout the troposphere. It is notable that in the numerical modelling of Parish et al. (1994), the model failed to reproduce the low pressure regions when the Antarctic topography was not present. This was also observed in the experiments of Walsh et al. (2000); the deepening of the circumpolar trough in this region was also seen to be heavily dependent on the presence of the Antarctic topography. When the height of the topography was removed, but the land/sea contrast still retained in the model, the characteristic wavenumber 3 was no longer recognisable.

The low in the ABS region is of particular interest, as it has a prominent role in the non-annular component of the Southern Annular Mode (see section 2.6) and has often been implicated in teleconnections with the lower latitudes (see section 2.7). Connolley (1997) examined the standard deviation of the mean sea-level pressure (MSLP) in the regions surrounding Antarctica as represented by five general circulation models. He found a peak in the variability in the ABS region extending into the Ross Sea, which he dubbed as the "West Antarctic Pole of Variability". The modelling experiment of Lachlan-Cope et al. (2001), who performed analysis with realistic topography, an axisymmetric representation of the continent as a dome centred on the South Pole, and the same dome with its axis offset to the location of the highest of the East Antarctic topography, confirmed that the non-axisymmetric nature of Antarctic provides enough forcing to generate this feature. The interannual variability was further studied by Fogt et al. (2012b), who found strong links between the density and depth of synoptic cyclones in the region and the size and position of the ABS low. They further found significant trends in the low that have been implicated in warming trends in West Antarctica (see section 2.8). A second in-depth analysis was provided by Turner et al. (2012), using slightly different methodology. Both authors found a seasonal variability in the depth and strength of the system, with the low being deeper and farther to the west in the winter than in the summer. The location of the low to the east of the Ross Sea aides the southerly circulation over the sea and ice shelf to the south. Further, on the east side of the low towards the

Antarctic Peninsula, the low aides northerly flow. Cohen et al. (2013) investigated the variability in MSLP conditions in the region using a k-means clustering approach. They defined six clusters based on the position and intensity of the low, and further used the synoptic classification to study precipitation at an ice core site on Roosevelt Island. Flow across the Ross Ice Shelf was seen to be sensitive to the location of the low.

The synoptic cyclones that skirt the coast of Antarctica are of much interest to meteorologists and forecasters as they are associated with high wind speeds and thus can adversely affect ground parties and air traffic. Further, they are an essential mechanism in the transport of moisture from lower latitudes to the Antarctic ice sheets (Turner et al., 1995; Noone and Simmonds, 2002; Nicolas and Bromwich, 2011a; Bromwich et al., 2011; Nicolas and Bromwich, 2011b; Uotila et al., 2011), and thus are of primary importance for accumulation studies, the unbiased interpretation of ice core temperature proxy records (Schlosser et al., 2010; Sinclair et al., 2010; Schlosser et al., 2011; Markle et al., 2012; Sinclair et al., 2012) and the Antarctic surface mass balance (Monaghan et al., 2006). Accordingly, a large amount of research has been performed on the presence of synoptic cyclones in the seas around Antarctica, their effects on the coast and hinterland, and their occasional intrusion into the continental interior. A review of the state of knowledge of extra-tropical cyclones and their predicted changes under anthropogenic forcing is given by Ulbrich et al. (2009). The Southern Hemisphere storm track was discussed in much detail by Hoskins and Hodges (2005). Simmonds and Keay (2000) used 40 years of reanalysis data and the University of Melbourne tracking scheme to describe variability in the frequency of cyclones. They found a distinct peak in cyclone density in the circumpolar trough, but particularly in the vicinity of the Ross Sea and in the Indian Ocean sector, where katabatic drainage is particularly prevalent. They found small, but statistically significant trends in cyclone tracks, consistent with observed trends in the Southern Annular Mode (see section 2.6). Simmonds et al. (2003) produced a climatology for the satellite era using the NCEP-DOE reanalysis. They found that the Antarctic coastline was highly cyclogenetic, with some cyclosis also occurring as systems move in from lower latitudes. They found a peak in cyclone density and cyclogenesis in the Ross Sea that was larger in winter than in summer. In this region and in the Amundsen and Bellingshausen Seas a large interannual variability was observed. The largest cyclones were seen in a band surrounding the continent at about 60 °S. They further found that winter cyclones were deeper, more intense and more frequent, while those in the summer tended to have larger radii.

Strong wind events that were recorded at coastal stations were investigated by Turner et al. (2009a) using data from the READER database (Turner et al., 2004). They found that synoptic cyclones were responsible for large numbers of strong wind events and were capable of reinforcing or hindering katabatic drainage in relation to their position relative to prevalent katabatic flows. This was particularly true in East Antarctica. They also calculated trends in strong wind events, but most were small and insignificant. As mentioned previously, Steinhoff et al. (2008) investigated a strong wind event at McMurdo Station caused by the interaction of a synoptic cyclone with local topography. Uotila et al. (2011) analysed surface conditions concurrent with synoptic cyclone occurrence and reported that the majority of synoptic cyclones were formed in the baroclinic environment of the circumpolar trough. The development of boundary layer conditions lagged that of the cyclones, and thus they concluded that the large size and strength of such systems meant that they were powerful enough to affect the boundary layer conditions. A climatology of surface tracks and fluxes from reanalysis output and satellite-born scatterometer data was reported by Yuan et al. (2009).

The high and steep nature of the Antarctic topography inhibits the movement of synoptic cyclones beyond the immediate hinterland. However, under hemispheric forcing, maritime intrusions occasionally

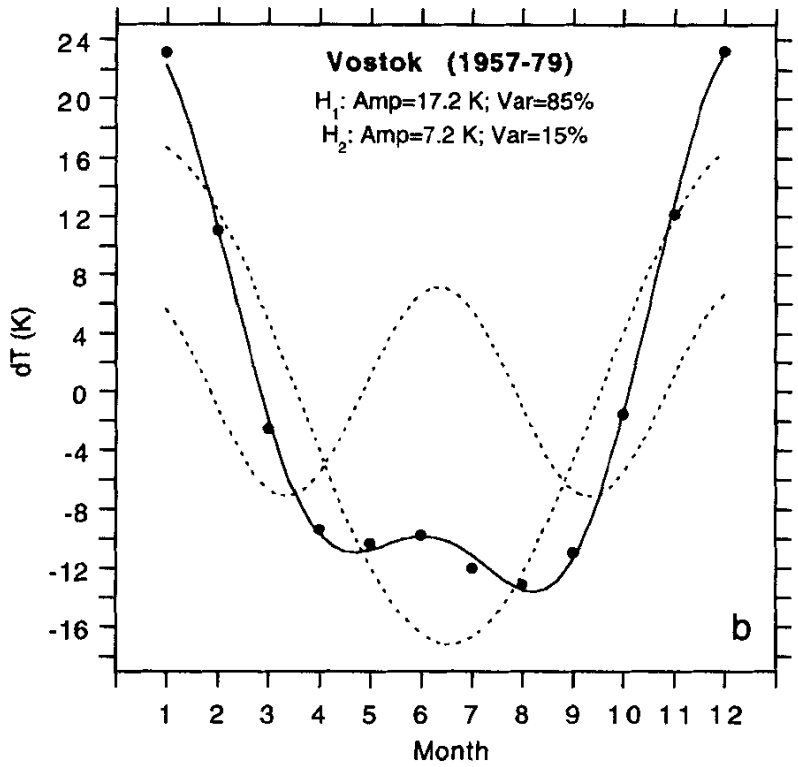

Figure 2.4: First and second harmonics of mean annual temperature cycle $H_1(T)$, $H_2(T)$ (dotted lines) and sum $H_1(T)$ and $H_2(T)$ (solid line) for the period 1957-79 at Vostok. Observations are represented by black dots. Reproduced from van den Broeke (1998a).

reach the interior of the continent, causing a dramatic rise in temperature and precipitation. These kind of intrusions were studied by Pook and Cowled (1999), Massom et al. (2004) and Schlosser et al. (2010), who note the importance of blocking-high patterns in the Southern Ocean on the movement of the intrusion.

2.5 The *coreless* winter and Semi-Annual Oscillation

The yearly temperature march in Antarctica is atypical of a global seasonal cycle. Due to its low angle of solar incidence, direct sunlight reaching the continent is low and the summer is brief. The so-called *coreless* winter of the Antarctic (Schwerdtfeger, 1984; King and Turner, 1997) is a further reflection of the short sun-lit period and the heat balance of the ice sheets. Antarctica experiences rapidly decreasing temperatures in the autumn as the sun disappears, but throughout the winter the temperature changes little until spring. We illustrate the effect with figure 2.4, which shows the first and second harmonics of the monthly mean temperature at Vostok, taken from van den Broeke (1998a). The total temperature change depicts the *coreless* winter effect and the Semi-Annual Oscillation, discussed later in this section. The depth of the winter temperature trough is limited as, despite the lack of solar heating, heat can still be transferred to the surface in a variety of ways. Mechanisms include vertical eddy flux, conduction from the ground, and heat of deposition (Schwerdtfeger, 1970). Thus, even under cloudless conditions, there is a limit to the degree of net heat loss from the surface of the ice sheet (King and Turner, 1997).

The location of Antarctica and its surface of ice ensure that temperature changes in the transition

months are fast and dramatic. This is in contrast to lower latitudes of the southern hemisphere, which are predominantly ocean-covered and thus are slower to respond to changing solar incidence. Consequently, the thermal gradient between the ice and ocean is not greatest in the mid-winter months, but in the transition periods of autumn and spring. Given that this temperature gradient is the primary driver of the winds over the southern ocean and the circumpolar trough, its peak in the transition months has a profound influence on the synoptic meteorology of the ocean and continent. The twice-yearly deepening and southward displacement of the trough with increasing continent-ocean temperature gradient, and associated peaks in synoptic activity in Antarctica, is known as the Semi-Annual Oscillation (SAO) and has been reported in a large number of temperature, pressure, and wind observational studies. During the late autumn and early spring periods, Antarctic temperatures are coldest, as enhanced circumpolar westerlies effectively isolate the continent from lower latitudes. Temperatures are warmest in summer, but a secondary peak is seen in mid-winter, as circumpolar westerlies abate. This structure is clearly visible in the Vostok temperature record (fig. 2.4). The transition months also show the lowest pressures and an associated large number of synoptic cyclones (Simmonds et al., 2003). Early research on the SAO was performed by van Loon (1967) using monthly temperature data at 500 hPa for the years of 1957-65. Meehl (1991) reexamined the mechanisms and emphasised the internal dynamics of the ocean in generating the required thermal contrast in the transition seasons. A modelling study of the phenomenon was performed by Simmonds and Jones (1998). They reported that the largest changes in pressure due to the oscillation were found near the coast of the continent. The maximum change in temperature gradient was found to be around 60 °S. van den Broeke (1998a) assessed the annual surface temperature march of long-period (1957-79) manned research stations by splitting records into the first and second annual harmonics. They found that the SAO had the largest impact on temperatures of the Antarctic Plateau, followed by coastal stations, and lastly the Antarctic Peninsula. They further found that a high correspondence between surface pressures and the second harmonic of temperature existed at coastal sites, suggesting that the movement of the ACT was responsible for changing temperatures. They addressed trends in the SAO in a follow-up report (van den Broeke, 1998b). The reanalysis study of Walland and Simmonds (1999) showed that while the meridional temperature gradient is strongest in March, the baroclinicity of the atmosphere over the Southern Ocean is greatest in October, consistent with the peak in SAO-related synoptic activity. Using 27 years of reanalysis output, Bromwich and Wang (2008) performed a review of Northern and Southern Hemisphere polar circulation. They noted the importance of the SAO on the Southern Hemisphere. A literature review of the several atmospheric oscillations, including the SAO and focusing particularly on their effects on synoptic activity is given in Simmonds (2003).

2.6 The Southern Annular Mode

The Southern Annular Mode, also known as the Antarctic Oscillation, or High-Latitude Mode, is an almost zonally symmetric pattern of variability that occurs in the Southern Hemisphere. The mode is generally described by its manifestation in the large-scale pressure anomaly field or the 500 hPa geopotential height and has been shown to account for a large amount of monthly variance in these variables across the hemisphere. SAM represents the periodic strengthening and weakening of the dominant large-scale pressure and wind patterns around the continent. In the positive (SAM+) phase, negative pressure and geopotential height anomalies are observed over Antarctica and the surrounding ocean. Positive anomalies are seen in the mid-latitudes, the circumpolar trough shifts to the south, and circumpolar

westerly winds are strengthened. The opposite conditions are observed during negative SAM (SAM-) phases. Kidson (1975) identified the SAM pattern in the second eigenfunction of the monthly mean Southern Hemisphere pressure for 1951-1960. Rogers and van Loon (1982) identified SAM in empirical orthogonal functions of 500 hPa geopotential height separately for the summer and winter seasons, and confirmed the finding with surface station records. They noted the highly barotropic nature of the phenomenon. SAM-like structure was also reported in the 500 hPa geopotential height by Kidson (1988) . Both Yoden et al. (1987) and Hartmann and Lo (1998) reported SAM-like structure in the leading EOF of the 1000-100 hPa thickness. Shiotani (1990) saw SAM-like variability in the first EOF of the zonal-mean 1000 hPa geopotential height. Gong and Wang (1999) described the oscillation using monthly mean MSLP output of the NCEP-NCAR reanalysis from January 1958 to December 1997. They used EOF analysis to extract the SAM signature and found that the first EOF, which explained $\approx 17\,\%$ to $\approx 33\,\%$ of the variance (depending on the month), described the SAM oscillation. They also defined the Antarctic Oscillation Index (AOI) as the difference in the zonal mean MSLP between $40\,^{\circ}$S and $65\,^{\circ}$S. Thompson and Wallace (2000) described annular modes in both the Northern and Southern Hemispheres. They further described the coupling of the modes to the stratosphere in seasons where the strength of the zonal flow allows planetary wave propagation between the troposphere and stratosphere: spring and summer in the Southern Hemisphere. Nan and Li (2003) examined the connections with SAM to locations as far north as the Yangtze River in China. They redefined the AOI as the difference between the zonal mean MSLP anomaly at $40\,^{\circ}$S and $70\,^{\circ}$S, after identifying that these two latitudes were more strongly anti-correlated.

The SAM pattern, as displayed by Kidston et al. (2009) from the NCEP-NCAR reanalysis is shown in figure 2.5. The authors defined the SAM pattern as the leading empirical orthogonal function (EOF) of the 500 hPa geopotential height south of $20\,^{\circ}$S, and used the principal component (PC) of this EOF as the SAM time series. The patterns in figure 2.5 were produced by calculating correlation coefficients between monthly mean 500 hPa geopotential height anomalies and the SAM PC. From these diagrams, both the annular and non-annular structure of SAM is evident. The non-annular structure is much more well-defined in the winter and occurs to due to associated variability within the Antarctic wavenumber 3 pattern. The non-annular structure of SAM was discussed further by Fogt et al. (2012a), who highlighted the especially large amount of variability in the ABS region, and investigated temperature dependence on the non-annual structure of the oscillation. Both Turner et al. (2009b) and Turner et al. (2012) discussed the deepening of the ABS low under SAM+ conditions. The authors suggested that enhanced flow splitting caused by stronger westerly winds around the continent caused a deeper ABS low during the SAM+ phase, which then induced stronger southerly winds over the Ross Sea and enhanced northerlies on the west coast of the Antarctic Peninsula. Turner et al. (2009b) suggested that this may have large effects on sea ice distribution. Recently, using a k-means clustering technique, Pohl and Fauchereau (2012) resolved the SAM oscillation into four regimes on daily time-scales. Their clusters described both the zonally symmetric and wavenumber 3 patterns of the mode.

The enhancement of circumpolar westerly winds under SAM+ conditions acts to isolate the Antarctic continent from lower latitudes. Thus, in the SAM+ phase Antarctica is generally colder than in the SAM- or intermediate phase. The Antarctic Peninsula provides an interesting exception to the general response. Its location to the east of the ABS low means that in on the west side during the SAM+ phase a higher incidence of warm advection from the north is observed (Fogt et al., 2012a; Turner et al., 2012). Further, its meridional protrusion into the field of strong westerly winds results in an increased foehn activity on the east side of the peninsula during the SAM+ phase (Marshall et al., 2006). Accordingly, temperatures

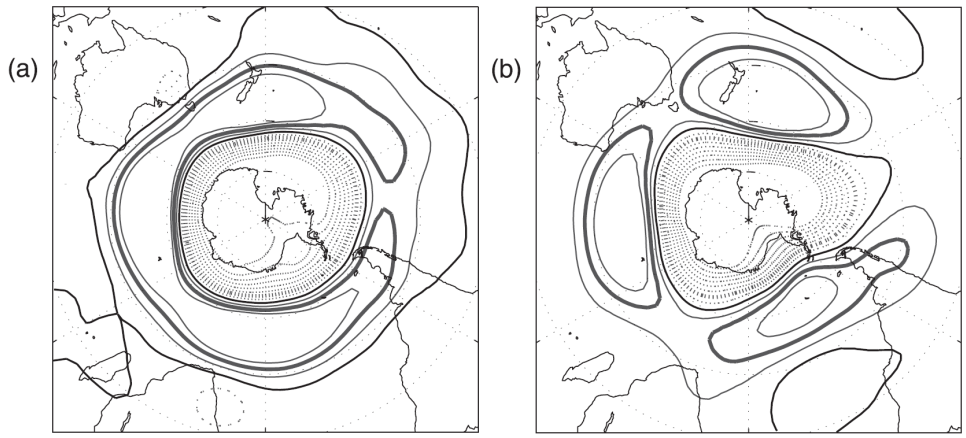

Figure 2.5: Correlation coefficient for monthly mean 500 hPa geopotential height anomalies and the SAM during (a) summer (DJF) and (b) winter (MJJ). The contour interval is 5 m std^{-1} (std = standard deviation) with the zero contour omitted and the $\pm$10 m std^{-1} bold. Figure and label reproduced from Kidston et al. (2009).

on the Antarctic Peninsula are seen to rise during the SAM+ phase, in contrast to the remainder of the continent. This pattern of warm peninsula/cold continent has been found repeatedly in investigations of climatic temperature trends, leading many authors to implicate trends in the SAM in forcing Antarctic climate change. This topic is covered in some detail in section 2.8. Schneider and Steig (2002) used principal component analysis to examine 21 years of satellite retrieved surface temperature data over the continent. After the seasonal cycle had been removed, the first principal component was highly correlated with the SAM index and displayed the cold continent/warm peninsula pattern. Kwok and Comiso (2002b) further used data taken from the Advanced Very High Resolution Radiometer (AVHRR) for 17 years to show that positive SAM phases are associated with cold anomalies over the continent and warm anomalies on the peninsula. Genthon et al. (2003) found a SAM signature in Antarctic precipitation variability. van den Broeke and van Lipzig (2004) performed a 14-year model integration and used the results to produce regressions of surface conditions to SAM variability. They reported stronger circumpolar westerlies in SAM+ years. The stronger winds advected warm, moist air over the peninsula, causing a rise in temperature and precipitation there. The remainder of the continent cooled during the SAM+ phase, and the reduction of southward transport of maritime air also made some parts of the continent drier. Schneider et al. (2004) used satellite thermal infrared and passive microwave brightness temperatures to study month-to-month variability of Antarctic surface temperature for 1982-99. They found a large amount of covariability between the data types, despite distinct differences in the physical properties to which the different wavelengths respond. The first principal component of both datasets was highly correlated with the SAM index of the NCEP-NCAR reanalysis and displayed the warm peninsula/cold continent pattern. Similar results were obtained from *in situ* observational data by Gillett et al. (2006). Marshall (2007) calculated regression coefficients between long-period temperature record from many Antarctic manned stations compiled in the READER database and the SAM index of Marshall (2003). He reported a temperature relationship in which peninsula stations, particularly those on the eastern side, showed warming in SAM+ years. The majority of East Antarctic stations displayed cooling during the SAM positive phase.

Variations in SAM are known to change the position of the circumpolar trough, and affect the strength of mid-hemisphere westerlies and the surface climate of Antarctica. There has also been a large amount of

research performed on the impact of these changes on synoptic activity around the coast of the continent, using a range of methods. Kidson and Sinclair (1995) studied the variation in the Southern Hemisphere storm track using 9 years of daily 500 hPa height data. The SAM index was defined as the leading principal component of data that had been filtered using a 10-day low pass method. They found that the positive phase of the SAM oscillation was associated with the Pacific split jet pattern. Kidson (1999) performed EOF analysis on the 300 hPa streamfunction of the NCEP-NCAR reanalysis. He found the SAM pattern manifested in the second and third EOFs on interannual time-scales. Vera (2003) used rotated empirical orthogonal functions to study interannual and interdecadal variations in the Southern Hemisphere storm track. The author reported that the second EOF of the stormtrack on interdecadal time-scales was related to the SAM. Using a Lagrangian cyclone tracking scheme, Pezza et al. (2008) showed a shift of high cyclone densities from mid-latitudes to high-southern latitudes during the SAM+ phase, consistent with the observed movement of the circumpolar trough. Pezza et al. (2012) reported similar results, with peaks in cyclone density in the familiar wavenumber 3 pattern around Antarctica in the SAM+ phase.

In recent years, much research has focused on trends identified in the SAM, with a significant tendency shown towards the positive phase (Thompson et al., 2000; Thompson and Solomon, 2002; Gillett and Thompson, 2003), which has been partially associated with anthropogenic ozone depletion in the stratosphere (Arblaster and Meehl, 2006). However, there is some debate as to the magnitude of the trends and the season in which they are largest, as the indices used to give a general impression of the strength and phase of the phenomenon are often calculated from reanalysis output which has been shown to be unreliable at high southern latitudes before the satellite era. In particular, the NCEP-NCAR reanalysis, upon which the AOI is defined, shows spurious negative pressure trends around the coast of Antarctica, due to a high bias early in the dataset that is sequentially reduced with the inclusion of increased observations over time (Hines et al., 2000; Bromwich and Fogt, 2004). As the SAM index is calculated using MSLP from this area, which has a negative pressure anomaly in the SAM+ phase, a larger trend than exists in reality has been shown to be contained in the NCEP-NCAR reanalysis (Marshall, 2003). Accordingly, several authors have made attempts to define indices of SAM based on observational data alone, but this has drawbacks in the Southern Ocean and Antarctica, where long-period records are sparse. Marshall (2003) defined a SAM index based on six station records on the coast of Antarctica at about 65 °S, and six at about 40 °S. Stations were chosen for the length of the record and for even an zonal distribution. The index was calculated from 1958-2000. The authors report that the NCEP-NCAR reanalysis over-represents the positive trend in all seasons, but particularly in winter. The station-based SAM index showed the largest trends in spring and summer, with the largest trends computed from the late 1970s onwards. Visbeck (2009) defined a further index, also based on station pressure records from the 1940s onwards. However, using the principle of conservation of mass, with pressure records at mid-latitudes the author was able to estimate the pressure in Antarctica prior to the beginning of the observational record there. With this method they constructed an index as far back as 1884. The authors reported an increasing trend in the SAM from the 1970s onwards, and a decrease observed in the 30 years surrounding 1945. The multiple ways of representing SAM are reviewed by Jones et al. (2009).

Modelling studies have been performed, specifically designed to identify the dominant forcing that is acting to generate the trend in SAM. For example, Fyfe et al. (1999) found trends towards the positive phase in global climate models for both the Arctic and Antarctic oscillations under climate change forcing. Sexton (2001) modelled the effects of ozone depletion on the phase of the SAM, and reported that a

tendency towards the positive was seen in the late spring and early summer. Shindell and Schmidt (2004) examined both ozone and greenhouse gas forcing, and found that both have pushed the SAM towards its positive phase in the last few decades, although ozone forcing dominates above the mid-troposphere. They further discuss the projected impacts. Given that the ozone hole is recovering, but greenhouse gas emissions are continuing to rise, they predicted little change in the SAM. Cai and Cowan (2007) examined simulations for the Intergovernmental Panel on Climate Change (IPCC) Fourth Assessment Report (AR4). They found that only those models that contained ozone depletion forcing reproduced realistic trends in SAM. Using climate model ensembles, Arblaster and Meehl (2006) found that ozone forcing was the largest contributor to the increasing trend in the circumpolar vortex in the stratosphere. However, contrary to Shindell and Schmidt (2004), they also reported that increasing greenhouse gas emissions would act to continue the trend into the 21st century, despite temperature increases across the Southern Hemisphere. These results were confirmed further by Arblaster et al. (2011). A review of the mounting evidence that the trend in SAM is forced by ozone depletion, and its effects on the surface of Antarctica is given by Thompson et al. (2011).

There is also some evidence that the SAM oscillation likely plays a significant role in controlling sea ice extent around the Southern Ocean, via the influence of direct wind-forced advection and Ekman drift. Hall and Visbeck (2002) used a 15000-year coupled ocean/atmosphere model integration to examine the influence of SAM on Antarctic sea ice on a month-to-month basis. They describe the SAM+ enhanced westerly winds as driving northward Ekman drift at the ocean surface. Associated anomalous up-welling was simulated around the Antarctic coastal margins, down-welling around 45 °S, and southward transport in lower ocean layers. The northward surface flux aides the northward advection of sea ice, and increased sea ice cover results during the SAM+ phase. Lefebvre et al. (2004) used an ice/ocean model with atmospheric forcing from the NCEP-NCAR reanalysis. Their results confirmed those of Hall and Visbeck (2002). However, they highlighted the importance of the non-annular component of SAM in the sea ice distribution. They also reported a sea ice concentration dipole between the Ross and Bellingshausen Seas. During the positive phase of SAM more cold air is advected into the Ross Sea, via SAM's modulation of the ABS low, aiding sea ice production. Conversely, northerly advection is enhanced in the Bellingshausen Sea, confining sea ice to the coast via both dynamic and thermodynamic processes. A similar mechanism was discussed by Turner et al. (2009b) and Turner et al. (2012). Sen Gupta and England (2006) used a coupled ocean/atmosphere model to further investigate the effects of SAM on sea ice. They emphasized the importance of oceanic processes such as meridional heat advection, surface heat fluxes, and changes in mixed layer depth in the generation of the SAM signature in sea ice. A review of the impacts of atmospheric modes, including SAM, on the sea ice system is given by Yuan and Li (2008), which portrays a complicated system in which many modes of variability play a role in controlling sea ice extent. More recently, the modelling study of Sigmond and Fyfe (2010) suggested that forcing linked to ozone depletion acted to decrease the extent of Antarctic sea ice in all seasons, due to a combination of sea-surface temperature shifts and Ekman transport. Clearly then, the question as to whether the trend in SAM impacts upon the trend in sea ice cannot be regarded as settled.

2.7 The El Niño-Southern Oscillation

The El Niño-Southern Oscillation (ENSO) is a coupled ocean/atmosphere mode which is forced in the tropical Pacific, and involves the modulation of atmospheric zonal circulation patterns by anomalous ocean currents and vice versa. During standard tropical Pacific conditions, up-welling of cold water at

the coast of South America causes a temperature gradient directed from east to west. Subsidence of air in the east, and rising in the west then forces the Walker circulation over the ocean, with easterly trade winds at the surface. In "El Niño", or warm event, conditions, the up-welling in the east is disrupted, causing warm anomalies to form in a tongue from South America across the Pacific. This is turn disrupts the atmospheric circulation, reducing subsidence in the east, which further reduces the up-welling there in an ocean/atmosphere feedback. Anomalous convection is seen in the central and eastern Pacific due to the warm sea surface temperature anomalies. In the opposite phase, coined "La Niña" or cold event, a reinforcement of zonal circulation and enhanced up-welling in the eastern Pacific is observed. Warm anomalies are forced farther west, causing anomalous convection and precipitation over the western Pacific. The cycle repeats itself approximately every five years, but shows a high degree of variability. Further, while peaks in the effect tend to appear around Christmas (hence the Spanish "the Little Boy"; referring to the Christ child), and each event follows broadly similar patterns, occurrences also show marked differences. A complete description of the manifestation of the phenomenon in the tropics is beyond the scope of this work. A thorough description of the mode, and different uses of the term "El Niño" is given by Trenberth (1997). The atmospheric portion of the oscillation is described at length from observational data by Trenberth and Caron (2000). In general, the term "El Niño" describes the oceanic portion of the coupled mode (and also refers specifically to warm events), whilst "Southern Oscillation" refers to its atmospheric component.

The ENSO mode is of direct interest for those wishing to understand aspects of the climate of Antarctica, as the anomalous upper-level convergence associated with the mode has been shown to force teleconnections that are observed as far south as the Amundsen-Bellingshausen Seas, as a result of a Rossby wave train and modulation of Hadley and Ferrel cells. In general, high geopotential anomalies are observed in the ABS region in warm events, and corresponding low anomalies in cold events. A review of the impacts of the ENSO phenomenon on Antarctica and surrounding ocean was given by Turner (2004).

Evidence for the ENSO high-latitude teleconnection has come from a wide range of sources, and generally describes a Rossby wave train observed in geopotential height or potential vorticity anomalies reaching from the tropical Pacific to the Southern Ocean. The dynamics of such a wave train, caused by anomalous upper-level convergence, were described by Hoskins and Karoly (1981). Karoly (1989) described the evolution of the wave train from several ENSO events and reported a centre of variability in the Amundsen-Bellingshausen Sea area, and a second on the opposite side of the Antarctic Peninsula in the Weddell Sea that acts out of phase with the first. In the ABS region lower pressures were observed under La Niña conditions and higher pressures in El Niño conditions. Thus, stronger cyclonic circulation is observed in the ABS region under La Niña conditions. In the summertime, they found a zonal wavenumber 3 pattern that circled the coast of the continent. In fact, two teleconnections that propagate from the tropical Pacific to the high southern latitudes have been identified. They are known as the Pacific South American (PSA) modes 1 and 2. The two wave trains were identified by Mo and Higgins (1998) as the first two principal components of reanalysis output of the 200 hPa eddy streamfunction, and found to be in quadrature with each other. The two EOF patterns from this analysis are shown in figure 2.6. Houseago et al. (1998) used Hovmöller analysis to illustrate the wave trains crossing the South Pacific. They found large variability in different events, with the 1982-83 El Niño highlighted as particularly anomalous, but observed broad similarities across events in general. The study was furthered by Houseago-Stokes and McGregor (2000). Renwick (1998) observed that blocking in the south-east Pacific was more common in El Niño periods than La Niña from a 16-year

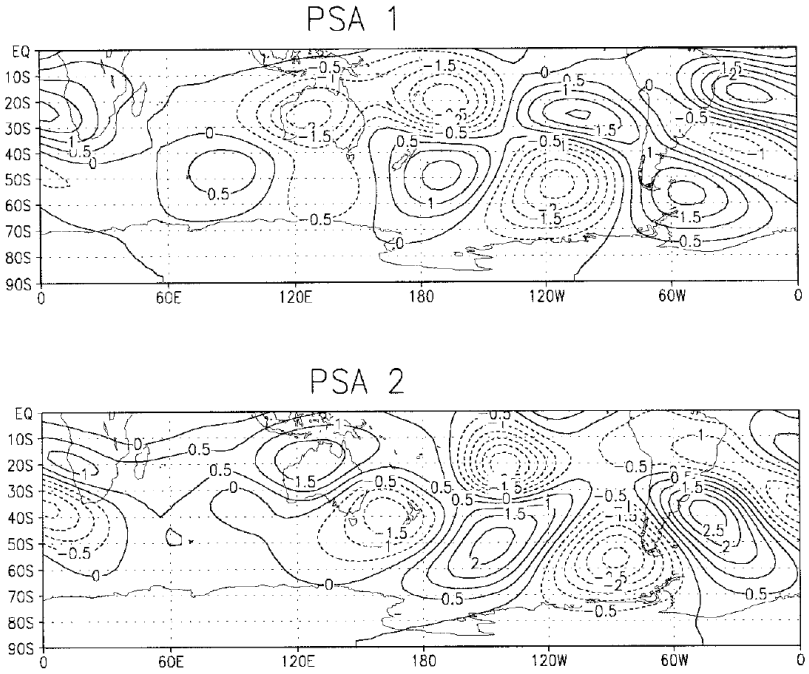

Figure 2.6: (a) EOF 1 and (b) EOF 2 for the 200 hPa eddy streamfunction. EOFs are normalized to 1 and time 100. Contour interval is 0.5 nondimensional unit. Figure and label reproduced from Mo and Higgins (1998).

dataset, consistent with the observed PSA modes. Renwick and Revell (1999) furthered this analysis with 39 years of data, and found that relationships were strongest in spring and summer. The modes also appeared in the principal components of the 300 hPa streamfunction in the analysis of Kidson (1999). Using reanalysis 500 hPa heights, Mo (2000) identified that the PSA1 was associated with the low-frequency part of the ENSO cycle, while the PSA2 is associated with its quasi-biennial component. The effects of the PSA modes on South American rainfall were discussed by Mo and Paegle (2001). Kidson and Renwick (2002) identified three ENSO-related principal components in a southern Pacific sea surface temperature (SST) dataset. They concluded that a large amount of variability ($\approx 29\,\%$) in the region was ENSO related at seasonal time scales. Harangozo (2004) reported that in El Niño warm events that displayed a strong teleconnection, deep tropical convection was observed in the Intertropical Convergence Zone. Convection was lacking in those events which did not have strong teleconnections. Lachlan-Cope and Connolley (2006) also performed an in-depth analysis into the generation of the PSA mode wave trains in the tropical Pacific. They too found that SST anomalies due to ENSO events caused deep convection in the tropics leading to convergence in the upper troposphere. However, the relationship between SST and convection was seen to be complex, and areas in which subsidence is usually found must pass an unrealistically high SST anomaly threshold in order for convection to occur. The geographic variation in heating between ENSO events then explained the observed variability in extra-tropical response. The authors explained the lack of extra-tropical response in the 1982-83 warm event noted elsewhere by the fact that the warm anomalies in the Pacific were only present in regions of climatological subsidence, and so little anomalous upper-level convergence was observed. As noted by Jin and Kirtman (2009), the extra-tropical response in the Southern Hemisphere tends to lead the evolution of the tropical anomalies. While, in the Northern Hemisphere, the peak is concurrent with that in the tropics. The authors reported that austral summer conditions inhibit the formation of the wave

train in the Southern Hemisphere, meaning that the peak in the teleconnection occurs prior to the onset of summer, in the austral spring. In a model experiment in which the ENSO peak temperature anomaly was shifted in time to the austral winter, the Southern Hemisphere extra-tropical response occurred at the same time as that in the tropics.

Much research has focused on the impacts of ENSO in the ABS and Weddell Seas, and area between, because of the modulation by the mode of geopotential heights in these regions via the PSA patterns. The ABS low, which is observed to be deeper in La Niña years, is responsible for the advection of warm, maritime air and moisture to the Antarctic Peninsula and West Antarctica. Thus, the ENSO teleconnection has been shown to modulate these variables. Some variation is seen between events, and on interdecadal time scales due to variation in the position of the pressure minimum, and the interaction of the PSA wave trains with other modes of variability such as SAM. Simmonds and Jacka (1995) found a significant correlation between sea ice extent in the south Pacific and ENSO forcing at zero-lag, which was consistent with anomalous circulation conditions. Cullather et al. (1996) studied the net accumulation (total precipitation minus total sublimation) of the Antarctic continent, and found that positive accumulation anomalies in West Antarctica were associated with La Niña events in the 1980-90 period. However, the correlation broke down after 1990. This finding was reproduced by Bromwich et al. (2000), using the ECMWF 15-year reanalysis. Genthon and Cosme (2003) also found an intermittent correlation between ENSO and precipitation in West Antarctica. Focusing on years of extreme temperature on the Antarctic Peninsula, Marshall and King (1998) produced geopotential height composites of warm and cold years that were highly reminiscent of La Niña and El Niño conditions. Although, the authors warn that not all extreme events on the peninsula have an associated ENSO peak. Harangozo (2000) found ENSO teleconnections to Antarctic Peninsula temperatures, via the mode's modulation of local sea ice extent. Using 17-years (1982-98) of satellite retrieved skin-surface temperature data, Kwok and Comiso (2002b) investigated correlations between the Southern Oscillation Index (SOI) and Antarctic surface temperatures. They found positive correlations in the Bellingshausen and Weddell Seas and in West Antarctica, corresponding to warming in La Niña years which is consistent with observed variability in circulation patterns. Kwok and Comiso (2002a) performed a similar analysis for the Southern Ocean as a whole, and again found temperature correlations which were consistent with the circulation changes induced by the PSA patterns. Renwick (2002) used the NCEP-NCAR reanalysis to examine links between ENSO, 500 hPa geopotential height, sea surface temperature and sea ice. They found that ENSO-induced advection anomalies caused a dipole in variability between the south Pacific and south-west Atlantic. Yuan (2004) examined the impact of this dipole on sea ice distribution, and found it was generated as a result of the well-known Rossby wave train, and modulation of Hadley and Ferrel cells due to anomalous convection in the tropics. Patterson et al. (2005) examined the moisture flux of an ice core taken in the McMurdo Dry Valleys. They found an ENSO signal, which they associated with the modulation of cyclonic circulation in the Ross Sea by the ENSO teleconnection. This research was furthered by Markle et al. (2012), who used a k-means technique to define clusters of back-trajectories of air reaching an ice core site in the Dry Valleys. They found that ENSO heavily influenced the observed tracks, with a higher degree of cyclonic tracks in La Niña years. Similar results were obtained by Cohen et al. (2013). Lee et al. (2010) reported on record maximum temperatures from a 30-year satellite retrieved SST dataset in the South Pacific near West Antarctica, associated with the strong El Niño in the austral summer of 2009/10. The timing of sea ice advance and retreat in the Ross Sea was studied by Stammerjohn et al. (2008), who found that advance began earlier in La Niña years, due to the enhanced southerly winds associated with a deeper ABS low. Schneider et al. (2012b) investigated the impact of the PSA patterns on the Antarctic Peninsula and West Antarctica.

They found the largest sensitivity in spring for temperature, pressure and precipitation, consistent with the peak in the tropical teleconnection in this season. Yu et al. (2012) computed correlations between surface manned station temperature records and an index of the PSA1 mode and SOI. They reported that significant correlations in pressure and temperature were present between Antarctic Peninsula stations and PSA for all seasons, while SOI had significant correlations with West Antarctic stations in spring.

The influence of cyclones tracking into the Amundsen and Bellingshausen Seas from the north-west is at least in part responsible for the creation of the climatological low pressure there. Given the impact that the ENSO-associated wave train has been shown to have on pressure anomalies in the area, it is not surprising that a large amount of research has been performed on the ENSO influence on synoptic cyclones and the Southern Hemisphere storm track. Sinclair et al. (1997) suggested a predominantly linear response of Southern Ocean cyclones to ENSO forcing, with more cyclones seen in a band from the subtropical Pacific towards South America, and fewer in the Indian Ocean sector in El Niño winters. The almost exact opposite conditions were observed in La Niña winters. Chen et al. (1996) examined the evolution of the split jet in the south Pacific in the 1986-89 ENSO cycle. They found a strong (weak) subtropical (polar) jet in the El Niño phase. The opposite conditions were reported under La Niña conditions, consistent with cyclone densities and the depth of the ABS low reported in numerous other studies. Similar conditions were reported by Marshall and King (1998). Vera (2003) used rotated empirical orthogonal functions to study interannual and interdecadal variations in the Southern Hemisphere storm track. The interannual variation of their first EOF was closely linked to ENSO variability, and resembled the PSA1 pattern. Pezza and Ambrizzi (2003) studied El Niño and La Niña composites of cyclone and anticyclone tracks over the Southern Hemisphere. They found that the total number of cyclones was not significantly affected by the ENSO phase, but that the distribution differed between warm and cold events. A thorough analysis of the impact of ENSO on cyclone activity, particularly regarding the rainfall in Australia was performed by Pezza et al. (2008). Pezza et al. (2012) further investigated the interaction of ENSO, SAM and sea ice.

Recently, the covarying aspect of SAM and ENSO has been investigated in some depth, with several reports implicating the recent in-phase nature of the phenomena as being mutually reinforcing, via the geographical placement of the loading centre in the Amundsen-Bellingshausen Sea region. It has been shown that both La Niña and SAM+ conditions involve reduced geopotential heights, and associated circulation changes, in the region. Further, the enhanced westerlies at southern mid-latitudes in the SAM+ phase have been shown to aid in the propagation of the ENSO-related wave train to high southern latitudes. Genthon et al. (2003) discussed the principal components of precipitation over Antarctica. They noted that the signals of both SAM and ENSO are found in one mode of precipitation, suggesting that they share a high degree of covariability. Carvalho et al. (2005), found a significant correlation between positive SAM and La Niña events. L'Heureux and Thompson (2006) reported that in the summer months, 25 % of the variance of ENSO is linearly related to that of SAM. Fogt and Bromwich (2006) found high correlations between the two modes in the spring of the 1990s, but lower correlations in the 1980s. They suggested that the in-phase relationship in the 1990s had essentially strengthened the PSA teleconnection pattern and enhanced its impact on the continent. Gregory and Noone (2008) examined the isotope record from a 100-year long ice core record from West Antarctica. They found that the strength of the ENSO teleconnection was highly dependent on the phase of SAM. When the two modes were in phase, the ENSO-teleconnection was observed to be more strongly apparent in the West Antarctic region, confirming the assertion of Fogt and Bromwich (2006) that an in-phase relationship is needed for the PSA wave train to propagate to the Antarctic. Fogt et al. (2011) reported that in a

50-year data set La Niña/SAM+ events and El Niño/SAM- events occurred concurrently at a higher rate than predicted by chance alone. They found that only when ENSO and SAM were in phase, or that the SAM was weak, did a strong teleconnection form from the tropics to the Southern Ocean. The authors examined the role of transient eddy flux in the mid-latitudes in the reinforcement of the ENSO-related wave train. They found that during in-phase events, eddy fluxes associated with each node reinforced each other, allowing the stronger propagation of the wave train to high-latitudes. In out of phase events, transient eddy fluxes oppose each other, retarding the wave train. Accordingly, the authors implicated the mechanism in the varying high-latitude response to the ENSO phenomenon. Recently, Schneider et al. (2012b) used Antarctic manned station and ice core proxy data to investigate coupling between the two modes, and confirmed earlier results. However, the short climate record in Antarctica has meant that mechanisms regarding the interaction of SAM and ENSO are still under debate.

2.8 Climatic trends

The troposphere above Antarctica is rather thin and dry, and is subject to large horizontal temperature gradients between the continent and surrounding ocean. Consequently, the surface climate of coastal regions of Antarctica is particularly sensitive to changes in circulation, as the advection of heat from lower latitudes can cause the temperature to rise dramatically. Considering current research priorities, it is no surprise that a large number of studies have focused on the characterization of temperature trends at the surface of Antarctica. The determination of trends on the continent is however a difficult task due to the short *in situ* and satellite-derived records, and the large interannual variability observed on the continent. The advent of reanalysis products may have improved the understanding of interannual and interdecadal variability over the data sparse continent, but these products have been shown to contain spurious trends and many authors have cautioned against their use in Antarctica before the satellite era (for example, Marshall (2002b, 2003); Bromwich and Fogt (2004); Bromwich et al. (2007)). The more recent development of the second generation of reanalysis datasets has addressed some of these issues (Nicolas and Bromwich, 2011b; Bromwich et al., 2011; Bracegirdle and Marshall, 2012), but the most reliable temperature trends from the continent are still computed from quality-controlled station records, which are thinly spread and almost entirely confined to the coastal margins of the continent for historical and logistical reasons. Clearly, the estimation and explanation of temperature changes in Antarctica is a large subject. While a consensus appears to have been reached regarding the general continental distribution of trends, with warming across the Antarctic Peninsula and West Antarctica and a small cooling in East Antarctica, trends are sensitive to the start and end dates and magnitudes vary between studies and datasets. Trends in West Antarctica are especially contentious, as the paucity of long-term records in the region is particularly severe. Several reviews have been published that cover the most pressing aspects of the field. Turner and Overland (2009) provide a synopsis of climate change research, compared to the state of knowledge of the Arctic. The case for ozone hole-related cooling of the Antarctic surface atmosphere is reviewed by Thompson et al. (2011). Schneider et al. (2012a) discuss at length the observed and interpolated trends in West Antarctica, and report the impact of the positive trend of the Pacific South American mode in the advection of warm maritime air over the region.

Early investigation of temperature trends across the Antarctic continent was performed by Raper et al. (1984) for the period 1957-82. In an early example of a reconstruction technique, the authors weighted 16 records from manned research stations and interpolated the records to a latitude-longitude grid. They then calculated a trend for the entire continent and found warming in all seasons. They

cautioned that results were more uncertain in West Antarctica after 1970 due to the cessation of the record at Byrd Station. Using a similar technique, Jones et al. (1986) produced a gridded dataset for the Southern Hemisphere, including several sub-Antarctic islands. Further, Jacka and Budd (1998) calculated trends from a similar set of research stations, with care to average temperatures on the Antarctic Peninsula first, as the high density (for Antarctica) of research stations in that area is capable of biasing trend estimates. A mean warming trend was calculated for the continent. Continuing in this vein of research, Jacka et al. (2004) took station records and averaged them depending on their location. Four separate regions were analysed: coastal Antarctica (excluding the peninsula), inland Antarctica, the Antarctic Peninsula, and Southern Ocean islands. Each of the four groups indicated warming in the time period, although the magnitude of the warming had slowed since the previous report. The authors cited the 1991 Pinatubo eruption as the cause of the slow down in warming. Since 2004, much analysis of Antarctic climatic trends has been performed with the records of the highly-quality controlled READER (REference Antarctic Data for Environmental Research) project, described by Turner et al. (2004). The READER project represents a catalogue of monthly mean climate data from a variety of manned research stations around the continent. Also contained in the project database are radiosonde records and long-period AWS data. Trend analysis of surface observations by Turner et al. (2005) revealed a dipole in temperature trends between the Antarctic Peninsula and East Antarctica. The eastern portion of the continent showed small cooling trends in the 1970-2000 period, while those stations on the peninsula almost invariably recorded a warming. Of the peninsula stations, those on the west side warmed in winter and spring, while those on the east showed more warming in the summer. Surface pressures were seen to drop over coastal East Antarctica in the same period, leading the authors to suggest that the observed trends were primarily caused by the trend of SAM towards positive polarity, as suggested in the work of Thompson and Solomon (2002) and Gillett and Thompson (2003). This regional pattern has also been suggested to be the result of the decline in the strength of the SAO since the 1970s, and subsequent strengthening of the wavenumber 3 MSLP pattern around the Antarctic coastline (van den Broeke, 1998b, 2000). The regional pattern is illustrated by figure 2.7, which shows annual and seasonal trends for long-term research stations of the READER database for 1951-2012. Turner and Overland (2009) provided further analysis of the READER database station temperatures. An interesting detail of their results is the difference in temperature trends between McMurdo Station and Scott Base, which are situated ≈ 2.2 km apart on the Hut Point Peninsula of Ross Island, and both have monthly climate records dating back to the mid-1950s. McMurdo Station was seen to have a larger positive temperature trend, despite the vicinity of the two stations, which may reflect the sensitivity of station records to localized conditions, and cast doubts on their representativeness of larger areas.

The Antarctic Peninsula has been a focus of interest in the Antarctic climate change debate, as it appears to be subject to increasing temperature trends that are in the upper bound of those observed anywhere on Earth (Vaughan et al., 2001). This is of particular interest, as results indicate that most of East Antarctica has cooled in the same time period, while the trends in West Antarctica indicate warming but are still poorly constrained (Bromwich et al., 2012; Schneider et al., 2012a). The warming of the peninsula region was identified by King (1994) using several stations on its west coast. Noting the persistent year-to-year nature of the temperature variability in the region. The author suggested that temperatures there were more sensitive to changes in sea ice cover than the remainder of the continent, which may have impacted upon the observed trend. Harangozo et al. (1997) calculated temperature trends for three locations on the peninsula, and found significant increases at all stations, citing the decreased albedo of the ocean due to ice retreat as the main cause. The warming of the peninsula was placed in a global context by Vaughan et al. (2001), and was shown to be one of three regions of the

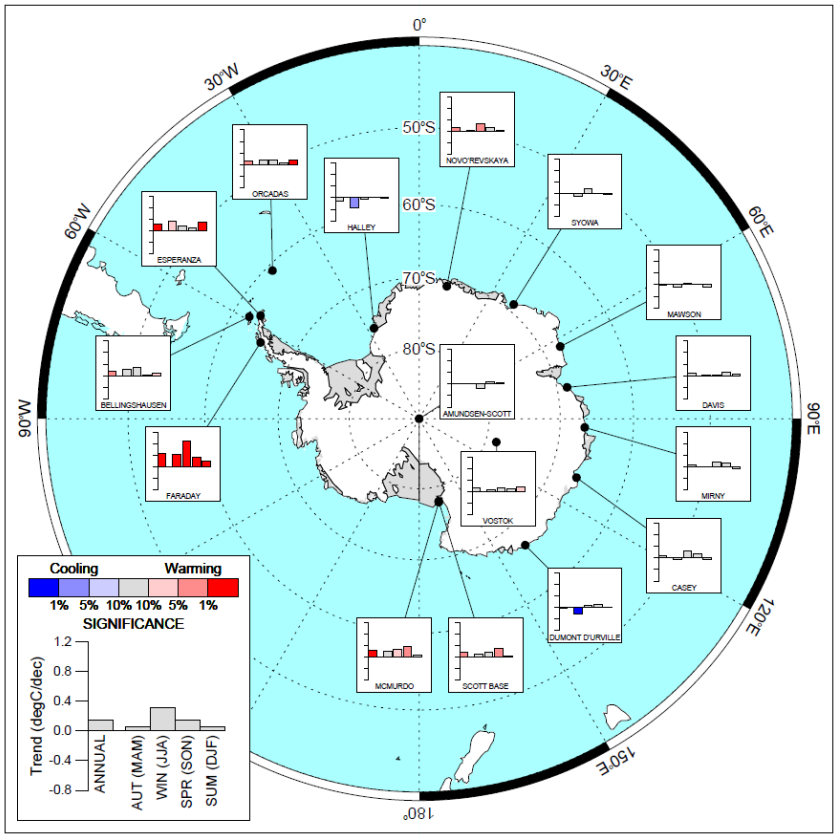

Figure 2.7: Temperature trends for selected Antarctic research stations for the years 1951-2012. Figure downloaded from the SCAR READER project website (http://www.antarctica.ac.uk/met/gjma/).

globe suffering from high-latitude amplification of warming trends, the other two locations being the north-west of North America and the Siberian Plateau. Vaughan et al. (2003) proposed three possible mechanisms for the peninsula warming: changing oceanic circulation, changing atmospheric circulation, or an ocean/atmosphere ice feedback that reinforced greenhouse gas warming. While the explanations of Thompson and Solomon (2002) and van den Broeke (2000) favoured the atmospheric circulation option, the analysis of Marshall (2002a) found no significant change in meridional heat advection and little evidence that increased westerlies due to SAM were forcing trends on the west side of the peninsula. Marshall et al. (2002) found that increasing trends in the troposphere were significantly reduced compared to those at the surface, suggesting that a feedback mechanism was taking place in the boundary layer that accelerated the warming there. In a later paper, Marshall et al. (2006) used a combination of observational and reanalysis data to determine that increased westerlies caused by trends in SAM were responsible for a higher amount of advection over the mountainous spine of the peninsula, causing foehn winds on the lee side that have a large warming impact. Stations on the east side of the peninsula were found to be three times more sensitive to SAM forcing than those on the west, where ocean/atmosphere feedback appears to dominate the warming. Marshall (2007) confirmed that the SAM influenced warming was most apparent on stations on the east side of the peninsula, and that the trend of SAM towards its positive phase had caused cooling in East Antarctica. Zazulie et al. (2010) studied the temperature record of the Argentinian Orcadas Station in the South Orkney Islands, which represents the longest record anywhere near the Antarctic continent, and consists of data at daily intervals starting in 1903. They

found no significant trends between 1903 and 1950, but a significant warming trend in all seasons between 1950 and 1970. The trends between 1970 and 2008 were double those of the middle period, and largest in austral autumn and winter. The authors note that this is consistent with the observed trend in SAM. However, recently Steig (2012) reported on the drilling of a deep ice core from the near-summit of Mount Haddington, James Ross Island. The recent temperature proxy record showed that warming started in the 1920s, well before the advent of chlorofluorocarbons (CFCs) that have caused ozone depletion in the stratosphere and the subsequent strengthening of SAM. Using a statistical significance technique, Steig (2012) further showed that the recent warming is unlikely to be a result of natural climate variability, and likely to be due to increased greenhouse gas emissions. This is in agreement with the work of Gillett et al. (2008), who found large warming trends at many locations around Antarctica after the influence of SAM had been removed. The authors also concluded that these warming trends were the result of anthropogenic greenhouse forcing.

Despite the existence of the READER database, the area of the continent that can be represented by manned station records is still low. This is partly due to the fact that the research stations utilized by the READER project are predominantly situated near the coast. A further problem is that records rarely extend backwards in time before the International Geophysical Year (1957-58), which profoundly limits both the time and spatial scales that can be assessed using no resources other than the *in situ* data. In regions without manned stations, AWS units do exist, but their initial introduction to Antarctica was rarely performed with climate monitoring in mind (Lazzara et al., 2012). Moreover, AWS records are short and they are known for their unreliability, due to their isolated locations in often hostile environments. The result is that little understanding of climatic trends can be attained over data-sparse areas from *in situ* data alone. In particular, trends in West Antarctica are poorly constrained, due to the closing of Byrd Station, the sole interior manned research base, in 1972. Thus, while temperature trends at Antarctic research bases are well known, trends in the large areas between bases are subject to debate. Attempts at characterising these trends with satellite retrieved remote sensing data have been performed. However, changes in emissivity at the surface due to melting in the warm season can profoundly affect the sensed temperature. Also, cloud masking must be performed on the dataset to ensure that the cloud-top temperature is not misinterpreted as the surface temperature. This procedure can be difficult, as the difference between clouds and ice is not large in the infrared. Comiso (2000) reported on a comparison between surface observation and satellite infrared temperature measurements from the AVHRR, finding cooling of annual temperatures across the continent in the time period of 1979-98. However, the analysis of Monaghan et al. (2008) for the same satellite dataset but 1982-2001 time-period shows warming over the Antarctic Peninsula, West Antarctica and East Antarctic coast, with cooling confined to the continental interior. Schneider et al. (2004) used a combination of infrared and AVHRR measurements and computed empirical orthogonal functions for the month-to-month temperature. They found that the third mode represented winter warming trends over the East Antarctic plateau, which they attributed to an increase in blocking events.

Recently, increasingly sophisticated statistical reconstruction schemes have been employed in an effort to better represent and understand the complex patterns of observed trends. Reconstruction analyses tend to use data from multiple sources, generally a mixture of *in situ* observations that represent the longest complete temperature records, and gridded satellite or reanalysis products that offer a higher spatial resolution than *in situ* measurements. Empirical statistical relationships are computed between the *in situ* and gridded products, and the resulting relationships are then used to fill in spatial gaps in the observations record by interpolating from available observations. Simpler schemes may use a single

data type from many observational sources and employ a spline type method to fill in spatial gaps. For instance, based on data from the University of East Anglia HadCRUT temperature data set (Jones et al., 1999), Doran et al. (2002b) were able to use Cressman interpolation to infer temperature trends across the continent for the period 1966-2000. They reported cooling trends in East Antarctica in all seasons except spring, when a large amount of warming was seen on the East Antarctic coast, the Ross Sea, and parts of West Antarctica. Antarctic Peninsula temperatures were seen to rise in all seasons. Similarly, Chapman and Walsh (2007) produced a synthesis of Antarctic monthly temperature data from manned stations, AWS units, ships, and buoys, on a latitude-longitude grid, using the correlation length scale to determine the spatial extent to which observations could be interpolated. They reported an annual mean warming over the continent for the period of 1945-2002, but identify that trends are sensitive to start and end dates. On a seasonal basis, cooling was seen at the East Antarctic coast in summer, and reaching farther inland in the autumn. Warming was seen in winter and spring on the coast and hinterland, but cooling on the plateau. West Antarctica and the Antarctic Peninsula were seen to warm in all seasons. Monaghan et al. (2008) combined data from the READER database with gridded data from the the ERA 40 reanalysis. After computing linear regressions between observations and grid points, they generated continental maps of temperature trends at a $1^\circ \times 1^\circ$ resolution for 1960-2005. Correlation length scales were again used to limit the influence of individual observations. They found weakly negative trends in late summer and autumn of the 1970-2005 period, consistent with observed trends in SAM. Cooling trends were interspersed with some warming, which was particularly apparent on the Antarctic Peninsula. Warming was also observed in winter and spring, especially in the recent period and over West Antarctica. Steig et al. (2009) continued in this vein by using the Regularized Expectation-Maximum algorithm of Schneider (2001) to produce two reconstructions of Antarctic temperature trends from READER surface data; the first utilizing satellite temperature measurements and the second from AWS records. Results were generally similar to those of other studies. However, the authors reported trends in West Antarctica in all seasons except autumn that were positive and much larger than those previously reported. A critique of the paper was published by O'Donnell et al. (2011), who re-evaluated the technique using an improved analysis. They reported trends that were about half the magnitude of Steig et al. (2009), although in most seasons they were of the same sign. The large warming of the Antarctic Peninsula and West Antarctica was confirmed in spring and summer.

Thus, while it is generally agreed upon from observations, satellite analysis, and reconstructions that recent temperature trends in East Antarctica are generally negative and are caused by the trend of SAM towards its positive phase, and trends on the Antarctic Peninsula are positive and caused by a combination of sea ice retreat and SAM, both the trends and forcing in West Antarctica are subject to discussion. This is mainly due to the fact that West Antarctica represents a large region with little available *in situ* data. Byrd Station, the only manned base in the interior of the ice sheet was closed in 1972. In order to alleviate this problem, Shuman and Stearns (2001) attempted to reconstruct missing temperature records at four West Antarctic AWS sites using statistically calibrated satellite microwave brightness temperatures to fill in gaps. They found an insignificant warming at both Siple and Byrd AWS units, that matched well with other studies. Reusch and Alley (2004) also reconstructed temperature trends in West Antarctica from AWS records, using a neural network technique. Siple AWS was found to have a significant warming trend in summer from 1979 to 1994, while Byrd lacked a significant trend. The unexplained warming of West Antarctica in winter observed in satellite temperature measurements and ERA-40 reanalysis output was investigated by Ding et al. (2011). They found that a teleconnection in the ABS region to increasing central tropical Pacific sea surface temperatures was forcing a change in circulation in the area, advecting warm air south over the West Antarctic plateau. They further tied the

observed decrease in sea ice concentration in the Amundsen Sea to the influence of the teleconnection. Recently Bromwich et al. (2012) performed a further reconstruction of the temperature record at Byrd Station, using statistical interpolation of the ERA 40 and ERA Interim reanalyses to fill gaps in the observations. The calculation of the springtime linear trend resulted in a linear increase in temperature of $2.4 \pm 1.2\,^{\circ}\mathrm{C}$ between 1958 and 2010, establishing the region as one of the fastest warming places on Earth, although clearly the uncertainty on the derived trend is large. The authors implicated teleconnections to the tropics in their explanation of the trends. In particular, they highlighted the more in-phase activity of SAM and ENSO in the recent period as possibly causing the trends in spring and summer.

Associated with trends in Antarctic temperatures, and equally complex in terms of spatial and temporal variability, are trends in the sea ice that surrounds the continent for the majority of the year. The total extent of sea ice has been shown to have a small increasing trend, and the maximum extent on record occurred in the winter of 2012. Within this small upward trend however, is a signal of asymmetric change within the distribution of sea ice, to which the dynamical impact of changing circulation patterns have been shown to contribute. The fact that reliable large-scale sea ice data is unavailable before the satellite era means that these trends, and the mechanisms that have caused them have only recently come to light. Zwally et al. (2002) used 20 years (1979-98) of passive microwave observations to classify variability and trends within the sea ice distribution. They found that the extent of sea ice cover, defined as pixels containing at least 15 % sea ice had increased at a rate of $\approx 1\,\%$ per decade. However, after splitting the area surrounding Antarctica into sectors, they reported positive trends in the Ross Sea and strongly negative trends in the ABS in all seasons. They discussed the possibility of increased snowfall in driving the trend.

Given the impact that both SAM and ENSO have been shown to have on sea ice extent, it is natural to consider trends in these modes and their ability to force sea ice trends. Liu et al. (2004) assessed the sea ice distribution with reference to changes in these modes, and found that while their effects were large the extent of sea ice changes could not be fully attributed to them. Stammerjohn et al. (2008) assessed patterns in the advance and retreat of the sea ice, rather than its total extent. They found that in the Bellingshausen Sea ice is retreating sooner in the spring and advancing later in the autumn in recent years. Trends in the western Ross Sea showed the opposite tendency. The authors stressed the importance of the in-phase relationship of ENSO and SAM in recent years in forcing the pattern, through modulation of the ABS low. Turner et al. (2009b) showed that the increase of sea ice in autumn in the Ross Sea was caused primarily by increased cyclonic circulation in the region. They cited the non-annular structure of SAM and its increase in magnitude due to ozone forcing as the cause. Comiso et al. (2011) performed a thorough assessment of the impact of cyclonic circulation in the Ross Sea on sea ice in the Ross, Amundsen and Bellingshausen Seas. They found that the modulation of the ABS low by SAM and the Antarctic Circumpolar Wave (White and Peterson, 1996) had probably forced trends in the area. Shu et al. (2012) examined sea ice trends and sea surface temperature trends, and found a well-defined inverse relationship. Stammerjohn et al. (2012) discussed the differences in trends in the Antarctic and Arctic. Recently, Holland and Kwok (2012) described the increasing total trend in sea ice and analysed the impact of dynamic and thermodynamic changes in the atmosphere on sea ice production and advection. They found that the majority of variance in the sea ice distribution near West Antarctica was dynamically wind-driven, while elsewhere thermodynamic processes dominated. The mechanism behind such changes in circulation remains unclear.

Chapter 3

The climatology of the Ross Sea region of Antarctica as represented by a k-means clustering routine

3.1 Introduction

In this chapter we describe the development of a clustering routine to describe the climate of the wider Ross Ice Shelf region, using surface wind data taken from the ERA Interim reanalysis (1979-2011). A description of the ice shelf circulation is given in section 2.3. In essence, any clustering routine uses some metric to aggregate time instances that display atmospheric conditions considered similar. As such, the approach produces results that can be considered as a compromise between a meteorological case-study and long-period climatological means. The aim of this analysis is to reduce the complexity of the reanalysis output, but to retain a level of detail that is lost in a simple averaging exercise. The technique identifies the set of states (or clusters) that contribute to the mean and, through the investigation of the variability of individual cluster conditions, variability in the mean state can be better understood.

We employ the widely-used k-means clustering technique due to its speed and simplicity. In a similar vein, Sinclair et al. (2010) and Markle et al. (2012) used reanalysis output and k-means clustering to define tropospheric back-trajectory patterns for moisture transport terminating over several ice core locations in the vicinity of the RIS. While these studies used upper-level information, the focus of interest of our study is the surface climate, which is much influenced by the topography in Antarctica due to the high stability of air over the ice sheets (King and Turner, 1997), and as such we employ surface variables in our analysis. Further, while the back-trajectory approach is apt for study of air reaching a single location or small area, we focus on describing the circulation of a wider region. In this sense, our analysis is more similar to that of Seefeldt and Cassano (2008) and Seefeldt and Cassano (2012), both of whom employed self-organising maps (SOMs) (Kohonen, 2001) to describe the surface and near-surface wind regime of the RIS and environs using archived AMPS forecasts. However, due to the experimental nature of AMPS, these analyses were limited to short periods (five years). The results are thus not directly applicable to the study of longer term variability within the climate system. A logical step therefore, is to extend the analysis using a similar technique and a longer period dataset, in order to describe the climate and investigate changes in synoptic patterns due to internal variability. Although

we focus on a smaller region, the approach is also similar to that used by (Pohl and Fauchereau, 2012) to describe the Southern Annular Mode (SAM), and (Cohen et al., 2013) to describe the movements of the climatological pressure minimum in the Amundsen-Bellingshausen Seas. As such, this chapter details the application of the clustering routine, its results and a comparison to *in situ* data sources to demonstrate its validity. Subsequent chapters describe the employment of the results of this chapter to the study of climatic variability in the Ross Sea region.

This chapter is organised as follows: section 3.2 describes the data used in the analysis, which consists of a combination of reanalysis and *in situ* observational sources. Section 3.3 details the clustering technique employed to produce a synoptic climatology of the Ross Sea region. Section 3.4 reports on the initial results of the clustering algorithm, and represents a description of the climatology of the Ross Sea region, as depicted by the ERA Interim reanalysis. These results are discussed with reference to similar research and conclusions are made in section 3.6.

3.2 Data

3.2.1 ERA Interim reanalysis

We use gridded data from the ERA Interim reanalysis project (Dee et al., 2011). Reanalysis output is generated by a global atmospheric model, which is temporally consistent and guided via the assimilation of observational data taken from *in situ* and remotely sensed sources such as automatic weather station (AWS) units, ship and aircraft measurements, buoys, radiosondes and satellite sounders. The ERA Interim is an updated and improved version of the older ERA-40 reanalysis. In particular, the ERA Interim uses a 4DVar assimilation technique and has improved model physics.

Surface output of the ERA Interim is available on a $0.75\,^{\circ} \times 0.75\,^{\circ}$ grid between $87.75\,^{\circ}$N and $87.75\,^{\circ}$S at 6-hourly time intervals. The atmospheric model employed by the reanalysis has 60 vertical levels (Dee et al., 2011). We turn to the ERA Interim reanalysis as it provides consistent records of multiple atmospheric variables from 1979 onwards at time and spatial resolutions that allow us to investigate the synoptic climatology of the region for an extended time period. This is particularly important when studying the effects of the El Niño-Southern Oscillation, which oscillates on 2 to 10 year time scales (Trenberth, 1984), as for statistically significant conclusions to be drawn many instances of extreme warm (El Niño) and cold (La Niña) events must be included in the study period.

Being a relatively recent product, little research has been performed in validating the ERA Interim reanalysis at high southern latitudes. A full treatment of the accuracy of reanalysis is beyond the scope of this study. However, before using reanalysis output we perform a brief comparison of wind data to available automatic weather station (AWS) records in the Ross Sea region. This is discussed fully in section 3.2.3. Recent research has shown a high degree of accuracy in the ERA Interim surface wind field over the RIS (Rodrigo et al.). Nicolas and Bromwich (2011b) tested the ERA Interim in an accumulation study in West Antarctica and concluded that of all the datasets included, ERA Interim was the best at capturing accumulation in the region. The ERA Interim was also found to be relatively free of anomalous trends in meridional wind around the Southern Ocean, suggesting that the new reanalysis is not as subject to large spurious pressure trends in the circumpolar trough seen in earlier reanalyses (Bromwich and Fogt, 2004). This was confirmed by Bromwich et al. (2011), who concluded that of six global reanalyses studied, ERA Interim had the best representation of accumulation and pressure trends. Further evidence of the superiority of the ERA Interim was given by Bracegirdle and Marshall (2012).

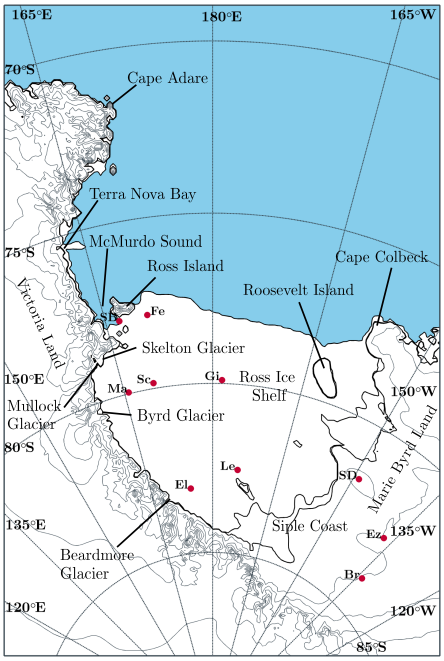

Figure 3.1: Map of greater Ross Ice Shelf and Ross Sea region. Sea is shown in blue and land and permanent ice in white. Ice cover around the sea margins is variable, such that depiction of the ice edge is approximate and for visual purposes only. Topographic contours shown are at 10 m, 80 m, 500 m and then every 500 m to 4000 m. Red dots show the locations of AWS units used in subsequent analysis. Abbreviations are listed in table 3.1. The location of Scott Base (SB) is also displayed as it is used in the ERA Interim-AWS comparison of section 3.2.3. Topographic data are sourced from the Radarsat Antarctic Mapping Project (RAMP) (Liu et al., 2001).

They compared ERA Interim output for surface temperature, MSLP and 500 hPa geopotential height (H500) to other reanalyses and records from Antarctic manned-stations between 1979 and 2008. Of all the reanalyses compared, the ERA Interim was found to have the highest correlations with surface temperature, and lowest decadal bias changes of MSLP and H500. Bracegirdle (2012) compared five reanalyses with independent drifting buoy MSLP measurements in the Bellingshausen Sea for the autumn and early winter of 2001. He reported that the ERA Interim was the most accurate of the reanalyses in terms of both the absolute pressure, and the pressure difference between buoys. The ERA Interim has been used previously at high southern latitudes by Schlosser et al. (2011), who investigated changes in sea ice in the Weddell Sea caused by enhancement of Rossby wave activity over West Antarctica, and Sinclair et al. (2012) who used reanalysis output to partially calibrate ice core proxy temperature records.

The rapid decrease in the distance between meridians at high latitudes means that the use of constant latitude-longitude gridded data in the Ross Sea region is not optimal. Thus, we bilinearly interpolate ERA Interim gridded data to a polar stereographic grid that encompasses the southern Ross Sea and Ross Ice Shelf and includes the western part of Marie Byrd land to the east and Victoria Land to the west. The extent of the region studied is shown in figure 3.1. Grid cells have sides of 40 km and represent an equal area over the entire domain. The grid has dimensions of 1440 km in the x-direction and 2120 km in the y-direction. At the latitude of 75 °S, which approximately bisects the region of our study, a

0.75 ° latitude-longitude grid cell has a north-south dimension of ≈ 80 km and an east-west dimension of ≈ 20 km. The latitude-longitude and stereographic grids then represent similar areal extents at this latitude.

We focus on surface variables from the ERA Interim reanalysis, such that they can be readily compared with *in situ* AWS records. We use the zonal and meridional wind components, which are given at 10 m above the surface, surface air temperature, which is given at 2 m above the surface, and mean sea-level pressure (MSLP). MSLP is considered accurate over the ocean and floating ice shelves. However, difficulties in interpolation to sea-level over land grid cells mean that MSLP is not representative of the pressure at these sites. Values of MSLP at these sites, particularly over the East Antarctic Plateau in the far south-west of the region, should then be interpreted with caution or disregarded. As shall be shown, the most salient areas of MSLP variability in the study region occur over the ocean and floating ice shelves. Data are acquired from 1979 to 2011, such that only complete years are included in the analysis.

3.2.2 Automatic weather station data

We use data from the automatic weather station (AWS) project of the University of Wisconsin, Madison. Over the course of several decades, a network of AWS units has been deployed over the Ross Ice Shelf for the purposes of meteorological and climatological study. A summary of the American Antarctic Program's AWS project is given by Lazzara et al. (2012). We focus on the long-term spatial variability of the near-surface wind regime, and therefore we use stations with the longest records available. All stations used are shown on the map in figure 3.1. In this map we also display the location of Scott Base, which is used to represent the area to the south of Ross Island in section 3.2.3. Wisconsin AWS records are provided at 10-minute intervals. We form 6-hourly time series by taking the closest available record to a particular hour within an hour-long interval. If no record exists within that hour then the record is deemed as missing. As the hostile environment encountered by AWS units in Antarctica can cause frequent failures and inaccurate data to be recorded, AWS records from the University of Wisconsin are quality controlled using a semi-automatic process prior to being made available online (Lazzara et al., 2012). However, despite automatic and semi-automatic quality control routines, it is still possible for anomalous data to exist in the records. Thus, we visually check all AWS records for anomalous values, trends or break points before using the data. Furthermore, as we plan to calculate long-term averages from AWS records, we operate a stringent data volume metric of allowing only months containing more than 90 % of usable data for a particularly atmospheric variable to be used in the analysis. This reduces the possibility of a month biased by a lack of data to further bias the long-term mean. A summary of the AWS data used in the study is given in table 3.1. We include information on the starting date and the number of records used in the cluster analysis in order to highlight the large volume of data available.

3.2.3 ERA Interim-AWS comparison

As there is little information on the ability of ERA Interim to reproduce accurate atmospheric information over Antarctica, we perform a brief intercomparison between *in situ* measurements of data taken from AWS records and reanalysis output. We collate time series from the reanalysis of those grid cells closest to AWS stations shown in figure 3.1. We interpolate ERA Interim 10 m winds to the nominal AWS wind vane height of 3 m using Monin-Obukhov similarity theory (Stull, 1988; Stearns and Weidner, 1993), with a constant roughness length of 10^{-4}m. Temperature and pressure records from Antarctic AWS units

Station name	Abbr	Altitude (m)	Start Year	No. records
Brianna	Br	525	1994	19125
Elaine	El	62	1986	25332
Elizabeth	Ez	519	1996	16819
Ferrell	Fe	45	1984	32165
Gill	Gi	53	1985	29276
Lettau	Le	39	1986	25575
Marilyn	Ma	62	1984	31990
Schwerdtfeger	Sc	54	1985	33883
Siple Dome	SD	668	1997	20383

Table 3.1: Metadata for AWS units used in the analysis of Ross Sea region circulation study. Stations are arranged in alphabetical order. Geographical locations are shown in figure 3.1. The start year is the year in which enough data is considered present to contribute to a long-term mean. All stations are maintained and records collated by the University of Wisconsin, Madison.

Station name	R_U	$\overline{\Delta U}$	R_u	$\overline{\Delta u}$	R_v	$\overline{\Delta v}$
Brianna	0.81	-0.63	0.84	0.89	0.65	0.25
Elaine	0.57	-0.04†	0.61	0.77	0.40	1.06
Elizabeth	0.76	0.04†	0.84	0.09	0.71	0.22
Ferrell	0.82	-1.49	0.71	-0.76	0.85	-1.10
Gill	0.63	0.41	0.54	-1.26	0.66	0.70
Lettau	0.74	0.28	0.75	0.24	0.79	0.24
Marilyn	0.69	-0.35	0.49	-0.78	0.68	0.36
Scott Base	0.45	-1.76	0.18	1.70	0.45	2.79
Siple Dome	0.52	0.28	0.67	-0.74	0.71	0.27
Schwerdtfeger	0.72	-0.21	0.52	-0.79	0.70	-0.10

Table 3.2: Wind speed comparison statistics for selected subset of Antarctic AWS units. Statistics are calculated only for times when AWS records are present. All wind speed values are given in ms^{-1}. All statistics are significantly different from zero at $p \leq 0.05$ using a 2-tailed Students t-test, except biases marked by †. Biases are calculated as ERA Interim - AWS.

are likely to pass the reanalysis quality control routines and thus these records will be assimilated into the ERA Interim system, which means that they are not totally independent. Accordingly, correlations between AWS temperature and pressure records and ERA Interim output are high ($\gtrsim 0.9$). Winds are not assimilated into the reanalysis, and as such we expect their correlations to be lower. Due to the focus of the study on the variation of wind patterns, in this section we will focus on a comparison of wind records. Correlations and biases are calculated between AWS data and reanalysis output for the entire time period of the AWS record. Results are shown in table 3.2.

Values of correlation of the scalar wind speed are consistently high across the AWS network. The lowest value is observed at Scott Base, which is in an exceptional location and discussed later. High correlations suggest that time variability in the strength of the wind is captured well in the reanalysis. Scalar wind biases tend to be small, and at some stations are not statistically different from zero. Brianna and Ferrell show high negative biases, that indicate that ERA Interim under-estimates the wind speed at these stations. A salient feature that remains unrevealed by either the correlation or bias statistics is that the distribution of wind speeds at AWS sites and ERA Interim grid cells is subtly different. AWS records tend to be variable, with large spikes during short periods and low wind speeds in others. ERA Interim winds are much smoother in time and lack extreme values. The result is that the mean wind

speeds are rather similar, despite the variance in the AWS wind speed being higher. Analysis of the variance shows that for the AWS sites shown in table 3.2, the observed variance is on average ≈ 2.5 times higher than that of the ERA Interim reanalysis. Stations with large magnitude biases tend to occur where winds are consistently strong and uni-directional. Speed distributions from these stations are skewed towards high values, and thus the AWS mean wind is significantly higher than ERA Interim. This is equally true of the biases for zonal and meridional components of the wind. Those stations where the wind is strongest and most highly uni-directional tend to have large biases. For instance, at Marilyn, Schwerdtfeger and Gill, ERA Interim shows zonal components that are too easterly (table 3.2), suggesting that the reanalysis does not capture the speed of the katabatic jet that often propagates from Byrd Glacier (Breckenridge et al., 1993). This effect probably occurs due to the difference in resolution between the two data sources. Firstly, AWS records represent point measurements, while the reanalysis model is likely to be smoother as it represents a much larger grid cell. Secondly, the topographic detail of the reanalysis is smoothed by the necessity of the grid employed, and thus it is likely that the reanalysis under-estimates the convergence, and subsequent strengthening, of winds caused by topographic channelling. Finally, the vertical resolution of the reanalysis may not adequately capture the present temperature inversion, meaning an under-estimation of the katabatic forcing would occur. Similar results were reported by Turner et al. (2009a) for the ERA-40 reanalysis. They concluded that, although the analysis captured synoptic variability well, the wind speed is often under-estimated if it is enhanced by localized topography.

Correlations of the zonal and meridional components are both relatively high, implying that the direction of the wind is captured well. The combination of high correlations and an under-estimation of the variance of the wind suggests that the ERA Interim under-estimates the strength of wind forcing, while estimating the direction of the forcing well. This may be expected in Antarctica, as the two dominant forcing mechanisms appear to generate winds that flow almost directly down-slope for the majority of the time (see section 2.2). This is confirmed by looking at the seasonal correlations and biases (not shown). Correlations do not show a large seasonal variation. In contrast, speed biases tend to be larger and more negative in winter and spring, when both katabatic and cyclonic forcing are strongest.

Scott Base is located in complex topography and localized flows in the north-west of the Ross Ice Shelf (see section 2.3). It is unrealistic to expect ERA Interim to be able to reproduce wind records in areas where flow is dominated by topography much smaller than the grid-spacing of the reanalysis. Correlations of the zonal and meridional components of the wind are predictably lower than the remainder of the AWS records and biases indicate that the direction of the wind is inaccurate. We include computed values from Scott Base however, to provide a comparison between this station and those on the ice shelf. The correlation of the scalar wind at Scott Base is still relatively high, suggesting that the large scale conditions influence the speed at Scott Base. This result and those described above indicate that the time variability of the large-scale forcing is captured well, even if the local-scale modulation of the wind is not resolved. This is important, as it suggests that the reanalysis is adequately reproducing the variation in the synoptic-scale pressure field.

3.3 Clustering technique

Due to its simplicity and speed, a particularly popular method for clustering is the k-means algorithm, which we also choose to employ. The algorithm proceeds by computing the Euclidean distance between

each instance of a particular field and centres of a series of predefined clusters. The cluster centre is defined as the mean of the instances that are designated as being within that cluster. The total Euclidean distance is minimised by including an instance into the cluster to which its Euclidean distance is lowest. This procedure is performed for every instance in the time series. The entire routine is then repeated, such that instances can be moved between clusters if they fall closer to another cluster centre than the one in which they currently reside. This occurs often, as cluster centres are updated according to new inclusions. The repetition continues up to the iteration in which no instances are moved between clusters. For time varying fields, in order to reduce the number of dimensions present in the time series, the clustering analysis is often performed on the most important principal components of the field rather than the field itself.

A notable caveat of the k-means algorithm is that the number of clusters (k) and an initial approximation of their centres must be specified in advance. The choice of these is highly non-trivial, as discussed at length by Christiansen (2007). A standard method for overcoming this problem is to seed the k-means routine with varied numbers of random instances as the initial clusters and repeat the routine a large number of times. A metric of the success of the clustering routine can then be used to determine how many clusters are present and which realization of the routine best represents the dominant modes. However, in order to better inform a first estimate of the number of clusters and their centres we choose to perform a simple hierarchical agglomerative clustering (HAC) routine on a subset of the ERA Interim output before running the k-means routine. The subset, which we will refer to as the "training" data, is necessary, as the HAC algorithm is computationally expensive to run on the entire time series (48,212 instances). The training data used in the HAC algorithm will determine the initial clusters of the k-means algorithm, in order to remove the initial uncertainty of the first-guess of the number and shape of clusters. As such, the data must be as representative of the time series as possible. We take a subset of data which is 1000 entries long and selected randomly from the entire data series. Once the HAC has defined the initial first-guess clusters the remainder of the data can be assigned to its closest cluster via the k-means algorithm. As the HAC is randomly seeded there is little *a priori* knowledge of the ability of the randomly selected data to represent the larger patterns. Thus, after choosing the number of clusters to be used, we run the algorithm a large number (100) of times and use the total sum of squared errors (defined as the mean Euclidean distance between each time instance and its associated cluster centre (Christiansen, 2007)), to choose the most representative of the cluster results. To reduce the dimensionality of the data we use the first 10 principal components of the scalar wind speed and the zonal and meridional components of the wind calculated over the greater Ross Sea region shown in figure 3.1. The inclusion of data of both the scalar wind speed and the directional components encourages the clustering algorithm to define clusters based on both the speed and direction of the wind. The first ten principal components of each wind time series constitute over 75 % of the variance contained within that time series. The HAC algorithm is described by Wilks (1995) and proceeds as follows:

1. The routine is initialized with each instance designated as an individual cluster;

2. The distance between each possible combination of two clusters is calculated. We use the weighted Euclidean distance in P dimensions. For two instances, i and j the Euclidean distance can be calculated as:

$$d_{i,j} = \left[\sum_{p=1}^{P} w_p \left(x_{i,p} - x_{j,p} \right)^2 \right]^{1/2} \tag{3.1}$$

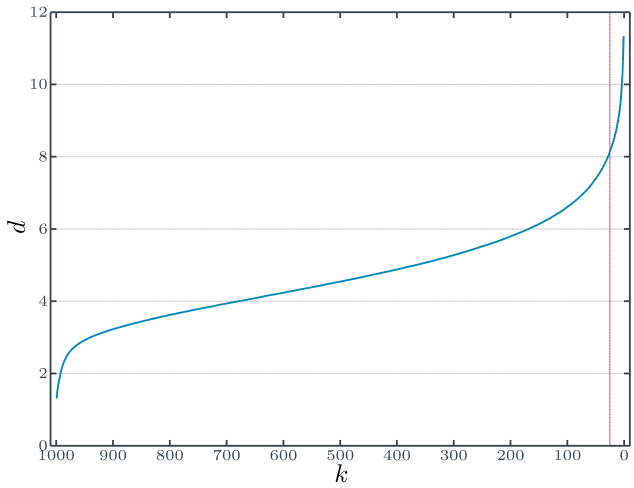

Figure 3.2: Weighted Euclidean distance between clusters as a function of the number of clusters. The vertical red line marks the $k = 25$ limit.

p designates the dimension, and P the total number of dimensions. w_p is the weight attributed to each dimension. Each principal component is weighted by the reciprocal of its standard deviation, such that each dimension has equal variance in the cluster algorithm. The normalization prohibits the algorithm from clustering solely on information contained within the first two or three principal components of the wind, which tend to have the highest variance.

For clusters containing more than one instance we use the average-linking technique. The distance between clusters is defined as the average distance over every possible combination of instances within those clusters. Hence, if cluster set s_1 contains n_1 instances and cluster set s_2 contains n_2 instances, then the average distance between the two clusters is:

$$d_{s_1,s_2} = \frac{1}{n_1 n_2} \sum_{i=1}^{n_1} \sum_{j=1}^{n_2} d_{i,j} \tag{3.2}$$

3. The combination of two clusters separated by the smallest Euclidean distance is grouped into a single, larger cluster;

4. The procedure is repeated until every instance is grouped into one cluster which contains the entire time series.

Of course, from a clustering perspective the start and end points of the algorithm are essentially useless. Having as many clusters as there are instances does nothing to reduce the data to an interpretable level, while obtaining one large cluster that represents the mean state of the region contains no information about the ability of the variables to change. It is important then, to stop the clustering algorithm when it reaches a number of clusters that is large enough to adequately describe the variability of the region, whilst being small enough that the number can be readily interpreted.

The advantage of initiating the k-means technique with the hierarchical scheme is that the latter provides a first guess at the number of clusters without having to perform a large number of randomly seeded cluster realizations. The Euclidean distance, d, generally increases as the number of clusters

decreases, as instances are grouped together which are increasingly less similar. It can then be viewed as a measure of the amount of information that is lost in every combinational step. If two similar clusters are combined then the Euclidean distance between them is small, which indicates that the amount of information lost when they are merged into a single cluster is also small. The cluster at which the gradient of d begins to increase dramatically can be used to inform the decision on how many clusters exist within the time series, as a large increase in d corresponds to a large loss in information when clusters are combined. A compromise must be made between the amount of information included in the clusters and the ability of the clusters to be interpreted. At this point, a subjective decision will always have to be made. However, the HAC algorithm provides a metric with which to inform this decision.

Figure 3.2 shows the mean development of d over the course of many realizations of the randomly trained HAC algorithm. d increases without exception over the routine. In the interval between $k = 25$ (marked in red) and $k = 1$ clusters the gradient of d rapidly increases, and thus we choose this interval to halt the clustering algorithm. The choice of one particular number (k) at which to halt the clustering is rather arbitrary, and thus we experimented with several values of k, in order to provide further robustness to the results. We choose values of $k = 24, 20, 16$, as values of k above this are considered too large for adequate interpretation of the clustering results and values below are considered too few to accurately depict the variability of conditions in the region.

In summary, the clustering technique first uses the HAC algorithm to gain information about the number of clusters contained in the data. From a large number of iterations of randomly trained HAC realizations we choose to investigate $k = 24$, $k = 20$ and $k = 16$ clusters. First-guesses from the HAC output are then used to seed a k-means algorithm that assigns the remainder of the data to one of the clusters defined by the HAC. This process is repeated a large number of times and the iteration that results in the lowest value of the total sum of squared errors is chosen as the most representative of the reanalysis output for each k. The results from the clustering routine are presented in the next section. We will focus on $k = 20$ clusters as results between different values of k tend to be similar.

3.4 Clustering results

Results from the clustering algorithm represent the climatology of the greater Ross Sea region as depicted by the ERA Interim reanalysis through broad-scale averaging of comparable synoptic conditions. By assigning each time-slice of the reanalysis data to a particular cluster, we are able to compile composites of mean conditions as depicted by that cluster. This provides the opportunity to view wind, MSLP anomalies and temperature anomalies for each cluster and further understand the forcing and influence of synoptic conditions on the surface atmosphere of the region. As the clustering algorithm focuses on the surface wind field, we first display mean wind conditions in figure 3.3. Arrows depict the wind direction, which is calculated as the resultant direction from the mean zonal and meridional wind components. Arrow directions are relative to the grid north of the polar stereographic map projection and are pointed in the direction in which the wind is propagating. The colour scale represents the mean wind speed, which is calculated as the resultant magnitude of the zonal and meridional components, for consistency with the direction. In each diagram, the topography of the Ross Sea region is overlaid to aid in interpretation. Topographic data is sourced from the Radarsat Antarctic Mapping Project (RAMP) (Liu et al., 2001). For clarity, we show only the 0 m, 10 m, 80 m and 100 m contours as they approximately depict the important features of the region. We also show mean composites of the MSLP in figure 3.4, which are particularly relevant to the wind field as the synoptic pressure gradient is the primary driver of the

synoptic wind conditions away from steep coastal slopes (Parish and Cassano, 2001; van den Broeke and van Lipzig, 2003). The MSLP is shown as an anomaly from the areal average, to highlight the pressure gradient rather than the absolute pressure. As has been demonstrated in the past (Seefeldt and Cassano, 2008, 2012; Cohen et al., 2013), we find that the surface wind field of the ice shelf and surrounding environs is highly dependent on the modulation of the background pressure gradient by the semi-permanent synoptic cyclone in the Ross Sea. Surface temperature anomalies for each of the clusters are shown in figure 3.5. Mean temperature anomalies are compiled from temperature data with the monthly climatological mean of each grid point removed, such that the anomalies represent the deviation during the cluster time-period from the mean temperature of the entire time period of the analysis. The process of calculating the anomaly also removes the seasonal temperature march, which would otherwise swamp the cluster temperature signal. To indicate the seasonal variation of the frequency of each cluster, we show bar graphs of frequencies as a function of the month in figure 3.6.

It is important before employing the clusters in further investigation of the Ross Sea region, to determine conclusively that the clusters described above fairly represent the synoptic climatology of the region, and that they represent statistically robust patterns that are not formed through chance combinations of the reanalysis output. To this end, we estimate the statistical significance of the anomaly of the wind, pressure and temperature from their mean values for each cluster. Significance is estimated via a two-tailed Student's t-test for each grid point in each cluster, to assess if that grid point shows a significant deviation from the mean for a particular cluster. We find that only the lowest magnitude anomalies are not significantly different from zero at $p \leq 0.05$ for all three variables. Thus, we choose not to display significance on the diagrams in this section as they are consistently significant. The high significance is at least partly a result of the long time series of the reanalysis output. We analyse 33 years of 6-hourly output, resulting in a time series that has a total of 48,212 members. Even a relatively infrequently occurring cluster, for instance (1,4) with 3.15 % total occurrence, will then have over 1500 instances associated with it. Even a small deviation from the total mean value is then likely to be highly significant.

We further assess the robustness of the clusters by estimating the significance of the difference between clusters, by using Hotellings T^2 test (von Storch and Zwiers, 1999). For a clustered variable X with dimensions p and two clusters i and j, the Mahalanobis distance is given by $D^2 = (\overline{X}_i - \overline{X}_j)^T \mathbf{S}^{-1} (\overline{X}_i - \overline{X}_j)$, where S is the pooled covariance of the two cluster sets: $\mathbf{S} = ((n_i - 1)\mathbf{S}_i + (n_j - 1)\mathbf{S}_j)/(n_i + n_j - 2)$. $\mathbf{S}_i$ and $\mathbf{S}_j$ are the covariances of the sets of clusters i and j, respectively, and n_i and n_j are the number of instances in each cluster. Assuming mutivariate normality, under the null hypothesis that the means of the two clusters are identical, the test statistic $T^2 = cD^2$ follows an F-distribution with degrees of freedom p and $n1 - n2 - p + 1$, where $c = (n_i n_j (n_i + n_j - p - 1))/((n_i + n_j)(n_i + n_j - 2)p)$. We are thus able to test the statistical significance of the distance between each combination of two clusters for each variable. We find that for all variables, the clusters are significantly different from each other at $p \leq 0.05$, indicating that the clustering algorithm is grouping instances in a statistically robust manner.

In order to aid understanding of cluster conditions, and in particularly, which clusters are most similar to each other, we arrange clusters into a 6×4 grid. From observation of figures 3.3 and 3.4 it is apparent that the winds of the region are highly dependent on the pattern and gradient of the pressure in the Ross Sea and over the ice shelf, as is to be expected. We thus determine the location of each cluster within the grid by the pressure conditions rather than by the wind, as it represents a slightly less complicated mean field. The position of each cluster is established by two measures of the strength of the effects of pressure minima over the sea and ice shelf. The first measure, which determines the location on the

x-axis, is the angle of the line linking the maximum and minimum pressure, measured clockwise from the y-axis. Clusters on the left of the diagrams show pressure minima in the north-west. These minima then move in a south-easterly direction towards the right of the diagram. Subsequently, clusters are located on the y-axis depending on the mean pressure gradient between the minimum and maximum MSLP. Clusters are arranged such that the strongest gradients are at the top and decrease downwards. It is important to note that clusters are arranged for their angle before their pressure gradient, and thus the pressure gradient is not entirely constant across the diagrams. Further, the arrangement process attempts to project a multi-dimensional field onto two axes, and thus is subjective and approximate, and for display purposes only. However, the resulting configuration of clusters appears to ensure that similar clusters are near each other, both in the x- and y-axes. Gaps are left in the grid in places where no cluster appears to fit. Plotted underneath each cluster diagram in figures 3.3, 3.4, 3.5 and 3.6 are the numbers (i, j), where i corresponds to the row and j to the column. Also shown is the frequency of the cluster, calculated over the entire range of the ERA Interim output employed (1979-2011).

The further grouping of clusters is a subjective exercise. However, from the ordering process described above, five larger groups of clusters become apparent. These groups are indicated in figures 3.3, 3.4 and 3.5 by grey boxes. At the bottom-left corner of each box is the name of the group. We will address each group in turn and discuss the differences and similarities between and within groups.

The first group depicted in figures 3.3 and 3.4 contains clusters that represent deep pressure minima in the north of the domain, and includes clusters (1,2), (1,3), (2,1), (2,2) and (2,3). This group is designated as the Strong Northern Cyclonic (SNC) group. As described above, pressure minima are located to the north-west on the left and move towards the east and south to the right. The wind induced by these lows is clearly highly dependent on the position of the low pressure centre (cf. figures 3.3 and 3.4). Geostrophic theory dictates that air will circulate clockwise around a low pressure region in the southern hemisphere. Thus, we observe southerly flow on the west side of the low and northerly to the east. The left side of the group (clusters (1,2), (2,1) & (2,2)) shows easterlies only in the north of the domain, with a peak in the north-west, where air converges around Cape Adare, and a jet is formed. The position of its peak wind speed changes in line with the movement of the pressure trough. Buzzi et al. (1997) analysed this feature from model output and determined that it constituted a tip-jet protruding from a barrier flow caused by the flow damning cold air against the Admiralty Mountains, at the northern tip of the Transantarctic Range. The authors noted that at the time of writing there was little observational evidence for the phenomenon, although it seems to be confirmed by the ERA Interim reanalysis, and also appears in several of the composites of Seefeldt and Cassano (2012). Winds over the ice shelf in these clusters tends to be low, but appears to be slightly higher in the second row, probably because of the alignment of pressure contours being more south-north in the lower diagrams. Conversely, (1,2) shows quite constant pressures from east to west across the shelf. Katabatic drainage over Victoria Land occurs in each of the clusters, and drainage is observed in clusters (2,2) and (2,3) over West Antarctica, perhaps aided by the synoptic gradient.

In clusters (1,3) and (2,3), which have pressure minima farther to the south (fig. 3.4), the flow on the westward flank of the trough appears to be generally stronger, as the northward moving air converges into the region over the sea between the Transantarctic mountains in northern Victoria Land and the low pressure centre. It is possible that the flow over the Ross Sea to the west of the cyclone constitutes a barrier wind regime. Similar structures in the area can be seen in the SOM of Seefeldt and Cassano (2012). Winds over the ice shelf are also heightened towards the north-west, in line with the pressure gradient. There is an area of low winds speeds, however, at the south-west of the ice shelf, against the

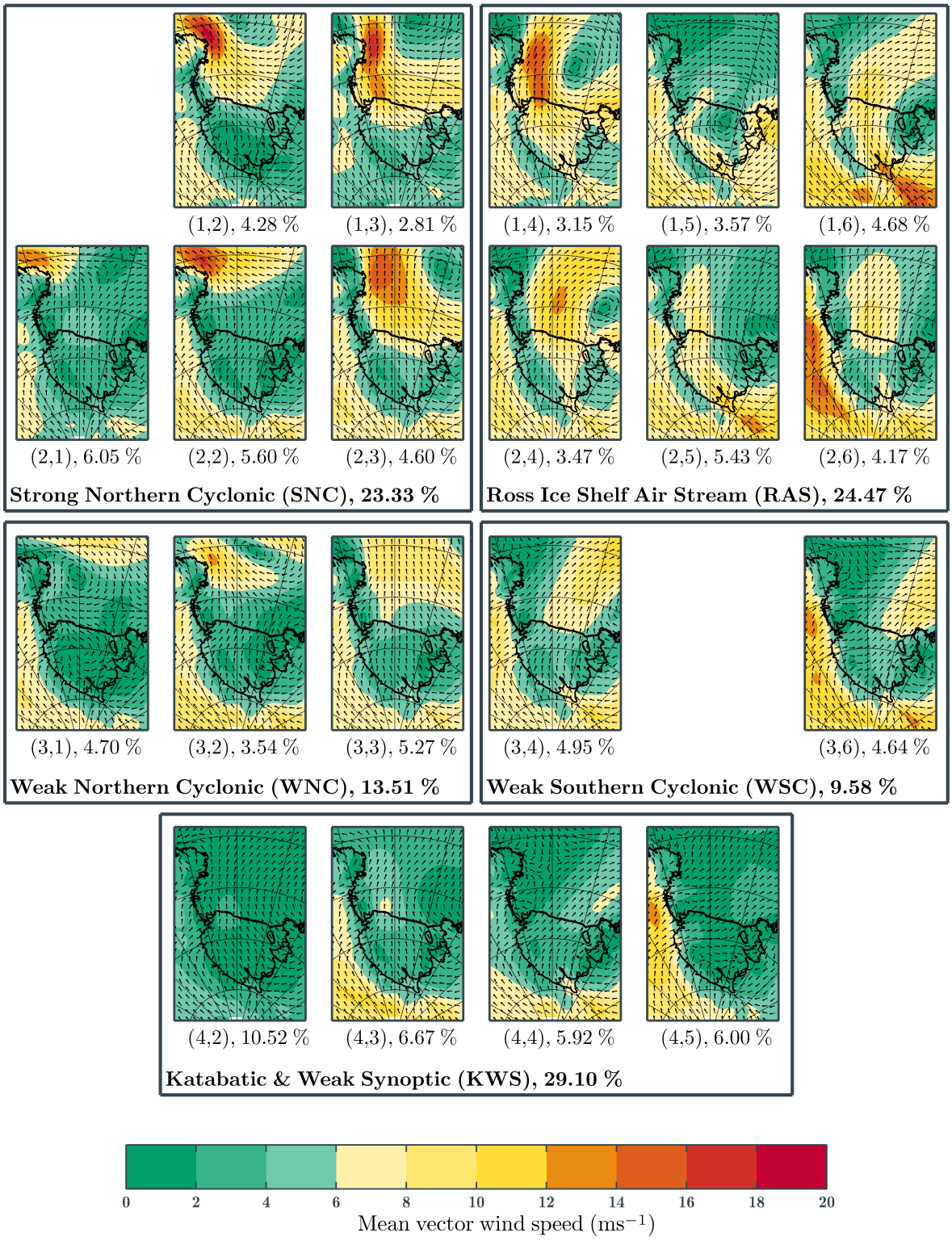

Figure 3.3: Ross Sea region clusters, surface wind speed and direction. Direction of arrows indicates direction in which wind is flowing. Arrows are plotted relative to grid north. Background colour represents the mean vector wind speed. Percentages under each diagram display the total frequency of the particular cluster. Bracketed numbers, (i,j), indicate i: row; and j: column. Topographic contours shown are at 0 m, 10 m, 80 m, and 100 m.

Transantarctic Mountains. Stronger winds tend to cross the centre of the ice shelf, but also propagate towards the north-east from Byrd Glacier. (2,3) shows more drainage over the ice sheets than (1,3), perhaps because of the position of the pressure minimum slightly farther east and the pressure contours being aligned south-north across the shelf.

The SNC group displays a distinct temperature signature (fig. 3.5). In all clusters in this group there appears to be a temperature anomaly dipole between northern and southern parts of the domain. We assume this to be caused by the effects of heat advection. Thus, the peaks of the dipole move depending on the areas of advection, which are in turn dependent on the wind direction and speed. Northerly winds on the eastern flank of the pressure minima advect warm air to the south, which is apparent by the regions of positive temperature anomalies in figure 3.5. Corresponding southerly winds on the western flank cool the ice shelf and ocean. The position of the minima in the far north of the domain in clusters (2,1) and (2,2) means that positive temperature anomalies are also confined to the north, while weak drainage from the ice sheets appears to cool the coastal slopes and ice shelf. Strong winds over the Ross Sea in the ice-covered seasons may also break sea ice and thus increase heat transfer from the ocean to the atmosphere, which may provide a further explanation for the warming associated with these clusters. On the ice shelf, the coldest clusters appear to be those with enhanced drainage from East Antarctica. Air originating in this region is likely to be cold (see section 2.4). Further, it is in areas of weak winds on the shelf that the surface temperature is lowest, suggesting that stronger winds may counteract surface cooling. This mechanism will be discussed in some detail later. The area of warm anomaly in cluster (1,3) is particularly large, reflecting the slight south-west to north-east slope of the pressure contours in the west of the domain.

Frequencies of this group indicate that the incidence of deep cyclones in the Ross Sea is quite common. Seasonal variation is also apparent from figure 3.6. Cluster (1,2) shows a peak in late summer and early autumn and a slight decrease in December and January, but is relatively constant in other months. (1,3) has peaks in the summer and mid-winter, but troughs in the transition seasons, while (2,1) shows troughs in the winter months. (2,2) is least frequent in summer and has peaks in transition months, suggesting a semi-annual component (Meehl, 1991; Simmonds and Jones, 1998; van den Broeke, 1998a). Finally, (2,3) has dips in frequency in the summer, but is relatively constant throughout autumn, winter and spring.

To the right of the SNC group is that of the Ross Ice Shelf Air Stream (RAS). We define RAS events by the presence of higher than average winds propagating along a corridor from the Siple Coast to the northern extent of the ice shelf. Of course, the distinction between this group and the previous is arbitrary, and several elements of the air stream exist within clusters on the right hand side of the SNC group. For instance, both clusters (1,3) and (2,3) show slightly heightened winds propagating from the Siple Coast to the ocean. However, these winds are not consistently above the average for those regions, and so these clusters are not included within the RAS group. Clusters immediately below the RAS group also show some elements of RAS, which will be discussed later.

As in the SNC group, each of the RAS group clusters displays a distinct pressure minimum in the domain. In the top-left of the group (fig. 3.4), this minimum is situated directly to the north of the ice shelf. The pressure minimum moves south-east and weakens from left to right and top to bottom, respectively. Thus in the top right of the group, a deep pressure minimum is observed over Marie Byrd Land. Cluster (1,5) shows a pressure minimum centred on the ice shelf itself. The position of this low is reminiscent of that discussed by Steinhoff et al. (2008), for an exceptionally strong wind event at McMurdo Sound in 2004.

The RAS signature is clearly visible within the wind diagrams (fig. 3.3). A low-level jet can be

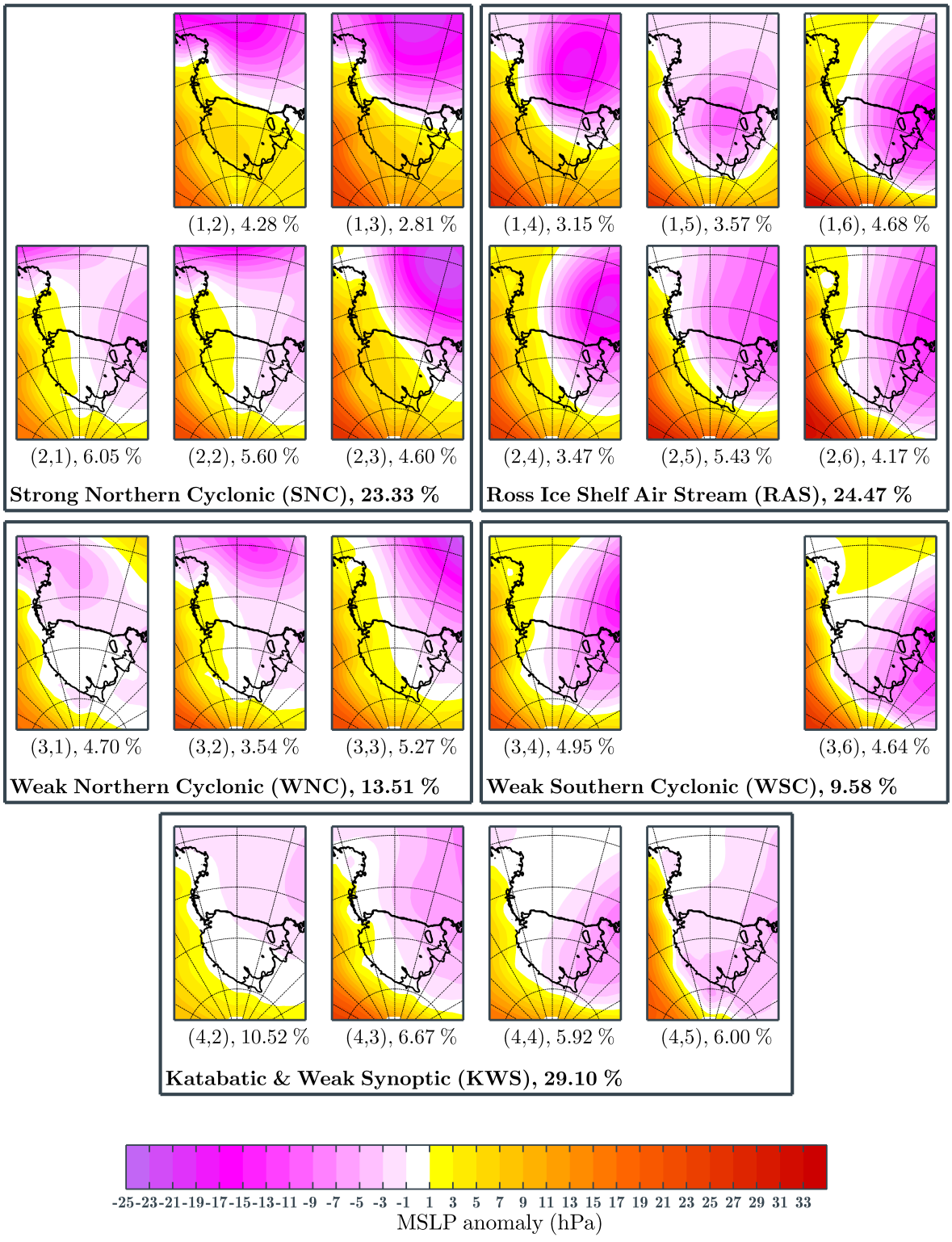

Figure 3.4: Ross Sea region clusters, MSLP anomaly. To highlight the importance of the pressure gradient, rather than the absolute pressure, MSLP diagrams are displayed as anomalies from areal means. Percentages under each diagram display the total frequency of the particular cluster. Contours shown are at 0 m, 10 m, 80 m, and 100 m. Bracketed numbers, (i,j), indicate i: row; and j: column.

observed propagating from the Siple Coast, parallel to the Transantarctic Mountains across the ice shelf, turning northwards near the coastal margin and becoming north-easterly over the sea, in line with the synoptic pressure gradient and steep topography of the mountain barrier. In clusters where the pressure minimum is located towards the east, there may also be an area of weak winds against the Transantarctic Mountains, such as in clusters (2,4) and (1,6). The shape and general features of the jet are similar to the thermal infrared wind signature shown by Bromwich et al. (1992) and Carrasco and Bromwich (1993b). The pattern was interpreted as a katabatic surge that propagated across the ice shelf forced by a synoptic pressure gradient, which appears to be essentially equivalent to the conditions displayed here. Clearly, as the synoptic forcing becomes greater both the speed and the width of this jet increase and the areas of strongest winds are clearly affected by the position of the maximum pressure gradient. Clusters on the left have the peak wind over the ocean near Victoria Land, similar to the SNC clusters in their vicinity. In group members to the right, we observe strong winds near the Siple Coast that appear to be enhanced by the synoptic gradient over West Antarctica as discussed by Bromwich et al. (1994), Bromwich and Liu (1996) and Liu and Bromwich (1997). Bromwich et al. (1994) found in particular that the synoptic pressure gradient was important to the forcing of winds on the Siple Coast, which is less steep than slopes farther into the interior of West Antarctica, and thus more readily influenced by cyclonic activity. We find similar results, with the cyclone forcing stronger winds with an enhanced down-slope direction. The location of strongest winds upwind of the Siple Coast at around 130 °W, 85 °S is equivalent to that seen by Seefeldt and Cassano (2008). On the ice shelf the jet is further fed by drainage from glaciers along the Transantarctic Mountains, which is particularly apparent in cluster (2,6). Also observed is drainage through glaciers in the hinterland of Terra Nova Bay, as previously reported by Kurtz and Bromwich (1983), Bromwich (1989b) & Cogliani et al. (1996).

These conditions are broadly similar to those designated as RAS events by Parish et al. (2006) and Seefeldt and Cassano (2012). Synoptic conditions are also similar to those shown by Steinhoff et al. (2009) for similar winds. These authors found that upper level pressures favoured the generation of a barrier wind along the Transantarctic Mountains that reinforced the flow at lower levels. Further evidence for this effect was provided by Seefeldt et al. (2007), although from these composites alone and without upper level information, it is difficult to tell if the mean conditions presented here constitute a barrier wind regime. Clusters which do not show strong winds in the vicinity of the mountains are unlikely to be affected by barrier flow forcing.

The RAS group shows much stronger winds over the Siple Coast than the SNC, presumably due to the reinforcement of katabatic winds by the synoptic pressure gradient. The stronger synoptic gradients over the ice shelf in the RAS group are especially relevant for the climatology of the domain, as the turbulent vertical mixing of air within the region of strong winds can transport air from upper layers downwards, effectively breaking the semi-permanent temperature inversion (Carrasco and Bromwich, 1993b; Vihma et al., 2011). This is apparent in figure 3.5. Marked temperature contrasts can be seen between the regions of slow (cold) and fast (warm) moving air on the ice shelf. In clusters (1,4), (1,5), (1,6) and (2,5), heightened temperatures are observed over almost all of the ice shelf and grounded ice sheets. Clusters (1,6) and (2,5) in particular show a warm tongue that follows the winds as they propagate from the Siple Coast along the Transantarctic Mountains, reaching as far as Ross Island and the south-western Ross Sea (over 1000 km distant). The winds in this region may also act to transport warmer air from West Antarctica across the ice shelf. The size and shape of the tongue is highly reminiscent of the thermal infrared images of Bromwich et al. (1992), Bromwich et al. (1993) and Carrasco and Bromwich (1993b). Warm temperatures over the elevated regions are perhaps also caused by a combination of warm air

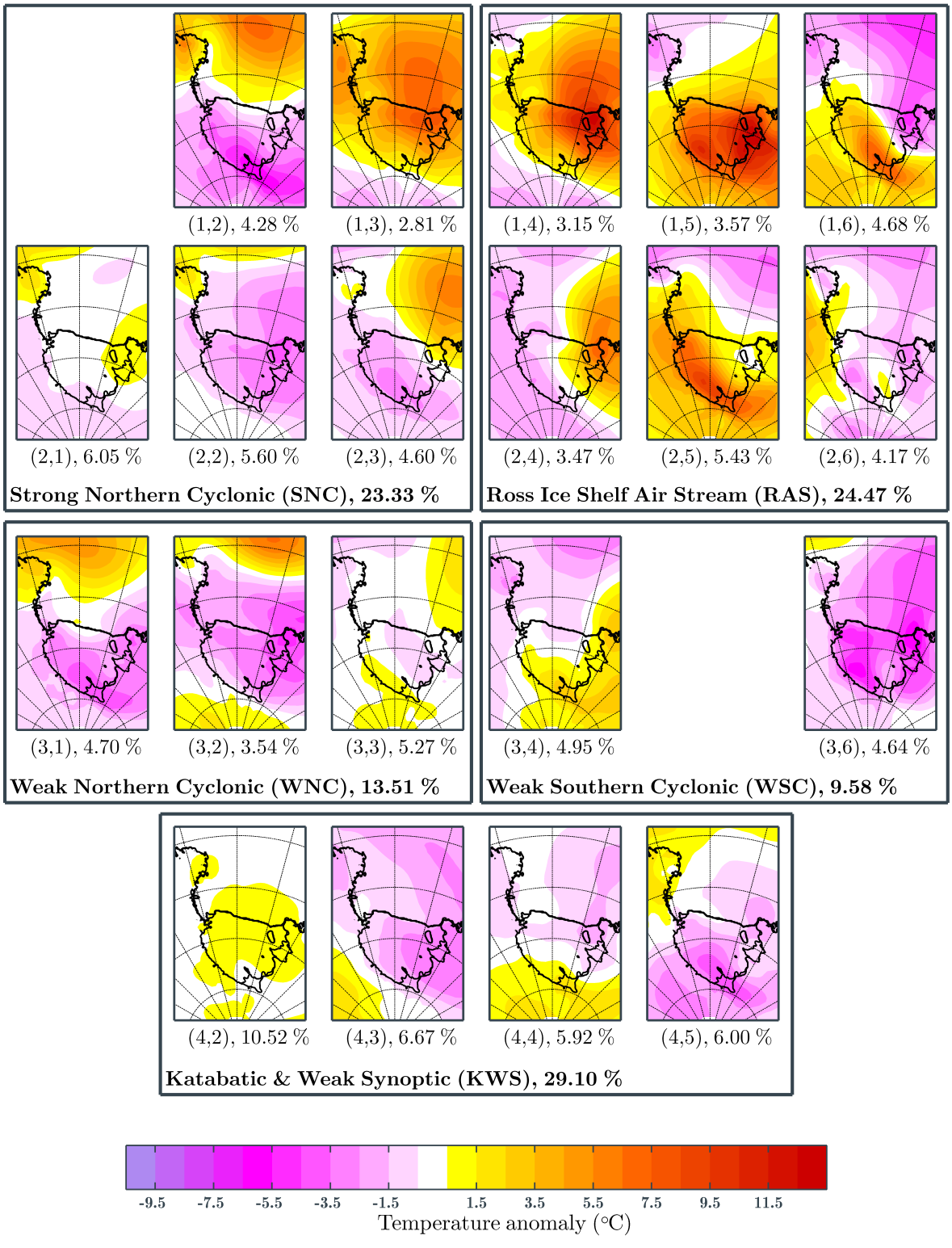

Figure 3.5: Ross Sea region clusters, as in figure 3.4, but for temperature anomaly.

advection and potentially increased vertical mixing due to the strong winds. The adiabatic heating of descending air is also likely to contribute. The strongest positive temperature anomalies are seen in cluster (1,5) over the north-east Ross Ice Shelf and surrounding coast. The large warming is probably

caused by the advection of warm, maritime air due to the location of the cyclone in the centre of the ice shelf to the west. Figure 3.3 shows strong northerly winds in this area. It should be noted, however, that these conditions are relatively rare. In general in the RAS group, temperatures over the sea are decreased, corresponding to the advection of colder ice shelf and continental air from the south. However, this is not true of cluster (1,4), which shows increased temperatures over the sea due to the position of the pressure minimum and associated warm air advection. Clusters (2,4) and (2,6) show cold pools in the west of the ice shelf, which form where the winds are observed not to be strong. The pool may be associated with colder air draining from East Antarctica.

Frequencies of this group (figure 3.6) show a marked sharpening of peaks from left to right. Peaks on the right hand side tend to occur slightly more often, but are heavily skewed towards the late winter. On the left, the total frequency is slightly reduced and the frequency is more evenly spread throughout the year. This suggests a modulation of the forcing of RAS events between different seasons, with more northern cyclonic systems generating RAS events in the summer, while more southern systems tend to generate RAS in the winter. Clusters (1,6) and (2,5) also show a semi-annual component consistent with heightened baroclinic conditions in the southern ocean in the transition months and a corresponding southward shift of the circumpolar trough (Meehl, 1991; Simmonds and Jones, 1998; van den Broeke, 1998a). Comparison of the seasonal frequencies of the RAS clusters with those of the self-organising maps (SOMs) of Seefeldt and Cassano (2012) (SC12) indicates a general agreement between studies in the seasonal variability. Following SC12, we discuss seasons organised into summer (DJ), autumn (FMA), winter (MJJA) and spring (SON), which depict the *coreless* winter cycle of the Antarctic (see section 2.5). The sum over RAS clusters shows a low incidence during summertime (9.57 %), which is consistent with the results of SC12. In the winter, we find a RAS frequency of 33.56 %, which is considerably smaller than that reported by SC12 (71 %), although the large increase from summer to winter is consistent between studies. This may occur due to a slightly different definition of RAS. SC12 designate their nodes as belonging to RAS if there is present a "pronounced corridor of atmospheric mass transport northward across the Ross Ice Shelf and Ross Sea from the continental interior." Our definition of RAS is similar, but with the extra criterion of the wind speeds being consistently above average within the corridor. If we further include those clusters which show RAS elements, but without higher than average wind speeds ((1,3), (2,3), (3,4) & (3,6)), then the wintertime frequency increases to 53.82 %, which is still lower than that of SC12. We suggest that the difference arises due to the SOM of SC12 being generated from the 5th lowest AMPS model level ($\sim$ 150 m), where wind speeds are likely to be stronger than those at the surface. Thus, it appears that the RAS is a more common occurrence above the surface in the wintertime. We find a higher frequency of RAS events in the springtime (29.03 %) than in autumn (17.62 %), which is consistent with the result of SC12 that cyclones in the Ross Sea occur more often in the spring.

The left-hand side of row three contains the group designated as Weak Northern Cyclonic (WNC). These clusters have much in common with the group above them, except that the pressure minima contained in the lower group is often located farther north, and thus affects the ice shelf to a lesser extent (see fig. 3.4). In general there exists a north-south directed pressure gradient, manifested as an intrusion of the circumpolar trough into the far north of the domain. The intrusion of the gradient induces easterly winds to the south of the pressure trough, and, where the trough intrudes farther south, westerly winds to the north (fig. 3.3). Northerly winds are also observed to the east, which are important for the advection of heat over the ocean. Westerly winds in the north are particularly apparent in clusters (3,1) and (3,2). The pressure minimum in cluster (3,3) is located much farther to the east, and

the corresponding wind shows strong southerlies and south-easterlies over the sea. Katabatic drainage appears to dominate in the south of the domain and synoptic pressure gradients in this region tend to be weak, but increase from east to west. Accordingly, these clusters tend to have weak winds over the ice shelf, and in (3,1) in particular they are variable in direction.

Temperature anomalies show a similar pattern to the SNC group, with increases in temperature in regions of northerly winds, and cool temperatures over the ice shelf and ice sheets, due to the katabatic movement of cold air north. Cold pools suggest that these flows are not strong enough to vertically perturb stably stratified air on the ice shelf. The seasonal frequency variability of this group varies across the members. (3,1) shows an erratic distribution with peaks in early autumn, winter and spring. (3,2) is somewhat similar, but with a larger reduction in frequency in summer, giving it an apparent semi-annual signal. (3,3) peaks in autumn but is quite constant throughout the remainder of the year.

The right-hand side of row three contains Weak Southern Cyclonic (WSC) clusters. These clusters represent a continuation of movement of pressure minima in the WNC group towards the south-east. The position of the pressure minimum also dictates that they have much in common with the RAS clusters, situated above this group. However, the pressure gradient over the ice shelf is weaker in these clusters (fig. 3.4), and thus winds are also weaker (fig. 3.3). Some heightened winds over the shelf are observed, particularly to the east, but these winds are not consistently above the average for those areas, meaning that these clusters do not meet the RAS requirements. Katabatic drainage is observed in both clusters, and is particularly strong in (3,6). This cluster also shows a stronger area of winds over the Siple Coast, presumably due to its pressure minimum being situated farther south relative to (3,4) (see fig. 3.4).

Temperature anomaly composites within the WSC group differ greatly. (3,4) shows warm anomalies in the south-east of the domain and cold anomalies in the north and west, which is similar to many of the RAS clusters, and appears to occur due to the synoptic forcing of drainage from West Antarctica. (3,6) shows deep cold anomalies across the ice sheets and ice shelf, with a small warm anomaly in the north-west. It is much more similar to clusters on the fourth row, located below it. It is possible that the cold anomalies on the ice shelf in the right-hand cluster are caused by the strong drainage from the East Antarctic ice sheets, which appears to be aided by the pressure gradient across the ice shelf (fig. 3.4). Winds on the shelf do not appear to be strong enough to thoroughly mix the boundary layer, and hence the surface is quite cold. Note that temperatures are not as cold in regions where winds are stronger, such as on the east side of the shelf, where a corridor of flow is seen from the Siple Coast. This may be due to turbulent vertical advection in these regions, or simply because air draining from West Antarctica is warmer than that from East Antarctica. The large difference in temperature reaction serves to highlight the sensitivity of the domain to slight changes in circulation, as the synoptic pressure aspects of these clusters are similar. Frequencies of these clusters are higher outside of summer, and a slight semi-annual component can be observed in cluster (3,4).

The final group of clusters includes the entire fourth row of figures 3.3, 3.4 and 3.5. This group contains wind and pressure conditions that depict katabatic drainage from the East Antarctic plateau, through glacial valleys in the Transantarctic Mountains. Some weak synoptic forcing is also apparent, with marginally lower pressures observed in the east of the domain, which acts to propagate flows across the ice shelf. Hence, this group is designated as the Katabatic and Weak Synoptic (KWS) group. Cluster (4,2) shows calm conditions and a weak pressure gradient directed from east to west. Slightly stronger southerly winds are seen in the far south-west of the region that are probably katabatic in origin. Winds turn to the east as they reach Victoria Land due to topographic channelling. (4,2) represents times of the lowest wind speed in the region. It occurs over 10 % of the time, but is mostly confined to

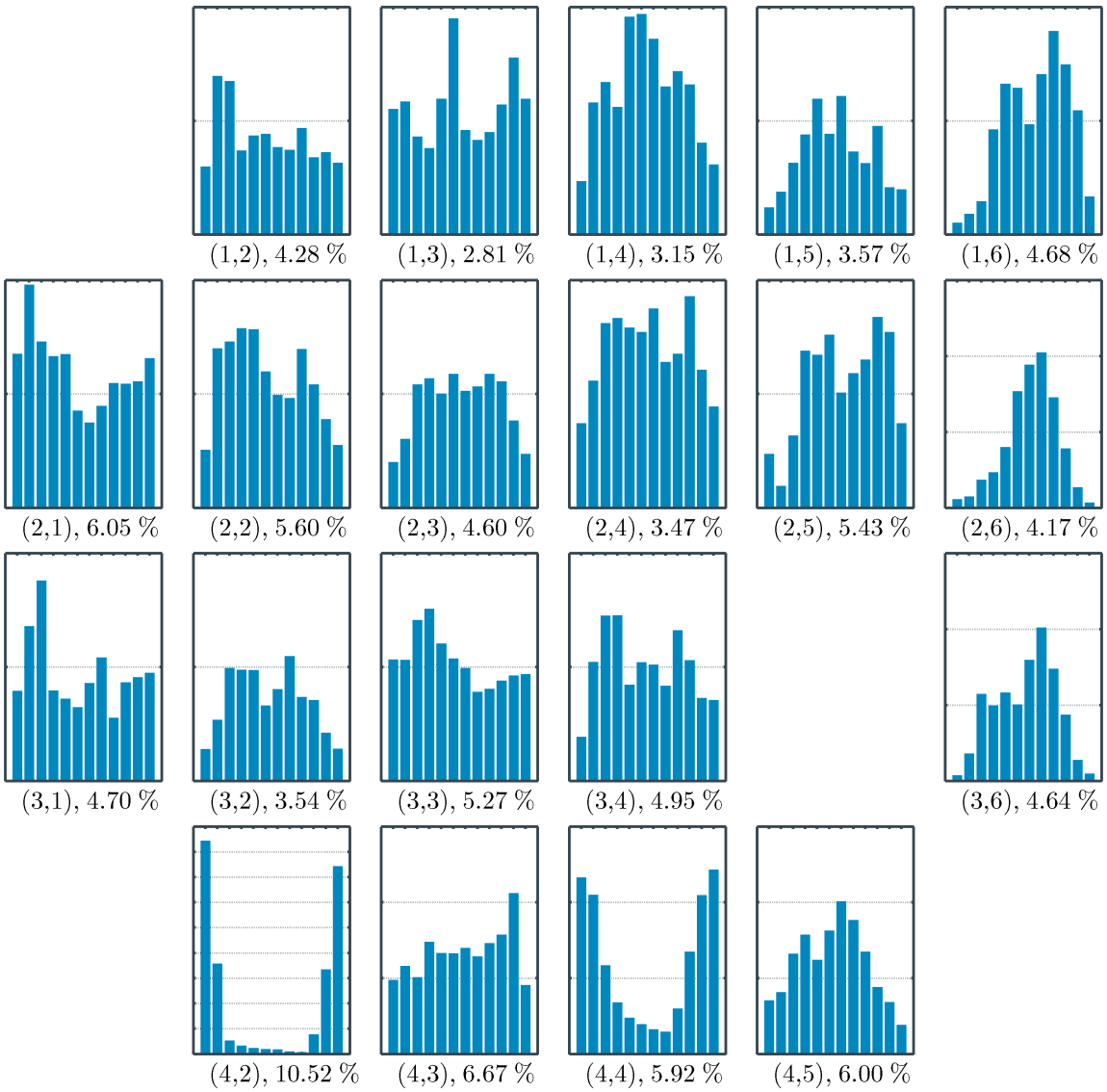

Figure 3.6: Ross Sea region clusters, monthly frequency. For clarity, axes labels are not shown. Months are shown on the x-axis from January to December. Frequency for the month is shown on the y-axis, with each increment representing 5 % of total occurrence.

the summer months, early autumn and late spring due to the decrease of both katabatic and synoptic forcing in the warmer months (figure 3.6). Winds in cluster (4,3) are increased across the south of the domain into Marie Byrd Land in West Antarctica, in line with the shape and depth of the pressure gradient. The strong barrier effect of the Transantarctic mountains is apparent in this cluster, with the wind propagating onto the ice shelf through only the glacial valleys such as Byrd, Skelton and Mullock Glaciers to the south of Minna Bluff. Other intrusions can be seen through Beardmore Glacier, at the south of the Siple Coast and over the Drygalski ice tongue in Terra Nova Bay. These are all areas that have been highlighted in previous studies as katabatic confluence zones (Parish and Bromwich, 1987; van Lipzig et al., 2004; Parish and Bromwich, 2007). Drainage onto the ice shelf through these channels can also be observed in many clusters outside of this group. Stronger winds do not propagate far from the

mountains, presumably due to the loss of the katabatic forcing over the flat ice shelf and the lack of a strong synoptic gradient. There is however, an area of heightened winds in the western Ross Sea, that appear to be synoptically driven. Interestingly, a calm area is observed in the lee of Ross Island. Similar conditions prevail in cluster (4,4). However, in this cluster stronger winds are observed in the east of the domain and directed to the north-east, consistent with the observed pressure gradient. Winds in cluster (4,5) are similar to others in the group, but show areas of stronger winds in Victoria Land, particularly upwind of Terra Nova Bay.

Temperature anomalies in this group follow the broad patterns described previously. Cold anomalies are observed in regions where southerly winds transport polar air northwards. Warm anomalies are also seen in the areas of strongest winds, which may be associated with down-slope adiabatic heating or mixing within the boundary layer.

Frequencies of these clusters indicate that they are common, although some disparity exists in their seasonal aspect. As mentioned earlier, (4,2) is almost wholly confined to the summer months. The same can be said of (4,4). (4,3) seems well spread across the year, but has a peak in November. Finally, (4,5) shows a peak in winter, which is consistent with the strong katabatic winds depicted by the cluster.

3.5 AWS comparison

To demonstrate further the validity of the derived clusters, we show in figure 3.7 composites of temperature derived in the manner of figure 3.5, but for AWS data described in section 3.2.2. To compute these means, we take 6-hourly AWS data and remove the climatological monthly mean, similar to the previous temperature diagram. However, for AWS data the procedure is complicated by the existence in the dataset of large amounts of missing values. In order to minimise biases due to the inclusion of months with missing data, after the quality control routine is performed, entire months are removed if they have fewer than 90 % of their data present. In order to ensure that a truly representative mean is calculated we also do not allow the calculation to be performed for a month if fewer than ten of those months are present in the AWS record. The records for AWS units shown in figure 3.7 all fit these criteria, and thus we are able to compute representative cluster composites for these locations. It should be noted that the temperature scale in figures 3.5 and 3.7 are equivalent, and so the two diagrams are directly comparable. The names of the AWS units are shown in the map in figure 3.1. They are not plotted on the temperature diagrams for clarity.

Temperature anomalies seen at AWS sites are consistently significant at $p \leq 0.05$. Anomalies that are significant at this level are marked with a cross. Temperature anomaly patterns are remarkably similar to those shown in figure 3.5. This is an important result, as it indicates that the mean temperature anomalies in the ERA Interim are accurate. It does little to validate the clustering routine, as the correlation between ERA Interim and AWS temperatures is already known to be high. If a subset of ERA Interim temperatures and AWS temperatures are compared, the correspondence is then also likely to be high. However, it does suggest that the patterns exist in reality, rather than as an artefact of the ERA Interim reanalysis. It also confirms the high degree of dependence of temperature on circulation patters seen earlier. Highly detailed features such as temperature gradients across the ice shelf in clusters (4,4) and (2,4) are well-resolved by the reanalysis (cf. fig. 3.5 & 3.7).

Wind conditions as derived from AWS records are exhibited in figure 3.8. Correspondence of cluster winds between ERA Interim and AWS is perhaps more important than that of the temperature, as it

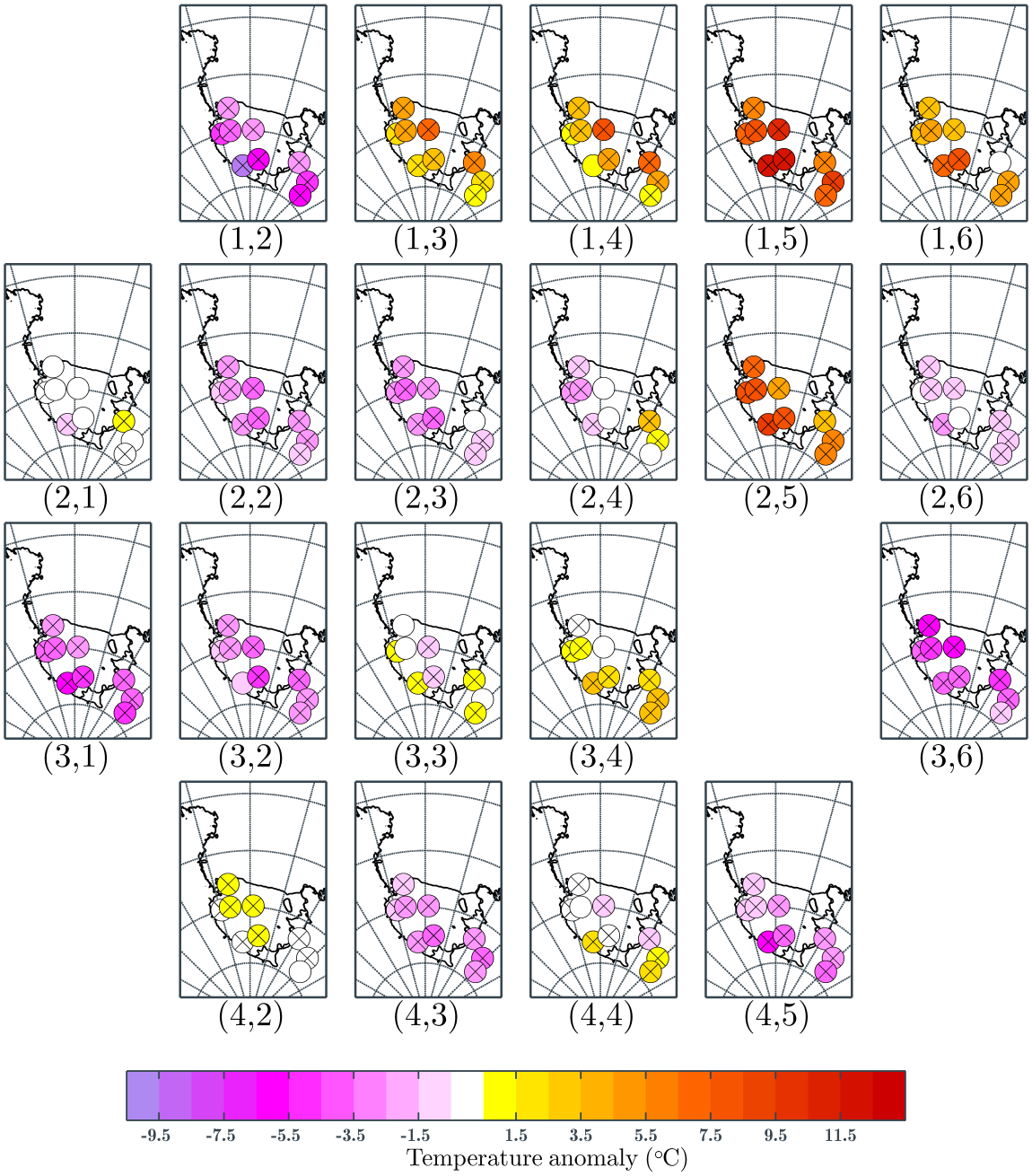

Figure 3.7: Ross Sea AWS clusters, temperature anomaly. Temperature scale is equivalent to that shown in figure 3.5. Means that are significantly different from zero at $p \leq 0.05$ are displayed with a cross.

has the capacity to provide more confidence in the clustering algorithm. At individual stations we can view wind roses that describe the climatology of the wind for each cluster. If the clustering algorithm is working well, then the wind direction and speed should be relatively constant for the instances within a cluster. We show all wind composites for comparison, but will focus on clusters (1,3), (1,6), (3,6) & (4,2) as these clusters give an adequate cross-section of wind conditions. AWS winds in figure 3.8 are compared with ERA Interim winds shown in figure 3.3. Cluster (4,2) describes low wind speed conditions, with light and variable winds over the ice shelf. This is mirrored well in the AWS record. It can even be

observed that the slightly increased wind speeds at Ferrell AWS are shown as a stronger region near the permanent ice edge in the cluster composite. Stronger winds are also observed at Brianna, upwind from the Siple Coast in both composites. Wind directions also show good correspondence.

For cluster (3,6), in the ERA Interim composite (fig. 3.3), strong winds are observed over Victoria Land, along the southern border of the Transantarctic Mountains and at the Siple Coast. Reduced winds are seen on the ice shelf, but a jet is seen to the north, directed towards the north east. A band of slightly stronger winds propagates from the Siple Coast to the south-east end of the jet, and is clearly feeding it. According to the AWS composite, the strength and direction upwind from the Siple Coast is represented well, as is the wind over the southern ice shelf. However, AWS composites show a region of stronger winds propagating from Byrd Glacier in a jet across the ice shelf to the east. These jets have been imaged with satellite thermal infrared data previously (Bromwich, 1989b; Breckenridge et al., 1993). The jet is recorded at Marilyn, Schwerdtfeger and Gill, but not well represented by the ERA composite. Unfortunately, there is no long-period AWS unit located on the western side of the ice shelf with which to compare the marginally heightened winds in the ERA Interim there.

For cluster (1,6) the ERA Interim composite shows good correspondence with all AWS records. In particular, we note the drainage from Beardmore Glacier that is shown at Elaine and replicated in the ERA Interim composite. The channelling of winds around Minna Bluff is also picked up well in the ERA Interim composite, as evidenced by the Ferrell records. Wind speeds are still slightly under-estimated propagating from Byrd Glacier, however.

Finally, for cluster (1,3) strong winds are seen over the sea along the east coast of northern Victoria Land, and as far south as the permanent ice shelf. These winds are clearly well depicted, as evidenced by the record at Ferrell. Winds further south at Schwerdtfeger, Marilyn and Gill are also relatively high and the ERA Interim represents both the speed and direction well. Good correspondence is also seen with weaker winds over the remainder of the ice shelf, but wind speeds at Brianna and Elizabeth are a little too low.

The directional constancy (q) can be used as a slightly more quantitative method of assessing the effectiveness of the clustering algorithm than direct examination of wind roses. q is a measure of the variability of the wind direction and is calculated as the ratio of mean vector to the mean scalar wind speeds. Expressed mathematically:

$$q = \frac{\sqrt{\overline{u}^2 + \overline{v}^2}}{\overline{U}} \tag{3.3}$$

where $\overline{U}$ is the mean scalar wind speed, $\overline{u}$ is the mean zonal wind speed and $\overline{v}$ is the mean meridional wind speed. The range of q is $[0, 1]$, where low values indicate that the wind direction is variable and values close to 1 indicate that the wind direction is constant. If the clustering algorithm efficiently groups instances displaying similar wind conditions, then within clusters we would expect the q value from AWS records to be high. We show q values for the AWS record for cluster times in figure 3.9. In the q diagram we also include an extra panel in the top-left, which displays the q value for all available records, for the purpose of comparison. As in temperature anomaly diagrams (fig. 3.7) we indicate whether q is significantly different from the value shown in the top-left at $p \leq 0.05$ with a cross. In this case, significance is assessed with a Monte Carlo method. For each AWS and each cluster, we calculate q for 100 randomly chosen subsets of records for an equal length of time to the total cluster occurrence. The normal distribution obtained from this random selection is then used to assess the significance of cluster results.

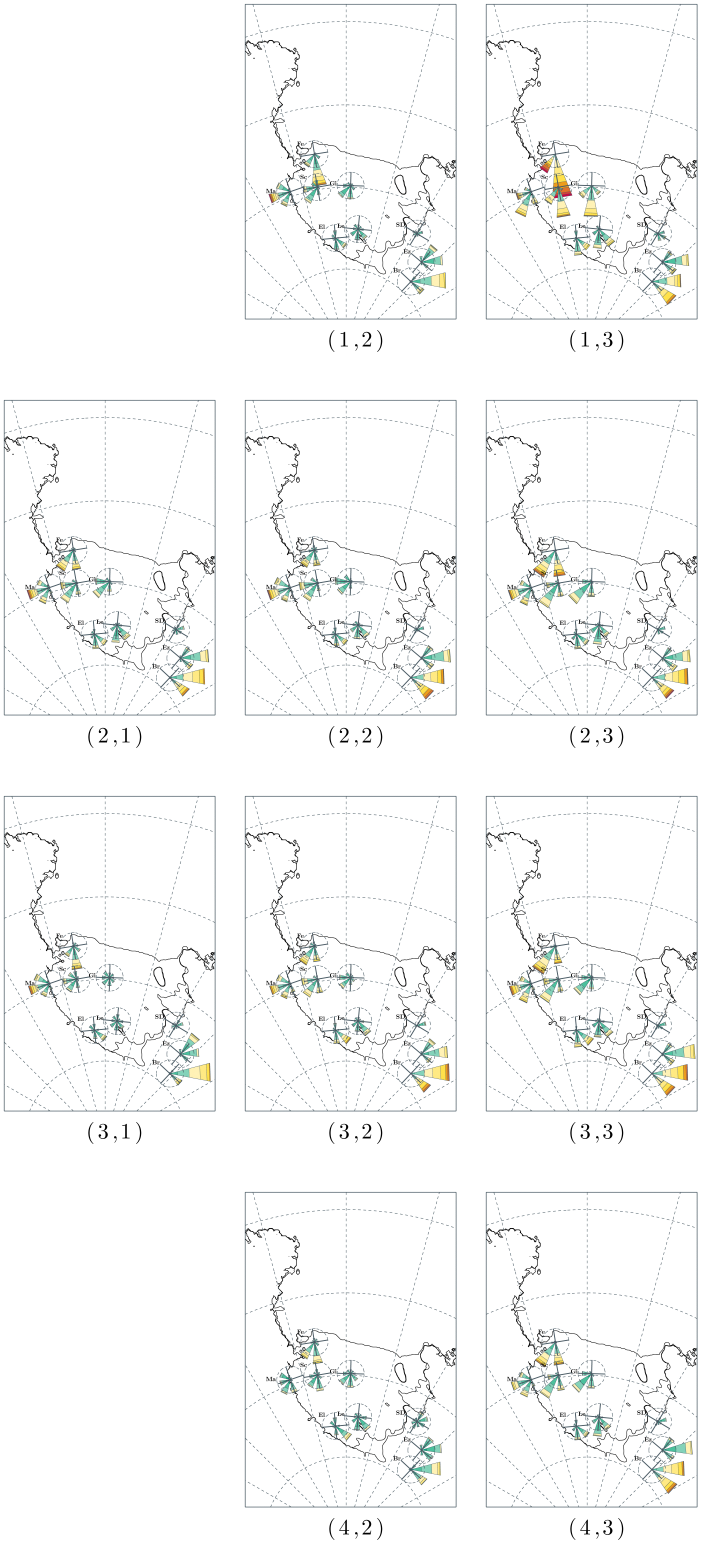

Figure 3.8

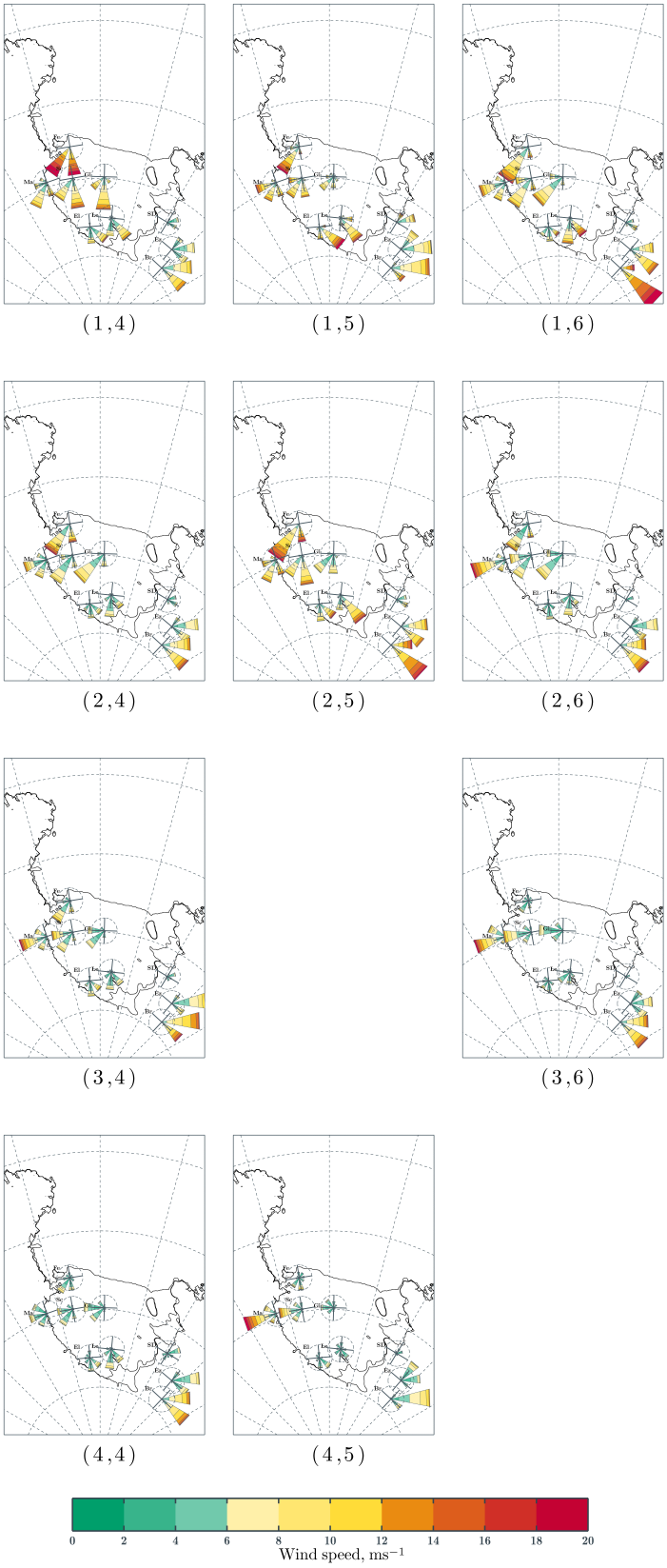

Figure 3.8

For the entire record, differences in q across the ice shelf are noticeable and appear to be mainly caused by the variation of small-scale topographic influences. Units on the margins of the ice shelf, either on steep coastal slopes (Brianna (Br), Elizabeth (Ez)), or in the vicinity of glacial valleys (Marilyn (Ma)), show highly directional flows and correspondingly high q values. The line of AWS sites including Marilyn (Ma), Schwerdtfeger (Sc) and Gill (Gi), shows a uniform decrease in q from west to east. Presumably, this is due to the decreased influence of katabatic drainage from Byrd Glacier and decreased topographic constraint of the Transantarctic Mountains. Generally speaking, stations situated more towards the centre of the ice shelf are less subject to topographically controlled flows, and as such the effects of synoptic forcing are more variable, hence q values are lower. For instance, q at Elaine (El) is larger than that at Lettau (Le), due to the vicinity of the former station to the mountains. The most variable record indicated by the q measure is that of the Siple Dome (SD) AWS, which is positioned on the peak of an elevated ice dome to the east of the ice shelf. The lack of an topographic forcing at this location means that the wind direction is variable. The wind direction is also sensitive to changes in the position of pressure minima in the Ross Sea.

Further examination of figure 3.9 indicates that the majority of q values for cluster times are significantly different from that of the entire data series. This can be interpreted as a positive assessment of the clustering algorithm, as it implies that similar wind patterns are grouped, which is the goal of the clustering process. There are a number of AWS sites and clusters where the value of q is lower within the cluster than for the record as a whole. The most salient example is cluster (4,2), where all the weather stations used show significantly reduced q values. Observation of figure 3.3 shows that this cluster represents times of low wind speeds across the ice shelf and surrounding area. With the low wind speeds and lack of synoptic forcing shown in this cluster, it is to be expected that the winds would be rather variable. The same can be said of all clusters to the left of figure 3.3, where synoptic gradients over the ice shelf are small (see fig. 3.4). In this respect, it is telling that a general increase in q is observed from the bottom-left of figure 3.9 to the top-right, as the wind speeds over the ice shelf increase.

Wind at stations mentioned above as being controlled predominantly by local topographic conditions tend to have high q values for all clusters, which again highlights the dominance of the local topography at these locations. An example is Brianna (Br), which shows q consistently close to one. Siple Dome (SD) provides an interesting counter example, as it is subject to limited topographic forcing. Wind directions are variable for the entire data record composite, and tend to also be variable for times of weak synoptic forcing, such as the leftmost column and bottom row of figure 3.9. Winds at this station are also more variable than at other stations towards the right of the diagram, when synoptic forcing over the ice shelf is strong. This is presumably due to the location of the station relative to the MSLP minima. With a minimum MSLP to the east of the domain, Siple Dome tends to be close to the region of lowest pressure, meaning that it exists within the area of low winds surrounding the minimum, and thus producing a reduced q value.

In general, the wind directions between ERA clusters and AWS wind composites match well. This is

---

Figure 3.8: Previous page: Ross Sea region cluster wind roses. Petals of the wind roses show the frequency of the wind from a particular direction. The dashed circle around each rose represents 20 % frequency. The colour of a particular petal indicates the speed of the wind from that direction. Roses are rotated to be aligned with grid north. The wind rose for Marilyn (Ma) is offset to the west of its true position, in order not to overlap with Schwerdtfeger (Sc). Brianna (Br) and Elizabeth (Ez) are also offset to the west, in order that their roses stay within the map boundaries.

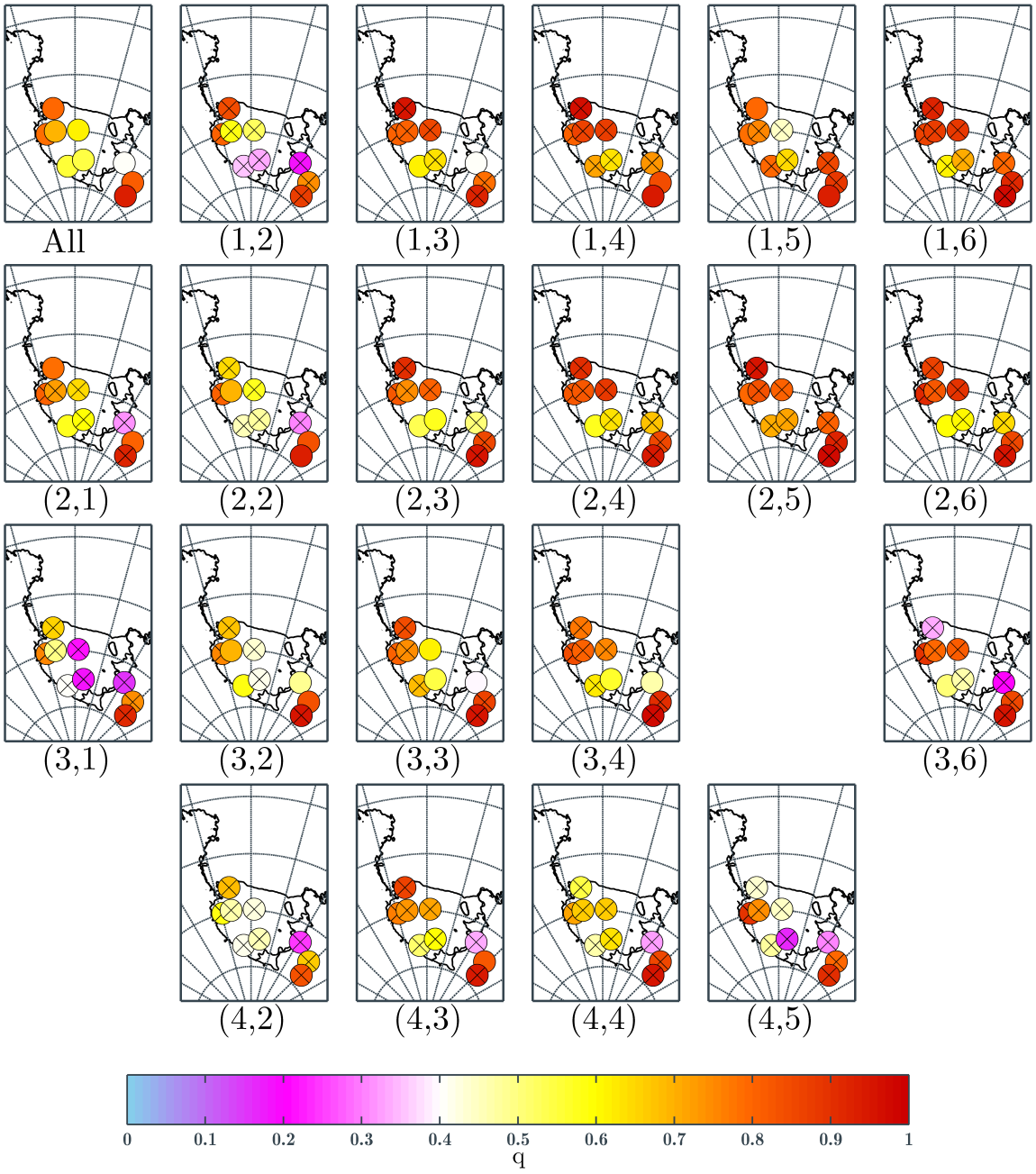

Figure 3.9: Ross Sea AWS clusters, directional constancy (q). Extra panel in top-left shows the q value for all times available. Details on the calculation of q are given in the text. q values that are significantly different from zero at $p \leq 0.05$ are displayed with a cross.

to be expected from the analysis in section 3.2.3. The constancy of the wind directions in each cluster suggest that surface wind regimes are well represented by the clustering results. This is true especially where winds are strong. In clusters that represent low wind speeds and a lack of synoptic forcing, low measures of directional constancy from AWS records are observed, which is to be expected. Strengths of the wind appear to be slightly too low in the ERA composites, which again is to be expected from section 3.2.3. Interestingly, it appears to be when the wind is not synoptically forced and is probably

generated katabatically that the wind speeds are most under-estimated. For instance, at Marilyn (Ma), Schwerdtfeger (Sc) and Gill (Gi) in cluster (3,6) and Brianna (Br) and Elizabeth (Ez) in cluster (1,3). Katabatic forcing could be reduced due to an under-estimated temperature inversion at the surface due to coarse vertical resolution, or topography considerations. The strength of the katabatic wind is dependent on the slope of the terrain and the topographically enhanced convergence of the wind. Both of which may be under-estimated at the grid resolution of the ERA Interim reanalysis.

3.6 Discussion and conclusions

In this chapter we have described the development and results of a modified k-means clustering algorithm, applied to the representation of the greater Ross Sea region of Antarctica of the ERA Interim reanalysis. Results from the algorithm have been shown to match well with data from AWS sites in the same region, and describe details of the meteorology that are well known. Using a simple organisational process, we have been able to split clusters into further larger groups, which describe the effects of strong and weak pressure minima in the northern Ross Sea, the Ross Ice Shelf Air Stream (RAS), weak pressure minima over eastern Ross Sea, and katabatic and weak synoptic forcing. By producing composites of wind, MSLP anomalies and temperature anomalies of the clustered instances we have been able to examine these conditions in some detail. Of all the groups, the RAS category is perhaps the most important in a climatological sense, as the strong winds over the ice shelf have a profound warming effect at the surface. Any changes in the frequency of such events may have large repercussions on the surface climate.

Throughout the description of clustering results we have noted how structures exhibited in cluster composites are reminiscent of meteorological features seen in many previous analyses. We believe that this indicates that the ERA Interim represents the surface meteorology well, except for a few cases, and that the clustering algorithm is effectively separating instances into legitimate patterns. We offer further validation of our method with reference to the analyses of Seefeldt and Cassano (2008) and Seefeldt and Cassano (2012), who performed similar synoptic classification schemes in the same region using five years of AMPS output. Composites produced by these studies compare favourably to those exhibited here and our study reproduces the main features of the region as described previously. One disparate feature of the analyses is that in the lowest model layer composites of Seefeldt and Cassano (2012), stronger winds were found descending through glaciers in the Transantarctic Mountains and onto the ice shelf than in the composites presented here. Having shown previously (section 3.2.3) that the ERA Interim under-estimates the drainage winds from the plateau to the west, we do not believe that the lower wind seen propagating across the ice shelf in our composites relative to AWS measures and AMPS are an artefact of the clustering algorithm. Rather, the ERA Interim under-estimates the strength of the wind at these times. The lower frequency of RAS events in our study than in Seefeldt and Cassano (2012) occurs due to the different model levels used and a slightly different definition of the phenomenon. The ERA Interim does not resolve the knob-jet observed from the protruding Prince Olav Mountains, as described by Seefeldt and Cassano (2008) and Nigro et al. (2012b). This is almost certainly a result of the reduced resolution of the ERA Interim relative to AMPS. We also do not see evidence of wind splitting around Ross Island (O'Connor et al., 1994; Seefeldt et al., 2003), or of mesoscale cyclones (O'Connor and Bromwich, 1988; Bromwich, 1991; Carrasco et al., 2003) which are also known to occur in the region. The small size and transient nature of mesocyclones means that they are difficult to capture in compositing studies (Seefeldt and Cassano, 2012), and given the resolution of the ERA Interim, the lack of these features is not surprising. The ERA Interim does however reproduce the wind direction at

Ferrell AWS unit rather well. It has been shown (Seefeldt et al., 2007) that the flow at this station is constrained by the topography of the Transantarctic Mountains to the west. This is an important point, as it suggests that the resolution of the ERA Interim is high enough to resolve the barrier of Minna Bluff in a meaningful way.

We mention that we also performed an equivalent clustering analysis using NCEP-DOE reanalysis (Kanamitsu et al., 2002) surface data for the same time period (1979-2011), albeit with reduced horizontal resolution (100 km stereographic grid). We found similar clusters to those presented here, further indicating that the structures described above are not artefacts of the ERA Interim reanalysis, but exist as dominant synoptic patterns in the Ross Sea region.

We believe that the clustering algorithm described in the previous section adequately distinguishes between synoptic conditions in the Ross Sea region. In essence, the analysis so far has provided corroboration to the previous work of Seefeldt and Cassano (2008) and Seefeldt and Cassano (2012) over a much extended time period and performed a validation of the ERA Interim reanalysis surface data over the region. The SOM technique of previous studies may have advantages over the k-means. In particular, the SOM algorithm is capable of automatically producing a map of clusters, where each cluster is placed in the vicinity of those to which it is most similar. Further, it is almost certainly true that AMPS output more accurately depicts Antarctic atmospheric conditions than the ERA Interim, and at a higher resolution. However, the advantage of using the reanalysis dataset lies in the ability to use the clusters presented in this chapter to better understand the climatology of the region with reference to large-scale circulation patterns, such as SAM and ENSO, and the production of temperature composites provides the potential of better understanding temperature trends in the region. We feel that the results of this chapter can be used to investigate the aforementioned effects in some detail. This will be the focus of the following two chapters. In addition, the Ross Ice Shelf Air Stream, and its variability related to synoptic activity has also been shown to impact heavily on open water formation and sea ice production in the Ross Sea (Bromwich et al., 1992; Carrasco and Bromwich, 1993a; Bromwich et al., 1993; Harangozo and Connolley, 2006; Comiso et al., 2011), and thus the characterization of its strength and variability on a climatological time-scale it relevant to sea ice studies. This is research which is particularly pressing due to recent increases in sea ice extent that have been tied to changes in wind patterns (Holland and Kwok, 2012). This will be an area of future work.

Chapter 4

The influence of the Southern Annular Mode and El Niño-Southern Oscillation on the climate of the Ross Ice Shelf

4.1 Introduction

Recently, much research has been performed on two modes of internal variability that profoundly affect the surface atmosphere of Antarctica. They are: the Southern Annular Mode (SAM), which is reviewed in section 2.6, and the El Niño-Southern Oscillation (ENSO), which is reviewed in section 2.7. Both modes have been shown to impact on the depth of the ABS low, which is located to the east of the Ross Ice Shelf.

Surface wind flows over the Ross Ice Shelf and its immediate surroundings have been shown to be important on a hemispheric scale for several reasons. Strong southerly winds over the ice shelf cause a net northerly outflow at the surface in the region (Parish and Bromwich, 2007). The meridional polar cell, which has been shown to be partly forced by southerly surface winds over Antarctica (James, 1989; Parish, 1992), is thus likely to be modulated by such events, which has been demonstrated by Parish and Bromwich (1998). Further, wind-forced polynyas, which exist at the northern edge of the ice shelf (Bromwich et al., 1993), have been shown to be net producers of Antarctic sea ice (Tamura et al., 2008; Comiso et al., 2011), and consequently highly-saline Antarctic bottom water. Sea ice production and subsequent advection and ocean currents are thus highly dependent on the circulation of the overlying atmosphere (Stammerjohn et al., 2008; Comiso et al., 2011; Holland and Kwok, 2012). This dependence has driven much research into characterising the circulatory variability over the Ross Sea with reference to large-scale modes. Sea ice in the south Pacific region has been shown to be highly coupled to SST variability in the tropical western and mid-Pacific (Yuan and Martinson, 2000), and has been observed to be related to SAM and ENSO-forced changes in atmospheric circulation through observational (Yuan, 2004; Stammerjohn et al., 2008; Yuan and Li, 2008) and model studies (Hall and Visbeck, 2002; Lefebvre et al., 2004; Turner et al., 2009b).

Despite the large potential impacts, and due to the short time periods of previous studies, the variability of ice shelf winds has not been characterised over climatological time periods. In the previous chapter we demonstrated that within the Ross Ice Shelf region the surface temperature has a high dependence on synoptic circulation conditions, due to the joint effects of anomalous horizontal advection and increased vertical mixing due to strong winds. Thus, it seems likely that modulation of the RAS effect through changes in the ABS low will have significant effects on the surface temperature field of the shelf. This has yet to be adequately characterised. In this chapter we discuss changes in the state of the atmosphere of the domain defined in chapter 3 that occur concurrently with variation in the phases of SAM and ENSO. We use the output of the clustering algorithm described in the chapter 3 in order to ascertain what impact these large-scale internal modes have on the synoptic climatology of the region. Rather than focusing only on differences in the mean fields, this approach affords us an insight into the ability of the hemispheric conditions to change the daily meteorology of the study area. Since the long-term mean state of the atmosphere is an integrated measure of the synoptic state, this approach allows us to ascertain which synoptic patterns in particular are responsible for any observed changes in the mean climate of the region. The structure of this chapter is as follows: section 4.2 describes the data sources and techniques used in the subsequent analysis. Sections 4.3 and 4.4, detail results of the analysis for SAM and ENSO, respectively. In section 4.5, we provide a summary of results and conclusions are made.

4.2 Data and techniques

In this chapter we employ output directly from the ERA Interim reanalysis (as described in section 3.2.1), to describe the total change of atmospheric parameters between positive and negative phases of the modes of variability, SAM and ENSO. To represent variation in the SAM, we use the Marshall SAM index (Marshall, 2003), which is derived from long-period records of mean sea-level pressure from coastal Antarctic manned-stations around 65 °S and stations in the Southern Ocean at approximately 40 °S. The SAM index is defined as the difference in normalized monthly zonal-mean sea-level pressure between these latitudes. The Marshall SAM index has been shown to be superior to indices of SAM derived from reanalysis datasets (eg. Gong and Wang (1999); Nan and Li (2003)), which suffer from spurious pressure trends (Hines et al., 2000; Marshall and Harangozo, 2000; Marshall, 2003), particularly at high southern latitudes before the satellite era.

The Southern Oscillation Index (SOI), which we use to represent the atmospheric component of the ENSO phenomenon, is computed as the twice-normalized MSLP anomaly difference between Tahiti and Darwin, Australia (Trenberth, 1984). Positive (negative) values indicate enhanced (decreased) trade winds, and thus represents the La Niña (El Niño) phase. As suggested by Trenberth (1997), we use 5-month running mean values of the SOI series, in order to reduce the effects of intra-seasonal oscillations at low latitudes.

In order to represent the total change in atmospheric conditions between positive and negative phases of SAM and ENSO, we produce composites of atmospheric variables extracted from the ERA Interim reanalysis and interpolated to a stereographic grid (as detailed in section 3.2.1). We take seasonal means of the data, using the canonical austral seasons: summer (DJF), autumn (MAM), winter (JJA) and spring (SON); such that seasonal variations in the effects of oscillations can be studied. We then use the Marshall SAM index and the SOI to determine the years in which each season shows extrema in the large-scale oscillations. The mean difference of reanalysis output between the five maximum and five

Month	SAM+	SAM-	SOI+	SOI-
	1979	1980	1979	1983
	1999	1983	1989	1987
DJF	2000	1985	1999	1992
	2002	1987	2008	1998
	2008	2006	2011	2010
	1982	1980	1989	1983
	1989	1981	1999	1987
MAM	1993	1986	2000	1992
	1998	1990	2008	1993
	2000	2002	2011	1998
	1979	1988	1988	1982
	1993	1992	1996	1987
JJA	1998	1995	1998	1993
	2004	1996	2010	1994
	2010	2007	2011	1997
	1983	1980	1988	1982
	1985	1988	1998	1991
SON	1999	1994	2008	1994
	2001	1997	2010	1997
	2010	2002	2011	2002

Table 4.1: Five most positive and negative years of the Marshall SAM index and SOI time series for all seasons.

minimum years of the oscillation index is computed (SAM + −SAM−, SOI + −SOI−). The procedure is similar to that used by Pezza et al. (2008) and Pezza et al. (2012) for a synoptic cyclone tracking study, and roughly corresponds to using the ± one standard deviation extrema of the indices identified above. We also experimented with using 4 and 6 years, and found only minor differences. The years used in the difference calculations for each season and oscillation are listed in table 4.1. Some overlap is observed in the SAM and ENSO years, particularly in the spring and summer, suggesting a degree of covariability between the modes (see section 2.7). The composites for the two modes thus are not independent during these seasons.

We are able to estimate the statistical significance of the mean difference from zero for each of the interpolated reanalysis grid points using a Student's t-test. Care must be taken when interpreting statistical significance when large numbers of similar calculations are performed, as multiple tests can often produce an over-estimate of the degree of significance. For instance, if 100 differences are calculated, then the expectation value for the number of differences that are significant at $p = 0.05$ is 5. Hence, when multiple differences are calculated the probability of incorrectly rejecting the null hypothesis (type I error) increases. However, the effects of large-scale oscillations are far-reaching, such that if one member of a field shows a significant difference, then those in its vicinity are likely to also. Thus, care must also be taken to avoid failing to reject the null hypothesis where a legitimate relationship actually exists (Type II error). A compromise must be reached that limits both types of error. To this end, we use the false discovery rate (FDR) procedure proposed by Ventura et al. (2004), which has been shown to be a reliable solution to this type of problem.

We also use output of the modified k-means clustering algorithm detailed in section 3.3. In the previous chapter, the algorithm was applied to ERA Interim surface variables for the years 1979-2011 over a polar stereographic grid encompassing the Ross Ice Shelf, Ross Sea, and surrounding regions of

East and West Antarctica. Output of the algorithm consists of a series of twenty clusters that describe frequent synoptic patterns over the studied area. Following the example of Cassano et al. (2007) and Cassano et al. (2011), for both SAM and ENSO and for each season, we calculate the frequency of each cluster for positive and negative instances (f_{+k} and f_{-k}, respectively), and the cluster mean atmospheric parameters (X_{+k} and X_{-k}, respectively, where X represents MSLP, zonal wind speed, meridional wind speed, or temperature anomaly at any grid point). k is an index that corresponds to a specific cluster. The change in frequency and cluster mean parameters between the positive and negative phases for any cluster can then be described by:

$$f_{+k} = f_{-k} + \Delta f_k, \tag{4.1}$$

and

$$X_{+k} = X_{-k} + \Delta X_k \tag{4.2}$$

where Δf_k and ΔX_k represent the change in frequency and cluster mean parameters between positive and negative phases, respectively. The sum over all clusters of any parameter, weighted by the frequency of each cluster within a particular time interval reproduces the total mean of that parameter in that interval. Thus:

$$X_+ = \sum_{k=1}^{K} f_{+k} X_{+k} \tag{4.3}$$

where K is the total number of clusters, which is twenty in this case. Substituting equations (4.1) and (4.2) into equation (4.3) yields:

$$X_+ = \sum_{k=1}^{K} (f_{-k} + \Delta f_k)(X_{-k} + \Delta X_k) \tag{4.4}$$

Which, upon expansion, becomes:

$$\begin{aligned} X_+ =& \sum_{k=1}^{K} (f_{-k} X_{-k} + f_{-k} \Delta X_k + X_{-k} \Delta f_k + \Delta X_k + \Delta f_k) \\ =& X_- + \sum_{k=1}^{K} (f_{-k} \Delta X_k + X_{-k} \Delta f_k + \Delta X_k \Delta f_k) \end{aligned} \tag{4.5}$$

Thus:

$$\begin{aligned} & \quad 1 \qquad\quad 2 \qquad\quad 3 \\ X_+ - X_- =& \sum_{k=1}^{K} (f_{-k} \Delta X_k + X_{-k} \Delta f_k + \Delta X_k \Delta f_k) \end{aligned} \tag{4.6}$$

As such, the difference for any parameter between the positive and negative phases ($X_+ - X_-$) can

be described by the three terms on the right-hand side of equation (4.6). Term 1 describes the variations due to changes in the mean composite of each cluster (intra-cluster changes). Term 2 describes the change due to variations in the frequency of each cluster (inter-cluster changes). Term 3 describes the two modes of change acting together. For each cluster, each of these terms is readily calculated from the ERA Interim output and the time series of cluster occurrence. In the next section, we exhibit the sum over all clusters of the three terms, and the total change as calculated directly from the ERA Interim output described previously. We can then explain changes in the total mean with respect to changes due to the three terms of equation (4.6). We also display the difference in frequencies (Δf_k) of each cluster between positive and negative phases of SAM and ENSO. While the difference in frequencies themselves are trivial to calculate, some attention must be given to the estimation of the significance of differences. In this case, the tested null hypothesis is that the difference between frequencies is zero. Following Cassano et al. (2007) and Cassano et al. (2011) once more, for each time period there are n_+ and n_- total records, and the frequencies of a cluster k are f_{+k} and f_{-k}, respectively. Assuming that the frequencies for each period are generated by two random, independent, binomial (cluster states can be considered binomial, as for any instance, either a particular cluster occurs, or it does not) processes, the frequency variances are given by $f_{+k}(1 - f_{+k})/n_+$ and $f_{-k}(1 - f_{-k})/n_-$, and the test statistic by $(f_{+k} - f_{-k})/\sqrt{f_{+k}(1 - f_{+k})/n_+ + f_{-k}(1 - f_{-k})/n_-}$. If the test statistic exceeds the value of 1.96, then we reject the null hypothesis, and the frequency change is said to be significant at $p \leq 0.05$.

Throughout this section we choose to use indices and ERA Interim output that have not had background trends removed. We do not perform the detrending procedure as, despite the potential of concurrent trends to bias results, the procedure does not conserve the inherent statistics of frequency changes. For instance, for any given time period $\sum_{k=1}^{K} f_k \equiv 1$. And, for any frequency change between two time periods $\sum_{k=1}^{K} \Delta f_k \equiv 0$. In practise, detrending data before calculating differences makes little difference to the results.

4.3 Southern Annular Mode results

In figures 4.1, 4.2, 4.3, and 4.4 we show changes in MSLP, vector wind and temperature associated with SAM for each season. To reiterate, the total change in the mean field (leftmost panel) is calculated directly from the ERA Interim output. The remaining three panels represent the three terms of equation (4.6), which were shown in section 4.2 to contribute to the total mean change. The first term (second from left panel) represents the change due to intra-cluster variability. Term 2 (second from right panel) represents the change due to inter-cluster variability. The final term (rightmost panel) represents changes due to intra- and inter-cluster changes working in tandem. Each panel represents a sum over all of the clusters defined in chapter 3. For the leftmost panel, we indicate the statistical significance of the total change, as estimated by a two-tailed Student's t-test and the FDR procedure of Ventura et al. (2004). For pressure and temperature, stippled areas indicate that changes are significant at $p \leq 0.05$. Indication of the significance of the vector wind difference is less straightforward, as the statistical significance of a vector is itself a vector. Vectors that are significant at $p \leq 0.05$ in the zonal direction are plotted in green. Those significant only in the meridional direction are plotted in blue. Vectors for which both components are significant are shown in red. The remainder of the arrows are plotted as grey. As in figure 3.3 the vectors are plotted so as to be relative to grid north of the polar stereographic projection. The vertical black arrow in the lower left corner shows the magnitude of a 1 ms^{-1} change. For reference,

	1	2	3	4	5	6
1		**-1.59**	0.19	**2.58**	-0.80	**1.41**
		0.65	**-2.39**	0.27	-1.14	0.16
		-0.98	**-3.59**	-0.33	-0.43	-1.14
		-1.92	**-2.80**	**1.43**	**-1.65**	**5.82**
2	**-3.10**	-0.16	0.14	-0.63	**-1.20**	-0.34
	-0.11	-0.76	**-1.58**	**2.77**	-0.11	**-1.74**
	-0.49	0.00	0.98	**1.63**	0.49	**-2.66**
	-4.07	**-1.59**	**-2.25**	1.21	-1.43	**1.70**
3	0.73	0.70	-0.07	**-1.79**		**-0.80**
	1.20	**1.79**	**-2.99**	0.98		-0.05
	0.76	0.82	**-3.48**	**2.23**		**5.98**
	2.09	**1.87**	**-3.13**	-0.38		**2.75**
4		-0.56	0.61	**3.11**	**1.58**	
		1.14	0.33	0.82	0.76	
		-0.05	1.20	0.60	-1.52	
		-5.22	**4.73**	**5.38**	**-2.53**	

Table 4.2: Cluster frequency difference (%) between most positive and most negative years of Southern Annular Mode index. Differences significant at $p \leq 0.05$ are shown in bold. Clusters are arranged in the orientation used in chapter 3. Each cluster has four frequency changes, these are ordered from the top: summer, autumn, winter, spring.

we also show the change in frequency for each cluster and each season in table 4.2. These changes are discussed throughout the text, in reference to changes observed in term 2. We will also refer to changes in the group frequencies, as defined in chapter 3. While the contribution from each cluster for each term can be calculated, to conserve space we choose not to display these diagrams. However, clusters that dominate observed changes will be referred to throughout. In order to aid in interpretation, we also show composites of surface conditions for SAM+ seasons in figure 4.5 and for SAM- seasons in figure 4.6. Note that scales are different between composite and change diagrams. As noted by Fogt et al. (2012a), the asymmetry between SAM+ and SAM- conditions may also mean that some variability is masked if only the differences between SAM+ and SAM- is examined.

In summer (fig. 4.1), changes indicate an enhanced pressure gradient from east to west across the ice shelf, with the largest negative changes observed in the east. A much deeper low pressure region is visible in the SAM+ phase (cf. fig. 4.5a and fig. 4.6a). A second, smaller, region of decreased pressure is observed to the west of the domain, over the slopes of Victoria Land. Observation of the three terms of equation (4.6) shows that the change in pressure is dominated by background changes, rather than those associated with changes in the frequency of clusters, although table 4.2 indicates that the frequency of many clusters changes appreciably between SAM positive and negative summers. Instances of the Strong Northern Cyclonic (SNC) group decrease, while those in the Katabatic & Weak Synoptic (KWS) group increase, which is mainly caused by a large increase in cluster (4,4). The resulting pressure changes are not large, however. The contribution of term 3 is also small. Examination of the individual cluster contributions to term 1 (not shown), indicates that an almost uniform decrease in pressure is observed across the region. However, a deep decrease is observed for cluster (4,2), which was shown in section 3.4 to be the most common cluster in the summer months. The largest MSLP decrease for this cluster is seen in the east of the domain, corresponding to the largest area of decrease in the total difference diagram.

As expected, changes in the wind correspond well to changes in the gradient of MSLP. Summer shows

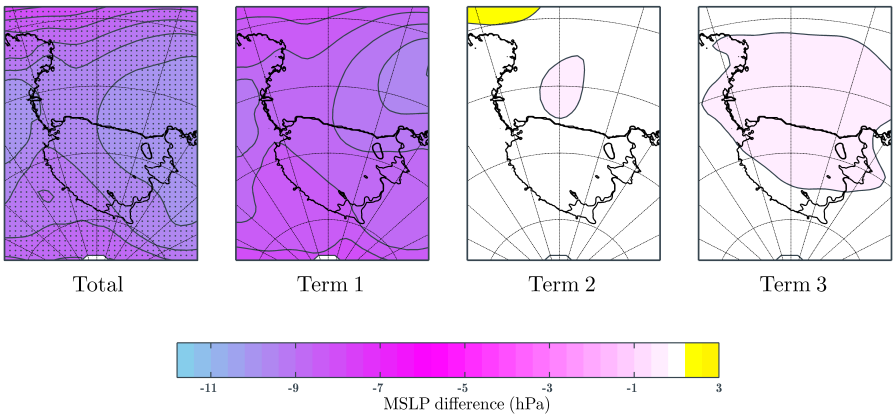

(a) SAM, MSLP.

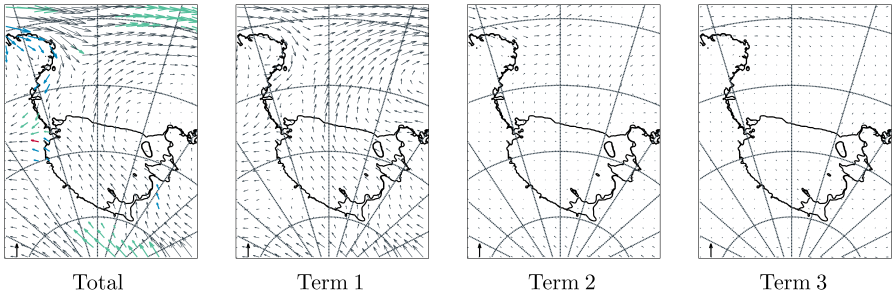

(b) SAM, wind speed.

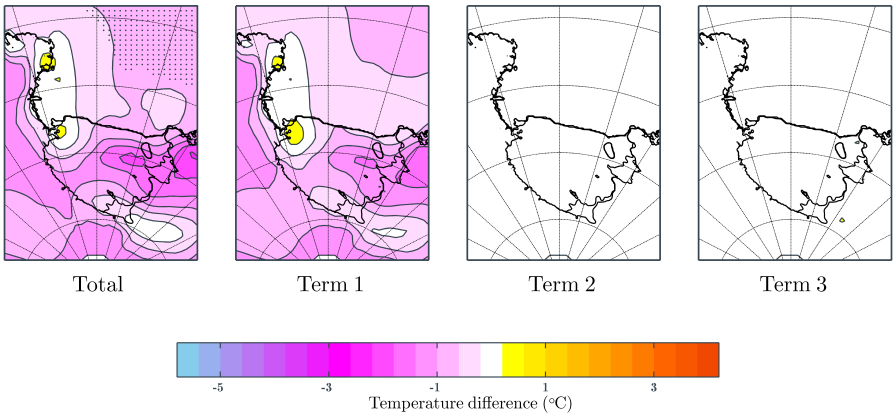

(c) SAM, temperature.

Figure 4.1: Difference between the extreme positive and negative summers (DJF) of SAM for (a) MSLP, (b) zonal and meridional wind, (c) temperature, for the total change and each term of equation (4.6). For the total change, for MSLP and temperature, significance at $p \leq 0.05$ is indicated by stippling. For wind speeds, green (blue) arrows show changes that are significant in the zonal (meridional) direction. Red arrows show changes that are significant in both. Grey arrows are not significant. A 1 ms^{-1} arrow is shown in the lower left corner of each diagram. Significance is not shown for the changes according to each term in equation (4.6).

some significant changes between positive and negative SAM years, particularly in the westerly winds in the far north of the region. The strengthening of westerly winds to the north of the Antarctic coast in positive SAM years is well known (see section 2.6). An area of increased northerlies is also seen off of the north-west tip of Victoria Land. Comparison of figures 4.5b and 4.6b indicates that the difference here is mainly associated with stronger southerlies in SAM- summers. Winds on the ice shelf are more south-easterly under SAM+, corresponding to the strengthening of the prevailing wind there. Some extra cyclonic motion is observed to the north-east of the shelf, corresponding to the change in the pressure gradient, and accordingly, more southerly flow is seen in the central Ross Sea. Changes in Victoria Land are in the up-slope direction, indicating a reduction in the instance of katabatic drainage in this region under SAM+ conditions. Some of these changes are significant. Increased down-slope winds are seen at the Siple Coast and in the south of the domain. Unsurprisingly, the majority of wind changes are forced by background pressure gradients, rather than inter-cluster changes. In particular, stronger zonal winds are observed in the north for almost all but are particularly apparent in clusters on the fourth row of figure 3.3. As discussed in section 3.4, these clusters are most prevalent in the summertime, and hence it is to be expected that changes associated with these clusters would heavily impact upon the mean. Stronger winds on the Siple Coast and ice shelf are predominantly related to pressure changes associated with cluster (4,2).

A high degree of temperature change is also observed for the summertime, with a net cooling in the domain. The cooling is only significant in the far north-east, however. The largest cooling signatures do not appear to be significant. This occurs because significance is dependent not only on the size of the change, but also the inter-annual variability present in the region. The largest magnitude cooling is observed over Marie Byrd Land and on the east of the ice shelf. Comparison of figures 4.5c and 4.6c indicates a general shift north of temperature contours in SAM+ summers.

Term 1 temperature changes are more difficult to interpret than those of term 2 as, while term 2 changes are caused solely by circulatory variation, those of term 1 include circulatory condition changes and changes forced by many other physical mechanisms, such as cloud cover and ocean-ice feedbacks, that are not included in term 2. However, the influence of circulation on temperature is also complex, particularly on the ice shelf where several mechanisms exist that can change the temperature depending on circulation. van den Broeke and van Lipzig (2004) discussed two mechanisms for SAM to produce temperature changes. Firstly, the reduced meridional transfer of air due to the stronger circumpolar westerlies effectively isolates the Antarctic continent from higher latitudes. This mechanism is consistent with the observed changes in zonal winds seen here, and thus the background decrease in temperature is probably explained by this mechanism. As mentioned above, cluster (4,2) dominates at this time of year, and the internal temperature change for this cluster is negative. The second mechanism is the turbulent mixing of the surface inversion due to strong winds (see section 2.2). Enhanced drainage over ice slopes may also warm the surface via adiabatic warming of descending air. Further, the origin of the air is also important. Results of chapter 3 indicated that enhanced drainage from West Antarctica may warm the ice shelf, while enhanced drainage from East Antarctica is likely to cool it. This temperature dipole is visible in the composites shown in figures 4.5c and 4.6c; in all seasons, and under both SAM+ and SAM- conditions, West Antarctica is notably warmer than East Antarctica. These mechanisms are evident to the south of Ross Island and in the areas of little change on the Siple Coast. Here, stronger winds from West Antarctica in the SAM positive phase, due to the increased pressure gradient, cause surface warming. Warming is most evident in the Ross Ice Shelf Air Stream (RAS) group clusters, and others which likewise show elevated winds over the ice shelf (clusters (3,6) & (4,5)), due to the decrease

in pressure to the east. Previous research (Marshall, 2007) has shown that the region around Ross Island cools in SAM positive years. This area may not be well represented by the ERA Interim (see section 3.2.3) and thus the warm spot to the south of Ross Island should be viewed with caution. However, the decreased cooling observed in regions where wind speeds increase is a notable feature of the temperature changes. The second warm spot on the tip of Oates Land is probably caused by the influx of warm air from the north due to anomalous northerly winds there, which occur in the change diagrams due to stronger southerlies in SAM- summers (fig. 4.6b). Temperature changes are almost entirely accounted for by term 1, while terms 2 and 3 are so small that they do not extend outside of the first contour interval (which represents the interval $[-0.2, 0.2]\,^{\circ}\mathrm{C}$).

In autumn (fig. 4.2), a large and significant negative change in MSLP is also apparent across the region, although the change appears to be reduced compared to the summer months. The largest negative change is observed in the far south-west of the domain in East Antarctica, which appears to be associated with raised pressures there in the SAM- phase (fig. 4.6a). Lower pressures in SAM+ autumns may indicate a relaxing of the polar cell, which may also account for the decreased drainage flows over the ice sheets (James, 1989; Parish, 1992). Pressure change contours over the northern ocean have a slight north-west to south-east slant. Those over the ice shelf appear to curve around the shape of the topography, due to subtle differences in the shape of the low pressure regions between SAM+ and SAM- conditions (cf. fig. 4.5a and 4.6a). Examination of the three terms of equation (4.6) suggests that the bulk of the change is due to intra-cluster pressure changes, although a large contribution is also given by changes in the frequencies of some clusters (term 2), which appears to reinforce negative background changes in the south-west and counteract them in the north-east. The gradient of the pressure changes appears to be higher in term 1 than term 2, which has important consequences for the resulting changes in the wind. For the intra-cluster changes, although all clusters show reduction in pressure between SAM positive and negative autumns, the largest contributions appear to arise from pressure changes for clusters in the third column of figure 3.3 (except (4,3)). These clusters show cyclones towards the north-east of the domain. Although there is a lowering of pressure across the domain, in these clusters there is enhanced deepening over East Antarctica and less so over the ocean to the north, suggesting that these cyclones are less pronounced with respect to the background pressure during SAM positive autumns, or indeed, more pronounced with respect to the background pressure in SAM- autumns. For term 2, a slight increase in pressure is observed in the north-east, and reduction in the south-west, which appears to be caused by a significant decrease in clusters from column 3 (except (4,3)) under SAM+ conditions. The reduction is apparent in table 4.2, suggesting that not only are these cyclonic systems less powerful in SAM positive autumns, they also occur less often. A net decrease is observed in the SNC clusters, which is countered by an increase in the KWS group. Term 3 shows a small increase in pressure in the south-west and a small decrease in the north-west.

Wind changes for autumn are similar to those for summer over the northern ocean, but autumn wind changes tend to be directed more towards the south-west, in line with the pressure gradient discussed above. Anomalous northerlies are also observed off the coast of Victoria Land, and in the far east over Oates Land. As in summer, these are caused by enhanced southerlies under SAM- conditions (fig. 4.6b). Over the western ice shelf, insignificant changes towards northerlies are also observed, corresponding to MSLP changes. Towards the east of the ice shelf, more southerly winds are observed. A minor number of changes over the ice shelf are significant, particularly to the south of Ross Island. These changes are in the opposite direction to the prevailing wind and so indicate a reduction in wind speeds over that part of the shelf. Slightly stronger winds are observed up-wind of the Siple Coast in West Antarctica. The

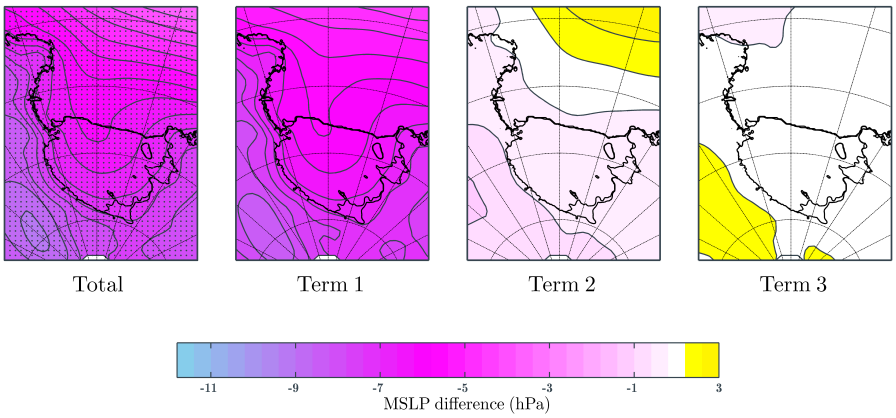

(a) SAM, MSLP.

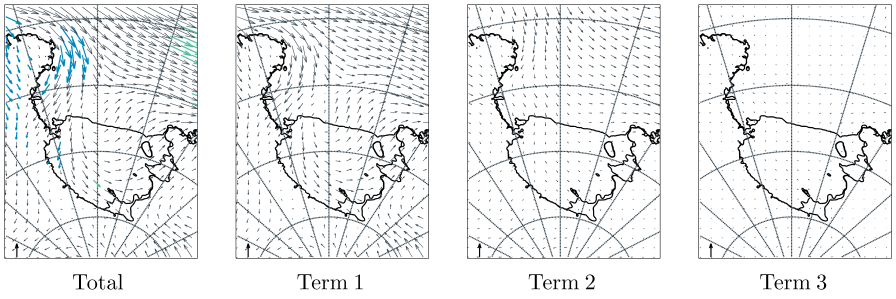

(b) SAM, wind speed.

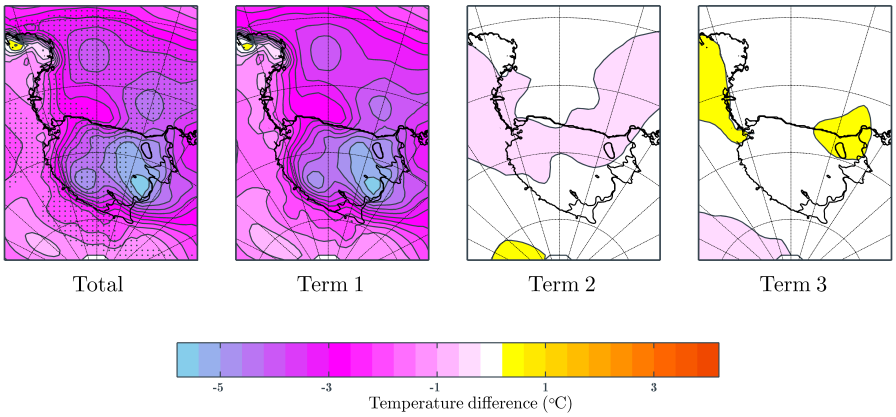

(c) SAM, temperature.

Figure 4.2: As in figure 4.1, but for autumn (MAM).

majority of wind changes appear to be generated by term 1, following the pressure changes discussed above. Stronger westerlies in the north are observed in all clusters for term 1. RAS clusters, at the top of figure 3.3, show decreased southerly winds on the western ice shelf in SAM+ autumns. Higher meridional winds are seen on the eastern part of the shelf, indicating a shift towards the east of the strongest winds under SAM+ conditions. This is consistent with the observed pressure changes. Term

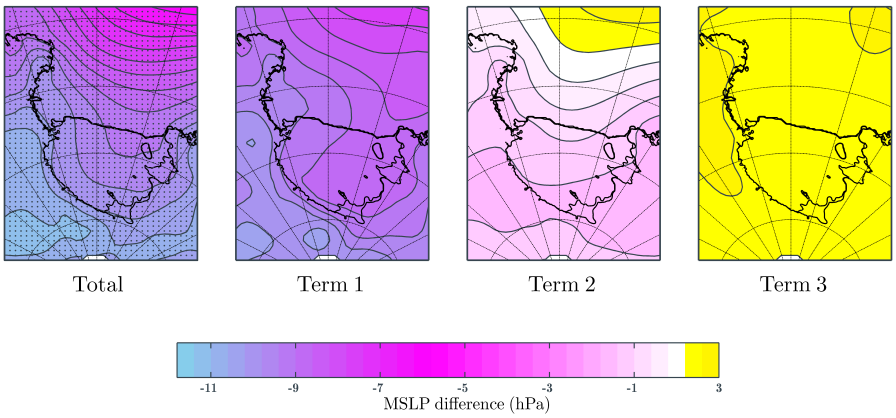

(a) SAM, MSLP.

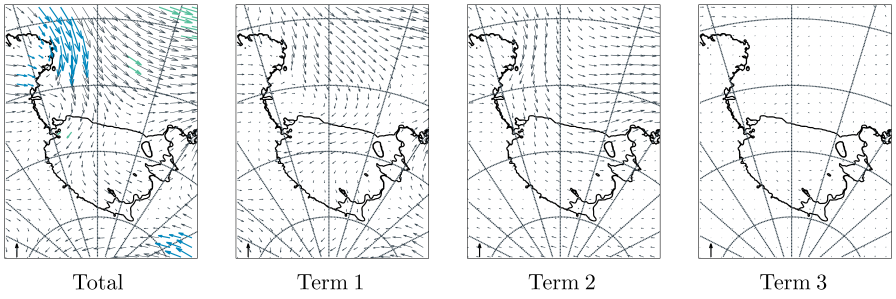

(b) SAM, wind speed.

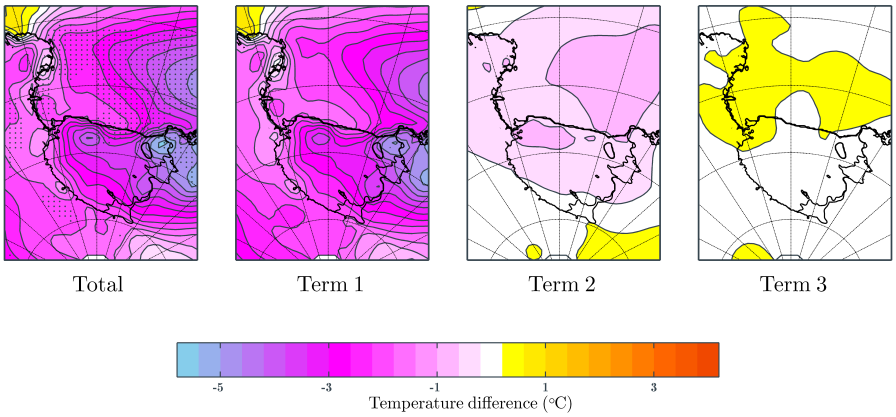

(c) SAM, temperature.

Figure 4.3: As in figure 4.1, but for winter (JJA).

2 also shows some more northerly winds in the north-west and more north-easterlies in the north-east that appear to reinforce the contribution from term 1, although the changes over the ice shelf for term 2 are small.

The temperature change for autumn is large and negative, and significant across the majority of the domain. The largest change is observed on the east of the ice shelf, but this change does not appear

to be significant. We note that this region has a high inter-annual variability and also relatively few observations with which to constrain the reanalysis. Large drops in temperature are also observed on the west of the ice shelf in the vicinity of the Transantarctic Mountains, corresponding to the reduction in wind speeds there. Changes over the ocean are slightly reduced to those over the ice shelf, although the smallest changes are observed in the far south over the East Antarctic Plateau. The contribution of term 1 almost exactly matches the total change, indicating that the temperature changes occur predominantly within clusters, rather than in changes between clusters. Cooling is seen in all clusters, perhaps due to the isolation of the continent as proposed by van den Broeke and van Lipzig (2004). The deep cooling over the south-eastern ocean appears to be associated with enhanced southerlies over the ice shelf to the south. Cooling over the northern ocean occurs in regions where the winds are anomalously northerly, suggesting that a different mechanism is responsible for the temperature change. Cooling is particularly acute off the coast of Oates Land in RAS clusters (especially (1,6) and (2,6)). SAM- years show stronger winds in the region propagating from Terra Nova Bay (fig. 4.6b). It is possible that these winds delay the onset of ice cover at this time of year and hence warm the surrounding atmosphere under SAM- conditions. The band of cooling seen in term 2 is a result of the large reduction in frequency of clusters (1,3) and (3,3), which cause warming in those areas.

The pattern of winter changes (fig. 4.3) in MSLP are broadly similar to those in autumn. However, the magnitude of the decrease is larger over the south-west of the domain, and change contours over the ocean show a more curved appearance. A similar pattern to the autumn is observed over the ice shelf. Despite the magnitude of the changes being larger in the wintertime, the gradient of changes is quite similar, which limits the changes in wind in winter to being about the same magnitude as those in autumn. The changes in winter are also much more broadly distributed between terms 1, 2 and 3. While term 1 still appears to contribute the largest change, terms 2 and 3 also have appreciable magnitudes. It appears that the contributions of terms 1 and 2 combine to produce the gradient seen in the total change. For term 1, the lowering of pressures over the south-west of the domain occurs for similar reasons for that in autumn. Clusters that show deep cyclonic systems in the region show negative pressure changes that are largest in the south-west, indicating that the strength of these clusters in winter is decreased in SAM positive winters compared to SAM negative. In autumn, this is particularly true for clusters in column 3, while in winter, the change is spread over almost all clusters that show strong synoptic gradients, especially those towards the right of the SNC group (top half of column three) and the RAS clusters. Table 4.2 indicates that the majority of change in term 2 is contributed by the decrease in frequency of clusters (1,3) and (3,3), which show cyclonic activity in the north-east of the domain. The decrease in frequency of these clusters causes an increase in pressure in the north and decrease towards the south. A large increase in frequency is observed for cluster (3,6), causing a decrease in MSLP over Marie Byrd Land. These changes in frequency indicate that clusters tend to shift from more northern MSLP minima in SAM negative years to more southern minima in SAM positive. Strong Northern Cyclonic (SNC) and Weak Northern Cyclonic (WNC) group clusters indicate a net decrease, which is offset by Weak Southern Cyclonic (WSC) clusters. This is consistent with the southward shift of the circumpolar trough observed in the SAM positive phase (Kidston et al., 2009; Pohl and Fauchereau, 2012)). Term 3 shows a wide increase in pressure over the entire domain.

As with other seasons, the wind changes for winter are broadly in line with those for the MSLP. Increased northerlies are seen off the coast of Oates Land, which appear to be stronger in the winter change composites than for summer and autumn. Again, these changes occur due to stronger southerly winds in the region under SAM- conditions (fig. 4.6b). The total change in the pressure gradient in that

region in winter is particularly large. In the north-east of the domain, some significantly more westerly winds are observed, which are of a similar magnitude to previous seasons. Wind changes opposite to the prevailing wind are seen over the western ice shelf, as in autumn, but the changes in winter are not significant. Changes on the west side of the ice shelf are indicative of a reduction in strong southerlies there due to changes associated with column 3 and RAS clusters. Unlike in autumn, winds are simply reduced over the ice shelf, rather than being shifted to the east. Over the sea to the north-east of the ice shelf more westerly and slightly more southerly winds are observed. Observation of terms 1 and 2 indicates that wind changes over the southern parts of the domain are mostly caused by intra-cluster changes, while those farther north over the ocean and ice shelf are a combination of both intra- and inter-cluster shifts. In term 1, some increased cyclonic circulation is observed to the north of Ross Island, which is linked to the kink in the pressure change contours. Term 2 shows reduced cyclonic circulation changes around the increase in pressure in the north of the region, indicating a reduced number of cyclones there, as reflected by changes observed in cluster frequencies. Over the ocean, terms 1 and 2 appear to reinforce each other. However, on the ice shelf, term 1 changes are north-easterly while changes due to term 2 are north-westerly. These appear to combine to become mostly northerly changes on the west side of the shelf in the total change diagram. As the change in pressure of term 3 is uniform, wind changes are small.

Temperature changes for winter are large and negative. Magnitudes are similar to those for autumn, but the distribution of changes is rather different. Further, winter changes are significant only over the ocean, Marie Byrd Land, and isolated regions of Victoria Land. Negative temperature changes are largest in the east and are organised into two maxima, one over the ocean and the other slightly farther south over Cape Colbeck. Some warming is observed in the far north-west of the domain, which appears to be associated with anomalous southerly circulation there under SAM- conditions (fig. 4.6b). As with other winter changes, those associated with terms 1 and 2 combine to produce the observed total, although for temperature the magnitude of contribution from term 1 is larger. For term 1, cooling over the ice shelf appears to correspond to a decrease in wind speed there that occurs across clusters. The temperature pattern of term 2 appears to be associated with the observed shift from (1,3) and (3,3) to (3,6). As such, similarly to the MSLP change, both the decrease in strength of cyclonic systems and the shift from clusters representing northern cyclones to those representing southern cyclones, acts to change the temperature between SAM positive and SAM negative winters over the ice shelf. For term 1, as in autumn, the large cooling in the eastern ocean does not appear to correspond to changes in circulation, and may be due to damming of sea ice due to the reduction in southerly winds. The southerly winds appear to be fed from Terra Nova Bay, and are stronger under SAM- conditions (fig. 4.6b). A persistent polynya is present in Terra Nova Bay, which is generated by drainage winds from glaciers in the area (Bromwich, 1989a). It is possible that stronger winds in SAM- conditions act to enlarge the polynya, and hence warm the atmosphere.

Similar to other seasons, the MSLP changes in spring (fig. 4.4) show a net reduction in pressure over the region, which is statistically significant. However, compared to other seasons, the gradient of the pressure change is much larger. This is particularly true over the ocean to the north of the ice shelf and in the far south of the domain. The gradient change occurs due to a region of large pressure reduction centred over Marie Byrd Land in the east. A deep low is observed in the SAM+ composite (fig. 4.5a). A second large reduction occurs in the west, over Victoria Land, somewhat similar to that seen in summer. Pressures over the majority of the ice shelf are also lower than those seen to the north and south, but not as low as those to the east and west, producing a saddle in the MSLP over the ice shelf. This

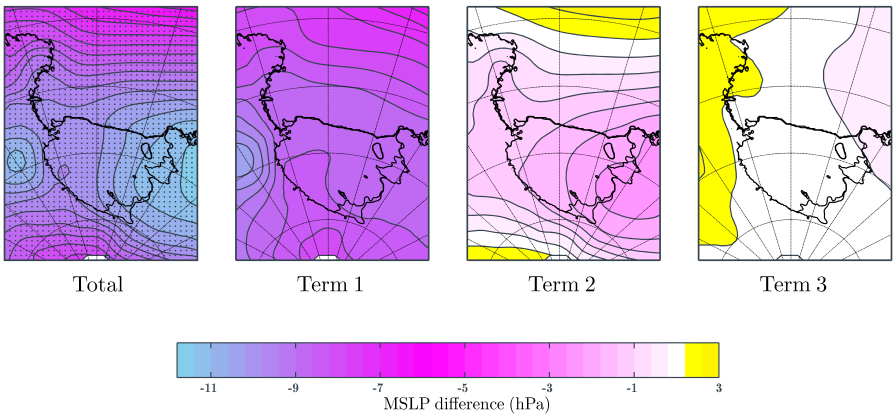

(a) SAM, MSLP.

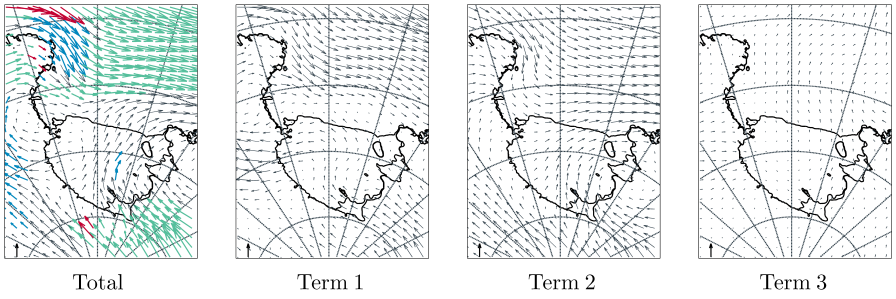

(b) SAM, wind speed.

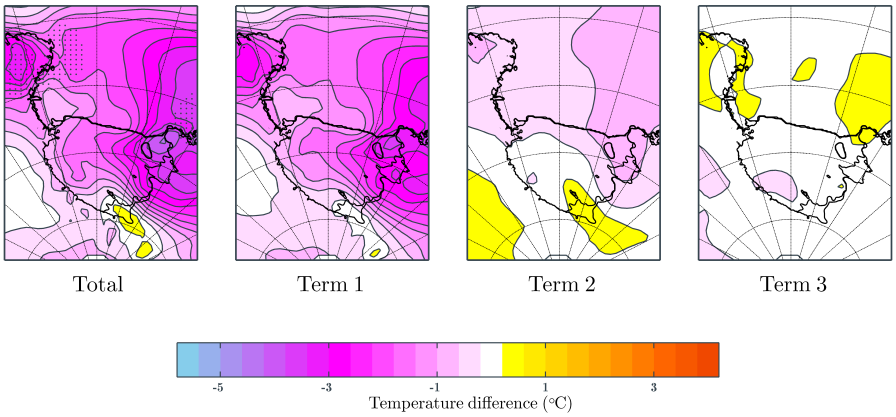

(c) SAM, temperature.

Figure 4.4: As in figure 4.1, but for spring (SON).

pressure change distribution appears to occur due a combination of term 1 and term 2. Both terms show large changes in the vicinity of the ice shelf, and smaller decrease to the north and south. Term 1 appears to be responsible for the deep change in Victoria Land, while term 2 displays raised pressure in the north and south and lower pressure in Marie Byrd Land. The pressure change for term 3 is less uniform than those in other seasons, with a raising of pressures in the west and lowering in the east.

The magnitude of these changes is still small relative to terms 1 and 2, however. For term 1 each cluster displays a lowering of pressures, but the largest magnitude appears to be in the west, counteracting the climatological east-west pressure gradient. The MSLP change pattern of term 2 appears to be due to a significant shift towards clusters on the 6th column (table 4.2), which show deep lows centred over Cape Colbeck and Marie Byrd Land. These clusters also show higher than average pressures in the south-west, and as such their increasing frequency causes higher pressures there. Large reductions in frequencies of clusters such as (1,2) and (1,3) cause higher pressures in the north of the domain. The SNC clusters show a net decrease, which is mostly offset by a net increase in RAS clusters. WSC and KWS clusters also contribute by increasing in frequency.

Corresponding to the large gradient observed in the pressure change, the wind change in the spring between SAM positive and SAM negative conditions are the largest and most significant of all seasons. A large increase in the strength of westerlies is observed in the north of the domain. As in other seasons, anomalous northerly circulation is seen off the coast of Oates Land. Unlike other seasons, many of the changes in this region are significant in both the zonal and meridional directions. Marked differences are also seen through comparison of the SAM+ and SAM- composites (fig. 4.5b and 4.6b). Significant changes are also seen over Oates Land itself. Some significant up-slope winds are seen in Victoria Land, indicating a reduction in katabatic drainage in this region. Very large increases are seen over and up-wind of the Siple Coast and cyclonic circulation changes are observed centred around the maximum pressure change in Marie Bryd Land. Some significantly stronger winds are observed on the ice shelf and the path of the strongest flow appears to be shifted to the east. As in winter, term 1 and term 2 appear to combine to cause changes over the ocean, with term 1 providing a slightly northerly component. Stronger westerlies are apparent in all clusters for term 1, but are particularly strong for clusters in the top-left corner: the SNC (strong northern cyclone) clusters. For term 2, westerlies in the north-east appear to be caused by the increase in frequency of those clusters on the right hand side of table 4.2, including the RAS clusters. The terms also reinforce each other over the Siple Coast, due to the deepening pressures and increased frequencies of RAS clusters. Up-slope winds in Victoria Land are primarily accountable to term 1, while cyclonic circulation changes on the ice shelf and Marie Byrd Land mostly originate in term 2. Changes from term 3 are small, and follow the pressure change distribution.

The change in temperature in spring is somewhat similar to winter, with the largest degree of cooling observed in the east of the domain. Unlike winter, some insignificant warming is observed on the Siple Coast, probably corresponding to increased turbulent mixing there due to stronger winds. As in summer, cooling on the ice shelf is counteracted in regions where winds are observed to be stronger, which may represent increased turbulent mixing or enhanced drainage from West Antarctica. The origin of air may be particularly important in spring, as the ice shelf is colder on average than West Antarctica at this time (see figures 4.5c and 4.6c), meaning that advection of air from West Antarctica is likely to significantly warm the shelf. A deep, significant cooling is also observed in Oates Land, while little or no change occurs over Victoria Land. Examination of the three term diagrams indicates that the large negative changes can be mostly attributed to term 1. Colder temperatures over the ocean are explained by the deeper lows associated with some RAS clusters, which advect cold southern air from the ice shelf northwards. Cooling in Oates Land appears to be forced by cyclonic circulation changes to the south, bringing cold air north. Ocean cooling is reinforced by term 2, caused by the more frequent occurrence lows to the east. Term 2 also appears to force a small warming over the Siple Coast, consistent with the increased incidence of RAS clusters. As in other seasons, the temperature contribution from term 3 is small and disorganised.

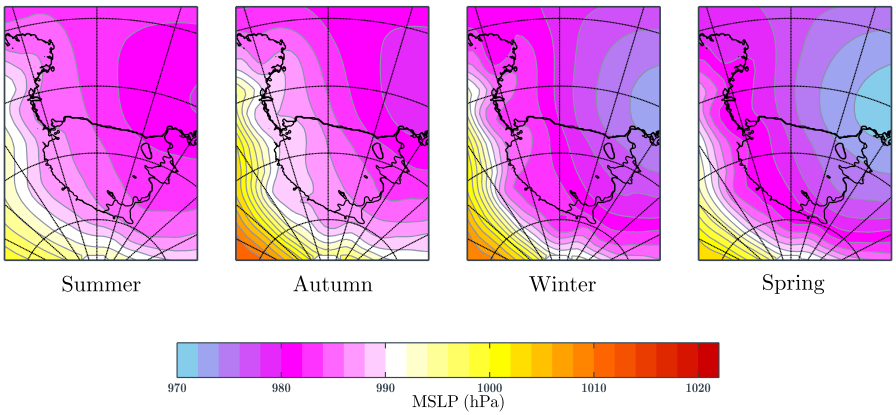

(a) SAM+, MSLP.

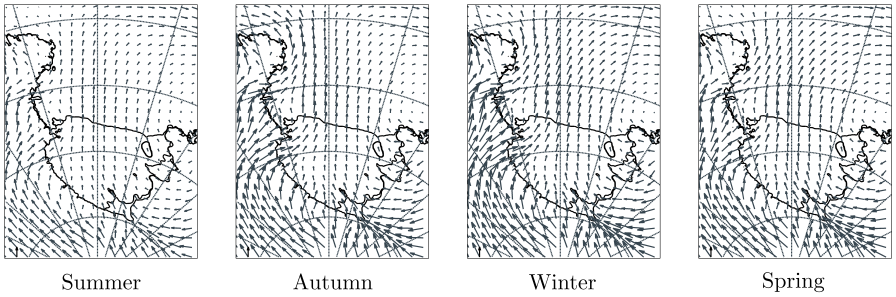

(b) SAM+, wind speed.

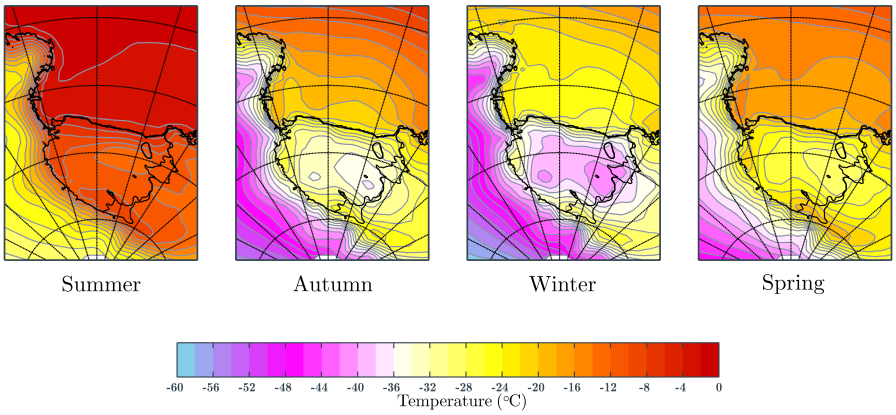

(c) SAM+, temperature.

Figure 4.5: Composites associated with the positive phase of SAM for (a) MSLP, (b) zonal and meridional wind, (c) temperature for each season. For wind diagrams an arrow representing 5 ms^{-1} is shown in the lower left corner.

4.4 El Niño-Southern Oscillation results

In a similar fashion to section 4.3, we now present the differences in atmospheric conditions over the Ross Sea, Ross Ice Shelf, and surrounding regions of East and West Antarctica between the positive

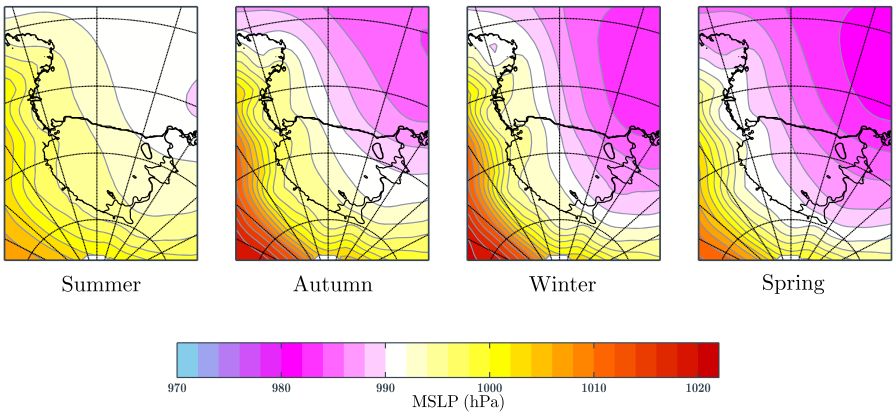

(a) SAM-, MSLP.

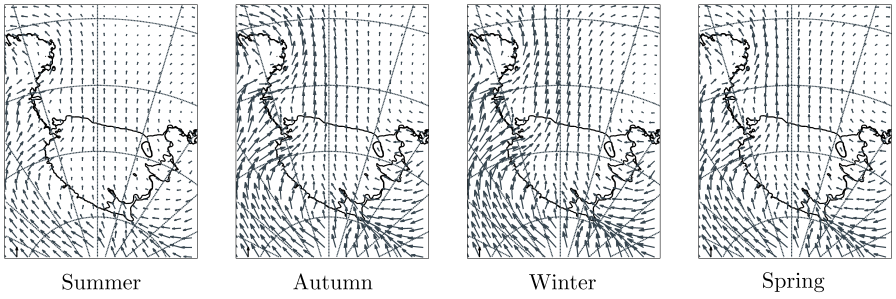

(b) SAM-, wind speed.

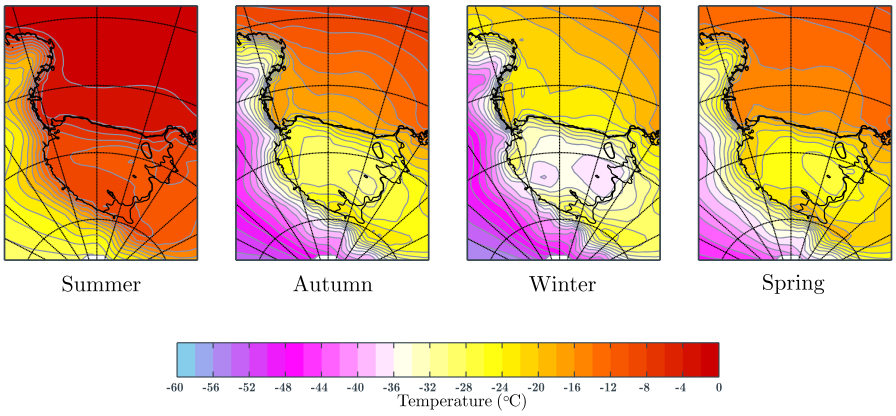

(c) SAM-, temperature.

Figure 4.6: As in figure 4.5, but for the negative SAM phase.

and negative phases of the El Niño-Southern Oscillation, as represented by the SOI. As in the previous section, we use the technique described in section 4.2 to split changes into three terms, the first being associated with changes within individual clusters, the second with changes between clusters, and the third representing the two changes acting at the same time. We also present the total change, which is calculated directly from ERA Interim seasonal means. Figures 4.7, 4.8, 4.9, and 4.10 show the ENSO

	1	2	3	4	5	6
1		**-3.38**	0.99	**1.19**	**-0.89**	**1.07**
		0.22	-0.27	-0.92	**-2.55**	1.09
		-4.08	-0.16	-0.98	**-1.79**	**3.97**
		-1.21	**-3.96**	**-1.76**	**-2.58**	**2.75**
2	-1.62	-0.02	0.81	-0.00	0.75	-0.07
	0.27	1.52	**3.97**	-0.87	0.27	**1.30**
	2.45	**-1.58**	**2.45**	0.22	0.49	**2.17**
	-0.55	**2.47**	**-1.59**	**-2.53**	**5.05**	-0.71
3	**-1.89**	**1.07**	**3.71**	0.05		**-0.74**
	-2.55	0.60	**-2.83**	0.92		0.38
	-0.65	-0.71	0.98	**-3.15**		**-1.85**
	-3.13	0.66	**-1.48**	**1.70**		0.66
4		-2.64	-0.41	**2.90**	-0.87	
		-0.38	-1.03	**1.68**	-0.82	
		-0.43	**3.70**	-0.16	-0.87	
		-1.70	**3.35**	**2.53**	**2.03**	

Table 4.3: As in table 4.2, but for SOI.

related changes for summer, autumn, winter, and spring, respectively. Table 4.3 shows the change in frequency of each cluster between the SOI positive and negative phases for each cluster and each season. The layout is correspondent to that of table 4.2. Figures 4.11 and 4.12 show composites for MSLP, winds, and temperature for La Niña and El Niño conditions, respectively.

During summertime, MSLP changes in the domain are large and negative. Statistical significance is attained in all regions, except for a small area to the south. The largest magnitude changes are in the north-east, and a secondary maximum is observed in northern Victoria Land. The deepening of pressure in the north-east under SOI+ conditions is extremely apparent in composites shown in figures 4.11a and 4.12a, and may correspond to a shift to the east of the low pressure region in El Niño summers (Turner et al., 2012). A large gradient in the change is apparent across the ice shelf. Examination of the three terms associated with the change shows that the largest contribution comes from term 1, which shows a pattern which largely matches the total. A smaller contribution is provided by term 2, which shows the largest reduction in the north-east of the domain, and an increasing gradient across the ice shelf. Some positive changes can be seen in the far north-west and south but these are small. Changes associated with term 3 are small, disordered and positive, and appear to counteract those of terms 1 and 2. Although similar patterns are seen for most clusters, as for the SAM changes in the summertime, the largest intra-cluster change (term 1) occurs due to the development of a pressure gradient resembling the total change in clusters to the left hand side of figure 3.3. The change in cluster (4,2) is particularly large, suggesting that this cluster dominates the observed changes. This is unsurprising, as this cluster is by far the most frequent in the summertime (fig. 3.6). For term 2, the decrease in pressure in the north-east and east of the domain is largely caused by an increase in incidence of clusters that represent low pressures in the east and north-east, in particular, clusters (1,4), (1,6) (both RAS clusters) and (3,3) show significant increases in frequency. (1,3) and (2,3) also contribute through positive frequency changes. Despite their increases being insignificant, the depth of the MSLP minima associated with these clusters is low. Thus, it appears that in La Niña summers, there is a higher degree of cyclonic activity in the Ross Sea, and the background synoptic MSLP gradient is also steeper than in El Niño summers. A net shift also occurs from SNC clusters towards the RAS group. An increase is also observed in the

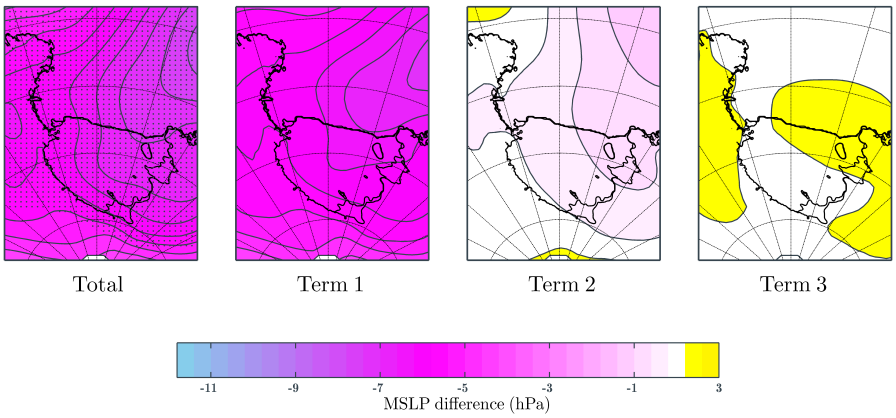

(a) SOI, MSLP.

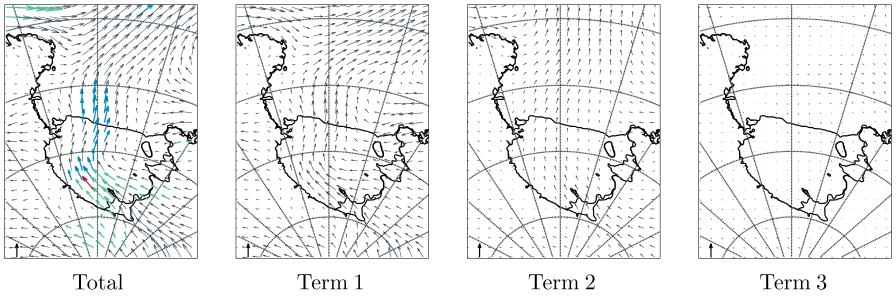

(b) SOI, wind speed.

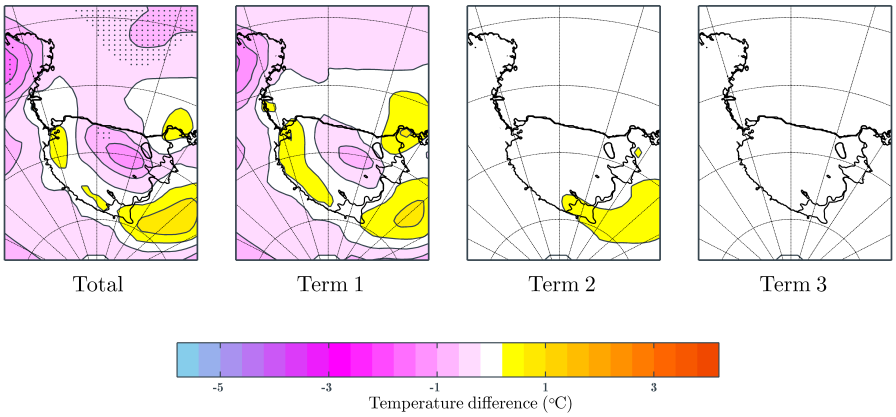

(c) SOI, temperature.

Figure 4.7: Difference between the extreme positive and negative summers (DJF) of SOI for (a) MSLP, (b) zonal and meridional wind, (c) temperature, for the total change and each term of equation (4.6). For the total change, for MSLP and temperature, significance at $p \leq 0.05$ is indicated by stippling. For wind speeds, green (blue) arrows show changes that are significant in the zonal (meridional) direction. Red arrows show changes that are significant in both. Grey arrows are not significant. A 1 ms^{-1} arrow is shown in the lower left corner of each diagram. Significance is not shown for the changes according to each term in equation (4.6).

WNC group, suggesting that cyclones still occur in the north of the domain, but they are less frequent and weaker under La Niña conditions.

The summertime pressure gradient changes force significant wind changes within the domain. A largely significant increase in the prevailing wind is seen propagating from the Siple Coast and across the ice shelf to the north, following the standard track of the Ross Ice Shelf Air Stream. This is particularly noticeable in comparison of figures 4.11b and 4.12b: SOI- summers show low wind speeds on the west of the ice shelf. Significance is attained until slightly north of the ice shelf. Insignificant changes towards south-westerly winds are observed over the ocean. In the far north-west, significantly stronger westerlies are seen. Changes over Victoria Land are generally small and up-slope. In the south of the domain, insignificant increases in down-slope winds are seen up-wind of the Siple Coast, and some significant changes are seen farther to the west. The general pattern of the flow change appears to be cyclonic around the deepest pressure change. As for the pressure, the largest contribution comes from term 1, which shows a pattern that matches the total, particularly over the ice shelf. Correspondingly, winds in this region in cluster (4,2) are stronger in SOI positive conditions than SOI negative. Wind changes shown for term 2 are similar to term 1, but are directed more towards the north, particularly over the ocean. As for the pressure, the increase in clusters representing deep pressure minima in the east appears to force wind changes.

The temperature pattern for summer reflects the changes in wind conditions. Some significant results are seen, but they are confined to an area of cooling in the far north-east. This cooling appears to be produced by the advection of cold air northwards due to stronger southerly winds in the region. Other areas of significant cooling are seen on the northern portion of the ice shelf and over Oates Land. Slight warming is observed across the ice shelf, parallel with the Transantarctic Mountains, broadly following the path of heightened wind speeds, and suggesting that an increase in the turbulent vertical heat flux is the cause. Warming up-wind of the Siple Coast may be due to the southward movement of maritime air. Term 1 appears to contribute the majority of temperature changes, with most clusters showing warming along the Transantarctic Mountains and cooling over the ocean, due to stronger winds being present over the ice shelf. Again, cluster (4,2) seems to dominate these changes. The cold spot in the centre of the ice shelf appear to be caused by changes in clusters (1,2) and (1,3), which show shifts in their lowest pressure towards the east, causing slightly higher meridional winds in this region. The winds appear to transport cold air north. The contribution of term 2 to temperature is smaller. Positive anomalies are seen over the Siple Coast area and into West Antarctica. These appear to be caused by enhanced drainage in the area due to an increased frequency of clusters with strong synoptic gradients, as discussed above.

MSLP patterns for autumn (fig. 4.8) do not show any regions in which the changes are significant. This may be expected, as in autumn and winter the forcing of the PSA wave train from the tropics is weakest (Jin and Kirtman, 2009), as ENSO events generally peak in the austral summer. The covariability of the ENSO and SAM modes is also weakest at this time of year (section 2.7). However, despite the pressure changes being insignificant, some wind changes do attain significance, and thus we will continue to discuss ENSO forcing. The pattern of pressure changes in the autumn is similar to that in the summer, with the deepest changes observed in the east of the domain. The area where MSLP drops the most in autumn is farther to the south, however. The magnitude of changes is also smaller. The region of lowest pressure does not appear to move much between SOI+ (fig. 4.11a) and SOI- (fig. 4.12a) autumns. An increase in pressure is observed over the high parts of East Antarctica in the far south-west of the domain. The contribution from term 1 appears to explain most of the pressure changes, while that from term 2 shows a small reduction in pressure in the east and increase in the west, which acts to reinforce

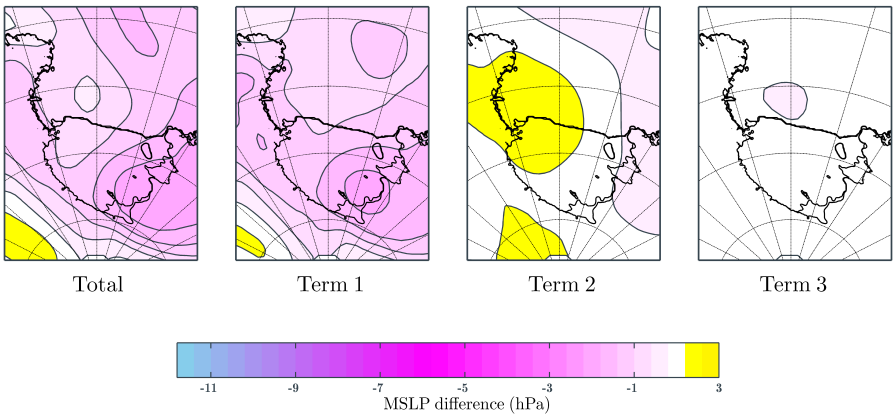

(a) SOI, MSLP.

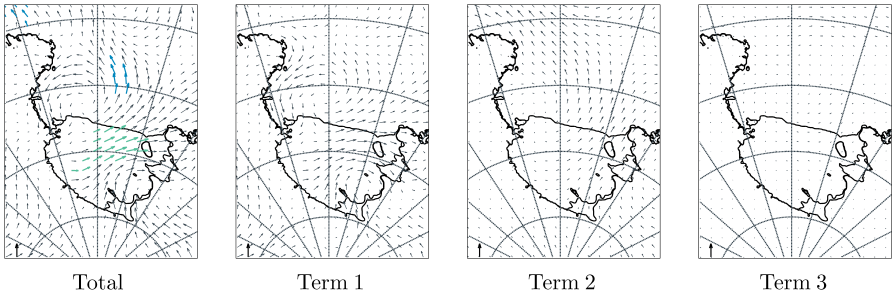

(b) SOI, wind speed.

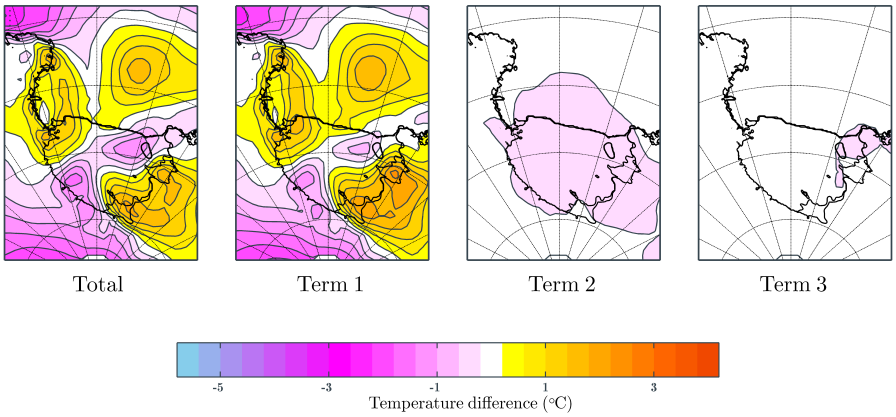

(c) SOI, temperature.

Figure 4.8: As in figure 4.7, but for autumn (MAM).

the gradient across the total change. As for other change composites, the contribution from term 3 is small. Changes in term 1 appear to be the result of the deepening of pressure over Marie Byrd Land in cluster (4,2), clusters on the left hand side of the RAS group, and in the SNC group. The contribution from term 2 appears to occur due to an increase in frequencies of clusters (1,6) and (2,3) and a decrease in frequency of (3,1). In autumn, a net increase is observed in the frequency of SNC clusters, which

mainly comes from cluster (2,3), the most RAS-like of the group. A corresponding decrease is seen in the WNC clusters.

The wind changes for the autumn months are significant across a large part of the ice shelf, and small areas of the ocean. Anticyclonic changes, indicative of a reduction in cyclonic winds, are observed following the pressure change contours over the southern Ross Sea, causing a more northerly wind component near Ross Island and south-westerly changes over the ice shelf. Significant changes towards southerlies are seen in the far north-west off the northern coast of Oates Land. These winds are more easterly under SOI- conditions (cf. figs 4.11b and 4.12b). Slightly enhanced drainage is seen over southern Victoria Land and southern Marie Byrd Land, although these changes do not attain significance. As for the pressure, the majority of wind changes are explained by term 1, due to the deepening pressure seen primarily over Marie Byrd Land and the eastern ice shelf. Smaller changes are seen in term 2. Specifically, anticyclonic changes are seen to the north of the ice shelf, following the pressure change contours, which mark a reduction in the number of cyclonic systems there.

Temperature changes appear to be quite large in autumn. They are not significant anywhere in the domain, but generally correspond to the changes in circulation described above. Warm patches are seen in the western Ross Sea, due to the reduced southerlies there. Enhanced drainage and stronger winds propagating across the ice shelf from south-west to north-east cause cooling in a path across the shelf, possibly due to the transport of cold air from East Antarctica. Warming is also seen at the Siple Coast, perhaps because of the slightly stronger down-slope winds there. As for other parameters, term 1 appears to match the total change in temperature well and dominates the overall change. Term 2 shows slight cooling in a broad area across the ice shelf, which appears to be caused by greater southerly motion in the region. Warming in the north-eastern Ross Sea is not explained by changes in circulation and may be the result of an oceanic ENSO teleconnection. This warming occurs in all clusters for term 1, except those on the far right of figure 3.3. These clusters show enhanced southerly winds, which may counteract the warming through the northward advection of polar air. Kwok and Comiso (2002a) showed warmer sea-surface temperature (SST) and surface air temperature (SAT) in this region under La Niña conditions, which suggests that the warm signature may be oceanic in origin. The warming appears to be contrary to that reported by Ledley and Huang (1997). However, this study defined the Ross Sea to extend northwards from the continental margin to the latitude of 50 °S and calculated the average SST change over this large region. Our results, and those of Kwok and Comiso (2002a) and Kwok and Comiso (2002b) suggest a warming in our domain in La Niña years. Farther to the north, Kwok and Comiso (2002a) display a cooling under the same conditions, as reported by Ledley and Huang (1997).

Similar to autumn, MSLP changes in the domain in the wintertime (fig. 4.9) are not significant, however, in many areas both the wind and temperature changes attain significance. The pattern of MSLP changes is similar to that in autumn, with the largest negative change occurring in the east of the domain. The maximum change is however larger than that of autumn and located farther to the north, which is also apparent from comparison of figures 4.11a and 4.12a. A secondary negative peak is seen over Victoria Land. The change contours over the ice shelf and ocean are generally aligned south to north. A region of raised pressure exists in the far south of the domain and spreads to the south-west. As for previous change composites, the largest contribution of pressure change occurs due to term 1, and is thus caused predominantly by changes within clusters. Examination of individual cluster diagrams (not shown) indicates that the pressure changes are associated mainly with clusters (1,2) and (2,2) which show large negative changes in the north-east, suggesting an eastward shift of the minimum pressure in these clusters under SOI+ conditions. Cluster (4,5) also shows a deepening of pressure in the north-east.

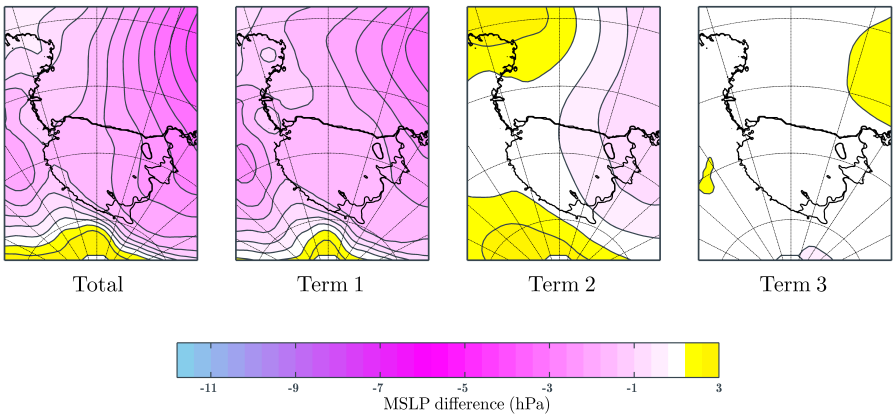

(a) SOI, MSLP.

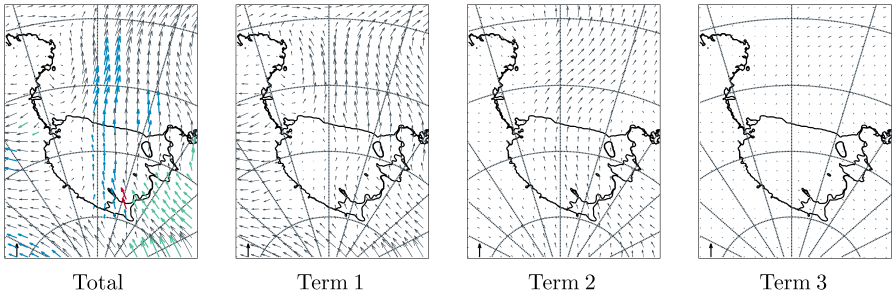

(b) SOI, wind speed.

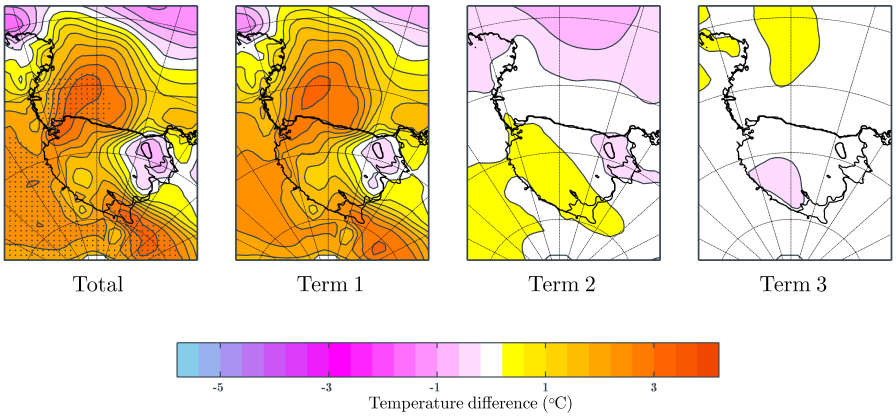

(c) SOI, temperature.

Figure 4.9: As in figure 4.7, but for winter (JJA).

A large shift towards positive MSLP is observed for cluster (1,5), with a peak in the south of the domain, which may dominate the positive change in the south for term 1. The contribution from term 2 is smaller than for term 1, but it is still evident in the total change, particularly in the south-west of the domain where the total and term 2 both show positive changes. Term 2 also acts to reinforce the deepening of pressures in the north-east and thus helps effect the gradient over the ice shelf. A net shift is seen

in frequencies from clusters in the WSC group to the RAS group, suggesting that low pressure systems exist in similar locations but are generally deeper with respect to the background pressure.

Wind changes in the winter attain significance in many areas, predominantly over the Siple Coast and West Antarctica, and in a path from the south-east across the ice shelf to the north, and over the ocean north of the shelf. Wind changes in this region appear to be mainly southerly. However, comparison of figures 4.11b and 4.12b indicates that the direction of winds does not change much, due to the symmetry in MSLP fields between SOI+ and SOI- events. Significantly reduced down-slope flow is observed over Victoria Land. Anomalous northerlies are seen north of Ross Island, although these are not significant. The general pattern is that of cyclonic changes around the largest reduction in pressure in the north-east of the domain. Unsurprisingly, the largest contribution comes from term 1, which displays a pattern similar to that of the total. Stronger southerly winds are observed over the ice shelf in almost all clusters and are often shifted towards the centre of the shelf. Observation of term 2 indicates that the frequency changes detailed above act to reinforce term 1 over the Siple Coast and ice shelf, and give the total change a slight westerly direction over the ocean to the north. The contribution from term 3 is small.

Temperature changes in the winter between positive and negative ENSO phases are large and mainly positive. Statistical significance is attained in large parts of the south-west of the domain, upwind of the Siple Coast and to the north of Ross Island. Some cold anomalies are also seen in the north of the domain and around Roosevelt Island. The cold changes are not significant, however. As for the pressure and wind, the largest contribution to temperature comes from term 1, which shows a pattern which matches the total. Term 2 appears to reinforce the warming over the western parts of the ice shelf and the cooling in the north and at Roosevelt Island. The contribution from term 3 is small. Term 1 temperature changes over the ocean appear to be forced partly by anomalous southerly winds and may be associated with the opening of polynya. Warming farther to the west may also be caused by oceanic effects, as proposed in the autumn. This is further evidenced by the fact that almost all clusters show warming there for term 1, irrespective of their wind conditions. The warming at the Siple coast appears to be associated with stronger drainage and may be caused by the adiabatic warming of air from West Antarctica. The large warming over East Antarctica seems to be associated with up-slope directed wind changes there. The positive temperature change appears in almost all clusters for term 1, which suggests that the change is not forced by circulation, but that the increased temperature acts to prohibit strong katabatic flows from forming, resulting in the up-slope directed wind changes. We note that Kwok and Comiso (2002b) also found positive temperature changes in this area. Further investigation is needed to ascertain its origin.

Finally, we discuss springtime changes associated with ENSO (fig. 4.10). MSLP differences do not reach significance anywhere in the domain. It is possible that the large variability observed between ENSO events prohibits statistically significant relationships from being attained (Karoly, 1989; Lachlan-Cope and Connolley, 2006). Further, the inclusion of September (essentially winter) conditions in spring is debatable and may have biased results. As in winter, many changes in the wind and temperature are significant despite insignificant changes in the MSLP. MSLP change composites show a net negative change across the domain. As in other seasons, the largest negative change is located in the east, although the maximum change exists over Marie Byrd Land, and thus has more in common with autumn than winter. An area of almost no change occurs in the middle of the Ross Sea, which can also be determined by comparison of figures 4.11a and 4.12a. The resulting pressure change gradient across the ice shelf and ocean is directed from south-east to north-west. MSLP changes for term 1 are largest, and are similarly organised as the total change. However, the pattern is clearly modulated by term 2, which

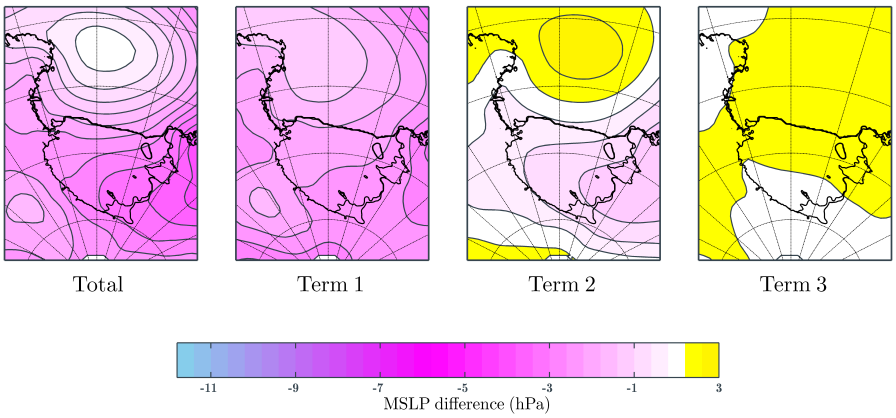

(a) SOI, MSLP.

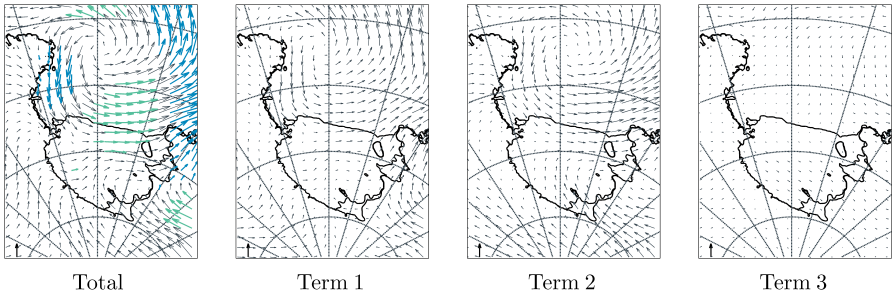

(b) SOI, wind speed.

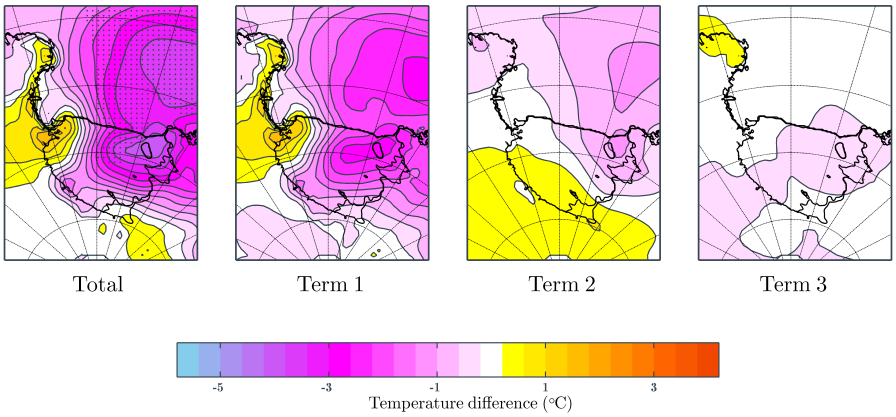

(c) SOI, temperature.

Figure 4.10: As in figure 4.7, but for spring (SON).

shows smaller, but important changes in MSLP. A slight positive change is seen in the Ross Sea, which appears to combine with term 1 to produce the lack of change there in total. Term 3 also seems to contribute to this a little. Term 2 acts to reinforce the decrease in pressure over the east of the domain and counteracts decreases in the south-west. Similar to the summer conditions, the pressure changes of term 1 appear to be forced by an increase of the pressure gradient across the ice shelf in cluster (4,2).

Table 4.3 indicates that the changes in term 2 are associated with the increase in frequency of clusters to the right of figure 3.3, which show deep lows over Marie Byrd Land. This coincides with a decrease in frequency of clusters with lows to the north of the domain, such as (1,3), (1,4), (2,3) and (2,4), which appears to cause the change towards higher pressures in the Ross Sea.

Wind changes for winter are significant in many places over the Ross Sea. The winds appear to change anticyclonically, following the pressure change gradient in the region. The changing wind directions follow subtle asymmetries between the pressure fields shown in figures 4.11a and 4.12a. Significantly more southerly winds are seen in the east of the domain. Northerlies in the west mark the weakening of the southerly component in SOI+ conditions (cf. figs 4.11b and 4.12b). Wind changes over the ice shelf are small, except for westerly changes at the northern extent of the shelf associated with the anticyclonic change. Increased drainage flows are also observed up-wind of the Siple Coast, consistent with the pressure change there. Springtime appears to be the only season in which the term 2 wind changes appear to be larger than term 1. This is particularly clear in the east of the domain, where the tight pressure change gradient of term 2 causes large shifts in the wind. In almost all areas, terms 1 and 2 act to reinforce each other to produce the total change pattern. Interestingly, despite the increase in frequency of some RAS clusters, particularly those on the far right-hand side of figure 3.3, winds over the ice shelf for term 2 do not increase significantly. This may be caused by a shift between different RAS states. For instance, clusters (1,6) and (2,5) have large increased frequencies, while those of all other clusters in the RAS group appear to decrease. This suggests that the change in frequency of RAS events is not large, but that the position of cyclonic systems forcing such event shifts to the east. Accordingly, the sum of frequency changes in the RAS group is only 0.22 %. A net decrease is observed in the SNC group, while an increase in the KWS occurs. As for other seasons, the contribution from term 3 is small.

The springtime change in temperature closely follows the changes in wind patterns. A significant cooling is seen over the ocean, particularly towards the north-east. This cooling appears to be associated with the enhanced advection of cold air to the north and reduction in southward transport of northern air, as forced by anomalous southerly winds in the area. Cooling is also observed over the ice shelf, and some is significant. Insignificant warming is observed near Ross Island and along the coast of Victoria Land, due to the reduced southerly winds observed there. A slight warming is also seen at the Siple Coast, due to the enhanced down-slope flows. The temperature pattern appears to be forced primarily by term 1, although term 2 appears to cause warming at the Siple Coast, due to the increase in frequency of clusters with strong drainage flows.

4.5 Discussion and conclusions

In section 4.3 we showed large and significant decreases in the MSLP in the study domain under positive SAM conditions compared to negative. This is unsurprising, given the vicinity of the region to the circumpolar trough at around 65 °S which is considered to be the most active SAM region and hence contributes to the strength of the SAM index as defined by Marshall (2003). We note, however, that neither of the long-period station records from the region (McMurdo Station and Scott Base on Ross Island) are employed in Marshall (2003)'s SAM index, as they are considered to be too far south. MSLP changes between SAM+ and SAM- conditions have been shown to vary across seasons. In summer and spring the change in the domain is most negative in the east, while in autumn and winter the largest change is in the south and a kink is observed in the pressure change that follows the contours of the ice shelf. This kink appears to be the result of subtle asymmetries between SAM+ and SAM- conditions.

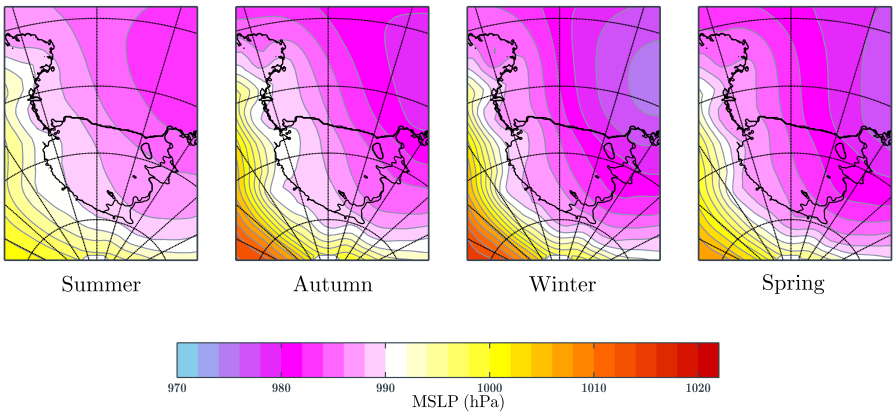

(a) SOI+, MSLP.

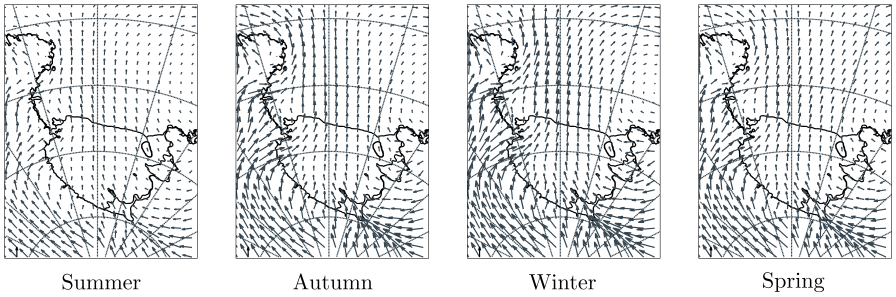

(b) SOI+, wind speed.

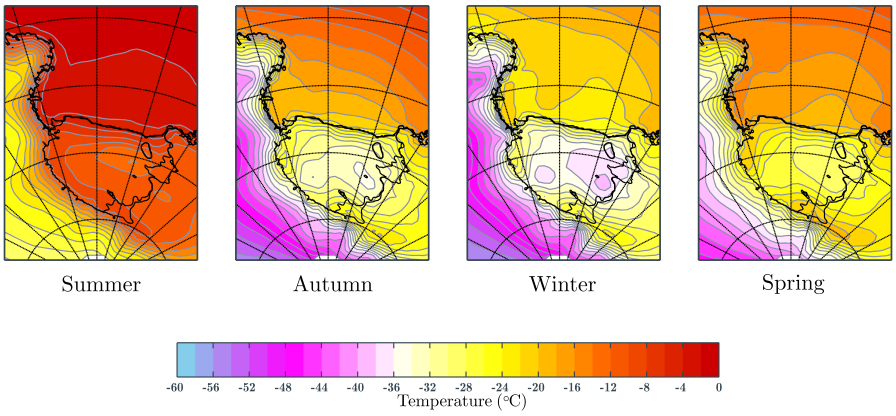

(c) SOI+, temperature.

Figure 4.11: Composites associated with the positive phase of SOI (La Niña) for (a) MSLP, (b) zonal and meridional wind, (c) temperature for each season. For wind diagrams an arrow representing 5 ms^{-1} is shown in the lower left corner.

Examination of the wider MSLP dependence on SAM reported by van den Broeke and van Lipzig (2004) (their figure 5) indicates that the most sensitive area to SAM changes occurs in the east of the Ross Sea in summer and spring, but moves east into the Amundsen Sea in the autumn and winter. Therefore, the lack of a large change in the east of our domain in autumn and winter is consistent with previous

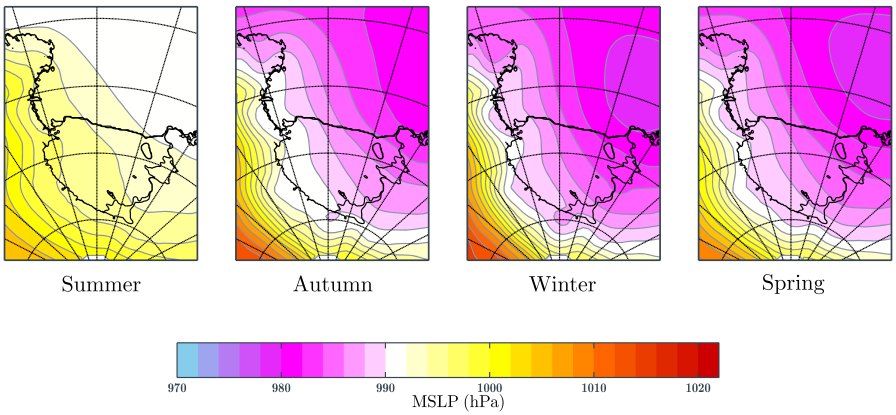

(a) SOI-, MSLP.

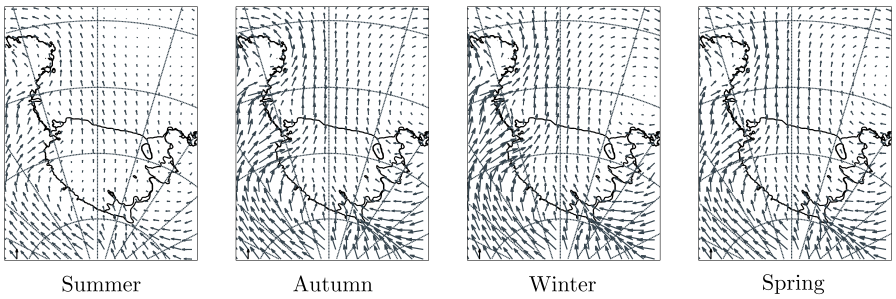

(b) SOI-, wind speed.

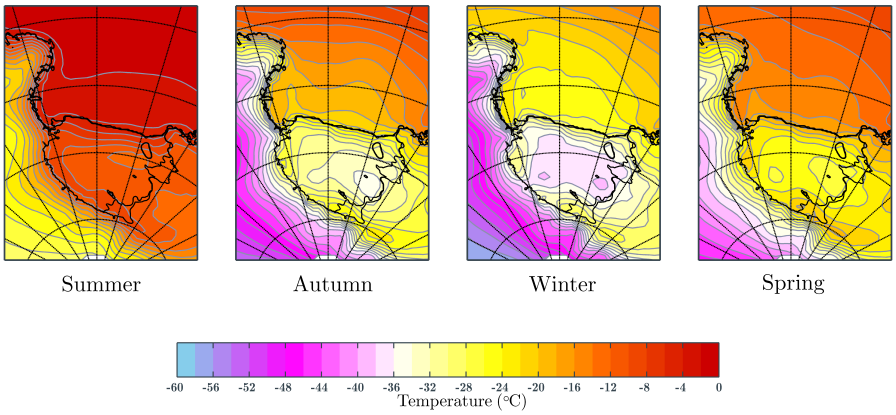

(c) SOI-, temperature.

Figure 4.12: As in figure 4.5, but for the negative SOI (El Niño) phase.

results. Similarly, Fogt et al. (2012a) showed a higher sensitivity of MSLP to SAM changes farther east in autumn and winter compared to spring and summer (their figure 9). The change in sensitivity is also visible in the correlations of 500 hPa height with the SAM index of Kidston et al. (2009) (their figure 2), and appears to be due to the less annular structure of SAM in the winter and a more pronounced zonal wavenumber 3 signal. The movement of the area of highest change to the east in winter seems

counter-intuitive, as the annual variability in the location of the ABS low reported by Fogt et al. (2012b) and Turner et al. (2012) indicates that the low exists to the west (in the Ross Sea) at this time. Thus, it appears that the location of the greatest change in pressure due to SAM may be independent of the location of the lowest absolute pressure.

Changes associated with term 1 appear to dominate the change in pressure. However, in spring in particular, inter-cluster changes act to reinforce the pressure gradient change and generate a steep gradient of pressure change over the Ross Sea. This change appears to occur due to a shift of cluster frequencies towards cyclonic activity in the east of the region. These clusters have been shown to represent RAS events. In all seasons we observe a net decrease in the Strong Northern Cyclonic clusters. A corresponding increase is seen in KWS clusters in the summer and autumn, WSC in winter, and RAS clusters in spring.

Wind differences between positive and negative SAM conditions resemble closely the well-known aspects of the SAM oscillation. In all seasons, increased westerly winds are observed in the north of the domain, which are induced by the increased north-south pressure gradient present in that region. The increase in circumpolar westerlies around the latitude of the circumpolar trough is a well-reported SAM effect (eg. Thompson and Wallace (2000)). An enhanced northerly component is also seen in the west as southerly winds south of Cape Adare are reduced in SAM+ conditions. A similar structure can be seen in van den Broeke and van Lipzig (2004)'s figure 4b. Wind changes predominantly follow the background pressure gradient changes of term 1, but in winter and spring, the term 2 changes are also large and generally act to reinforce those of term 1. In autumn and spring, MSLP changes act to shift the strongest winds across the ice shelf to the east, while in summer the winds in the west of the shelf are enhanced. This appears to be caused both by a shift in frequencies towards RAS clusters and modulation of the winds by the background pressure changes. In all seasons except winter, southerly flow is enhanced in a large portion of the ice shelf. In winter, kinks in the MSLP changes cause enhanced southerly and westerly winds just to the north of the shelf but weaker winds over the shelf itself. Modelling experiments of Turner et al. (2009b) indicated that the deepening of the ABS low in positive SAM conditions was caused by increased westerly winds and thus increased flow separation around high coastal topography. They suggested that the resulting more active cyclonic conditions forced stronger southerly winds over the Ross Ice Shelf and Ross Sea. This appears to be reflected in our results, although in summer, autumn, and spring the region of strongest flow is shifted to the east, and in winter the flow is increased more in the westerly direction than the southerly. It is unclear how these changes might affect sea ice production and advection, and this requires further study.

Reductions in temperature are seen across the region for all seasons, but seem to be weakest in summer and strongest in autumn. Large cooling seen in SAM positive years is consistent with findings from numerous other studies (Gong and Wang, 1999; Thompson and Wallace, 2000; Thompson and Solomon, 2002; Gillett et al., 2006). Very large decreases in autumn are particularly apparent surrounding and to the south of Roosevelt Island, although these are not significant. The deep cooling here is consistent with the results of Kwok and Comiso (2002a), however. The highest dependence of temperature being in autumn is consistent with temperature variability reported by Marshall (2007), van den Broeke and van Lipzig (2004) and Schneider et al. (2012b). Most of the change in the temperature occurs due to intra-cluster changes (term 1), partly due to changes in horizontal advection and the potential formation of strong inversion layers due to decreased wind speeds. We find that the cooling in autumn and winter on the west of the ice shelf is enhanced by the lower wind speeds observed in these regions in SAM+ years. In spring and summer, higher wind speeds in this area offset the cooling caused by the isolation of

the continent. Some background changes are harder to classify, however, due to the complex and varied nature of the processes involved. For instance, the cooling of the ocean in autumn is not consistent with circulation changes, and could be associated with ocean-ice feedbacks.

For ENSO-related MSLP changes, results indicate a lowering of the pressure in the study domain under La Niña conditions, and a heightening under El Niño conditions. This is true in all seasons, but particularly apparent and significant in the summertime, when the ENSO phenomenon tends to peak. A distinct asymmetry exists in the lowering pressure patterns, with larger magnitudes invariably observed in the east of the region. The reduction in pressure appears to be mainly caused by background changes in the pressure field of particular clusters. However, some inter-cluster changes also contribute appreciably. This is particularly true in winter and spring. It is well known that during cold phases of the ENSO phenomenon, a deepening of the area of low pressure in the Amundsen-Bellingshausen Seas is observed, while in ENSO warm phases, the pressure in the area is higher (Turner et al., 2012), although this relationship has been shown to be variable and dependent on factors such as the location of convection in the tropical pacific (Karoly, 1989; Lachlan-Cope and Connolley, 2006), the time of year (Jin and Kirtman, 2009), and possible interconnections with the SAM phenomenon (Fogt and Bromwich, 2006; Fogt et al., 2011). That the largest MSLP changes are seen in summer and spring is consistent of the results of the seasonal analysis of Jin and Kirtman (2009). However, Turner et al. (2012) reported the largest ENSO-related MSLP variable being in winter. It is possible that the large variability in the location of the ABS low at this time (Fogt et al., 2012b; Turner et al., 2012) masks the ENSO-related variability in the eastern Ross Sea. The results presented in the previous section, in which clusters with cyclonic systems in the east of the domain increase in frequency in La Niña years is in agreement with the results of Markle et al. (2012). Further, the cyclone tracking study of Pezza et al. (2008) showed a shift of cyclone densities from the north and west of the Ross Sea in El Niño years to the east in La Niña years (their fig 3a), which corresponds to the shift in frequencies observed here. Chen et al. (1996) and Yuan (2004) also reported a higher incidence of synoptic storms in the Ross/Amundsen Seas under La Niño conditions, in accordance with the southward shift of the eddy-driven jet.

We have shown significant wind changes between La Niña and El Niño conditions. Specifically, an increase in northward flow is observed over the ice shelf in all seasons except spring. In these seasons, wind increases are forced by the reduction of pressure in the east of the domain, as discussed above and thus the largest contribution comes from term 1. An appreciable contribution towards wind changes is given by term 2, particularly in winter. For inter-cluster changes, the shift towards cyclonic activity in the east appears to be the most important factor in driving southerly winds over the ice shelf and ocean directly to the north. Similar wind patterns were reported by Kwok and Comiso (2002a) and suggested by the analysis of Stammerjohn et al. (2008). Clusters in the RAS group contribute heavily to increasing southerly wind speeds at the northern edge of the shelf, and appear to be highly dependent on SOI conditions, as suggested by Bromwich et al. (1993). In spring, terms 1 and 2 appear to contribute in roughly similar amounts to increased cyclonic motion over West Antarctica and decreased cyclonic motion in the Ross Sea. Winds over the ice shelf are not significantly increased, although more southerly winds occur over the eastern Ross Sea, which may be important for sea ice movement. These wind changes occur due to highly asymmetric responses of MSLP between SOI+ and SOI- conditions in the spring, and are a combination of changes associated with terms 1 and 2. The sea ice study of Harangozo and Connolley (2006) found comparable meridional wind changes in the springtime.

Temperature changes between positive SOI and negative SOI conditions also show many areas of significant change. In La Niña conditions, warming is seen over the ice shelf in regions where the prevailing

wind is strengthened. We suggest that this occurs due to the disruption of the strong temperature inversion, as proposed by van den Broeke and van Lipzig (2004). This is particularly apparent in the area covered by the RAS. The temperature pattern also corresponds in many areas to regions of anomalous advection due to changes in wind patterns. As with the pressure and wind changes, the largest contribution appears to come from term 1, but winter and spring also show a high dependence on term 2. Kwok and Comiso (2002b) calculated regression coefficients between surface temperature data derived from the AVHRR satellite-borne sensor and the SOI. For annual averages, they found significantly positive relationships on areas of the ice shelf, in similar regions to those described in section 4.4. They also found positive coefficients on the East Antarctic ice sheet, in a similar location to the winter results displayed here (fig. 4.9c). Significantly positive results were also obtained over regions of the Ross Sea directly north of the permanent ice shelf. Term 1 changes in temperature are harder to interpret than term 2, as the former contains contributions from both dynamic and thermodynamic processes. As such, the much larger temperature changes contributed by term 1 may be associated with non-circulatory changes, such as cloud cover and ocean-ice feedbacks. As for the unexplained temperature changes between SAM+ and SAM- conditions, those for ENSO variability require further investigation.

A notable aspect of the changes reported in the previous two sections is that for both spring and summer, ENSO and SAM related changes appear to be rather similar. This apparent similarity between the two oscillations has been noted before, and occurs because of the modulation of both modes of the low pressure region in the ABS, due to the non-annular structure of SAM and the ENSO-related wave train. Several authors have suggested that in phase variability of the modes tends to reinforce each other and that they share a high degree of variance, particularly in recent decades (Fogt and Bromwich, 2006; L'Heureux and Thompson, 2006; Fogt et al., 2011). Further, Fogt et al. (2012a) note that the impact of ENSO on SAM variability causes a higher degree of asymmetry in the SAM structure. It is clear from table 4.1, that there is some cross-over between the years used to represent SAM and SOI maxima and minima. As such, the two modes cannot not be regarded as being fully independent, particularly in the summer and spring. An investigation into the covariant forcing of winds and temperatures in the Ross Sea region will be the focus of further research. Further, while the dependence of winds in the Ross Sea region has been soundly demonstrated to be dependent on the SAM and ENSO modes, the impact of these winds on sea ice remains unclear, and will be investigated in the future.

A second aspect of the summer results that deserves further consideration is that, in summer, the total change is heavily dependent on changes in cluster (4,2), which dominates the synoptic conditions at this time of year. This is apparent from both SAM and ENSO changes. The dominance of a single cluster at this time suggests that the clustering algorithm is biased towards representing non-summer conditions, and thus may not capture summer variability. This may occur because the variability in summer is much lower than that of other times of the year. Due to the coreless winter effect, the Antarctic summertime is short and conditions quite different to other seasons. A useful extension of the clustering process may be to perform the analysis for a second time, but cluster only on summer conditions. At present, variability at this time of year appears to be swamped by that in other seasons.

Chapter 5

The impacts of synoptic circulation in the Ross Ice Shelf region upon Ross Island

5.1 Introduction

Circulation in the lower atmosphere around Ross Island is complicated and subject to control by high and complex topography, as well as synoptic forcing conditions. The wind dynamics of the region are described in detail in chapter 1 in sections 2.3, and a case study is given later in chapter 7. As established in chapter 3, the surface temperature of the Ross Ice Shelf is sensitive to changes in circulation. Strong wind events, such as instances of the Ross Ice Shelf Air Stream, have the ability to dramatically raise the temperature by temporarily disrupting the surface temperature inversion and may be particularly important from a climatological perspective. As such, in order to fully understand the climates of Scott Base and McMurdo Station, it is first necessary to understand the impact of synoptic conditions upon these locations. While past studies of the climate, in particular the wind dynamics, of the Ross Island region have aided the understanding of the area, research has tended to focus on mean conditions over long periods (Sinclair, 1982, 1988), isolated case studies or short period model output (Bromwich, 1988; O'Connor and Bromwich, 1988; Seefeldt et al., 2003), or individual field seasons (Liu and Bromwich, 1993). A climatology of the region was performed by Monaghan et al. (2005) using one year of the finest grid resolution AMPS output (June 2002 to May 2003). The study focused on annual and seasonal mean depictions of the wind field, pressure, temperature and cloud fraction of the McMurdo Sound area, as described by AMPS. However, the time period of the study was rather short, and the onus on prevailing conditions.

In this chapter, we investigate the conditions around the Ross Island, with respect to synoptic forcing over the Ross Ice Shelf and Ross Sea. We then apply this knowledge to better understand the observed trends at Scott Base and McMurdo Station, paying particular attention to the difference between the two observed trends. The chapter is ordered as follows: the data employed is described in section 5.2. A description of the climate of Ross Island is given in section 5.3, through the application of the clustering results of chapter 3 to the region. In this section we also address several salient meteorological questions regarding the region, such as the conditions under which southerly winds are observed at

Scott Base and the notable difference in temperature between Scott Base and McMurdo Station. In section 5.4 we perform an analysis of temperature trends at the two long-period bases in the region. The contribution of changes in circulation upon the observed trends is estimated through the application of a novel reconstruction technique. A summary is given and conclusions made in section 5.5.

5.2 Data and methods

Three main sources of data are used within this chapter. Firstly, we employ the output of the clustering algorithm developed in chapter 3. A time series of clusters is produced which spans the period from 1979 to 2011. The development of the clustering algorithm and its results are discussed at length in sections 3.3 and 3.4, respectively.

Considering the resolution of the ERA Interim reanalysis (and its subsequent interpolation to a 40km $\times$ 40km stereographic grid), we do not expect the reanalysis to adequately depict atmospheric processes in the boundary layer surrounding Ross Island, which is a region that contains complex topography of a scale much smaller than the resolution of the reanalysis. That the ERA Interim does not well represent local flows in this area is demonstrated in section 3.2.3. However, the location of a collection of long-period AWS units in the region, deployed specifically to aid in understanding the meteorology, allows us to compile data for the clusters defined in chapter 3 directly from observations. This technique was used previously in chapter 3 to validate the results of the clustering algorithm against observational data. In this chapter, we use the same technique to provide an insight into the interaction of the larger-scale flow with the detailed topography of Ross Island that cannot be derived from the ERA Interim reanalysis alone.

As in chapter 3, we use data from the automatic weather station (AWS) project of the University of Wisconsin, Madison. AWS records included in this analysis are subject to the same requirements of those used in chapter 3 to ensure adequate representation of long-term means and the removal of spurious records. One station, Ferrell (Fe), located to the east of Minna Bluff, is used in both analyses. Aside from the University of Wisconsin units, we also use temperature and wind records from Scott Base, at which the AWS unit is maintained by NIWA. Hourly records are available from the location from 1979 onwards. However, there exists a gap in the record from 1991 until 1997. Viewing of the wind data between the two periods shows clear differences in wind velocities before and after the break, possibly caused by the relocation of the AWS unit. As such, we choose only to use the Scott Base wind data from 1997 onwards, which still allows for a long enough complete record to calculate representative anomalies from climatological means. We also obtain 6-hourly data from McMurdo Station from the National Climatic Data Center. McMurdo Station data are available from 1973 onwards. We perform an automated quality control procedure on Scott Base and McMurdo Station data before including it in the analysis. Data are also visually checked prior to inclusion. Table 5.1 summarizes the AWS records employed in this analysis. The start year and number of data records available for the clustering analysis are displayed to demonstrate the large quantity of records available. A map of the Ross Island region, with weather stations and prominent geographic features marked, is displayed in figure 5.1.

Means for each cluster of wind and temperature displayed in the following sections are calculated by averaging over the times for which particular clusters occur. As in section 3.4, temperature data are displayed as a mean anomaly over all cluster times. Prior to averaging, the temperature anomaly is computed with respect to the long-term monthly mean. This allows us to view the temperature sensitivity of AWS locations without the signal being swamped by the seasonal cycle.

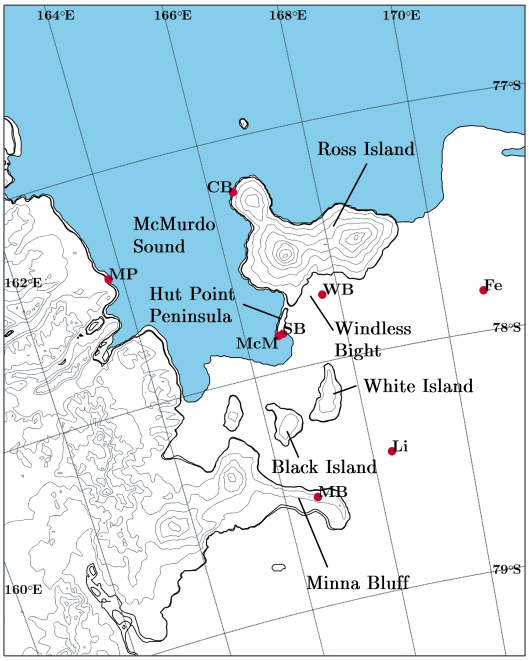

Figure 5.1: Map of the region surrounding Ross Island to the north-west of the Ross Ice Shelf. Sea is shown in blue and land and permanent ice in white. Ice cover around the sea margins is variable, such that depiction of the permanent ice edge is approximate and for visual purposes only. Topographic contours shown are at 10 m, 80 m, 500 m and then every 500 m to 4000 m. Red dots show the locations of AWS units used in subsequent analysis. Abbreviations are listed in table 5.1. Topographic data are sourced from the Radarsat Antarctic Mapping Project (RAMP) (Liu et al., 2001).

Station name	Abbr	Altitude (m)	Project	Start Year	No. records
Cape Bird	CB	38	Wisc	1999	16862
Ferrell	Fe	45	Wisc	1984	32165
Linda	Li	42	Wisc	1991	22134
Marble Point	MP	108	Wisc	1984	36245
McMurdo	Mc	24	NCDC	1979	37895
Minna Bluff	MB	895	Wisc	1991	22107
Scott Base	SB	20	NIWA	1997	19950
Windless Bight	WB	40	Wisc	1999	13442

Table 5.1: Metadata for AWS units used in the analysis of Ross Island region circulation study. Wisc denotes that the AWS is maintained by the University of Wisconsin, Madison. NIWA denotes that it is maintained by NIWA, New Zealand's National Institute of Water and Atmospheric Research. NCDC indicates that the data is sourced from the National Climatic Data Center. Stations are arranged in alphabetical order. Geographical locations are shown in figure 5.1. The start year is the year in which enough data is considered present to contribute to a long-term mean.

In addition to 6-hourly automatic weather station data, for the study of long-term temperature trends of the region, we also use data from Scott Base and McMurdo Station from the READER (REference Antarctic Data for Environmental Research) database (Turner et al., 2004). READER data is provided as highly-quality controlled and temporally complete monthly means. Only months that have at least 90 % of 6-hourly data present are included. As such, the READER database is essentially the gold-standard

for investigating long-term temperature trends in Antarctica.

5.3 The impacts of Ross Ice Shelf clusters on Ross Island

5.3.1 Wind analysis

Wind roses for the eight weather stations on Ross Island itself and in its immediate vicinity are shown in figure 5.2. Rose petals show the frequency of wind from the eight cardinal compass directions, and are essentially histograms on polar axes. The colour of the petal corresponds to the observed speed of the wind. Colours are equivalent to those depicted in figures 3.3 and 3.8. Clustered winds show a low degree of variability within clusters, suggesting that the clustering algorithm works effectively to group similar conditions within this region. This is an important point, as the clustering algorithm focuses on a much larger area than that shown in figure 5.1. Comparison of the wind speeds and directions with those shown in figure 3.3 reveals a significant correspondence between conditions, particularly at the AWS sites of Ferrell (Fe) and Linda (Li), which are located to the east of Ross Island and therefore slightly removed from the complex topography. Unsurprisingly, given what is known about the localised flows in the area, the conditions at Scott Base (SB) and McMurdo Station (McM) are not well-matched between the observations and reanalysis. However, despite the inconsistencies, the stations and those in the vicinity show little variation within the clusters, suggesting that the clustering algorithm can adequately depict the variation in conditions there.

Wind directions across clusters in figure 5.2 indicate that the directionality of the wind within the Ross Island region is relatively constant between clusters with different synoptic aspects, which suggests that observations are strongly influenced by local topography. Winds to the south and south-east of the island, at Minna Bluff (MB), Linda (Li) and Ferrell (Fe) AWS sites show southerly and south-westerly winds for the majority of the time, although the speed varies greatly depending on the cluster. The lightest and most variable winds seen at these positions are present in clusters (3,6), (4,4) and (4,5), located in the bottom-right corner of figure 3.3, the areas that represent mainly katabatic forcing over East Antarctica. In these clusters, winds to the south drain from the glaciers of Victoria Land and propagate over the ice shelf in a north-easterly direction, effectively bypassing the Ross Island region, which is sheltered by Minna Bluff, resulting in low wind speeds there. The strongest wind speeds are seen in clusters on the top row and to the right. In particular, clusters (1,4) and (2,5), which represent strong RAS events (fig. 3.3) show high wind speeds at these three stations, due to pressure minima situated to the north and south-east, respectively. Minna Bluff winds tend to be higher than those at Linda and Ferrell. This is probably because the Minna Bluff weather station is located at 895 m above sea-level on a narrow ridge, and thus is less subject to the surface friction of the ice shelf.

Cape Bird (CB), which is located on the north-western tip of Ross Island, has the most variable wind record of any of the weather stations used. The dominant wind is from the north-east, but in most cluster conditions the wind is generally light and quite variable. This is due to the fact that CB is located in the lee of Ross Island, which constitutes a considerable barrier to the large-scale southerly flow. The north-east wind at CB appears to be caused by the recirculation of air around Ross Island from a tip jet on the eastern side of the island. The jet is visible in the climatology of Monaghan et al. (2005) (their figure 3), as is the resulting vortex, and is further evidenced by the persistent polynya on the east flank of the island (Bromwich, 1988). The jet is also visible in figures in chapter 7. Accordingly, the north-east wind at CB is most apparent when the synoptic-scale southerly wind is strong; in general,

it appears in clusters that occur in the top right of figure 3.3, which correspond to RAS events. CB also displays some strong southerly winds, which concur with southerlies at Scott Base and occur at times of particularly strong southerly synoptic flow.

Winds along the Hut Point Peninsula have been studied in depth and are well-known to be particularly constant in direction and light compared to winds farther to the east (Sinclair, 1982, 1988; O'Connor and Bromwich, 1988; Seefeldt et al., 2003). This relative calm is caused by a combination of topographic and atmospheric conditions surrounding these locations. The north-easterly prevailing wind at Scott Base is discussed in section 2.3. In times when most of the AWS records show light and variable winds, the record at Scott Base appears to be strongly directional and of slightly higher speed (for instance, cluster (3,6)). This is because of the barrier wind effect, and the fact that convergence occurs towards Scott Base along the Hut Point Peninsula (see figure 6.5).

In the majority of the clusters, despite strong winds occasionally being present at MB, Li and Fe, the wind at Scott Base is moderate and from the north-east, while that of McMurdo Station is more easterly. Winds from the southern sector are observed at SB and McM in some clusters, notably (1,3), (1,4) and (2,5). They are further present in (1,5) and (1,6) but reduced. Despite strong winds at MB, Li and Fe in clusters (2,3) and (2,4), few southerlies are observed at SB. This variability in the presence of southerly winds at SB and McM is notable, as it provides an insight in to the conditions necessary for the southerly winds to occur. This information is inherently useful, as these winds tend to be the strongest observed in the region (Sinclair, 1982, 1988) and directly affect surface logistics and aircraft movements.

Examination of figure 3.3 shows strong winds over the ice shelf to the south of the island during instances of clusters (1,5) and (1,6). Corresponding strong winds are also observed at MB, Li and Fe in figure 5.2. However, the winds to the south and south-east show a south-westerly direction which causes air flow to turn before Minna Bluff rather than approaching the barrier perpendicularly, making it difficult for the air to surmount the barrier (section 2.1). Thus, only the incidences of these clusters in which the strongest winds occur are capable of producing southerlies at SB.

The lack of southerly winds at SB and McM in clusters (2,3) and (2,4) is indicative of a variation in vertical stratification between these clusters and (1,3), (1,4) and (2,5), which do display numerous southerlies. That clusters (2,3) and (2,4) display the hallmarks of the barrier wind mechanism (north-easterly at SB), while (1,3), (1,4) and (2,5) do not, at times when wind speeds in the region are similar, is indicative of the boundary layer of the first group being more stably stratified than that of the second. An indication of why this might be the case can be seen in figures 3.3, 3.4 and 3.5. Clusters (1,3), (1,4) and (2,5) show low pressure centres that are much farther south than those in clusters (2,3) and (2,4). Over the ice shelf to the south of Ross Island, winds in clusters (1,3), (1,4) and (2,5) are higher than those in clusters (2,3) and (2,4). While strong winds are observed over the ice shelf in clusters (2,3) and (2,4), they occur to the south-east and east of Ross Island. It is in these regions of strong flow that the semi-permanent temperature inversion is broken down by turbulent vertical mixing (Bromwich, 1989b), bringing warm air to the surface and reducing the static stability of the boundary layer, as evidenced by high temperatures in regions of strong winds in figure 3.5. Figure 3.5 shows that, in clusters (2,3) and (2,4), air advected towards Ross Island from the south originates from a region of calm, cold surface air, while in clusters (1,3), (1,4) and (2,5) this air is turbulently mixed (warm air signature). Thus, winds in clusters (2,3) and (2,4) are less likely to surpass the high topographic barriers surrounding Ross Island, leading to the north-easterly flow at SB and a lack of southerly winds. The difference in stratification is confirmed by calculating the difference in temperature between SB and MB. MB has an altitude of

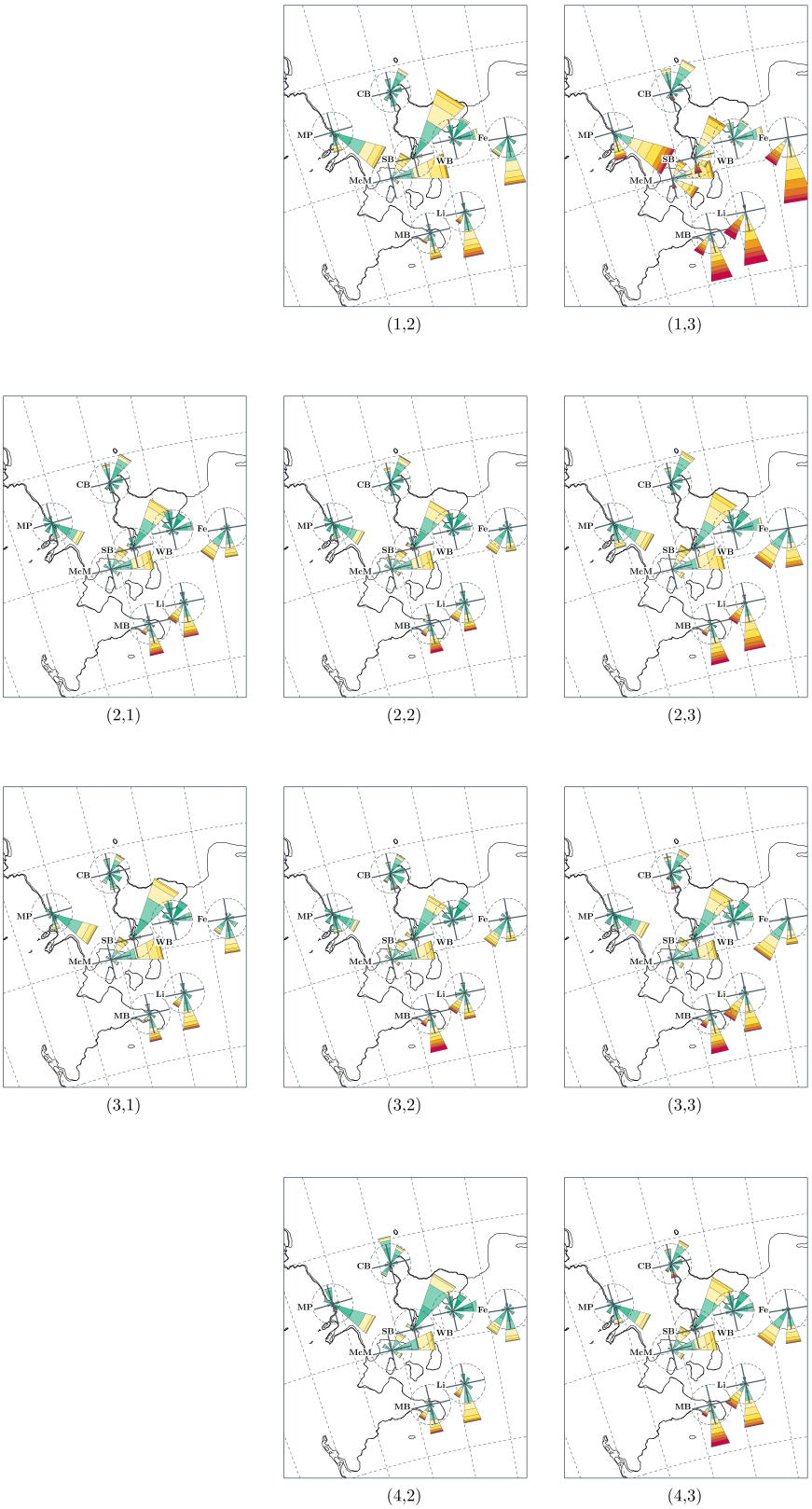
CB
MP
SB
WB
Fe
McM
Li
MB
(1,2)
(1,3)
(2,1)
(2,2)
(2,3)
(3,1)
(3,2)
(3,3)
(4,2)
(4,3)
0
2
4
6
8
10
12
14
16
18
20
Wind speed, ms^{-1}

Figure 5.2

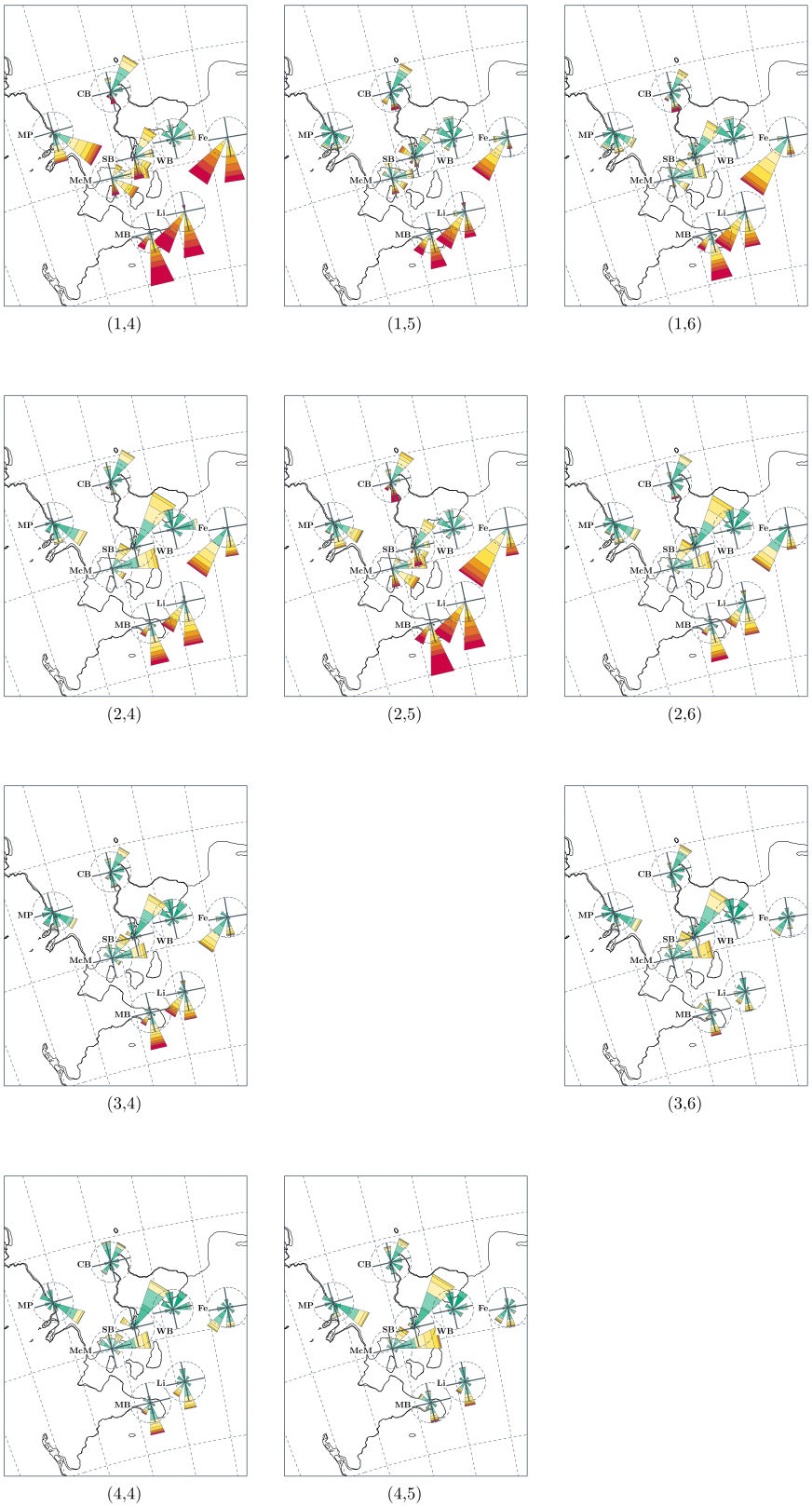
CB
MP
Fe
SB
WB
McM
Li
MB
(1,4)
(1,5)
(1,6)
(2,4)
(2,5)
(2,6)
(3,4)
(3,6)
(4,4)
(4,5)
0
2
4
6
8
10
12
14
16
18
20
Wind speed, ms^{-1}

Figure 5.2

895 m, and thus the temperature difference gives an indication of the vertical structure of the boundary layer. The technique is similar to that used by Holmes et al. (2000). Temperature differences between SB and MB are shown in figure 5.3. We use absolute temperatures rather than anomalies, meaning that the difference is likely to be highly dependent on the time of year as well as the wind speed. For instance, cluster (4,2), which is frequent in the summer, shows a relatively high and positive temperature difference. Rather than being caused by disruption by strong winds, this is likely to be simply because strong inversions do not form as often in the summer. Holmes et al. (2000) suggested that a temperature difference above 8.9 °C is indicative of unstable conditions in the region. Averages shown in figure 5.3 never surpass this limit. Similarly, only one average temperature difference is less than zero. The range of the averages is no doubt limited by averaging across many instance of similar conditions. Temperature differences displayed here are also likely to be more positive than those discussed by Holmes et al. (2000) because at the lower level we use data from Scott Base, while Holmes et al. (2000) used records from the Pegasus North AWS. Pegasus North is located over an ice surface, meaning that it is likely to be colder than Scott Base, which is situated over exposed rock (see chapter 6). We further note that SB and MB are separated by ~ 70 km, and thus the temperature differences are merely indicative of wider conditions. Despite these caveats, we observe a large degree of variability in the temperature difference, which appears to coincide with wind speeds shown in figure 5.2. Importantly, we find that in clusters (1,3), (1,4) and (2,5) vertical temperature differences (SB temperature - MB temperature) are more positive than those observed during (2,3) and (2,4), confirming that more stable conditions are present during occurrences of (2,3) and (2,4).

The direction of the pressure gradient (fig. 3.4) and wind direction (fig. 3.3) to the south of Ross Island in clusters (1,3), (1,4) and (2,5) ensure that air not only approaches the region from the south, ensuring a perpendicular alignment with Minna Bluff. They also display the strongest wind speeds and advect unstably stratified air from the south into the region. The largest proportion of southerly winds is seen during occurrences of these clusters, which are reminiscent of the second numerically modelled example given by Seefeldt et al. (2003). The observation of southerly winds at SB and McM is thus clearly dependent on the alignment of the pressure gradient and hence the position of the pressure minimum as well as the speed of the wind to the south of Minna Bluff.

Cluster (1,5) shows a wind rose peak from the north-west at SB, which is rarely observed during any other cluster. Peaks from this direction were also observed by SNOW-WEB nodes in the two-month deployment over the summer of 2011/12 (fig. 6.5). The peak is also seen in cluster (4,4), although it is less frequent and its associated wind speeds are reduced. Little in the ERA Interim composites exists to explain the origin of these winds, although in the area to the north of Ross Island in cluster (4,4), a north-westerly wind can be observed propagating from Terra Nova Bay. Similar winds were observed in this region by Marshall and Turner (1997) using satellite-borne scatterometer retrievals. The authors explained the turning of the wind by the influence of a mesoscale cyclone, which are frequent events in the region (Carrasco et al., 2003). The north-westerly flow at SB is not visible in the ERA composite

---

Figure 5.2: Previous page: Ross Sea region cluster wind roses. Petals of the wind roses show the frequency of the wind from a particular direction. The dashed circle around each rose represents 20 % frequency. The colour of a particular petal indicates the speed of the wind from that direction. Roses are rotated to be aligned with grid north. The wind rose for McMurdo Station (McM) is offset to the south-west of its true position to avoid overlap with that of Scott Base (SB). Similarly, The Windless Bight (WB) wind rose is offset to the east.

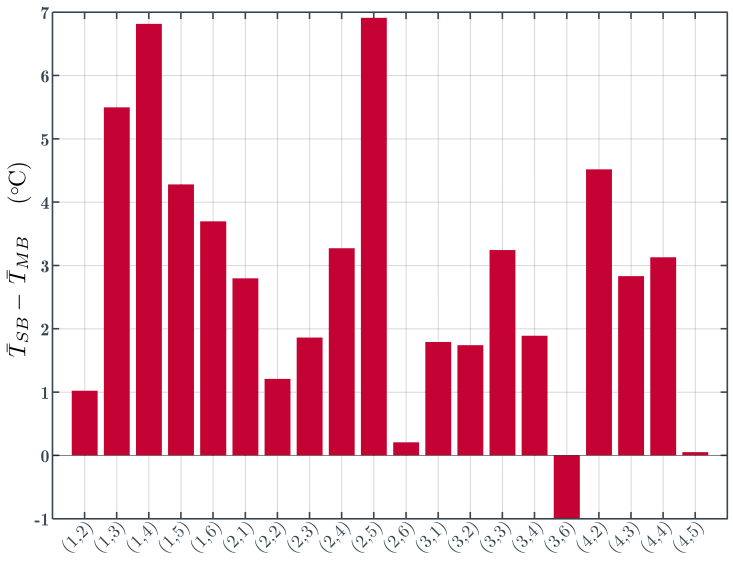

Figure 5.3: Scott Base - Minna Bluff temperature difference dependent on cluster conditions.

(fig. 3.3) for cluster (1,5), which describes a RAS event caused by a cyclonic system in the centre of the Ross Ice Shelf. It is conceivable that a westward shift of the low pressure centre of cluster (1,5) would result in winds from the north-west at SB. Thus, it is possible that these types of events are averaged into this cluster. For an example of a similar event producing a north-westerly wind at SB see chapter 7.

Upwind of Scott Base to the north-east lies the region of Windless Bight, where a University of Wisconsin weather station, WB, is located. Windless Bight was observed to have anomalously calm winds by early explorers (Simpson, 1919), due to its position in the high pressure stagnation zone formed as southerly winds encounter the steep slopes of Mount Erebus and Mount Terror (O'Connor and Bromwich, 1988; Seefeldt et al., 2003). Observation of figure 5.2 confirms the calm and quite variable winds in the bight, for all cluster instances, with wind speeds less than 5 ms^{-1} typical. At times of strong winds induced by cyclones to the north, such as clusters (1,3) and (1,4), WB may show a slightly stronger easterly wind, but aside from these occurrences, the wind there is remarkably weak.

The Marble Point (MP) AWS, to the west of Ross Island on the opposite side of McMurdo Sound, displays predominantly south-easterly winds. These may occur due to the channelling of air between Ross Island and high topography to the south. However, the north-east direction of winds at Cape Bird during strong wind events suggests that recirculation around Ross Island may also affect locations on the west of McMurdo Sound. It is possible that strong winds from the south-east at MP then represent a barrier regime against the Transantarctic Mountains. Further evidence for this effect was recorded in the case study examined in chapter 7. As with other stations the direction is quite constant, suggesting that it is determined by the local topography. Wind speeds vary according to synoptic conditions, and appear to be well correlated with those at SB, suggesting that the sheltering effect of Minna Bluff plays a further role here. For instance, during incidences of cluster (1,5), winds at MP are light and variable. MP also has an occasional westerly and south-westerly component, presumably due to flows from McMurdo Dry Valleys, which have outlets towards these directions and are subject to localised katabatic flows and

foehn winds below the ERA Interim resolution (Nylen et al., 2004; Speirs et al., 2010).

5.3.2 Temperature analysis

Temperature anomalies, which are compiled in the same manner as those in figure 3.7, and thus represent the change from the average temperature owing to circulation conditions, are shown in figure 5.4. The temperature scale is equivalent to temperature diagrams in chapter 3. Crosses representing statistical significance at $p \leq 0.05$ indicate that all but the smallest magnitude anomalies are significantly different from zero, which suggests that circulation is an important control on the temperature. Comparison of the AWS records in figure 5.4 and ERA Interim records of figure 3.5 in general shows a high degree of correspondence. Remarkably, even temperature gradients across the smaller region shown in the AWS record also appear to be well-resolved in the ERA Interim, such as those seen in clusters (3,3), (3,4) and (3,6). Thus, despite the wind directions not being well-resolved in the ERA Interim analysis, the temperature of the region does seem to be reproduced effectively, perhaps because of the direct assimilation of the AWS temperature records into the reanalysis.

As discussed in section 3.4, strong winds over the Antarctic ice shelves act to more thoroughly mix the surface air and thus break the inversion layer. This was shown to induce surface warming over coastal ice masses during periods of strong winds. Evidence of the effect occurring in the Ross Island region has been given by Sinclair (1982) and Sinclair (1988) from surface measurements at Scott Base, and Holmes et al. (2000) for Pegasus North. It is likely then, that during the cluster instances that show strong winds in the Ross Island region, that high temperatures will also be observed. The situation is complicated by a second mechanism: that of horizontal advection of warmer or cooler air from a distant area, which is also highly dependent on the wind speed and direction. However, the general relationship can be observed via comparison of figures 5.2 and 5.4. Those clusters that show strong winds in the Ross Island region and the ice shelf to the south tend to have the highest temperatures, while those with weak winds have lower temperature anomalies. Clusters with strong winds in the area may also promote the growth of polynyas around Ross Island (Bromwich, 1988), which would also act to raise the temperature in seasons when McMurdo Sound and the Ross Sea are ice-covered. To illustrate further, we compute the areal mean temperature anomaly and scalar wind speed across the region from six of the AWS sites shown in figure 5.1, for each cluster. We omit data from the Minna Bluff (MB) AWS from the averages, as this station is located at 895 m above sea-level and does not represent conditions at the surface of the ice shelf. We also exclude Windless Bight (WB), as conditions there are anomalously calm. A plot of the mean temperature anomaly against the mean wind speed is shown in figure 5.5. There is a clear positive relationship between the wind speed and the temperature, which plateaus towards high wind speeds. Clusters with strong winds, such as (2,5), (1,3), and (1,4) show high temperature anomalies. Those with weak winds, such as (3,6), show largely negative temperature anomalies.

The high degree of similarity in wind direction between clusters, in particular those with moderate wind speeds such as group 2, suggests that the meteorology of the Ross Island region could in fact be described with fewer clusters, and thus slightly less complexity. A contrasting (but complementary) clustering approach could be to determine clusters based on local conditions, and then average over the wider area. However, gaps in AWS records ensure that obtaining consistent cluster results is fraught with difficulty if these data are used. Further, the inability of the ERA Interim reanalysis to depict winds in the region makes it unsuited to this task. By using the technique of projecting a clustering algorithm based on a wider area upon the Ross Island region, we have revealed that rather different wind

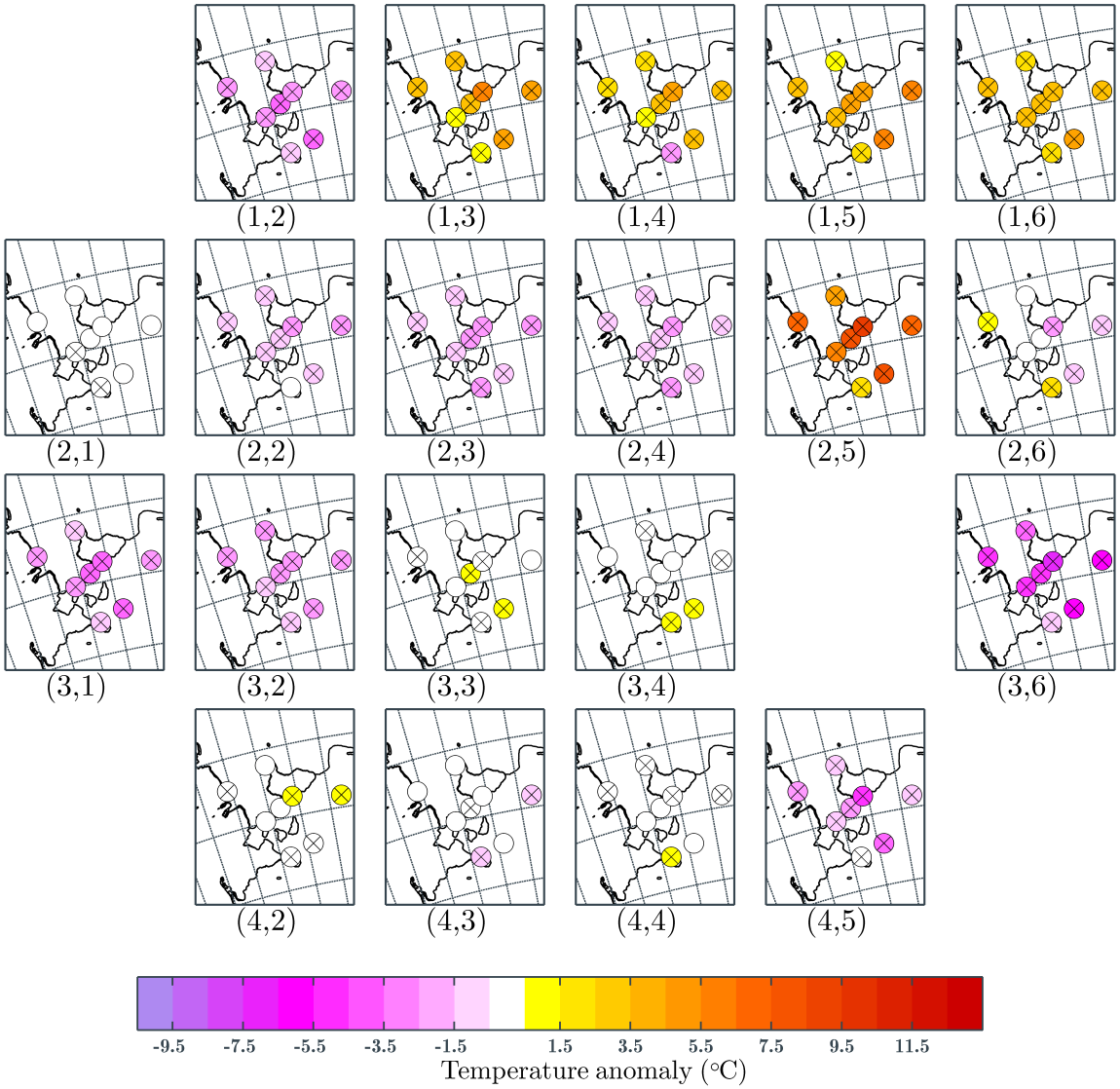

Figure 5.4: Cluster temperature anomalies for AWS units in the Ross Island region. AWS labels are not plotted for the sake of readability. McM is offset from its true location to avoid overlap with SB. Temperature anomaly scale is equivalent to that used in figure 3.5. Means that are significantly different from zero at $p \leq 0.05$ are displayed with a cross. Significance is estimated using a two-tailed Student's t-test.

conditions over the ice shelf can induce similar conditions at Ross Island, due to its sheltered nature and wind flows dominated by local topography. Rather similar synoptic conditions have also been shown to cause subtle differences in the response at Ross Island. The temperature response has also been shown to be sensitive to wind speeds in areas far removed from the region. As such, the temperature response may not have been well represented if clustering was performed only on the island itself.

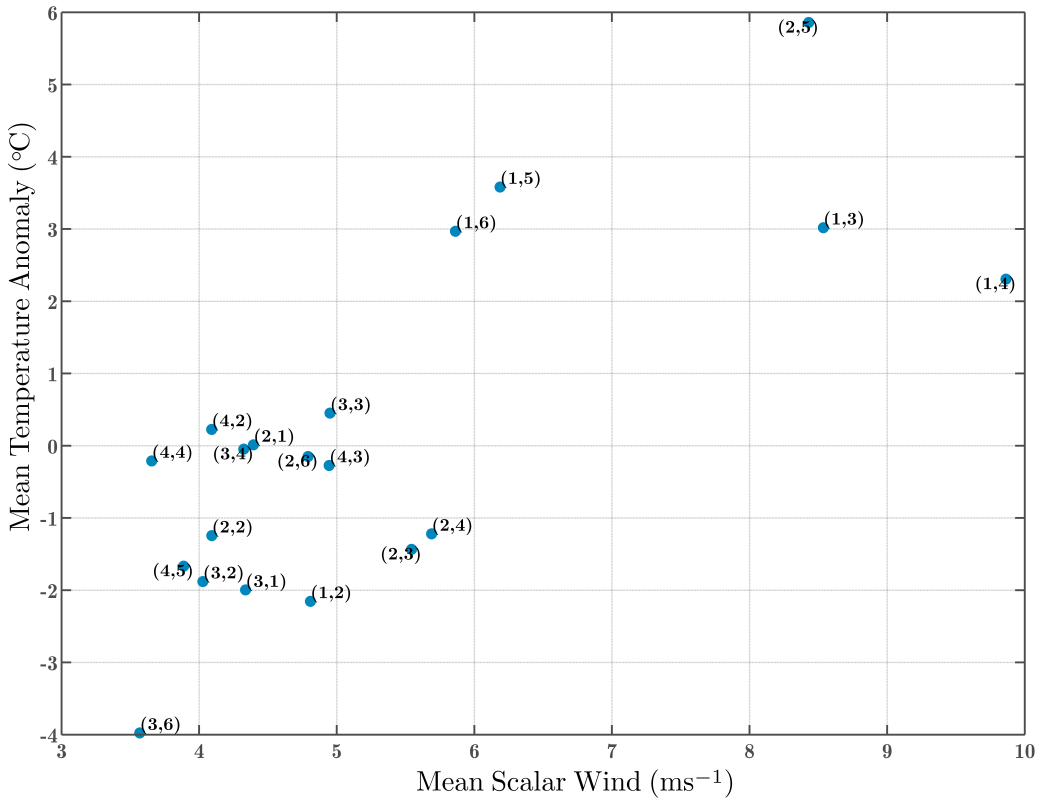

Figure 5.5: Average temperature anomalies against average scalar wind speed for AWS locations shown in figure 5.1. Minna Bluff (MB) and Windless Bight (WB) AWS unit records are excluded from the means. Bold black writing identifies the cluster. Red ellipses and writing designate groupings. Green ellipses and writing designates sub-groupings.

5.3.3 Scott Base - McMurdo Station comparison

Despite being separated by only 2.2 km, Scott Base and McMurdo Station show prominent differences in their long-term mean temperatures; annual averages computed from READER database records show that McM records are on average $\approx 3\,^{\circ}$C warmer than those from SB. To illustrate, we show the long-term mean monthly temperature at SB and McM from 1957-2011 in figure 5.6. A well defined seasonal cycle is observed at both locations, but SB shows a much deeper temperature trough in the winter months, particularly in August. The difference between the two means is much reduced in the summer months with the prevalence of warmer temperatures. The remarkable temperature difference was mentioned by Sinclair (1982), who suggested that it was brought about by the relative altitudes and locations of the two stations and their positions relative to the prevailing flow. SB is located at a lower elevation and close to the ice shelf, while McM is located at a higher elevation and farther from the shelf. Sinclair (1982) suggested that these conditions meant that SB was subject to a strong, shallow boundary layer temperature inversion, both around the base and present in air advected towards the location from Windless Bight. The highly constant north-easterly wind at SB is evidence of the barrier flow regime there, which exists because of the low-level inversion. Observations from the area and modelling experiments have shown that the layer in which the flow occurs is shallow (Sinclair, 1988; Seefeldt et al., 2003). This

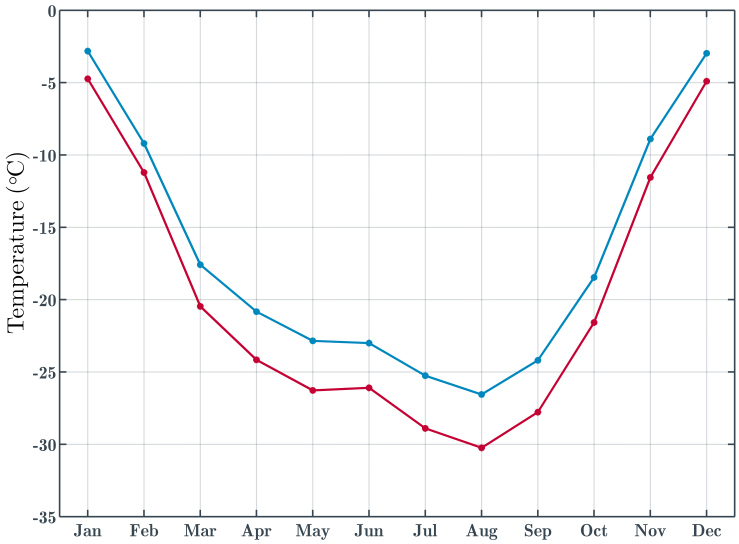

Figure 5.6: Mean monthly temperatures for SB (red) and McM (blue) for 1957-2011.

strong inversion is not manifest at McM for three reasons: its slightly higher elevation, its distance from the ice shelf, and its slightly higher mean wind speed. Hence, SB is naturally colder than McM. Stearns et al. (1993), who also noted that the difference between the two bases was largest when the temperature was low, explained the difference with reference to the sheltering effect of the Hut Point Peninsula on McM with respect to wind direction. SB is located on the south-east side of the peninsula and is thus highly sensitive to cold air advection, which is a frequent occurrence at the location. McM is situated on the opposite side of the peninsula, and thus is rather more sheltered from the cold wind from out of Windless Bight.

AWS wind and temperature composites presented in figures 5.2 and 5.4 afford the opportunity to study the climatic differences between SB and McM. Observation of the respective anomalies of the bases shows a marked difference in their reactions to circulatory forcing. Figure 5.2 identifies that wind directions at McM are more variable than those at SB, and speeds tend to be slightly higher. While the wind direction at SB is primarily from the north-east and directionally constant, winds at McM appear to be directed more towards the east. The notable difference is observed over a small distance, and is therefore probably caused by the diminished steering effect of the Hut Point Peninsula at the McM station location. Sinclair (1982) suggests that the gusty and variable nature of the wind at McM is partly caused by hills upwind of the station. In contrast to the prevailing conditions, in clusters which show strong southerly winds at SB ((1,3), (1,4), (1,5), (1,6) & (2,5)), winds appear to be more southerly at SB than at McM. SB winds are also stronger when they are from the south. This appears to be caused by the McM AWS being located in the lee of the Hut Point Peninsula with respect to the southerly wind. The sheltered location of McM was also noted by Turner et al. (2009a) in relation to strong wind events.

Comparison of temperature anomalies in figure 5.4 reveals that both positive and negative anomalies at SB tend to have higher magnitudes than those at McM, indicating that the change away from the mean at SB is larger than at McM. The temperature anomaly essentially provides a measure of the sensitivity of the AWS location to synoptic forcing. To further illustrate the sensitivity of the two stations, in figure

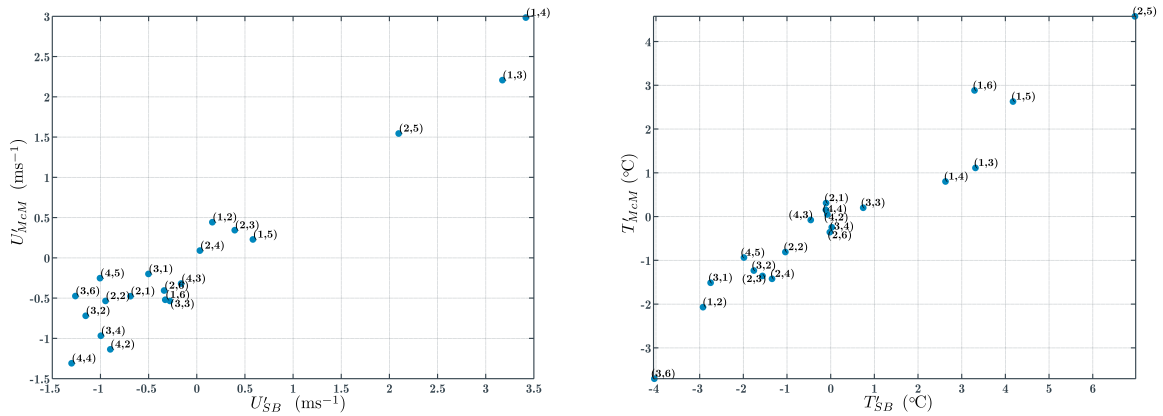

(a) Scalar wind speed anomaly

(b) Temperature anomaly

Figure 5.7: Mean scalar wind anomaly, U', (a) and temperature anomaly, T', (b) at SB and McM for each cluster. Cluster number is displayed next to the computed value.

5.7 we display a comparison of the wind anomaly and temperature anomaly conditions from SB and McM. Figure 5.7a shows a comparison of the scalar wind speed anomaly, which reveals that anomalies are marginally larger at SB during high wind speed events, which evidences the suggestion that SB is relatively less sheltered to such events. Similarly, in figure 5.7b, which compares the temperature anomalies, a generally positive linear relationship is found, with SB showing larger magnitude anomalies than McM, especially during strong wind events. This is a strong indication that SB is more sensitive to changes in temperature due to circulation than McM, as suggested by Stearns et al. (1993).

The lower temperatures at SB and higher sensitivity are thus produced by a combination of the localised topography and its interaction with the synoptic flow and inherent stability of the Antarctic atmosphere. In prevailing conditions, winds at SB are low due its low altitude position and the blocking effect of the peninsula. This means a stable boundary layer develops with cold air pooling towards the surface. The reinforcement of this inversion layer during anomalously calm events (such as (3,6)) causes much larger negative anomalies at SB than at McM. In contrast, the mixing of the inversion layer during strong wind events warms SB significantly more than McM, where the inversion layer is not as strong.

5.4 Scott Base and McMurdo Station temperature trends

In order to better understand trends at McM and SB and their variation over the yearly cycle, we separate temperatures on an annual, seasonal and monthly basis and calculate trends according to a linear least-squares fit for the period of 1979-2011. Statistical significance is determined by a two-tailed Student's t-test, with the effective degrees of freedom adjusted for autocorrelation according to Santer et al. (2000). The effective degrees of freedom is then used in the calculation of the standard error and the t-distribution. Trends are shown in table 5.2. Scott Base shows almost no trend on an annual basis. We find that SB has a small and statistically insignificant decreasing trend in summer and autumn during this time period. April and May show the strongest cooling trends, which are insignificant due to the large interannual variability at this time of year. The cooling trend in the summer and autumn has been tied to SAM activity over the longer time period (Thompson and Solomon, 2002; Marshall, 2007). The

Period	$m_{obs,SB}$	$m_{obs,McM}$	Month	$m_{obs,SB}$	$m_{obs,McM}$
Annual	0.02	0.24	Jan	-0.12	0.37
Summer (DJF)	-0.14	0.32†	Feb	-0.11	0.27
Autumn (MAM)	-0.51	-0.23	Mar	-0.31	0.11
Winter (JJA)	0.11	0.32	Apr	-0.51	-0.32
Spring (SON)	**0.60**	**0.77**	May	-0.73	-0.29
			Jun	0.29	0.57
			Jul	0.19	0.55
			Aug	-0.19	-0.11
			Sep	**1.13**	0.91†
			Oct	0.43	**0.67**
			Nov	0.26	**0.78**
			Dec	-0.11	0.31†

Table 5.2: Observed temperature trend statistics for Scott Base and McMurdo Station. $m_{obs,X}$ represents the observed temperature trend in °C/decade between 1979 and 2011. Significance at the $p \leq 0.05$ level is indicated by bold font. Significance at $p \leq 0.10$ is marked by a †. Observed McMurdo trends that are significantly ($p \leq 0.10$) more positive than at Scott Base are underlined. See main text for details of calculations.

trend in winter varies across months and is not statistically significant. In spring the trend is generally positive, and dominated by the large and statistically significant September value.

McM shows a larger positive trend in annual means than SB, but is not statistically significant. McM shows increasing trends throughout spring and summer that are statistically significant in September through December. As at SB, slight cooling is seen in the autumn and slight warming in the winter, although trends are variable across months. Perhaps the most salient detail of the temperature trends is that on an annual basis and in all seasonal averages, McM shows significantly more positive trends than SB. Significance of the difference in trends is estimated by calculating time series of the difference between McM and SB temperatures, computing a least-squares fit and assessing the significance of that fit via the method of Santer et al. (2000). As demonstrated previously, temperatures at SB are more sensitive to changes in circulation than those at McM, which may in part generate the disparity of the observed trends. We now assess the ability of regional circulation to determine the temperature at either location, and further investigate the forcing of the observed temperature trends via the application of a novel reconstruction technique.

5.4.1 Reconstruction technique

The reconstruction algorithm proceeds as follows: we first determine the frequency of the clusters described in section 3.4 for every calendar month for the period of the ERA Interim reanalysis (1979-2011). For every month, we then multiply the temperature anomaly associated with a particular cluster by its frequency. This combination of the frequency and temperature anomaly describes the contribution to the monthly temperature anomaly from a particular cluster. Finally, we sum over all the clusters to compute an estimation of the temperature anomaly as described solely by the circulation conditions present within that month. Expressed mathematically, the reconstructed temperature anomaly for any month is given by:

$$T_i' = \sum_{k=1}^{K} T_k' f_{k,i}$$

In which i is an index corresponding to the calendar month from 1979 to 2011, k an index corresponding to the cluster and K the total number of clusters, 20 in this case. T_k' is the temperature anomaly associated with the cluster k. This temperature anomaly is estimated from values for each station taken over the entirety of the 6-hourly data record. Temperature anomalies are calculated from data that has had the long-term monthly mean removed, and are thus independent of the month i. $f_{k,i}$ is the frequency of the cluster k within month i. It is calculated as the proportion of the total time, such that for any month:

$$\sum_{k=1}^{K} f_{k,i} \equiv 1$$

The reconstructed temperature anomaly is thus essentially a weighted average of the cluster temperature anomalies, with the weights estimated by the frequency of the clusters. The reconstruction scheme is limited to the years 1979-2011, as it is dependent on clustering output from the ERA Interim reanalysis. The interpolation routine underestimates the variance of the temperature anomaly in all months. This is a result of the assumption that every instance of a particular cluster forces an equivalent temperature anomaly. In reality, this isn't the case as variation also occurs within clusters (intra-cluster changes). We renormalize the reconstructed record to the variance of the respective temperature record, estimated from the READER database monthly means, in order to account for the restriction of variance introduced by not including intra-cluster changes in the reconstruction method. Clearly, this is not as accurate a method as assessing the contribution to changes individually as in chapter 4. However, the short and incomplete nature of SB 6-hourly records precludes the use of the technique used in the previous chapter. We feel that the renormalisation technique is justified by the high correlations between the observed and reconstructed temperature series (shown in table 5.3), which indicate a well-defined linear relationship. Changes in the frequency of clusters (inter-cluster changes) can then essentially be used as a proxy for the intra-cluster changes.

The reconstruction routine assumes that the anomaly associated with each cluster is constant with time. Any changes seen in the reconstructed temperatures are due solely to changes in the frequency of occurrence of each cluster and thus reflect changes in circulation. To illustrate the degree of accuracy that is achieved in the reconstruction experiment, scatter plots of the observed and reconstructed temperature anomalies are shown in figure 5.8 for SB and McM. Cluster temperature anomalies for SB are calculated for each cluster from 6-hourly data that is available from 1997 onwards. McM 6-hourly data is available from 1973, but we use only the data after 1997 for the sake of consistency. Thus, observed temperature records and reconstructed temperature records shown in figure 5.8 are entirely independent prior to the beginning of the 6-hourly temperature record in 1997.

5.4.2 Reconstruction validation

In order to assess the ability of cluster anomalies and frequencies to reconstruct monthly temperature anomalies at SB and McM, we perform a comparison exercise. We calculate correlations, biases and root-mean-square errors (RMSE) between the observed and reconstructed temperature anomalies for

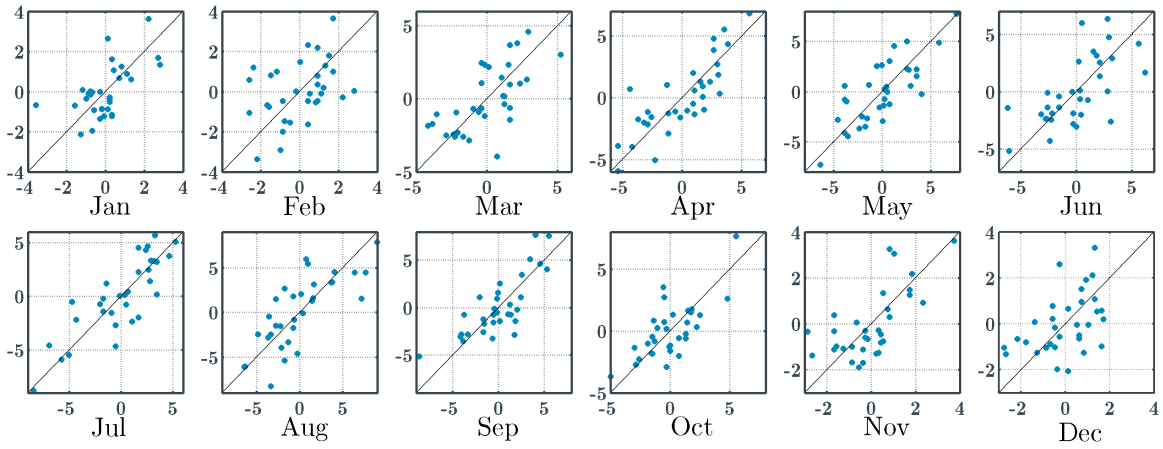

(a) SB

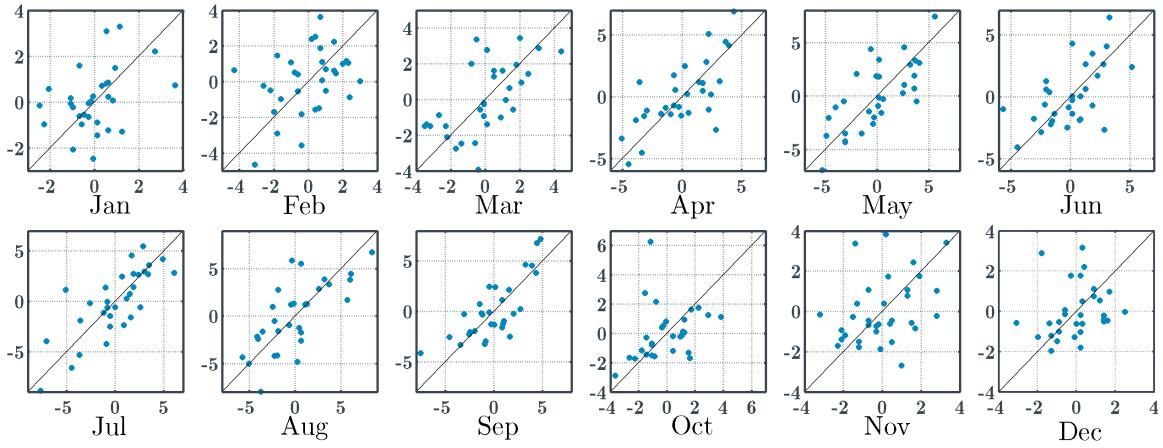

(b) McM

Figure 5.8: Scatter plot of reconstructed (ordinate) versus observed (abscissa) monthly temperature anomalies for 1979-2011 at (a) SB and (b) McM. Temperatures are given in °C. Diagonal black line marks a 1:1 relationship. Plots are separated into monthly values to illustrate variability in correlations.

the entire data series and two subsets. The first subset is the period from 1979 to 1996, during which time no temperature data from either SB or McM is used in the reconstruction. The second subset is the more recent period of 1997 to 2011 for which data from SB and McM are employed in the reconstruction. Validation statistics are shown in table 5.3.

Remarkably, correlations at SB and McM are high. The correlation at McM in the early time period is somewhat reduced but still significant at $p \leq 0.05$. The high correlations shown in table 5.3 suggest that the temperature anomaly at SB and McM is heavily influenced by regional circulatory conditions. Correlation statistics compare favourably to those computed by other statistical reconstruction schemes (Monaghan et al., 2008; Steig et al., 2009; O'Donnell et al., 2011) for times when the observed and reconstructed time series are independent. High correlations are probably a result of the dependence of the monthly temperature anomaly on three or four primary clusters that cause large deviations from the mean state (as described in section 5.3.2), ensuring that the mean temperature record in the area is sensitive to circulation changes. The correlation findings are reinforced by the temperature anomaly

	R_{SB}	Bias_{SB}	RMSE_{SB}	R_{McM}	Bias_{McM}	RMSE_{McM}
1979-1996	**0.70**	0.10	1.98	**0.57**	**0.38**	2.25
1997-2011	**0.80**	-0.07	1.66	**0.77**	**-0.38**	1.67
1979-2011	**0.74**	0.02	1.84	**0.65**	0.04	2.01
Jan	**0.59**	0.01	1.12	**0.48**	-0.08	1.46
Feb	**0.39**	-0.03	1.61	**0.36**	-0.05	1.96
Mar	**0.66**	0.00	1.78	**0.64**	-0.04	1.67
Apr	**0.82**	-0.00	1.75	**0.73**	-0.14	2.03
May	**0.77**	-0.00	2.06	**0.73**	0.02	2.21
Jun	**0.66**	0.00	2.39	**0.60**	-0.08	2.24
Jul	**0.84**	-0.06	1.97	**0.81**	0.09	2.21
Aug	**0.78**	-0.11	2.67	**0.74**	-0.06	2.68
Sep	**0.78**	-0.09	1.98	**0.76**	-0.12	1.95
Oct	**0.74**	-0.02	1.64	$0.34^{\dagger}$	-0.04	2.07
Nov	**0.66**	0.02	1.16	**0.34**	-0.00	1.79
Dec	**0.45**	-0.01	1.31	0.23	0.00	1.59

Table 5.3: Computed correlations (R_X), biases and root-mean-squared errors (RMSE) between observed and reconstructed time series for time periods shown in far left column. Biases are calculated as reconstructed-observed, and have units of °C. Significance is estimated by a two-tailed Student's t-test. Significance at the $p \leq 0.05$ level is indicated by bold font. Significance at $p \leq 0.10$ is marked by a †. Correlations for individual months are calculated over the entire 1979-2011 time range.

biases, which are low and not significant at SB. Biases are slightly increased at McM, and change from positive to negative before and after 1997. The bias of the early record indicates that the reconstruction over-estimates the temperatures at this time. The bias in the latter period indicates an under-estimation. The bias of the time period as a whole is low and not significant, although this may simply reflect the fact that both time series are anomalies, and thus the mean of both is likely to be close to zero. As a more absolute statistical measure we include the RMSE, which shows similar low values at SB and McM in the later and full periods. The earlier RMSE at McMurdo is a little larger. The higher magnitude biases and RMSE and lower correlations at McM indicate that the circulation reconstruction does not work as well at this station, which is also apparent from plots in figure 5.8. This is likely because of the reduced sensitivity to circulation seen at McM relative to SB, as discussed in previous sections.

We now split the reconstruction into monthly time periods in order to focus on the seasonal aspect. Correlations between reconstructed data and station records are shown in table 5.3 for individual months of the period 1979-2011. Correlations are high, particularly in the autumn, winter and spring. All correlations shown in table 5.3 are statistically significant at $p \leq 0.05$, except those for McM in October and December. Correlations tend to be lower in the summer, indicating that synoptic-scale circulation is not as dominant a factor in determining the temperature at SB or McM during this time. We also note that, as mentioned in chapter 4, summer conditions are dominated by cluster (4,2) and thus ability to represent temperature anomalies by inter-cluster variability at this time may be limited. Lower correlations may also reflect the fact that the Ross Sea region is perpetually sunlit during the summer months, and so radiative effects become far more important in controlling the temperature. The increased incidence of mesocyclones in the area in the summer and autumn (Carrasco et al., 2003) may also play a role; the influence of these features would is missing in the cluster analysis as it is incapable of resolving such small-scale and transient phenomena. Furthermore, particularly in the late summer there is likely to be open water in McM Sound, and so sensible and latent heat transfer to and from the ocean also play a more dominant role than in the winter and transition months when the ocean is ice-covered. This

Month	$m_{obs,SB}$	$m_{con,SB}$	$m_{res,SB}$	$m_{obs,McM}$	$m_{con,McM}$	$m_{res,McM}$
Jan	-0.12	-0.12	0.09	0.37	-0.18	**0.76**
Feb	-0.11	-0.02	-0.06	0.27	0.07	0.07
Mar	-0.31	-0.22	0.04	0.11	-0.13	0.31
Apr	-0.51	-0.88	0.54	-0.32	-0.88	**0.83**
May	-0.73	-0.51	-0.05	-0.29	-0.32	0.17
Jun	0.29	-0.06	0.38	0.57	-0.08	**0.71**
Jul	0.19	-0.19	0.42	0.55	-0.35	**0.99**
Aug	-0.19	-0.81	0.84†	-0.11	-0.80	**0.98**
Sep	**1.13**	0.66	0.23	0.91†	0.39	0.35
Oct	0.43	-0.12	**0.59**	**0.67**	-0.05	**0.83**
Nov	0.26	0.13	0.06	**0.78**	0.06	0.57†
Dec	-0.11	-0.09	0.10	0.31†	-0.02	**0.42**

Table 5.4: Observed and reconstructed temperature trend statistics for Scott Base and McMurdo Station. $m_{obs,X}$ represents the observed temperature trend in °C/decade between 1979 and 2011. $m_{con,X}$ is the temperature trend in the observed temperature that is linearly congruent with the trend in the temperature reconstructed solely from circulation information, in °C/decade. $m_{res,X}$ is the residual trend. For observed and residual trends significant at the $p \leq 0.05$ level is indicated by bold font. Significance at $p \leq 0.10$ is marked by a †. Observed McMurdo trends that are significantly ($p \leq 0.10$) more positive than at Scott Base are underlined. See main text for details of calculations.

is especially true at McM, where the correlations are generally slightly lower than at SB, and distinctly reduced in the late spring and summer. Biases at both sites are again small and do not have a consistent seasonal variation. Conversely, the RMSE shows higher values in the winter, despite higher correlations at this time. This is likely due to the higher interannual variability observed in the winter months. RMSE values are consistently higher at McM compared to SB.

5.4.3 Reconstruction trend analysis

Interestingly, the circulation based reconstruction shows trends in some months. Following the technique of Schneider et al. (2012a), we assess the contribution of circulation changes to the temperature trend at SB and McM by calculating the linear congruence of the trend in the observed temperature (from the READER database) with the corresponding trend in the reconstructed temperature. Linear congruence is calculated by computing linear regression coefficients between the detrended time series of observed and reconstructed temperatures. The regression coefficient is then multiplied by the trend in the reconstructed temperature. The reconstructed temperature trend is calculated using only the same data points that are present in the observed record to avoid potential biasing of trends. The congruent trend gives information on the extent of the trend in the observed temperature that is forced by temperature anomalies associated with changes in circulation. Congruent trends are displayed in columns three and six of table 5.4. We also calculate the residual trends at each station, which are defined as the trend in the difference between the observed temperature and the reconstructed. Values are shown in columns four and seven of table 5.4. The residual trend provides an indication of the background trend at each station, that is not caused by a change in circulation but by some other effect.

We find that the congruent trend at SB accounts for a high degree of the cooling trends in summer and autumn and the warming in spring, suggesting that trends at these times are forced predominantly by changes in circulation. Particularly prominent is the large positive congruent trend in September. The congruent trends are more negative than those observed in all months except February, May and

December. The more negative values are caused by the reconstructed temperatures over-estimating the anomaly towards the beginning of the record. This indicates that the observed trend is associated with a warming trend in the temperature anomaly associated with each cluster, rather than the change in the frequency of clusters. This suggests that a forcing other than inter-cluster circulation changes is at work. This is an effect that we are unable to take account for in the reconstruction experiment, which assumes a constant temperature anomaly for each cluster. In February and December it may also reflect the fact that these months show the lowest degree of accuracy of the reconstructed temperature, with reduced correlations of 0.39 and 0.45, respectively. Residual trend values are consistently positive, further suggesting a background warming. The only exception are the months of February and May, in which the residual trends are slightly negative. Again, in February, this may reflect a lack of correspondence between observed and reconstructed time series. The May correlation is rather high, and both the more highly negative observed trend and negative residual trend suggest that some cooling factor is taking place other than inter-cluster circulatory changes.

At McM, the congruent warming trend in September accounts for just under half of the observed. In the autumn, congruent and observed trends are of the same sign, but the congruent trend is too negative. In winter, observed trends are generally positive while congruent trends are negative. Again, this suggests that some effect other than circulation change is taking place, which is confirmed by the positive values for the residual trend. It also explains the negative bias in the early period seen in table 5.3. Similarly, in late spring and summer the observed trend is positive, but congruent trends are negative, as at SB. During these months at McM, the reconstructed temperatures do not reproduce the observed well, and as such it might be expected that trends in the circulation do not dictate trends in the observed temperature.

Examination of the congruent and residual trends, allows us to conclude that circulation changes dominate the observed temperature changes at SB in January, April, May, September, November and December. Circulation changes are clearly important at McM in April, May and September. But, unlike SB, the summer temperature change cannot be accounted for by trends in circulation. Residual trends at McM in particular indicate that a background warming has taken place at this location independently of changes in circulation. Earlier analysis revealed that the temperature at SB is more susceptible to circulation changes. Thus, the cooling impact of the circulation changes impacts more heavily on SB and appears to dominate changes there. Due to its exposed position, SB is almost certainly more representative of the temperature trends of the surrounding region. McM, in its more sheltered position, is less susceptible to circulation changes and thus congruent changes in circulation explain less of the observed trend there.

The difference in residual trends at SB and McM is also striking. Both stations show consistently positive residual trends, but those at McM are consistently much larger than those at SB, particularly in the summer months. While the generally positive residual trends at both sites may be forced by anthropogenic greenhouse gas emissions as suggested by Gillett et al. (2008), this forcing mechanism is unable to explain the observed disparity. In the summer it is possible that the location of McM nearer to open water in McMurdo Sound causes McM to be more susceptible to sensible and latent heat fluxes from the ocean. However, the warming trend and differences in trend are also present in winter, when the entire sea area is ice-covered and thus unlikely to play a role. Thus, it seems unlikely that maritime thermal mechanisms are effecting the changes. These results lead us to consider the possibility that the larger positive trends at McM are the product of a heat-island effect that is not present at SB, due to the much larger size and degree of human activity present at the American station. We believe that local

scale modelling over a climatological period would shed more light on the temperature changes seen at SB and McM, and aid in the explanation of the background warming that cannot be explained through changes in circulation.

5.4.4 Circulation forcing

A further advantage of applying the clustering technique to understanding temperature trends at the location of SB is the fact that contributions to the temperature trend can be assessed with reference to a particular synoptic weather pattern. As such, we are able to explain the temperature trends with respect to their dependence on specific conditions. We now attempt to attribute temperature trends due to changes in circulation to particular clusters. We will focus on SB temperatures in this section, as we have already shown that they are far more sensitive to circulation changes than those at McM. We note that the results in this section represent a preliminary investigation only.

In order to investigate which clusters in particular are forcing the observed changes at SB, we compute the trend in the temperature anomaly associated with each cluster. The cluster temperature anomaly trend is used instead of the trend in the frequency of the cluster because, as shown in figure 5.4, different clusters cause drastically different temperature anomalies. As such, a large increase in a cluster such as (4,1) will not affect the temperature to a high degree, because the anomaly associated with this cluster is small. Conversely, even a small increase in the frequency of (2,5) will force a large temperature difference, due to its extreme warming capability.

Trends are normalised by the total absolute temperature trend as computed from the reconstructed temperature anomaly, and thus represent the proportion of the trend that they contribute. The total absolute trend is used in order to conserve information on the direction of the temperature trend. We choose to discuss further only three representative months as they give the best examples of general patterns. We focus first on January, as in this month trends at SB and McM are opposite and significantly different, although neither trend is significant. We also look at May, as in this month both SB and McM show cooling trends, with SB being significantly more negative than McM. Finally, we investigate September, as SB and McM both show warming trends in this month that are not significantly different. Bar graphs of the cluster temperature anomaly trends are shown in figure 5.9 as the proportion of the total trend in the reconstruction. In these figure, positive temperature anomaly trends are shown in red and negative trends in blue. Positive trends represent either an increase in a cluster that has a positive temperature anomaly or decrease in a cluster that has a negative temperature anomaly, as both act to increase the reconstructed temperature anomaly. Conversely, negative trends represent either an increase in the frequency of negative anomaly clusters or a decrease in positive anomaly clusters. To schematically indicate the sign of the trend in the frequency, rather than the trend in temperature that the trend in frequency contributes, arrows in the direction of the frequency trend are also shown for each cluster.

The month of January shows a slight negative trend at SB and slight positive trend at McM (table 5.2). Trends congruent with the change in circulation (table 5.4) indicate that the negative trend at SB is explained by circulation changes, while that at McM is not. Figure 5.9a shows positive temperature trends caused by an increase in clusters (1,4) and (1,3), and negative temperature trends caused by increases in clusters (4,5), (3,1) and (1,2) at SB. There are also several smaller shifts that cause decreases in temperature, such as in clusters (3,6), (2,3), (2,4) and (2,5). The result is a slightly negative trend, although the interaction between changes in cluster frequencies is clearly complicated and it is difficult to

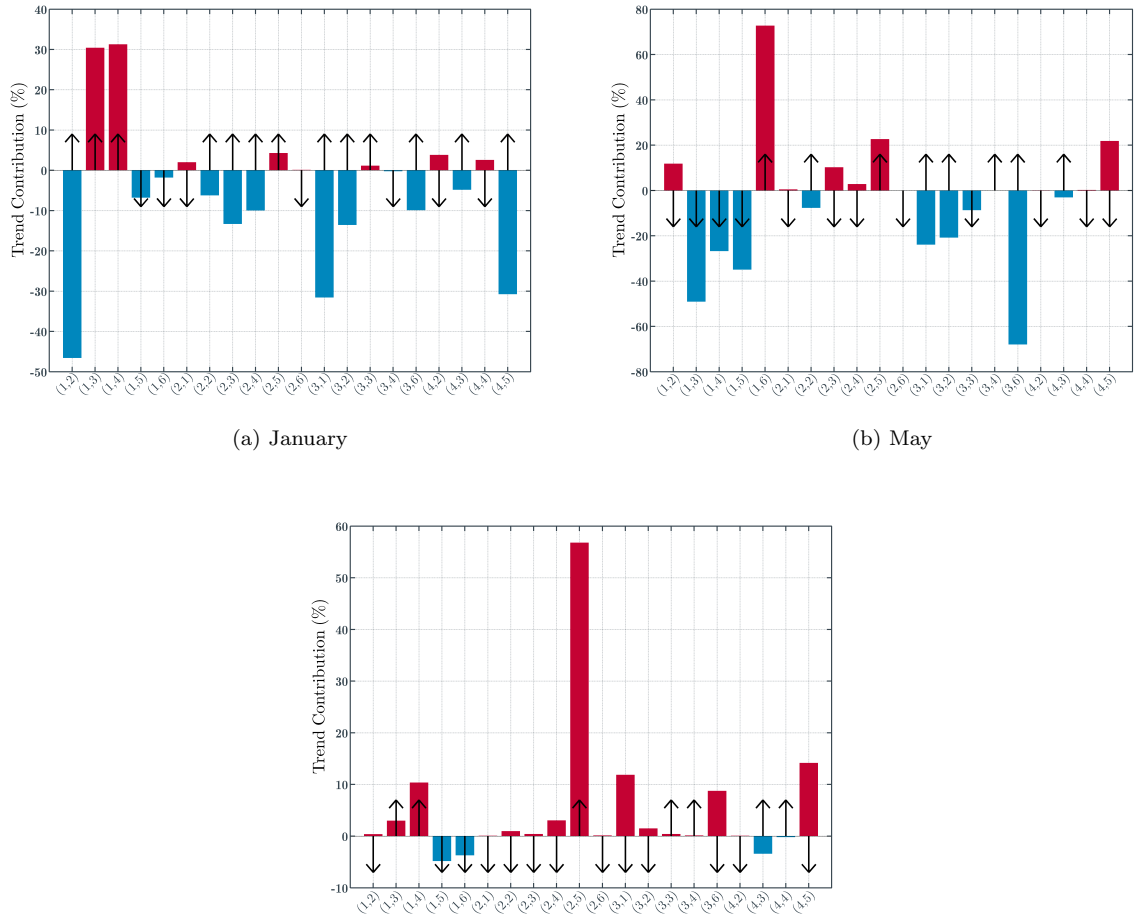

(a) January

(b) May

(c) September

Figure 5.9: Contribution of each cluster to total trend observed in reconstructed temperature series. Positive (negative) trends, shown in red (blue), represent either an increase (decrease) in incidence of a cluster associated with a positive temperature anomaly or a decrease (increase) in incidence of clusters associated with a negative temperature anomaly. Arrows indicate the sign of the frequency trend of the associated cluster.

determine which cluster, if any, is forcing the trend. Previous work on the cooling in the summer at Scott Base and McMurdo has revealed that the positive trend in the Southern Annular Mode accounts for a large amount of the observed temperature trend (Marshall, 2007). This relationship cannot be observed between the presented cluster trends and the assessment of cluster frequency dependence on SAM for summer performed in section 4.3. As discussed in section 4.3, the temperature change attributed to SAM occurs mostly within clusters, rather than changes in the frequency of clusters, due to stronger circumpolar westerly winds and the enhanced isolation of the continent. It is also possible that the low summer reconstruction correlations means that this technique is unsuited to examining temperature trends at this time of year.

In May both bases show decreasing temperature trends that are approximately accounted for by the congruent trend in the circulation. Figure 5.9b shows that trends in May are varied and complicated. Both clusters (1,6) and (3,6) show increases that lead to warming and cooling trends, respectively. Both

of these clusters show low pressures over the eastern part of the domain, and differ primarily by the depth of the pressure trough and resulting wind speeds. Cluster (1,6) shows a deeper low, and thus favours strong drainage over the Siple Coast and warm temperatures over the ice shelf. (3,6) favours lighter katabatic drainage from the East Antarctic Plateau, and hence cools the ice shelf. The temperature trends associated with these clusters are thus opposite and essentially equal, and counteract each other. Lesser negative temperature trends caused by an apparent shift away from clusters on the left of row 1 ((1,3), (1,4), & (1,5)) to the left of row 3 then appear to dominate the observed cooling. As in summer, autumn temperature reductions have also been attributed to increasing positive SAM activity (Marshall, 2007). In section 4.3 we demonstrated that clusters on the first row generally, in particular (1,3), decrease in SAM positive years in autumn, suggesting that the shift in circulation may be caused by the SAM influence. Cooling not described by the congruent trends shown in table 5.4 may be associated with intra-cluster changes which were shown to be large between SAM phases.

In chapter 4 we also demonstrated that in the summertime negative temperature changes associated with SAM around Scott Base are reduced due to stronger winds over the ice shelf. Strong winds raise the temperature at SB by mixing the surface inversion. Stronger events occur during the SAM+ phase due to the deepening of the ABS low (Turner et al., 2012). In the autumn, in the SAM positive phase we showed that winds are lower on the west side of the ice shelf and higher on the east. This may explain the larger magnitude cooling observed at SB in the autumn compared to the summer (see table 5.2), as the influence of stronger winds is not present at Ross Island in the autumn under SAM+ conditions.

Temperature trends associated with cluster frequencies in September (fig. 5.9c) show a dominance of an increase in the frequency of cluster (2,5). This cluster represents a relatively deep low over the eastern part of the greater Ross Sea region, which forces cyclonic circulation and displays a strong RAS signal. Figure 3.5 indicates that the combination of adiabatic warming and turbulent vertical mixing warms the ice shelf and cold air advection cools the ocean. The resulting temperature anomalies at both SB and McM are extremely positive, and as such the increase in frequency drives a positive trend. Both locations appear to be particularly sensitive to circulation changes at this time of year, as evidenced by congruent trends shown in table 5.4. This is perhaps because of the strong temperature inversion present at the end of the winter and the large sea ice extent present in September.

Several studies have shown significant trends in circulation in the eastern Ross Sea and Amundsen Sea. Simmonds et al. (2003) found an increase in the cyclone density in a similar location as the central low of cluster (2,5) for the period 1979-2001. Cyclones appeared to shift from farther north towards the Antarctic coast during the time period (their figure 9b). Fogt et al. (2012b) reported a deepening of the Amundsen-Bellingshausen Seas (ABS) low in September, when the low is located in the eastern Ross Sea, and a general decrease of cyclone central pressures in the region, which was linked to changes in the Semi-Annual Oscillation. The deepening trend of the ABS low in spring was confirmed by Turner et al. (2012). Schneider et al. (2012a) suggested that a deepening of the low was caused by anomalous convection in the western tropical and sub-tropical Pacific. They found a trend in the PSA-1 mode (Mo and Higgins, 1998), which is often associated with ENSO activity. They further noted that the lack of a trend in SAM in the springtime meant that its enhanced cooling influence was not present. Schneider et al. (2012b) confirmed that warm temperatures at Scott Base were associated with a deeper ABS low and La Niña-like signals in the tropical Pacific in all seasons. Both Markle et al. (2012) and Cohen et al. (2013) showed a higher degree of cyclonic activity in the Ross Sea under La Niña conditions and Turner et al. (2012) confirmed that the ABS low deepens during the La Niña phase. Bromwich et al. (2012) suggested that concurrent warming in West Antarctica might be caused by the more in-phase SAM and

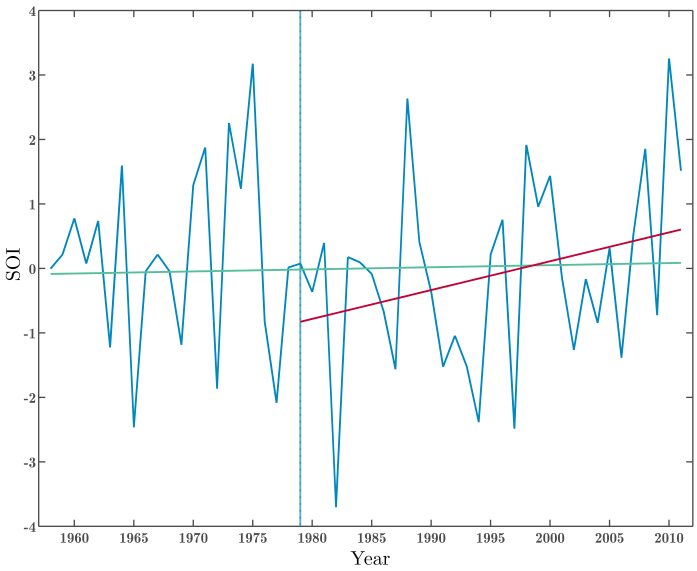

Figure 5.10: SOI running mean (JASON) time series for 1958 to 2011. Vertical dashed line marks 1979. Blue (red) line shows linear least-squares for period 1958-2011 (1979-2011). Index is normalised by its standard deviation, such that it is dimensionless.

ENSO activity in recent years, which is known to reinforce the observed deepening of the ABS low (Fogt and Bromwich, 2006; Fogt et al., 2011). Results from chapter 4 indicate that the frequency of cluster (2,5) is highly dependent on ENSO conditions, and more common in the La Niña phase, which appears to be consistent with the body of previous research.

In order to assess the proposed link between warming at Scott Base in the spring and ENSO activity, we compute trends for the Southern Oscillation Index (SOI) (see section 4.2) for the month of September, using a 5-month running mean (JASON) centred on the month. The time series of the SOI for the period 1958 to 2011 is shown in figure 5.10. While significant spring warming at Scott Base has been observed from the late 1950s onwards (Schneider et al., 2012a; Turner et al., 2005; Turner and Overland, 2009), we do not find a significant trend in the SOI between the founding of Scott Base (1958) and the present day, which suggests that ENSO-related changes have not forced Scott Base trends. The linear least-squares fit for the time period is shown in figure 5.10 in green. However, upon splitting the observed SB temperature and SOI time series into segments from 1958 to 1978 and 1979 to 2011 we find that neither the temperature or SOI has a significantly increasing trend in the earlier time period before the lower time limit of our reconstruction. In fact, the trend in temperature at SB is marginally negative in the earlier period. In the later time period both the SB temperature and SOI have increasing trends which are significant at $p \leq 0.1$. The positive linear least-squares fit for this time period is shown in red in figure 5.10. It is then possible that the increasing spring temperatures at SB and McM are forced in part by increasing incidence of La Niña conditions, although this requires further investigation.

While Bertler et al. (2004) suggested that increased drainage from West Antarctica onto the Ross Ice Shelf would cool Scott Base, we find that in springtime the increased frequency of events in which strong winds propagate from the Siple Coast act to warm Scott Base. This is due to the disruption by such events of the surface temperature inversion at the station. Given that cluster (2,5) warms large portions

of the ice shelf (fig. 3.5), it is possible that it is an increase in the frequency of this cluster that forces the upward trends reported over the shelf by Schneider et al. (2012a) and Shu et al. (2012). These trends will be a focus of future research. In particular, an obvious development of these findings is to apply a similar technique to that used in chapter 4 to temporal changes over the wider region. Circulation changes may also explain the observed differences in trends between the temperature at Scott Base and those observed in ice cores drilled to the west in the Transantarctic Mountains (Sinclair et al., 2012). The warming at SB appears to be linked to its position within the path of the strong winds of the Ross Ice Shelf Air Stream, to which the ice core sites are not subject. The temperature reaction to such events may then be fundamentally different.

5.5 Summary and conclusions

Clearly, a large amount of information on the meteorology and climate of the Ross Island region can be obtained through the use of cluster analysis. Using the clustering algorithm output developed in chapter 3 we have been able to composite conditions from Ross Island automatic weather stations for a variety of synoptic conditions. Using these composites we are able to study conditions in the vicinity of the island. In particular, the application of the clustering algorithm, trained on the Ross Sea and Ross Ice Shelf, has allowed us to ascertain the extent of the interaction and dependence of the smaller area on conditions in the wider region.

The occurrence of southerly winds at Scott Base has been studied in some detail and with respect to conditions across the ice shelf. We found that strong winds in the Ross Island region are not enough to cause the prevailing north-easterly wind at Scott Base to turn to the south. This is due to the sheltering aspect of Minna Bluff and the presence of a persistent low-level inversion at Scott Base, and the associated barrier flow along the Hut Point Peninsula. In order for southerly winds to occur, the wider area flow must overcome the slopes of Minna Bluff and the Hut Point Peninsula. Southerly winds show some dependence on temperature conditions to the south of the bluff, with warm surface air, indicative of a turbulently mixed boundary layer, more capable of surmounting the barriers. These conditions were confirmed by composites of the temperature difference between Scott Base and the peak of Minna Bluff, indicating less stable stratification when southerly winds occur at Scott Base. As we have shown, the conditions identified are highly dependent on the position of the pressure minimum relative to Ross Island. The clustering algorithm also produces several wind composites that appear similar around Ross Island, suggesting that the prevailing wind in the region is insensitive to some changes in synoptic conditions, and highlighting the dominance of local topography when synoptic forcing is not strong.

Examination of the temperature reaction to each cluster incidence is particularly important due to the demonstrated high dependence of temperature on synoptic circulation conditions, especially high temperatures experienced during RAS events. Accordingly, results detailed in this chapter have indicated that the temperature around Ross Island is highly dependent on the wind field of the island, and also that of areas to the south. While strong winds tend to generate positive temperature anomalies through the turbulent vertical mixing mechanism, it has been shown that in several cases weather stations around the area show a different temperature reaction to wind conditions that appear rather similar. The difference lies in the wind conditions in regions to the south of Ross Island, which are dependent on the size and position of pressure minima in the Ross Sea and over the ice shelf. Hence, it seems likely that, had the clustering algorithm been trained on the island rather than the wider region, these differences in the temperature reaction may not have been captured.

The importance of local topographic forcing to temperature is further highlighted by the temperature difference between the sites of Scott Base and McMurdo Station, which are separated by ≈ 2.2 km, but experience a temperature difference of $\approx 3\,^{\circ}$C over a long-term annual average. Previous research has suggested that Scott Base is situated in a region of a persistent shallow temperature inversion (Sinclair, 1982, 1988). The slightly higher altitude of McMurdo Station removes it from this layer, and precludes it from experiencing the coldest temperatures at Scott Base. As noted by Stearns et al. (1993), the location of the bases with respect to the localised flows is also important in determining their temperature. Winds at McMurdo are slightly higher, which may also prohibit the existence of a strong inversion there. Further, Scott Base is more subject to the cold wind out of Windless Bight. We have shown that these conditions cause a large distinction in the sensitivity of the locations to synoptic forcing. The presence of the inversion at Scott Base, and the dominance of the associated localised flow, means that if the inversion is disrupted, the temperature rise at Scott Base is dramatic. Consequently, the temperature at Scott Base is far more dependent on synoptic conditions than that at McMurdo Station.

We have calculated trends at Scott Base and McMurdo Station from observational data and using a novel reconstruction technique that is capable of reproducing the temperature from information on the circulation conditions and their variability, we have further investigated the sensitivity of these locations to changes in synoptic forcing. At Scott Base, the reconstruction technique works extremely well, further confirming the dependence of the temperature at Scott Base on synoptic conditions. At McMurdo Station, the reconstruction works reasonably in the winter, although not as successfully as at Scott Base. The reconstruction also appears to fail in the summer when the temperature is far more dependent on solar conditions than circulation and a single cluster dominates the synoptic conditions. The significant difference between observed trends at Scott Base and McMurdo Station have been analysed, and it has been shown that part of the disparity is due to the lack of sensitivity to synoptic forcing encountered at McMurdo Station. However, we are unable to explain the source of the positive trends at McMurdo Station that are not observed at Scott Base. That the trends appear to be so localised suggests that they may be the result of a heat island effect, but we are unable to confirm this. We have attempted to attribute changes in circulatory conditions to wider influences, and tentatively concluded that the temperature rise in spring may be associated with an increased tendency towards La Niña conditions since the late 1970s. This appears to cause an increasing incidence of cyclones centred over Marie Byrd Land, in accordance with similar studies (Markle et al., 2012; Schneider et al., 2012a; Cohen et al., 2013) and the results of section 4.4. However, other studies have highlighted the dependence of the depth of the ABS low in September on Semi-Annual Oscillation amplitudes (Fogt et al., 2012b; Turner et al., 2012) and we feel that this requires further enquiry. A logical extension of the trend analysis would be an extension to the ice shelf region by applying the technique of chapter 4 to characterise differences in mean conditions between the first and second halves of the ERA Interim record. This will be the focus of further study.